

Distribution Agreement

In presenting this thesis of dissertation as a partial fulfillment of the requirements for an advanced degree from Emory University, I hereby grant to Emory University and its agents the non-exclusive license to archive, make accessible, and display my thesis or dissertation in whole or in part in all forms of media, now or hereafter known, including display on the online submission of this thesis or dissertation. I retain all ownership rights to the copyright of the thesis or dissertation. I also retain the right to use in future works (such as articles or books) all or part of this thesis or dissertation.

Signature:

Caitlin M. B. Farr

Date

Allylic C-H Arylation, Enantioselective Catalyst Development, and Enantioselective Allylic C-H
Amidation

By

Caitlin M. B. Farr
Doctor of Philosophy

Chemistry

Simon B. Blakey, Ph. D.
Advisory

Frank E. McDonald, Ph. D.
Committee Member

Nathan T. Jui, Ph. D.
Committee Member

Accepted:

Dean of James T. Laney School of Graduate Studies

Date

Allylic C-H Arylation, Enantioselective Catalyst Development, and Enantioselective Allylic C-H
Amidation

By

Caitlin M. B. Farr
B. S., University of North Carolina at Asheville, 2015

Advisor: Simon B. Blakey, Ph. D.

An abstract of
A dissertation submitted to the Faculty of the
James T. Laney School of Graduate Studies of Emory University
in partial fulfillment of the requirements for the degree of
Doctor of Philosophy
in Chemistry
2020

Abstract

Allylic C-H Arylation, Enantioselective Catalyst Development, and Enantioselective Allylic C-H Amidation

By Caitlin M. B. Farr

The allylic substitution reaction, developed by Tsuji and Trost, was an important advancement in natural product synthesis and drug molecule design which proceeds via a π -allyl intermediate. The Tsuji-Trost reaction allowed for a disconnection that provided the opportunity for the convergent synthesis of natural products like strychnine. Instead of utilizing an allylic leaving group in the olefin substrate to access the π -allyl intermediate, our group developed allylic C-H functionalization of internal and terminal olefins with rhodium(III) and iridium(III) pentamethylcyclopentadienyl catalysts. This methodology provided a class of reactions that were efficient and highly useful. We have previously described the successful development of a rhodium catalyst system capable of activating unsymmetrical 1,2- disubstituted olefins for regioselective allylic C-H amination and etherification, and described the mechanistic investigations in detail. Herein, we will disclose the development of a rhodium catalyzed regioselective allylic C-H arylation and amidation to enable access to motifs present in natural products and drug molecules. Also, we expand on the regioselective allylic amidation and describe the development of a planar chiral rhodium(III) catalyst for the enantioselective allylic amination of unactivated terminal and internal olefins.

Allylic C-H Arylation, Enantioselective Catalyst Development, and Enantioselective Allylic C-H
Amidation

By

Caitlin M. B. Farr
B. S., University of North Carolina at Asheville, 2015

Advisor: Simon B. Blakey, Ph. D.

A dissertation submitted to the Faculty of the
James T. Laney School of Graduate Studies of Emory University
in partial fulfillment of the requirements for the degree of
Doctor of Philosophy
in Chemistry
2020

Acknowledgements

The pathway from a bachelor's degree to achieving a PhD in chemistry requires a copious amount of time, commitment and mental fortitude. I would not be where I am today without the help and encouragement of many important people. Firstly, I want to thank my advisor Professor Simon Blakey for his support and encouragement during my career at Emory University. You taught me to trust my chemical intuition and encouraged me to pursue my own projects and ideas, which helped me develop confidence in myself as a chemist, researcher and scientist. You were always available to discuss new ideas, interesting papers, and confusing and exciting results while keeping me focused on the end goals. You also provide a safe space to discuss any issues that arose in graduate school beyond reactions and projects. I would also like to thank my committee members, Professor Frank McDonald and Professor Nathan Jui. You have both provided invaluable advice and encouragement that shaped me into the chemist and scientist I am today. I would like to thank every member of the Blakey lab, both past and present, who provided a supportive laboratory environment. Specifically, I would like to thank Amaan Kazerouni for pushing me to be the best chemist and person over the last five years. You have been a great friend and fellow researcher. I would like to thank Jacob Burman, Taylor Nelson and Christopher Poff who worked beside me on multiple projects and helped shape an amazing body of work for my thesis. I would like to thank my family for the endless support and encouragement. You gave me the confidence to pursue such a difficult degree. Lastly, and definitely not least, I would like to thank my amazing husband for following me 200 miles, relocating a huge city, and loving me through the ups and downs of a doctoral degree. You pushed me to never give up and you always keep me grounded. I would have never made it through graduate school without you and I love you whole bunches. There is one more person to acknowledge, my beautiful son who arrived just in time to celebrate. You are truly the best thing that happened during my PhD and I love you so much.

Table of Contents

1. Metal catalyzed functionalization of olefins via π -allyl intermediates	
1.1 Introduction to Allylic Substitution.....	1
1.2 Allylic C–H Functionalization of terminal olefins.....	4
1.3 Rhodium(III) catalyzed Allylic C–H Functionalization.....	6
1.4 Development of rhodium(III) catalyzed Allylic C–H Functionalization of unsymmetrical 1,2-disubstituted olefins.....	8
1.5 Conclusions.....	12
1.6 References.....	13
2. Development and progress towards the regioselective allylic C–H arylation of 1,2-disubstituted allyl benzene derivatives.	
2.1 Introduction to allylic C–H arylation.....	19
2.2 Reaction discovery: allylic C–H arylation.....	20
2.3 Reaction discovery: benzylic site selective allylic C–H arylation.....	25
2.4 Rhodium(III) catalyzed allylic C–H functionalization mechanism and kinetic studies..	30
2.5 Conclusion.....	36
2.6 Experimental Procedures.....	38

2.7 Spectral Data.....	48
2.8 References.....	55
3. Development of a Novel Chiral Indenyl Catalyst for Regio- and Enantioselective C–H Amidation of Unactivated Olefins	
3.1 Introduction: Allylic C–H Amidation.....	56
3.2 Chiral group IX catalysts for allylic C–H amidation.....	58
3.3 Development of Catalyst for enantioselective allylic C–H amidation.....	63
3.4 Determining Catalyst and Substrate Stereochemistry.....	69
3.5 Reaction development: rhodium(III) indenyl catalyzed allylic C–H amidation.....	71
3.6 Reaction Mechanism and Stoichiometric Studies.....	77
3.7 Conclusion and Future Directions.....	81
3.8 Experimental Procedures.....	82
3.9 Spectral Data.....	119
3.10 References.....	175

Table of Figures

Figure 1-1. Allylic substitution via π -allyl intermediates.....	1
Figure 1-2. Tsuji and Trost seminal publications for the development of the allylic substitution reaction (Tsuji-Trost reaction).....	2
Figure 1-3. Key allylic substitution step in the synthesis of strychnine and colombiasin A.....	3
Figure 1-4. General palladium catalyzed allylic C–H functionalization and common nucleophiles.....	5
Figure 1-5. General allylic C-H oxidation mechanism proceeding through an σ -allyl intermediate.....	6
Figure 1-6. Cossy and Takana's rhodium catalyzed allylic C–H functionalization.....	7
Figure 1-7. Allylic C–H amination selected examples from amine nucleophile scope.....	10
Figure 1-8. Allylic C–H amination selected examples from olefin scope.....	10
Figure 1-9. Allylic C–H etherification selected examples from alcohol nucleophile scope.....	11
Figure 1-10. Allylic C–H etherification selected examples from olefin scope.....	12
Figure 2-1. Structure of tetrahydrocarbozole (THC) and tetrahydro- β -carboline (THBC) scaffolds.....	19
Figure 2-2. Effects of <i>N</i> -Cbz indole substitution on allylic C–H arylation.....	24
Figure 2-3. Proposed reaction mechanism for allylic C–H amination.....	31

Figure 2-4. Proposed reaction coordinate diagram for S _N 1 reaction of allylic acetate 53 with N-methyl indole.....	33
Figure 2-4. Proposed reaction coordinate diagram for S _N 1 reaction of allylic acetate 53 with N-Cbz indole.....	35
Figure 3-1. Proposed mechanism for allylic C-H amidation via nitrene intermediate.....	56
Figure 3-2. Rhodium(III) and iridium(III) catalyzed regioselective intermolecular allylic C-H amidation with dioxazolone reagents.....	57
Figure 3-3. Rhodium(III) chiral Cp and Cp* catalysts for asymmetric induction.....	58
Figure 3-5. Simplified asymmetric rhodium(III) complex with simplified ligand structure.....	63
Figure 3-6. Allylic C-H amidation with novel rhodium(III) and iridium(III) planar chiral indenyl complexes.....	68
Figure 3-7. Stereochemical assignment of rhodium(III) complex 86 and stereochemical determination of aryl and alkyl amide products.....	70
Figure 3-8. Scope of dioxazolone substrates for enantioselective allylic C-H amidation of 4-methylpentene.....	74
Figure 3-9. Scope of olefin substrates for enantioselective allylic C-H amidation with <i>tert</i> -butyl dioxazolone and <i>N</i> -phth-glycine dioxazolone.....	76
Figure 3-10. Complete energy profile diagram for the enantioselective allylic C-H amidation of allylbenzene and <i>tert</i> -butyl dioxazolone.....	79

Figure 3-11. Proposed catalytic cycle for enantioselective allylic C–H amidation with planar chiral

rhodium(III) indenyl complex (*R,R*)-86.....81

Table of Schemes

Scheme 3-1. Baker's discovery of an enantioselective allylic C–H alkylation utilizing asymmetric rhodium(III) π -allyl complexes.....	60
Scheme 3-4. Baker's synthesis and structure of planar chiral bidentate indenyl-sulfinyl complexes of rhodium(III).....	61
Scheme 3-5. Baker's oxidation of (pS)-70 for chiral resolution protocol.....	62
Scheme 3-6. Synthesis of substituted indenyl ligands.....	64
Scheme 3-7. Proposed complexation of indene ligands 74-75 and 78 with rhodium(III) chloride.....	65
Scheme 3-8. Complexation of indene ligands 78 and 75 via rhodium(I) cyclooctadiene ([Rh(COD)Cl] ₂).....	66
Scheme 3-9. Complexation of indene ligands 79 and 75 via iridium(I) bisethylene ([Ir(C ₂ H ₄)Cl] ₂).....	67
Scheme 3-10. Stoichiometric reaction with (S,S)-95 and 2-pentene.....	77

Table of Tables

Table 2-1. Exploration of N-protected indoles as nucleophiles.....	20
Table 2-2. Reaction optimization for regioselective <i>N</i> -Cbz indole addition.....	23
Table 2-3. <i>N</i> -Bn Indole Addition: Temperature and Nucleophile Concentration Effects.....	26
Table 2-4. Condition screening for benzylic site-selective <i>N</i> -Bn indole addition.....	27
Table 2-5. Condition Screening for Regioselective <i>N</i> -Bn Indole Addition.....	29
Table 3-1. Optimization of enantioselective allylic C–H amidation.....	72

Chapter 1. Metal catalyzed functionalization of olefins via π -allyl intermediates

1.1 Introduction to Allylic Substitution

The reaction of an allylic electrophile with a carbon or heteroatom nucleophile to afford products where the group in the allylic position on the electrophile is substituted for the nucleophile is an allylic substitution reaction. This class of reaction is a powerful tool for the synthesis of complex natural products, medicinally relevant molecules and drug candidates and targets.¹⁻⁴ Many allylic substitution reactions utilize a transition metal catalyst and proceed via a transition metal π -allyl intermediate (**Figure 1-1**). The allylic electrophile is historically an allylic halide, acetate, carbonate, phosphate, epoxide or aziridine typically derived from an allylic alcohol, while recent advances have used allenes and alkynes as pre-oxidized alternatives.⁵⁻⁹ The nucleophile employed is commonly a soft nucleophile which is less electronegative and more polarizable, like the anion of a dimethyl malonate derivative as a carbon based nucleophile or amines as heteroatom nucleophiles.¹⁰

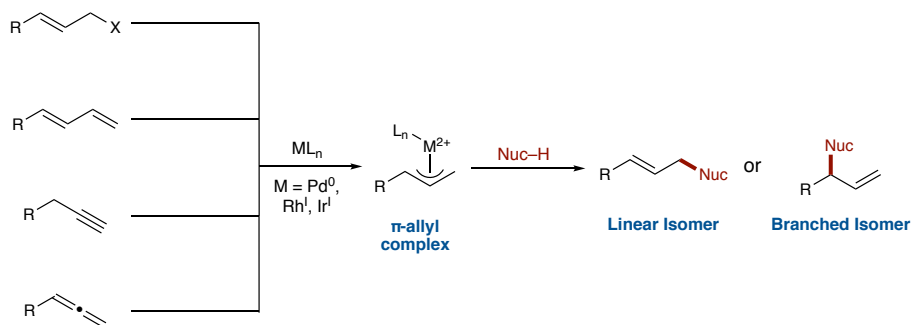


Figure 1-1. Allylic substitution via π -allyl intermediates.

It is widely accepted that the seminal allylic substitution publication was published by Tsuji in 1965 where he demonstrated that palladium-allyl complex **1** can undergo attack by malonate derivative **2** to generate allylic product **3** which contained a new carbon-carbon bond (**Figure 1-2a**).¹¹ The palladium-allyl or π -allyl complex **1** bears an electrophilic allyl ligand due to the η^3 -

bonding configuration, where all three carbons of the extended π -system are interacting with the metal, thus allowing for the flow of electrons from the ligand to the metal. This publication established that palladium π -allyl complexes are electrophilic and can undergo carbon-carbon bond forming reactions with stabilized carbon nucleophiles. In 1977, Trost and co-workers published the seminal publication for enantioselective allylic C–H alkylation (**Figure 1-2b**).¹² Due to Tsuji's seminal work in stoichiometric reactions of palladium-allyl complexes and Trost's discovery of an enantioselective variant, the reaction is referred to as the Tsuji-Trost reaction.

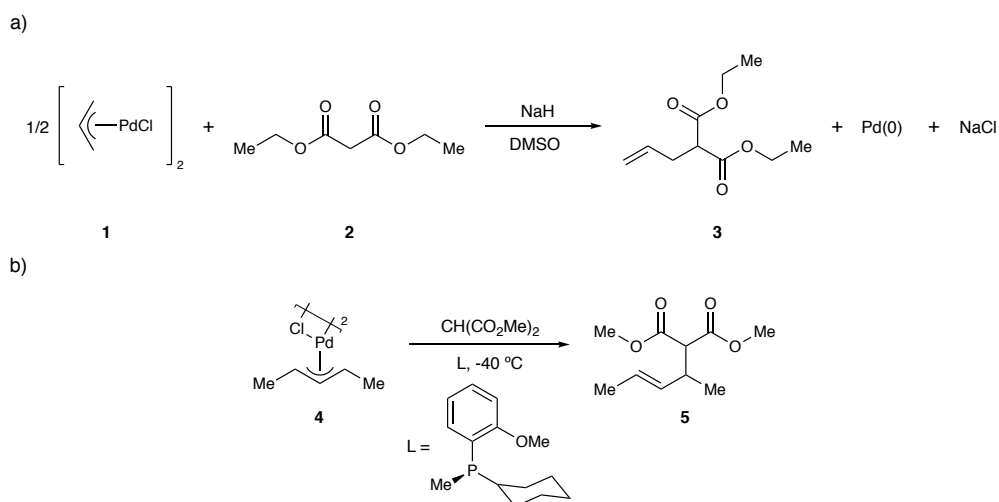


Figure 1-2. Tsuji and Trost seminal publications for the development of the allylic substitution reaction (Tsuji-Trost reaction).

The palladium catalyzed Tsuji-Trost reaction has been utilized in modern synthetic strategies and applied to the synthesis of complex natural products, such as strychnine and colombiasin A.¹³ Overman and co-worker's synthesis of strychnine in 1993 employed an enantioselective allylic alkylation at the convergence point of the synthesis (**Figure 1-3a**).¹³ The use of palladium catalyzed enantioselective allylic alkylation was one of the major factors which allowed for Overman to succeed in the first enantioselective synthesis of strychnine. Nicolaou and co-workers used a decarbonylative Tsuji-Trost reaction to introduce the allyl fragment for future ring-closing reaction

to afford one of the rings of the tetracyclic core (**Figure 1-3b**).¹³ The regioselectivity necessary for the subsequent ring-closure required the less favored isomer **11** compared to the more favored nucleophilic attack at the terminal position. However, Nicolaou and co-workers proposed that modifying electronic factors, rather than sterics, could provide the regioselectivity necessary for the synthesis of colombiasin A by taking advantage of the partial positive charge on the secondary carbon of the allyl functionality. The phosphine ligand on palladium was essential to enabling the accumulation of positive charge on the correct carbon to favor regioisomer **11**. This synthesis was the first complex molecule synthesis which controlled the regioselectivity of the Tsuji-Trost reaction beyond only steric control.

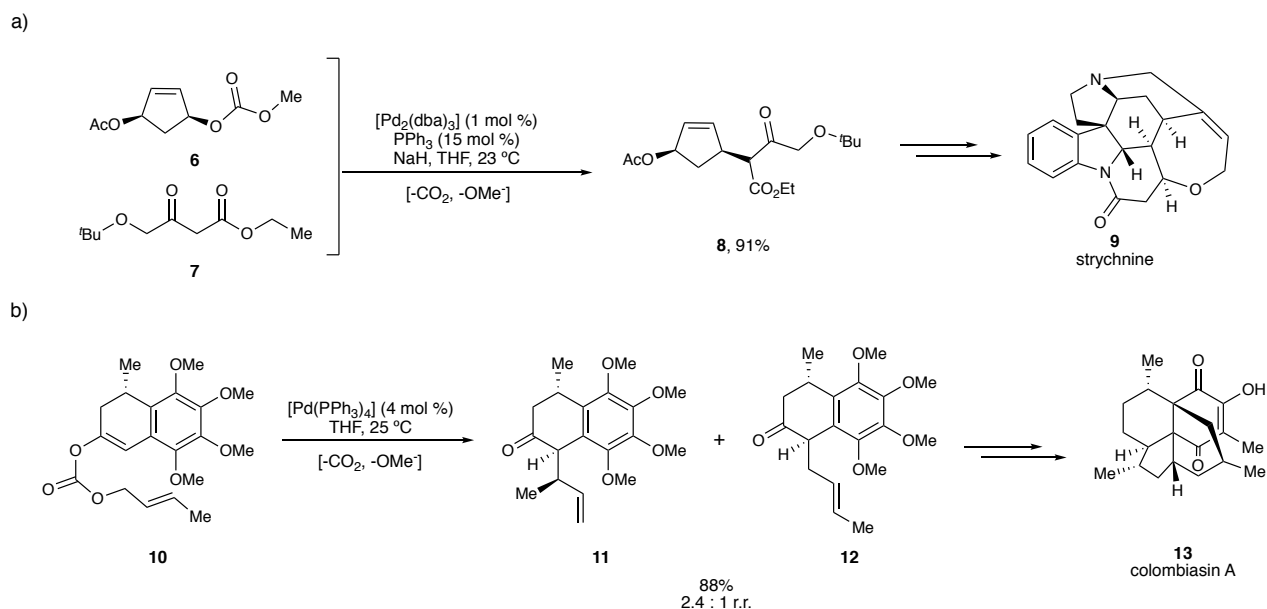


Figure 1-3. Key allylic substitution step in the synthesis of strychnine and colombiasin A.

In recent literature, rhodium, iridium and copper have made an appearance as metals for catalyzing allylic substitution, beyond classical palladium catalyzed allylic substitutions.¹⁴⁻⁶¹ Recent advances have expanded the scope of allylic substitution by broadening nucleophile compatibility and addressing regioselectivity issues with choice of metal catalyst and ligand. Typically, palladium

catalysts provide nucleophilic attack at the less hinder position of the π -allyl but are often limited to soft nucleophiles. Rhodium and iridium catalysts afford products from attack at the more hindered position and are compatible with soft and hard nucleophiles. The complementary reactivity observed with palladium versus rhodium and iridium provides the ability to tailor an allylic substitution to the needs of a complex molecule or natural product synthesis. A major disadvantage of allylic substitution is the necessity of the pre-oxidation of the π -allyl precursor. This is not a major synthetic challenge for small molecules but for complex intermediates, installing the allylic halide, acetate or other functionality would not be trivial.

1.2 Allylic C–H Functionalization of terminal olefins

Accessing transition metal π -allyl complexes directly from the parent or feedstock olefin would eliminate the need for the pre-oxidation, but require the development of a new class of catalysts. This reaction would utilize allylic C–H functionalization, where instead of the allylic substrate already being in the correct oxidation state, the allylic C–H bond would be oxidized and functionalized at the same time. The use of C–H functionalization would allow for the direct functionalization of natural products isolated from nature, minimize the number of transformations required for de novo synthesis of complex molecules and reduce the number of functional group manipulations. These advantages would allow syntheses to approach ideality by reducing the number of “concession” steps, such as functional group interconversions, while providing a “constructive” reaction in the C–H functionalization step.⁶²

In the last three decades, the development of palladium catalyzed allylic C–H functionalization has attracted the attention of the organic and organometallic chemistry community (**Figure 1-4**). In 2004, White and co-workers reported a major intellectual advance in field of allylic C–H functionalization with the development of a sulfoxide-promoted, palladium catalyzed allylic C–

H acetoxylation.⁶³ While this was not the first allylic C–H functionalization, the White group popularized and expanded the scope of nucleophilic partners to include carbon, nitrogen and oxygen.^{64–77} The sulfoxide-promoted allylic C–H functionalization has high conversion, large functional group tolerance, mild oxidants and with terminal olefins. Under previously published conditions underwent a Wacker oxidation instead of the desired C–H functionalized products.⁷⁸

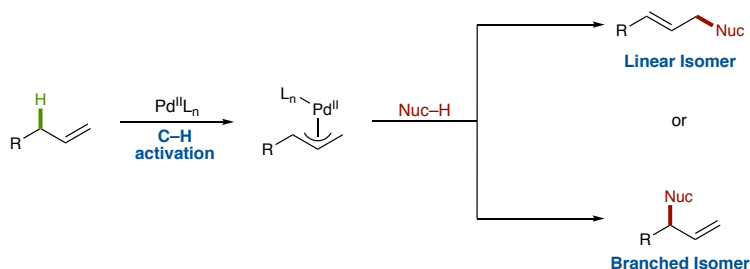


Figure 1-4. General palladium catalyzed allylic C–H functionalization.

The proposed mechanism for palladium-catalyzed allylic C–H acetoxylation is nearly identical to the mechanism invoked for catalytic allylic substitution (**Figure 1-5**).⁷⁷ The first difference is that the π-allyl is formed via C–H activation, presumably through a concerted-metalation-deprotonation (CMD) mechanism, in contrast to the oxidative addition of an allylic acetate or halide. Both reactions then undergo nucleophilic addition and ligand exchange of the alkene product for another ligand, in the allylic C–H functionalization this can be the oxidant or carboxylate. In the case of allylic substitution, the catalytic cycle is complete because the low valent metal is necessary for the oxidative addition. The last step for the allylic C–H functionalization is oxidation of palladium(0) to palladium(II) to complete the catalytic cycle. All of the differences can be attributed to whether the alkene is pre-oxidized or the an external oxidant is used.

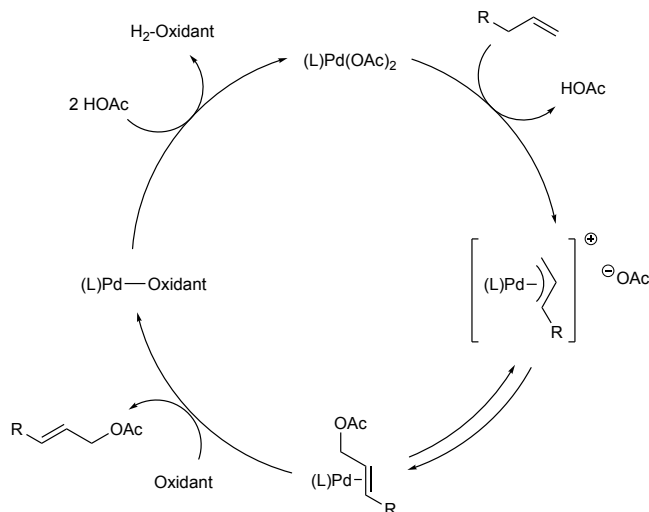


Figure 1-5. General allylic C-H oxidation mechanism proceeding through an π -allyl intermediate.⁷⁷

While the palladium catalyzed allylic C–H functionalization reactions developed in the past 20 years provide a more atom economical alternative to the pre-oxidized allyl electrophiles used in allylic substitutions, limitations and challenges still remain. The methodology requires carboxylates, doubly activated amine nucleophiles, containing two electron withdrawing groups, or stabilized nucleophiles, such as malonate derivatives. The reaction is also limited to terminal olefins and often requires elevated temperatures. Lastly, in the case of intermolecular allylic C–H functionalization, the nucleophilic attack often occurs at the least hindered position which provides the linear product as the major isomer.⁷⁸ There are exceptions with limited number of catalyst systems, like Itami and co-workers sulfoxide-oxazoline (sox) ligand which provides branched allylic C–H acetoxylation products in up to a 98:2 regiomer ratio.⁷⁹

1.3 Rhodium(III) catalyzed Allylic C–H Functionalization

Recent literature by Cossy, Tanaka, and Rovis give evidence that electron deficient rhodium(III) complexes can activate allylic C–H bonds of terminal and internal olefins.⁸⁰⁻⁸² In 2012,

Cossy and co-workers developed the first rhodium(III) catalyzed intramolecular allylic C–H amination using amines with a single electron-withdrawing group (**Figure 1-6a**).⁸³ They proposed that their intramolecular C–H amination was proceeding through a rhodium π -allyl intermediate in the formation of a tosyl-protected piperidine (**15a**) and tosyl-protected allylic pyridine (**15b**).⁶ This seminal work demonstrated the viability of rhodium(III) pentamethylcyclopentadienyl (Cp*) complexes for allylic C–H functionalization while also expanding nitrogen nucleophiles beyond doubly activated amines. The formation of **15b** from alkene **14** would require the formation of an internal π -allyl complex, if the reaction in fact proceeds through a π -allyl intermediate followed by nucleophilic attack. This is speculation because Cossy and co-workers did not isolate or observe the π -allyl complexes.

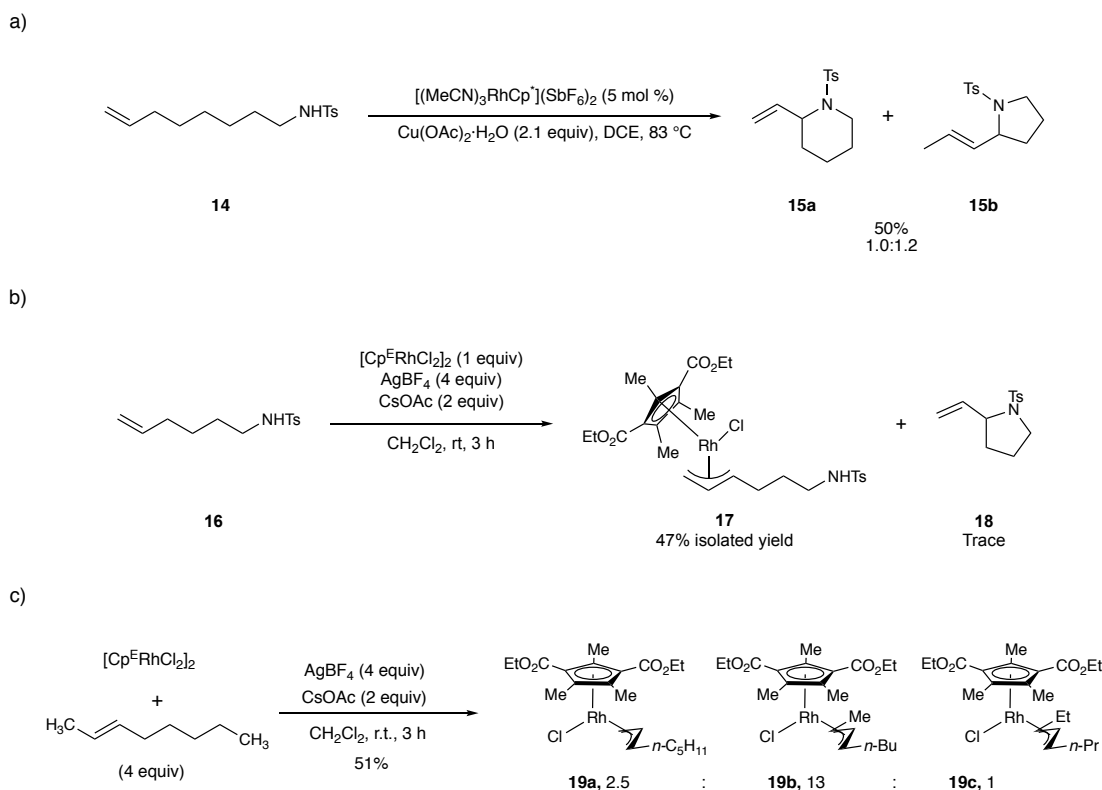


Figure 1-6. Cossy and Tanaka's rhodium catalyzed allylic C–H functionalization.

After Cossy's initial disclosure, Tanaka and co-workers utilized their novel electron-deficient cyclopentadienyl rhodium(III) complex $[\text{RhCp}^{\text{E}}\text{Cl}_2]_2$ to investigate Cossy's proposed mechanistic hypothesis.⁸⁴ In a previous publication, the novel $[\text{RhCp}^{\text{E}}\text{Cl}_2]_2$ displayed high catalytic activity in oxidative sp^2 C–H olefination of electron-rich arenes.⁸⁵ Since Tanaka knew that their $[\text{RhCp}^{\text{E}}\text{Cl}_2]_2$ could activate the C–H bond and afford a π -allyl complex, they optimized reaction conditions for the preparation of π -allyl complex **17**. They observed that with a terminal olefin **16**, the terminal rhodium(III) π -allyl complex **17** was favored in a >20:1.0 regiomer ratio (**Figure 1-6b**). Thus the proposed rhodium(III) π -allyl intermediate **16** in Cossy's publication, was isolated with Tanaka's Cp^{E} ligand on rhodium. The isolated π -allyl complex **16** was subjected to reaction conditions and pyrrolidine was observed. This provided strong evidence for Cossy's proposed rhodium(III) π -allyl intermediate invoked in the proposed mechanism.

Terminal π -allyl formation with rhodium(III) is a conceptual advance because the amine nucleophile does not require two electron-withdrawing groups, but the outcome with an internal olefin is more intriguing. When 2-octene underwent C–H activation, Tanaka and co-workers were able to isolate and characterize a terminal rhodium(III) π -allyl complex **19a** and two internal rhodium(III) π -allyl complexes **19b** and **19c** (**Figure 1-6c**). The stoichiometric allylic C–H activation of a di-substituted olefin is a conceptual advance because it the formation of an internal π -allyl complex provides a platform for expanding allylic C–H activation beyond terminal olefins. Our group proposed intercepting rhodium(III) π -allyl complexes, similar to the complexes isolated by Tanaka and co-workers, with a variety of nucleophiles toward the development of a rhodium(III)-catalyzed intermolecular allylic C–H functionalization with di-substituted olefins.⁸⁶⁻⁸⁷

1.4 Development of rhodium(III)-catalyzed Allylic C–H Functionalization of unsymmetrical 1,2-disubstituted olefins.

Our group, specifically Jacob Burman, successfully discovered and developed the regioselective allylic C–H amination of 1,2-disubstituted olefins.⁸⁶ Our initial investigations expanded the field of rhodium(III)-catalyzed allylic C–H amination to include internal olefins, an intermolecular reaction mechanism, and expand the nucleophile scope to other amines with one electron-withdrawing group (**Figure 1-7**). The reaction tolerates a variety of electron-withdrawing groups with halide, nitro and carbonyl functionality while providing high yields of allylic amine product (**21-26**). Amine nucleophiles with a alkyl group, in addition to the electron-withdrawing group, provided moderate to high yields of allylic amines **21**, **22**, and **26**. Jacob found that our allylic C–H amination is regioselective on aryl-alkyl disubstituted olefins, affording the conjugated allylic amine product (**Figure 1-8**). Electron-withdrawing and donating groups on the olefin substrate did not drastically reduce yield of allylic amines **27-30**. With electron-withdrawing groups, like CF₃, we observed lower regioselectivities (4.0:1.0 r.r.) of allylic amine product **29**. Notably, heteroaromatic functionality (**31-32**), present in natural products and drug molecules, can be incorporated into the olefin substrate. The allylic C–H amination is the first example of intermolecular allylic C–H amination of internal olefins, efficient for a variety of common nitrogen nucleophiles, and provides high regioselectivities on aryl-alkyl 1,2-disubstituted olefins.

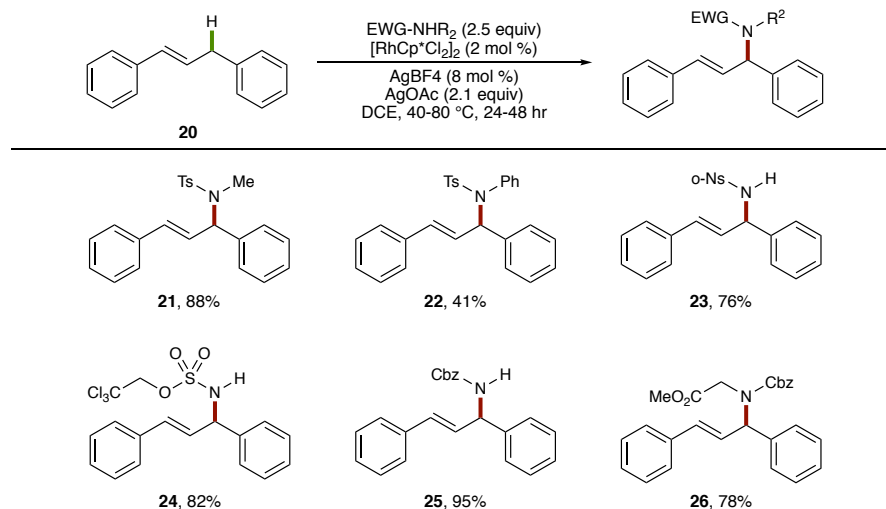


Figure 1-7. Allylic C–H amination selected examples from amine nucleophile scope.

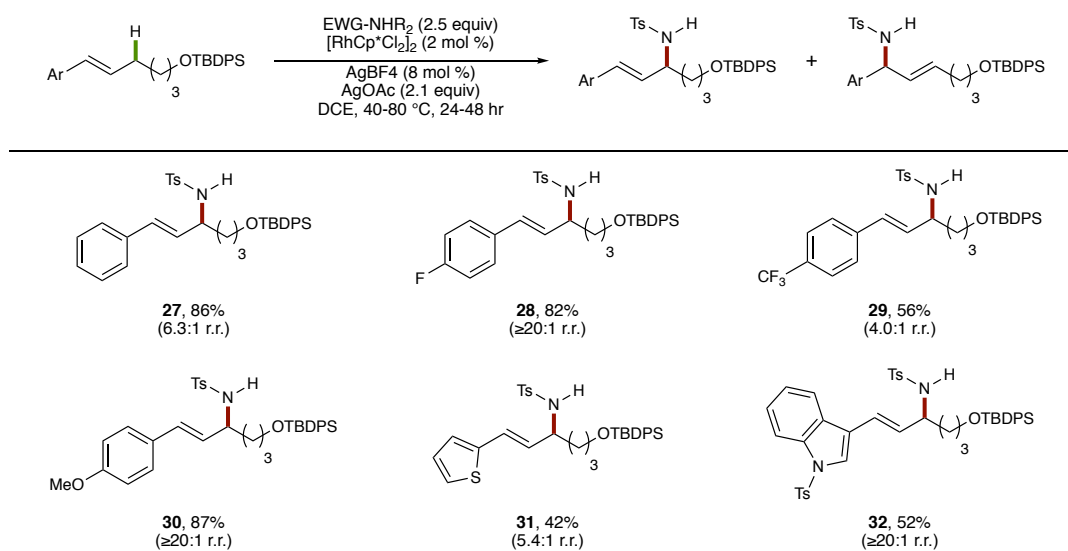


Figure 1-8. Allylic C–H amination selected examples from olefin scope.

After Jacob's initial disclosure of rhodium(III)-catalyzed allylic C–H amination, Taylor Nelson saw the opportunity to expand the methodology to include alcohols as nucleophiles (**Figure 1-9**).⁸⁶ Allylic alcohols are present as importation structural motifs in natural products and medically relevant molecules. Taylor observed primary (**33**, **34** and **36**), secondary (**35**) and tertiary (**37**) simple alcohols are efficient nucleophiles for the regioselective allylic C–H etherification of (*E*)-

tert-butyldiphenyl((6-phenylhex-5-en-1-yl)oxy)silane. Allylic ether **35** was produced in a 2.1:1.0 diastereomeric ratio from an enantiopure benzyl alcohol, which is the best selectivity observed but is not to synthetically useful levels. Alcohols with medically relevant functional groups, like aziridines, sugar derivatives and morpholines, afforded allylic ethers **39**, **40** and **41** in moderate to excellent yields, but allylic ethers **40** and **41** were observed with little to no diastereoselectivity. An alcohol nucleophile derived from serine provided allylic ether **42** in good yield but with low diastereoselectivity. The olefin substrate allowed for ortho functionality (**43-44**), amine functionality (**45**), and introduction of biologically relevant molecules (**46-47**) (Figure 1-10). This is the first example of intermolecular allylic C–H etherification of internal olefins and is tolerant of oxidatively sensitive alcohols.

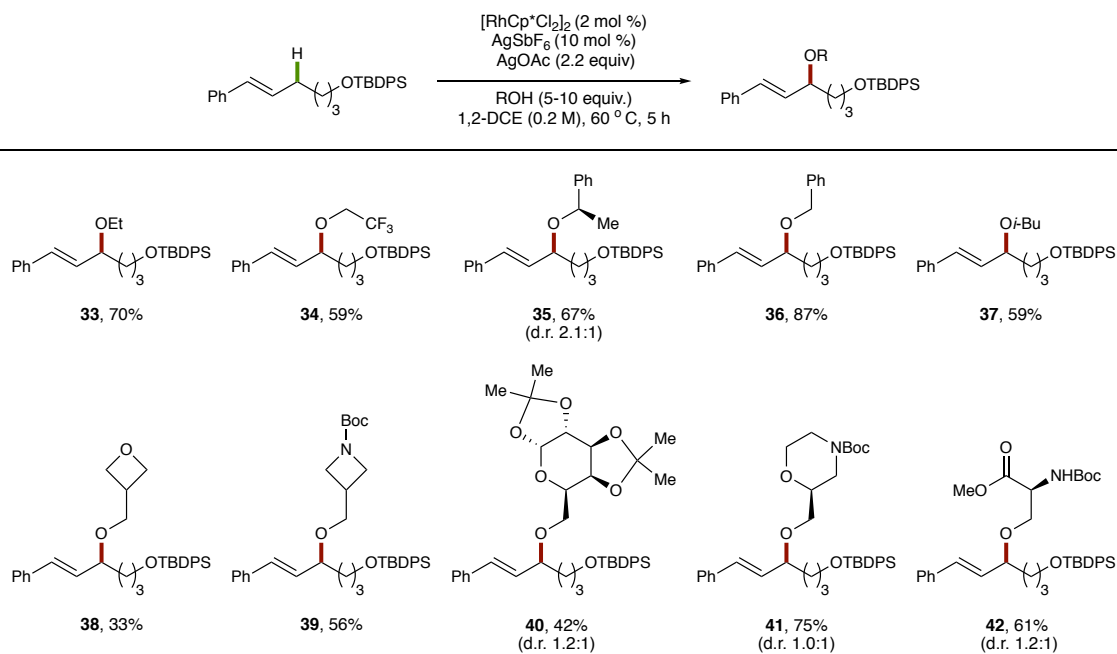


Figure 1-9. Allylic C–H etherification selected examples from alcohol nucleophile scope.

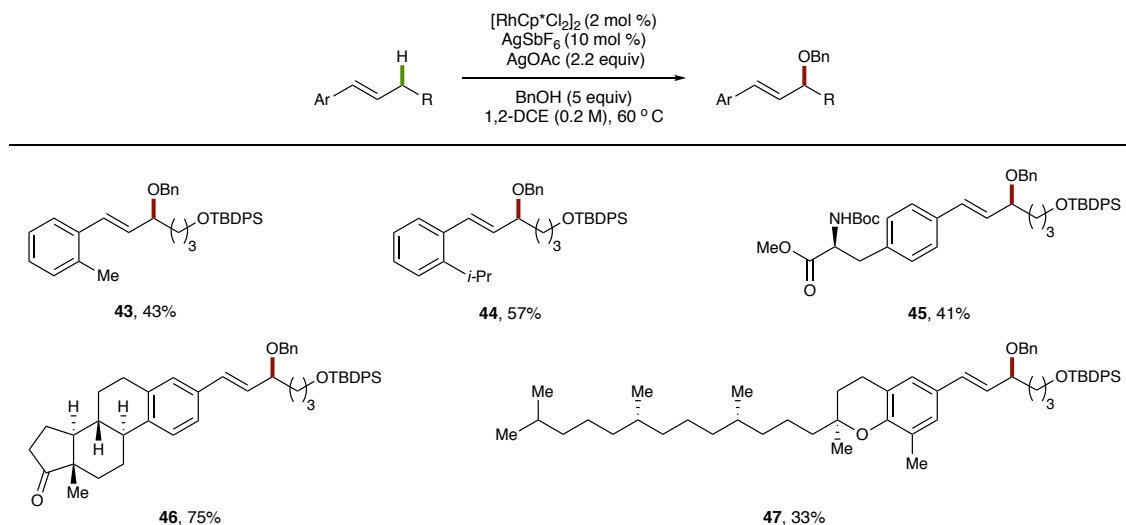


Figure 1-10. Allylic C–H etherification selected examples from olefin scope.

1.5 Conclusions

Our group has developed the regioselective allylic C–H amination and etherification of 1,2-disubstituted olefins. The discovery of rhodium(III) catalysts for allylic C–H functionalization expanded the previous palladium catalyzed allylic C–H amination beyond terminal olefins and doubly activated amine nucleophiles. Our methodology employed oxidatively sensitive alcohol nucleophiles for the formation of pharmaceutically relevant molecules. Despite what has been accomplished, investigation of the mechanism of rhodium(III)-catalyzed allylic C–H functionalization will provide information for further optimization and the potential development of an enantioselective allylic C–H functionalization.

1.6 References

- (1) Wright, T. B.; Evans, P. A. Enantioselective Rhodium-Catalyzed Allylic Alkylation of Prochiral Alpha,Alpha-Disubstituted Aldehyde Enolates for the Construction of Acyclic Quaternary Stereogenic Centers. *Journal of the American Chemical Society* **2016**, *138* (47), 15303–15306.
- (2) Evans, P. A.; Clizbe, E. A.; Lawler, M. J.; Oliver, S. Enantioselective Rhodium-Catalyzed Allylic Alkylation of Acyclic Alpha-Alkoxy Substituted Ketones Using a Chiral Monodentate Phosphite Ligand. *Chemical Science* **2012**, *3* (6), 1835–1838.
- (3) Turnbull, B. W. H.; Evans, P. A. Enantioselective Rhodium-Catalyzed Allylic Substitution with a Nitrile Anion: Construction of Acyclic Quaternary Carbon Stereogenic Centers. *Journal of the American Chemical Society* **2015**, *137* (19), 6156–6159.
- (4) Grange, R. L.; Clizbe, E. A.; Counsell, E. J.; Evans, P. A. Enantioselective Construction of C-Chiral Allylic Sulfilimines via the Iridium-Catalyzed Allylic Amination with S,S-Diphenylsulfilimine: Asymmetric Synthesis of Primary Allylic Amines. *Chemical Science* **2015**, *6* (1), 777–781.
- (5) Sundararaju, B.; Achard, M.; Bruneau, C. Transition Metal Catalyzed Nucleophilic Allylic Substitution: Activation of Allylic Alcohols via [Small Pi]-Allylic Species. *Chemical Society Reviews* **2012**, *41* (12), 4467–4483.
- (6) Trost, B. M. Designing a Receptor for Molecular Recognition in a Catalytic Synthetic Reaction: Allylic Alkylation. *Accounts of Chemical Research* **1996**, *29* (8), 355–364.
- (7) Tsuji, J. *Palladium Reagents and Catalysts: New Perspectives for the 21st Century*; John Wiley & Sons: Chichester, 2004.
- (8) Pouy, M. J.; Hartwig, J. F. INOR 157-Enantioselective Iridium-Catalyzed Allylic Amination with Ammonia and Ammonia Surrogates. *Abstracts of Papers of the American Chemical Society* **2007**, *233*, 268.
- (9) Evans, P. A.; Leahy, D. K. Regioselective and Enantiospecific Rhodium-Catalyzed Intermolecular Allylic Etherification with Ortho-Substituted Phenols. *Journal of the American Chemical Society* **2000**, *122* (20), 5012–5013.
- (10) Trost, B. M.; Crawley, M. L. Asymmetric Transition-Metal-Catalyzed Allylic Alkylations: Applications in Total Synthesis. *Chemical Reviews* **2003**, *103* (8), 2921–2944.
- (11) Tsuji, J.; Takahashi, H.; Morikawa, M. Organic Syntheses by Means of Noble Metal Compounds .17. Reaction of Pi-Allylpalladium Chloride with Nucleophiles. *Tetrahedron Letters* **1965**, No. 49, 4387.
- (12) Trost, B. M.; Strege, P. E. Asymmetric Induction in Catalytic Allylic Alkylation. *Journal of the American Chemical Society* **1977**, *99* (5), 1649–1651.
- (13) Nicolaou, K. C.; Bulger, P. G.; Sarlah, D. Palladium-Catalyzed Cross-Coupling Reactions in Total Synthesis. *Angewandte Chemie International Edition* **2005**, *44* (29), 4442–4489.
- (14) Turnbull B. W. H., Oliver S., Evans P. A. Stereospecific Rhodium-Catalyzed Allylic Substitution with Alkenyl Cyanohydrin Pronucleophiles: Construction of Acyclic Quaternary Substituted alpha,beta-Unsaturated Ketones. *Journal of the American Chemical Society* **2015**, *137* (49), 5374-5377.
- (15) Turnbull B. W. H., Evans P. A. Enantioselective Rhodium-Catalyzed Allylic Substitution with a Nitrile Anion: Construction of Acyclic Quaternary Carbon Stereogenic Centers. *Journal of the American Chemical Society* **2015**, *137* (19), 6156-6159.
- (16) Grange R. L., Clizbe E. A., Counsell E. J., Evans P. A. Enantioselective construction of C-chiral allylic sulfilimines via the iridium-catalyzed allylic amination with S,S-

- diphenylsulfilimine: asymmetric synthesis of primary allylic amines. *Chemical Science* **2015**, *6* (1), 777-781..
- (17) Grange R. L., Evans P. A. Metal-Free Metathesis Reaction of C-Chiral Allylic Sulfilimines with Aryl Isocyanates: Construction of Chiral Nonracemic Allylic Isocyanates. *Journal of the American Chemical Society* **2014**;136(34):11870-3.
 - (18) Evans P. A., Clizbe E. A., Lawler M. J., Oliver S. Enantioselective rhodium-catalyzed allylic alkylation of acyclic alpha-alkoxy substituted ketones using a chiral monodentate phosphite ligand. *Chemical Science* **2012**, *3* (6), 1835-1838.
 - (19) Evans P. A., Clizbe E. A. Unlocking Ylide Reactivity in the Metal-Catalyzed Allylic Substitution Reaction: Stereospecific Construction of Primary Allylic Amines with Aza-Ylides. *Journal of the American Chemical Society* **2009**, *131* (25), 8722.
 - (20) Evans P. A., Nelson J. D. Regioselective rhodium-catalyzed allylic alkylation with a modified Wilkinson's catalyst. *Tetrahedron Letters* **1998**, *39* (13),1725-1728.
 - (21) Evans P. A., Brandt T. A. Asymmetric palladium catalyzed allylic alkylation using vinylogous sulfonates. *Abstracts of Papers of the American Chemical Society* **1998**, *216*, U512-U.
 - (22) Evans P. A., Brandt T. A., Robinson J. E. Palladium-catalyzed rearrangement and substitution reactions of acyclic vinylogous carbonates and sulfonates: Development of a new leaving group for Pd-allyl chemistry. *Tetrahedron Letters* **1999**, *40* (16), 3105-3108.
 - (23) Jackowski O., Alexakis A. Copper-Free Asymmetric Allylic Alkylation with Grignard Reagents (vol 49, pg 3346, 2010). *Angewandte Chemie-International Edition* **2010**, *49* (30), 5026.
 - (24) Jackowski O., Alexakis A. Copper-Free Asymmetric Allylic Alkylation with Grignard Reagents. *Angewandte Chemie-International Edition* **2010**, *49* (19), 3346-3350.
 - (25) Langlois J. B., Alexakis A. Identification of a Valuable Kinetic Process in Copper-Catalyzed Asymmetric Allylic Alkylation. *Angewandte Chemie-International Edition* **2011**, *50* (8), 1877-1881.
 - (26) Langlois J. B., Emery D., Mareda J., Alexakis A. Mechanistic identification and improvement of a direct enantioconvergent transformation in copper-catalyzed asymmetric allylic alkylation. *Chemical Science* **2012**, *3* (4),1062-1069.
 - (27) Li H. L., Alexakis A. Enyne Chlorides: Substrates for Copper-Catalyzed Asymmetric Allylic Alkylation. *Angewandte Chemie-International Edition* **2012**, *51*(4), 1055-1058.
 - (28) Grassi D., Alexakis A. Copper-Free Asymmetric Allylic Alkylation of Trisubstituted Cyclic Allyl Bromides Using Grignard Reagents. *Angewandte Chemie-International Edition* **2013**, *52*(51), 13642-13646.
 - (29) Grassi D., Alexakis A. Transition metal-free asymmetric and diastereoselective allylic alkylation using Grignard reagents: construction of vicinal stereogenic centers via kinetic resolution. *Chemical Science* **2014**, *5*(10), 3803-7380.
 - (30) Alexakis A., Polet D. Very efficient phosphoramidite ligand for asymmetric iridium-catalyzed allylic alkylation. *Organic Letters* **2004**, *6*(20), 3529-3532.
 - (31) Tissot-Croset K., Polet D., Alexakis A. A highly effective phosphoramidite ligand for asymmetric allylic substitution. *Angewandte Chemie-International Edition* **2004**, *43*(18), 2426-2428.
 - (32) Falciola C. A., Tissot-Croset K., Alexakis A. beta-disubstituted allylic chlorides: Substrates for the Cu-catalyzed asymmetric S(N)2' reaction. *Angewandte Chemie-International Edition* **2006**, *45*(36), 5995-5998.
 - (33) Malda H., van Zijl A. W., Arnold L. A., Feringa B. L. Enantioselective copper-catalyzed allylic alkylation with dialkylzincs using phosphoramidite ligands. *Organic Letters* **2001**, *3*(8), 1169-1171.
 - (34) Lopez F., van Zijl A. W., Minnaard A. J., Feringa B. L. Highly enantioselective Cu-catalysed allylic substitutions with Grignard reagents. *Chemical Communications* **2006**, 409-411.

- (35) Mao B., Geurts K., Fananas-Mastral M., van Zijl A. W., Fletcher S. P., Minnaard A. J., Feringa B. L. Catalytic Enantioselective Synthesis of Naturally Occurring Butenolides via Hetero-Allylic Alkylation and Ring Closing Metathesis. *Organic Letters* **2011**, *13*(5), 948-951.
- (36) Perez M., Fananas-Mastral M., Bos P. H., Rudolph A., Harutyunyan S. R., Feringa B. L. Catalytic asymmetric carbon-carbon bond formation via allylic alkylations with organolithium compounds. *Nature Chemistry* **2011**, *3*(5), 377-381.
- (37) Teichert J. F., Fananas-Mastral M., Feringa B. L. Iridium-Catalyzed Asymmetric Intramolecular Allylic Amidation: Enantioselective Synthesis of Chiral Tetrahydroisoquinolines and Saturated Nitrogen Heterocycles. *Angewandte Chemie-International Edition* **2011**, *50*(3), 688-691.
- (38) Giannerini M., Fananas-Mastral M., Feringa B. L. Z-Selective Copper-Catalyzed Asymmetric Allylic Alkylation with Grignard Reagents. *Journal of the American Chemical Society* **2012**, *134*(9), 4108-4111.
- (39) Hornillos V., van Zijl A. W., Feringa B. L. Catalytic asymmetric synthesis of chromenes and tetrahydroquinolines via sequential allylic alkylation and intramolecular Heck coupling. *Chemical Communications* **2012**, *48*(31), 3712-3714.
- (40) Guduguntla S., Fananas-Mastral M., Feringa B. L. Synthesis of Optically Active beta- or gamma-Alkyl-Substituted Alcohols through Copper-Catalyzed Asymmetric Allylic Alkylation with Organolithium Reagents. *Journal of Organic Chemistry* **2013**, *78*(17), 8274-8280.
- (41) Hornillos V., Perez M., Fananas-Mastral M., Feringa B. L. Cu-Catalyzed Asymmetric Allylic Alkylation of Phosphonates and Phosphine Oxides with Grignard Reagents. *Chemistry-a European Journal* **2013**, *19*(17), 5432-5441.
- (42) Zhao D. P., Fananas-Mastral M., Chang M. C., Otten E., Feringa B. L. Asymmetric synthesis of N,O-heterocycles via enantioselective iridium-catalysed intramolecular allylic amidation. *Chemical Science* **2014**, *5*(11), 4216-4220.
- (43) Jiang X. Y., Chen W. Y., Hartwig J. F. Iridium-Catalyzed Diastereoselective and Enantioselective Allylic Substitutions with Acyclic -Alkoxy Ketones. *Angewandte Chemie-International Edition* **2016**, *55*(19), 5819-5823.
- (44) Chen M., Hartwig J. F. Iridium-Catalyzed Enantioselective Allylic Substitution of Enol Silanes from Vinylogous Esters and Amides. *Journal of the American Chemical Society* **2015**, *137*(43), 13972-13979.
- (45) Chen M., Hartwig J. F. Iridium-Catalyzed Regio- and Enantioselective Allylic Substitution of Silyl Dienolates Derived from Dioxinones. *Angewandte Chemie-International Edition* **2014**, *53*(45), 12172-12176.
- (46) Ueda M., Hartwig J. F. Iridium-Catalyzed, Regio- and Enantioselective Allylic Substitution with Aromatic and Aliphatic Sulfinates. *Organic Letters* **2010**, *12*(1), 92-94.
- (47) Stanley L. M., Bai C., Ueda M., Hartwig J. F. Iridium-Catalyzed Kinetic Asymmetric Transformations of Racemic Allylic Benzoates. *Journal of the American Chemical Society* **2010**, *132*(26), 8918.
- (48) Yamashita Y., Gopalarathnam A., Hartwig J. F. Iridium-catalyzed, asymmetric amination of allylic alcohols activated by Lewis acids. *Journal of the American Chemical Society* **2007**, *129*(24), 7508.
- (49) Ohmura T., Hartwig J. F. Regio- and enantioselective allylic amination of achiral allylic esters catalyzed by an iridium-phosphoramidite complex. *Journal of the American Chemical Society* **2002**, *124*(51), 15164-15165.
- (50) Hamilton J. Y., Sarlah D., Carreira E. M. Iridium-Catalyzed Enantioselective Allylic Alkylation with Functionalized Organozinc Bromides. *Angewandte Chemie-International Edition* **2015**, *54*(26), 7644-7647.

- (51) Roggen M., Carreira E. M. Enantioselective Allylic Thioetherification: The Effect of Phosphoric Acid Diester on Iridium-Catalyzed Enantioconvergent Transformations. *Angewandte Chemie-International Edition* **2012**, *51*(34), 8652-8655.
- (52) Roggen M., Carreira E. M. Enantioselective Allylic Etherification: Selective Coupling of Two Unactivated Alcohols. *Angewandte Chemie-International Edition* **2011**, *50*(24), 5568-55671.
- (53) Defieber C., Ariger M. A., Moriel P., Carreira E. M. Iridium-catalyzed synthesis of primary allylic amines from allylic alcohols: Sulfamic acid as amonia equivalent. *Angewandte Chemie-International Edition* **2007**, *46*(17), 3139-3143.
- (54) Sandmeier T., Krautwald S., Zipfel H. F., Carreira E. M. Stereodivergent Dual Catalytic alpha-Allylation of Protected alpha-Amino- and alpha-Hydroxyacetaldehydes. *Angewandte Chemie-International Edition* **2015**, *54*(48), 14363-14367.
- (55) Breitler S., Carreira E. M. Formaldehyde N,N-Dialkylhydrazones as Neutral Formyl Anion Equivalents in Iridium-Catalyzed Asymmetric Allylic Substitution. *Journal of the American Chemical Society* **2015**, *137*(16), 5296-5299.
- (56) Krautwald S., Schafroth M. A., Sarlah D., Carreira E. M. Stereodivergent alpha-Allylation of Linear Aldehydes with Dual Iridium and Amine Catalysis. *Journal of the American Chemical Society* **2014**, *136*(8), 3020-3023.
- (57) Krautwald S., Sarlah D., Schafroth M. A., Carreira E. M. Enantio- and Di Aereodivergent Dual Catalysis: alpha-Allylation of Branched Aldehydes. *Science* **2013**, *340*(6136), 1065-1068.
- (58) Lafrance M., Roggen M., Carreira E. M. Direct, Enantioselective Iridium-Catalyzed Allylic Amination of Racemic Allylic Alcohols. *Angewandte Chemie-International Edition* **2012**, *51*(14), 3470-3473.
- (59) Roggen M., Carreira E. M. Stereospecific Substitution of Allylic Alcohols To Give Optically Active Primary Allylic Amines: Unique Reactivity of a (P,alkene)Ir Complex Modulated by Iodide. *Journal of the American Chemical Society* **2010**, *132*(34), 11917-11919.
- (60) Becker N., Carreira E. M. Hydroxyl-directed nitrile oxide cycloaddition reactions with cyclic allylic alcohols. *Organic Letters* **2007**, *9*(19), 3857-3858.
- (61) Lyothier I., Defieber C., Carreira E. M. Iridium-catalyzed enantioselective synthesis of allylic alcohols: Silanolates as hydroxide equivalents. *Angewandte Chemie-International Edition* **2006**, *45*(37), 6204-6207.
- (62) Gaich, T.; Baran, P. S. "Aiming for the Ideal Synthesis". *The Journal of Organic Chemistry* **2010**, *75* (14), 4657-4673.
- (63) Chen, M. S.; White, M. C. A "Sulfoxide-Promoted, Catalytic Method for the Regioselective Synthesis of Allylic Acetates from Monosubstituted Olefins via C-H Oxidation." *Journal of the American Chemical Society* **2004**, *126* (5), 1346-1347.
- (64) Delcamp, J. H.; White, M. C. Sequential Hydrocarbon Functionalization: Allylic C-H Oxidation/Vinylic C-H Arylation. *Journal of the American Chemical Society* **2006**, *128* (47), 15076-15077.
- (65) Pattillo, C. C.; Strambeanu II; Calleja, P.; Vermeulen, N. A.; Mizuno, T.; White, M. C. Aerobic Linear Allylic C-H Amination: Overcoming Benzoquinone Inhibition. *Journal of the American Chemical Society* **2016**, *138* (4), 1265-1272.
- (66) Strambeanu II; White, M. C. Catalyst-Controlled C-O versus C-N Allylic Functionalization of Terminal Olefins. *Journal of the American Chemical Society* **2013**, *135* (32), 12032-12037.
- (67) Young, A. J.; White, M. C. Allylic C-H Alkylation of Unactivated Alpha-Olefins: Serial Ligand Catalysis Resumed. *Angewandte Chemie-International Edition* **2011**, *50* (30), 6824-6827.
- (68) Chen, M. S.; Prabakaran, N.; Labenz, N. A.; White, M. C. Serial Ligand Catalysis: A Highly Selective Allylic C-H Oxidation. *Journal of the American Chemical Society* **2005**, *127* (19), 6970-6971.

- (69) Young, A. J.; White, M. C. Allylic C-H Alkylation of Unactivated Alpha-Olefins: Serial Ligand Catalysis Resumed. *Angewandte Chemie-International Edition* **2011**, *50* (30), 6824–6827.
- (70) Reed, S. A.; Mazzotti, A. R.; White, M. C. A Catalytic, Bronsted Base Strategy for Intermolecular Allylic C-H Amination. *Journal of the American Chemical Society* **2009**, *131* (33), 11701–11706.
- (71) Vermeulen, N. A.; Delcamp, J. H.; White, M. C. Synthesis of Complex Allylic Esters via C-H Oxidation vs C-C Bond Formation. *Journal of the American Chemical Society* **2010**, *132* (32), 11323–11328.
- (72) Covell, D. J.; White, M. C. A Chiral Lewis Acid Strategy for Enantioselective Allylic C-H Oxidation. *Angewandte Chemie-International Edition* **2008**, *47* (34), 6448–6451.
- (73) Ammann, S. E.; Rice, G. T.; White, M. C. Terminal Olefins to Chromans, Isochromans, and Pyrans via Allylic C-H Oxidation. *Journal of the American Chemical Society* **2014**, *136* (31), 10834–10837.
- (74) Rice, G. T.; White, M. C. Allylic C-H Amination for the Preparation of Syn-1,3-Amino Alcohol Motifs. *Journal of the American Chemical Society* **2009**, *131* (33), 11707–11711.
- (75) Reed, S. A.; White, M. C. Catalytic Intermolecular Linear Allylic C-H Amination via Heterobimetallic Catalysis. *Journal of the American Chemical Society* **2008**, *130* (11), 3316.
- (76) Strambeanu, I. I.; White, M. C. Catalyst-Controlled C-O versus C-N Allylic Functionalization of Terminal Olefins. *Journal of the American Chemical Society* **2013**, *135* (32), 12032–12037.
- (77) Campbell, A. N.; White, P. B.; Guzei, I. A.; Stahl, S. S. Allylic C-H Acetoxylation with a 4,5-Diazafluorenone-Ligated Palladium Catalyst: A Ligand-Based Strategy To Achieve Aerobic Catalytic Turnover. *Journal of the American Chemical Society* **2010**, *132* (43), 15116–15119.
- (78) Fernandes, R. A.; Nallasivam, J. L. Catalytic allylic functionalization via π -allyl palladium chemistry. *Organic and Biomolecular Chemistry* **2019**, *17*, 8647–8672.
- (79) Kondo, H.; Yu, F.; Yamaguchi, J.; Liu, G.; Itami, K. Branch-Selective Allylic C–H Carboxylation of Terminal Alkenes by Pd/sox Catalyst. *Organic Letters* **2014**, *16*, 4212–4215.
- (80) Chen, M. S.; White, M. C. A Sulfoxide-Promoted, Catalytic Method for the Regioselective Synthesis of Allylic Acetates from Monosubstituted Olefins via C-H Oxidation. *Journal of the American Chemical Society* **2004**, *126* (5), 1346–1347.
- (81) Campbell, A. N.; White, P. B.; Guzei, I. A.; Stahl, S. S. Allylic C-H Acetoxylation with a 4,5-Diazafluorenone-Ligated Palladium Catalyst: A Ligand-Based Strategy To Achieve Aerobic Catalytic Turnover. *Journal of the American Chemical Society* **2010**, *132* (43), 15116–15119.
- (82) Archambeau, A.; Rovis, T. Rhodium(III)-Catalyzed Allylic C(Sp³)-H Activation of Alkenyl Sulfonamides: Unexpected Formation of Azabicycles. *Angewandte Chemie-International Edition* **2015**, *54* (45), 13337–13340.
- (83) Cochet, T.; Bellosta, V.; Roche, D.; Ortholand, J. Y.; Greiner, A.; Cossy, J. Rhodium(III)-Catalyzed Allylic C-H Bond Amination. Synthesis of Cyclic Amines from Omega-Unsaturated N-Sulfonylamines. *Chemical Communications* **2012**, *48* (87), 10745–10747.
- (84) Isolation of π -Allyl Complexes from Aliphatic Alkenes and an Electron-Deficient Rh(III) Complex: Key Intermediates of Allylic C–H Functionalization. *Organometallics* **2016**, *35* (10), 1547–1552.
- (85) Takahama, Y.; Shibata, Y.; Tanaka, K. Oxidative Olefination of Anilides with Unactivated Alkenes Catalyzed by an (Electron-Deficient η^5 -Cyclopentadienyl)Rhodium(III) Complex Under Ambient Conditions. *Chemistry A European Journal* **2015**, *21*, 9053–9056.
- (86) Burman, J. S.; Blakey, S. B. Regioselective Intermolecular Allylic C–H Amination of Disubstituted Olefins via Rhodium/ π -Allyl Intermediates. *Angewandte Chemie International Edition* **2017**, *56* (44), 13666–13669.

- (87) Nelson, T. A. F.; Blakey, S. B. Intermolecular Allylic C–H Etherification of Internal Olefins. *Angewandte Chemie International Edition* **2018**, *57* (45), 14911–14915.

Chapter 2. Development and progress towards the regioselective allylic C–H arylation of 1,2-disubstituted allyl benzene derivatives.

2.1 Introduction to allylic C–H arylation

Indoles are a key structural motif in various molecules with application in materials chemistry, pharmaceuticals, natural products synthesis and agrochemicals.^{1,2} One of the indole scaffolds considered a “privileged scaffold” is the tryptophan derivatives or molecules that contain a tryptamine moiety.³ Specifically, polycyclic indolyl scaffolds are structural motif found in naturally occurring compounds, such as tetrahydro- β -carboline (THBCs).⁴ A simple tetrahydrocarboline used as a drug candidate is Lycoprodine, which binds to the parathyroid calcium-sensing receptor extracellular domain hinge region.⁵ It acts as a calcimimetic which functions as a calcium-sensing receptor agonist. Synthesizing a privileged ligand scaffold like tetrahydro- β -carboline (THBCs) in an efficient, convergent sequence of steps would provide access to drug candidates and conduct structure-activity relationship (SAR) studies.⁵

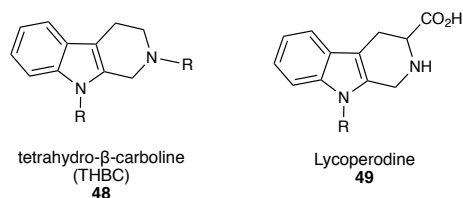


Figure 2-1. Structure of tetrahydro- β -carboline (THBC) scaffold and a THBC drug candidate, Lycoprodine.

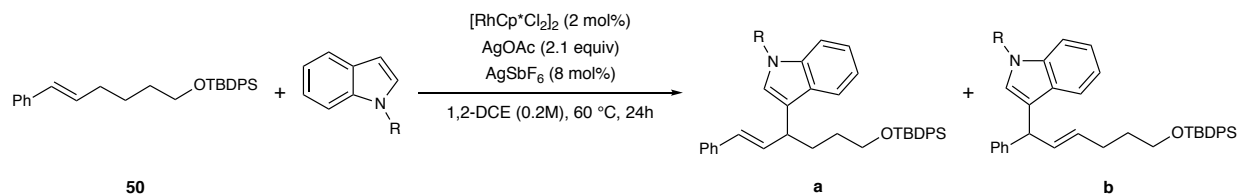
Our previous discovery that rhodium(III) Cp* allows for allylic C–H amination and etherification of 1,2-disubstituted olefins provided the foundation for the development of an allylic C–H functionalization with a carbon nucleophile. One of the nucleophiles utilized in our allylic C–H

functionalization was indole derivatives. We could provide access to structures like Lycoperodine via regioselective intramolecular allylic C–H arylation of terminal olefins.

2.2 Reaction discovery: allylic C–H arylation

Our initial investigation utilized indole and indole derivatives and unsymmetrical di-substituted olefin **50** with $[\text{RhCp}^*\text{Cl}_2]_2$ as the precatalyst, AgSbF_6 as a halide scavenger, and AgOAc as the oxidant and carboxylate source for the proposed concerted-metalation-deprotonation (CMD) mechanism. These conditions are adopted from the optimized reaction conditions developed for the rhodium(III) Cp^* catalyzed allylic C–H amination and etherification (Table 2-1). In the case our allylic C–H amination and etherification, modest to excellent regioselectivities for the conjugated isomer are observed in all cases.⁷ We hypothesized that indole nucleophiles would proceed through a mechanism similar to amine and alcohol nucleophiles, thus providing high regioselectivities for the conjugated isomer.

Table 2-1. Exploration of N-protected indoles as nucleophiles.



Entry	R	% yield ^a	a : b	% RSM[50]
1	H	0% ^b	N/A	83%
2	Me	43%	1.3 : 1.0	42%
3	Bn	61%	1.0 : 1.0	23%
4	TIPS	12%	2.0 : 1.0	60%
5	Ph	81%	1.3 : 1.0	12%
6	Boc	60%	19 : 1.0	3%
7	Cbz	65%	>20 : 1.0	0%
8	Ts	60%	>20 : 1.0	15%

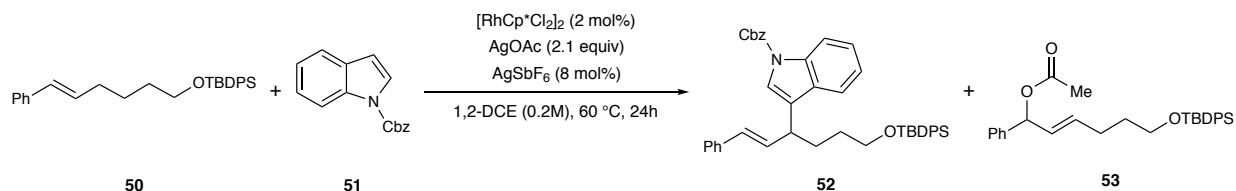
^aYields determined using 1,4-dinitrobenzene as an internal standard

Our initial investigation began with unprotected indole and unsymmetrical di-substituted olefin **50**, which did not afford a productive reaction (**Table 2-1, entry 1**). We hypothesize that the unprotected nitrogen can bind to the rhodium(III) catalyst leading to catalyst arrest, this is supported by the 83% recovery of olefin **50**. A catalyst arrest mechanism is not the only explanation for high olefin recovery, the unprotected indole could also be oxidized by silver which would leave the olefin unreacted. In order to prevent indole binding, we decided to block the indole nitrogen with a methyl group. The choice of a methyl group was twofold; firstly, the methyl is an electron donating group which increases the nucleophilicity of the 3-position of the indole and secondly, the methyl group should be highly stable to the acidic and oxidizing reaction conditions. The reaction of 1-methyl indole and olefin **50** proceeded with moderate efficiency (43% yield) and good mass balance (42% RSM) (**Table 2-1, entry 2**). We observed products **Me-a** and **Me-b** in a 1.3:1.0 regiomic ratio.

We were unable to separate regioisomers **Me-a** and **Me-b**, so we replaced the terminal silyl group for an acetate. We hypothesized that the ester functionality would provide enough polarity to achieve some separation between the two regioisomers. In fact, the acetate group did allow us to separate the two regioisomers (**Me-a-OAc** and **Me-b-OAc**) and identify the structure using chemical shift and splitting patterns. The conjugated isomer (**Me-a-OAc**) had the indicative doublet and double-doublet in the 6.25-6.60 ppm region which strongly suggests a styrenyl olefin. The non-conjugated or benzylic isomer (**Me-b-OAc**) displayed a double-doublet and double-triplet which accompanies the presence of a 1,2-disubstituted olefin which is not in conjugation with an aromatic ring. We also assigned the products structures by analogy to Simon Meek and co-workers similar indole products.⁶ Next, we used the nuclear overhauser effect (NOE) to determine whether the 2- or 3-position of the indole had undergone nucleophilic attack (in Supplemental Information). When we irradiated the methyl group on the nitrogen of the product molecule, we observed a correlation to a proton in the correct region for the 2-position of the indole moiety. We detected this

correlation for both of the regioisomers. This data strongly suggest the presence of isomers **Me-a-OAc** and **Me-b-OAc** and we then assigned the structure of all indole products by analogy.

In order to probe the origin of regioselectivity, or lack thereof, we explored a variety of substituents on the indole nitrogen in order to observe their effects on regioselectivity and conversion. Initially, we explored a small subset of electron donating substituents on the indole nitrogen. The allylic C–H arylation of olefin **50** with 1-benzyl-1*H*-indole afforded good yield (61% yield), however the reaction was not regioselective (1.0:1.0 r.r., **Bn-a:Bn-b**) (**Table 2-1, entry 3**). An indole bearing a TIPS protecting group offered a 2.0:1.0 regiomeric ratio, favoring conjugated isomer **TIPS-a** (**Table 2-1, entry 4**). We speculate the electronics of the indole did not cause the shift in regioselectivity, and instead that the sterics of the TIPS group slightly disfavored the formation of non-conjugated isomer **TIPS-b**. Next, we explored a weakly inductively electron-withdrawing group on the nitrogen, 1-phenyl-1*H*-indole which provided an excellent yield (81% yield) with no significant selectivity for either regioisomer (1.3:1.0 r.r., **Ph-a:Ph-b**, **Table 2-1, entry 5**). In contrast to the electron donating nitrogen substituents, we explored a small selection of electron withdrawing groups on the indole nitrogen. The reaction with *tert*-butyl 1*H*-indole-1-carboxylate proceeded in good yield (60% yield) and regioselectivity. We observed that the ratio of products shifted to greatly favor the conjugated isomer **Boc-a** (19:1.0 r.r.) (**Table 2-1, entry 6**). Other indoles bearing electron withdrawing substituents such as benzyl-1*H*-indole-1-carboxylate and (*E*)-*tert*-butyldiphenyl((6-phenylhex-5-en-1-yl)oxy)silane proceeded efficiently in 65% yield and 60% yield, respectively, with selectivity for exclusively conjugated isomer **Cbz-a** and **Ts-a** (>20:1.0 r.r.) (**Table 2-1, entries 7-8**). All of the indole derivatives afforded high yields of the products or displayed good mass balance.

Table 2-2. Reaction optimization for regioselective *N*-Cbz indole addition.

Entry	temp (°C)	oxidant	time (h)	equiv 51	solvent	% yield 52 ^a	52 : 53	% RSM[50]
1	60	AgOAc	24	4	DCE	65%	>20 : 1.0	0% ^b
2	60	AgOAc	24	2	DCE	53%	>20 : 1.0	0% ^b
3	40	AgOAc	24	4	DCE	60%	>20 : 1.0	0% ^b
4	40	AgOAc	24	2	DCE	74%	>20 : 1.0	0% ^b
5	25	AgOAc	24	2	DCE	46%	5.0 : 1.0	7%
6	25	AgOAc	24	1.5	DCE	34%	12 : 1.0	17%
7	25	AgOAc	48	2	DCE	43%	4.0 : 1.0	14%
8	40	Ag ₃ PO ₄	48	2	DCE	6%	>20 : 1.0	58%
9	40	AgOAc	24	2	Dioxane	0%	0.0 : 0.0	79%
10	40	AgOAc	24	2	THF	13% ^c	4.3 : 1.0	53%
11	40	AgOAc	24	2	Toluene	0%	0.0 : 0.0	95%

^aYields determined by integration of products in crude ¹H NMR against 1,4-dinitrobenzene as an internal standard. ^bNot observed by in crude ¹H NMR. ^c 7% of benzylic regioisomer of **52** was observed.

After exploring the effects of indole electronics on regioselectivity, we decided to pursue the development of a regioselective allylic C–H arylation with benzyl-1*H*-indole-1-carboxylate. We chose this nucleophile because it provided the best combination of regioselectivity and yield of all of the indole derivatives explored. In the previously developed allylic C–H amination and etherification, Jacob and Taylor observed allylic acetate **53** as common side product. We chose to track the recovery of **50** and the ratio of desired product **52** to allylic acetate **53**, as we optimized the reaction conditions for intermolecular allylic C–H arylation with *N*-Cbz indole. Under initial reaction conditions, adapted from the allylic C–H amination and etherification, we observed a 65% yield of **52** with no evidence of allylic acetate **53** or recovered **50** (Table 2-2, entry 1). Halving the equivalences of nucleophile at 60 °C decreased the efficiency of the reaction for **52** (53% yield) (Table 2-2, entry 2). While reducing the temperature to 40 °C with 4 equivalents of indole **51** did not improve the yield (60% yield), a combination of 40 °C and 2 equivalents of indole **51** afforded **52**

in 74% yield (**Table 2-2, entries 3-4**). As we changed temperature and equivalents of **51**, we observed high selectivity for **52** over allylic acetate **53** (**Table 2-2, entry 1-4**). Lowering the temperature to 25 °C did not increase the efficiency of the reaction (46% yield), nor did reducing the equivalents of **51** (34% yield) (**Table 2-2, entries 5-6**). When the temperature was decreased to 25 °C, we saw allylic acetate **53** emerge as a side product. Extending the reaction time to 48 hours at 25 °C with 2 equivalents **51** provided no improvement to the yield of **52** (43% yield) (**Table 2-2, entry 7**). The yield of **52** dropped to 6% yield when silver acetate was exchanged with silver phosphate, but crude proton NMR showed that 58% of **50** was left unreacted (**Table 2-2, entry 8**). A small solvent screen of organic solvents, commonly used in the C–H functionalization literature, performed with decreased efficiency compared to 1,2-dichloroethane (1,2-DCE) (**Table 2-2, entries 9-11**). After investigating a variety of reaction conditions, we found 40 °C for 24 hours in 1,2-DCE provided the optimal reaction conditions for regioselective allylic C–H arylation with benzyl-1*H*-indole-1-carboxylate (**52**) (**Table 2-2, entry 4**).

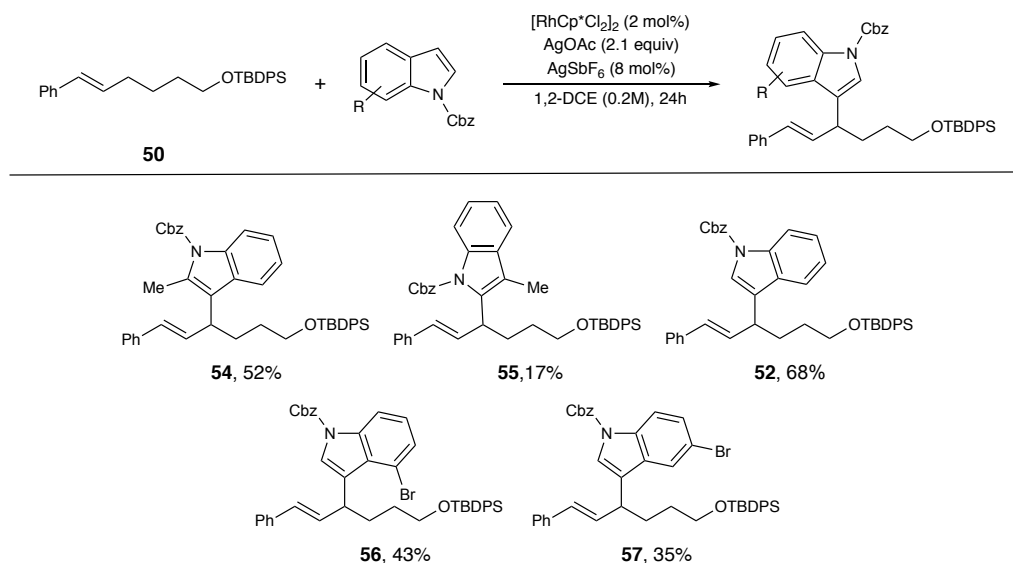


Figure 2-2. Effects of *N*-Cbz indole substitution on allylic C–H arylation.

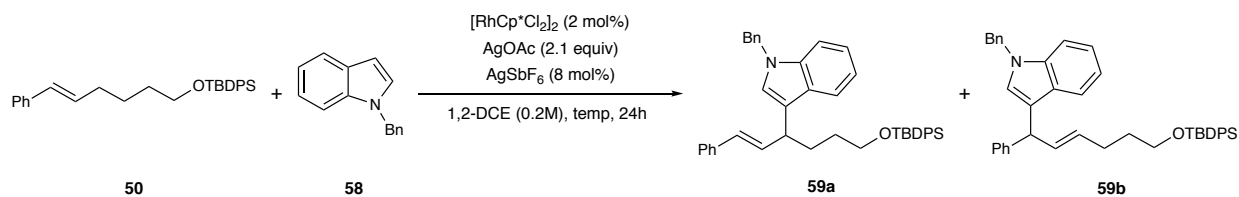
After establishing conditions for efficient regioselective allylic C–H arylation, we sought to explore functional group tolerance with a small set of substituted *N*-Cbz protected indoles (**Figure 2-2**). Addition of a methyl group at the 2-position of *N*-Cbz indole afforded olefin product **54** in good yield (52% yield), which suggests that increasing steric bulk adjacent to the nucleophilic carbon did not impede product formation. Blocking the nucleophilic 3-position with a methyl group led to the formation of olefin product **55**, where the 2-position of *N*-Cbz indole acts as the nucleophilic carbon. While we did observe a reduction in reaction efficiency with benzyl 4-bromo-1*H*-indole-1-carboxylate and benzyl 5-bromo-1*H*-indole-1-carboxylate (**56**, 43% yield and **57**, 35% yield), the reaction did tolerate the presence of the functional group. These substrates were important to the scope of the reaction because the bromine could be used a synthetic handle to introduce molecular complexity via cross-couplings like the Suzuki reaction. After a short exploration of the regioselective allylic C–H arylation, which favors the conjugated olefin isomer, we sought to discover conditions to provide complementary regioselectivity.

2.3 Reaction discovery: benzylic site selective allylic C–H arylation

Our initial investigation focused on optimization for the conjugated olefin regioisomer of allylic C–H arylation with an indole nucleophile bearing an electron-withdrawing nitrogen substituent, we hypothesize that use of an indole nucleophile bearing an electron-donating substituent would provide the platform for development of a benzylic selective allylic C–H arylation. We initiated our investigation by screening reaction temperature and nucleophile equivalents utilizing 1-benzyl-1*H*-indole (**58**) and unsymmetrical di-substituted olefin **50**, which provided a completely unselective reaction in the initial nucleophile examination (**Table 2-3, entry 1**). Since benzyl-1*H*-indole (**58**) afforded the only unselective reaction, we hypothesized that this reaction

allowed the best opportunity for discovering reaction conditions for a benzylic site-selective allylic C–H arylation. At 60 °C with 2 equivalents of nucleophile, we observed the reaction yield decrease by 6% which is contrary to the trend seen for *N*-Cbz indole (**Table 2-3, entry 2**). Further reducing the temperature to 40 °C, lead to a drastic decline in efficiency (10% yield) (**Table 2-3, entry 3**). None of the temperature or nucleophile equivalent variations provided a more efficient reaction than the original conditions.

Table 2-3. *N*-Bn Indole Addition: Temperature and Nucleophile Concentration Effects



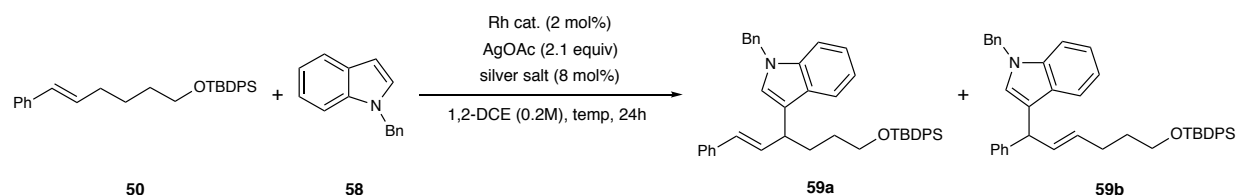
entry	58 (equiv)	temp (°C)	% yield ^a	59a : 59b	%RSM [50]
1	4	60	61%	1.0 : 1.0	23%
2	2	60	55%	1.0 : 1.0	22%
3	2	40	10%	1.0 : 1.0	46%

^aYields determined by integration of products in crude ¹H NMR against 1,4-dinitrobenzene as an internal standard.

We continued the reaction optimization with the best conditions found while varying temperature and equivalents of **58** (**Table 2-4, entry 1**). Tanaka and co-workers utilized electron-deficient rhodium(III) catalyst, $[\text{RhCp}^{\text{E}}\text{Cl}_2]_2$, to isolate and characterize π -allyl complexes from aliphatic alkenes.¹⁴ While the bulk of the investigation was focused on isolating π -allyl intermediates and the reactions of the stoichiometric π -allyl complexes, the authors did show that $[\text{RhCp}^{\text{E}}\text{Cl}_2]_2$ catalyzes an intramolecular allylic C–H amination. Based on the observed catalytic activity, we investigated $[\text{RhCp}^{\text{E}}\text{Cl}_2]_2$ as a catalyst for site-selective *N*-Bn indole (**58**) addition. We hypothesized that the electron deficient rhodium(III) would shift the regioselectivity but could not speculate which regioisomer would be favored because we did not know the mechanism of the reaction. Under optimized reaction conditions from **Table 2-3**, $[\text{RhCp}^{\text{E}}\text{Cl}_2]_2$ did not afford any

product at 60 °C (**Table 2-4, entry 2**) or 80 °C (**Table 2-4, entry 3**). Screening a small set of halide scavenger silver salts reduced the yield (**Table 2-4, entry 4-5**) and provided no significant change in regioselectivity (1.0:1.2 r.r.). We explored tetrahydrofuran (THF) as a solvent but yield and regioselectivity were not improved (**Table 2-4, entry 6**). Diluting the reaction to 0.05 M, reduced the yield (23% yield) and did not provide a significant shift in regioselectivity (**Table 2-4, entry 7**). Changing the silver halide scavenger, diluting the reaction concentration, and utilizing an electron deficient rhodium(III) catalyst did not provide optimal reaction conditions for site-selective benzylic *N*-Bn indole addition.

Table 2-4. Condition screening for benzylic site-selective *N*-Bn indole addition.



entry	Rh cat.	concentration (M)	silver salt	% yield ^a	59a : 59b
1	[RhCp*Cl ₂] ₂	0.2 M	AgSbF ₆	61%	1.0 : 1.0
2	[RhCp ^F Cl ₂] ₂	0.2 M	AgSbF ₆	0%	N/A
3 ^b	[RhCp ^F Cl ₂] ₂	0.2 M	AgSbF ₆	0%	N/A
4	[RhCp*Cl ₂] ₂	0.2 M	AgBF ₄	40%	1.0 : 1.2
5	[RhCp*Cl ₂] ₂	0.2 M	AgOTf	48%	1.0 : 1.2
6 ^c	[RhCp*Cl ₂] ₂	0.2 M	AgSbF ₆	36%	1.0 : 1.1
7	[RhCp*Cl ₂] ₂	0.05 M	AgSbF ₆	23%	1.0 : 1.3

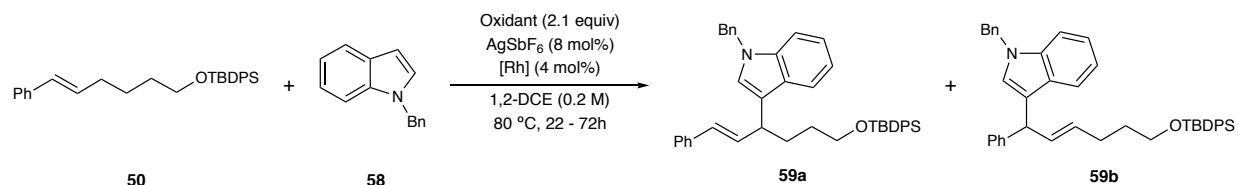
^aYields determined by integration of products in crude ¹H NMR against 1,4-dinitrobenzene as an internal standard. ^bReaction was ran at 80 °C.

^cReaction was ran in THF as solvent.

Next, we explored how rhodium(III) Cp* source and oxidant effected reaction efficiency and the distribution of product regioisomers (**Table 2-5**). When investigating oxidants, we hypothesized that it is necessary to use an oxidant with a carboxylate present or add an external carboxylate source for the C–H activation step via concerted metalation deprotonation (CMD) mechanism. We determined reaction efficiency by the conversion of starting material **50** to products

59a and **59b** observed in the crude proton NMR. The reaction of 1-benzyl-1*H*-indole (**57**) and olefin **50** with $[\text{RhCp}^*\text{Cl}_2]_2$ and copper oxidants, CuOAc and $\text{Cu}(\text{2-ethylhexanoate})_2$, favored reactants over products by 10 fold (**Table 2-5, entries 2-3**). While the reaction with $\text{Cu}(\text{2-ethylhexanoate})_2$ had low conversion, we observed a shift to favor benzylic regioisomer **59b** in a 1.0:3.6 regiomic ratio (**Table 2-5, entry 3**). The use of an organic oxidant, benzoyl peroxide ($(\text{BzO}_2)_2$), afforded similar conversion to AgOAc but favored conjugated isomer **59a** in a 5.0:1.0 regiomic ratio. Switching to a monomeric rhodium(III) catalyst allowed for the selective introduction of oxidant without the added complication of the presence of AgSbF_6 in the reaction. We observed that in the presence of AgOAc as the oxidant, $\text{RhCp}^*(\text{CH}_3\text{CN})_3(\text{SbF}_6)_2$ afforded lower conversion and no improvement in regioselectivity compared to $[\text{RhCp}^*\text{Cl}_2]_2$ (**Table 2-5, entry 5**). In the case of $\text{Cu}(\text{OAc})_2$, we observed no reaction (**Table 2-5, entry 6**). This is likely due to the lower conversion of the monomer coupled with $\text{Cu}(\text{OAc})_2$ acting as a less efficient oxidant. Copper ethylhexanoate ($\text{Cu}(\text{2-ethylhexanoate})_2$) and $\text{RhCp}^*(\text{CH}_3\text{CN})_3(\text{SbF}_6)_2$ did provide enhanced conversion compared to $[\text{RhCp}^*\text{Cl}_2]_2$ and $\text{Cu}(\text{2-ethylhexanoate})_2$ but the reaction was unselective at 2.1 equivalents and 4.2 equivalents of oxidant (**Table 2-5, entries 7-8**). With $(\text{BzO}_2)_2$ and $\text{RhCp}^*(\text{CH}_3\text{CN})_3(\text{SbF}_6)_2$, the product distribution favored conjugated isomer **59a**. The use of $\text{RhCp}^*(\text{OAc})_2$ did not provide a selective reaction with AgOAc or $\text{Cu}(\text{2-ethylhexanoate})_2$ (**Table 2-5, entries 10-11**). The more electron-deficient rhodium(III) heptamethylindenyl catalyst, $[\text{RhInd}^*\text{Cl}_2]_2$, was less efficient than the Cp^* variant, yet we observed a 1.0:2.0 regiomic ratio in favor of benzylic isomer **59b** (**Table 2-5, entry 12**). Lastly, iridium(III) Cp^* dimer, $[\text{IrCp}^*\text{Cl}_2]_2$, proceeded at lower efficiency and favored conjugated isomer **59a** in a 2.4:1.0 regiomic ratio (**Table 2-5, entry 13**).

Table 2-5. Condition Screening for Regioselective N-Bn Indole Addition



entry	Rh source	Oxidant	RSM[50] : 59a & 59b ^a	59a : 59b ^a
1	[RhCp*Cl ₂] ₂	AgOAc	1.0 : 3.0	1.0 : 1.3
2	[RhCp*Cl ₂] ₂	Cu(OAc) ₂	1.0 : 0.18	1.0 : 1.1
3	[RhCp*Cl ₂] ₂	Cu(2-ethylhexanoate) ₂	1.0 : 0.14	1.0 : 3.6
4	[RhCp*Cl ₂] ₂	(BzO) ₂	1.0 : 3.1	5.0 : 1.0
5	[RhCp*(CH ₃ CN) ₃ (SbF ₆) ₂] ^b	AgOAc	1.0 : 1.2	1.0 : 1.0
6	[RhCp*(CH ₃ CN) ₃ (SbF ₆) ₂] ^b	Cu(OAc) ₂	1.0 : 0.0	N/A
7	[RhCp*(CH ₃ CN) ₃ (SbF ₆) ₂] ^b	Cu(2-ethylhexanoate) ₂	1.0 : 0.23	1.0 : 1.3
8	[RhCp*(CH ₃ CN) ₃ (SbF ₆) ₂] ^b	Cu(2-ethylhexanoate) ₂ (4.2 equiv)	1.0 : 0.23	1.0 : 1.3
9	[RhCp*(CH ₃ CN) ₃ (SbF ₆) ₂] ^b	(BzO) ₂	1.0 : 0.28	1.5 : 1.0
10	RhCp*(OAc) ₂ ^b	AgOAc	1.0 : 3.3	1.0 : 1.2
11	RhCp*(OAc) ₂ ^b	Cu(2-ethylhexanoate) ₂	1.0 : 0.47	1.2 : 1.0
12	[RhInd*Cl ₂] ₂ ^c	AgOAc	1.0 : 1.3	1.0 : 2.0
13	[IrCp*Cl ₂] ₂	AgOAc	1.0 : 0.20	2.4 : 1.0

^aRatio determined by integration of products in crude ¹H NMR. ^bReactions were run without AgSbF₆.

^cReaction ran at 60 °C.

After exploration of effects of temperature, concentration, silver halide scavenger, oxidant and catalyst on the regioselectivity of allylic C–H arylation with *N*-Bn indole, we found that the conditions to achieve best observed selectivity for the benzylic isomer **59b** are an electron rich *N*-Bn indole, copper(II) ethylhexanoate as the oxidant, and [RhCp*Cl₂]₂. These conditions afford the most drastic shift towards benzylic isomer **59b** in a 3.6:1.0 ratio, which was not a synthetically useful regioselectivity when these two regioisomers are not separable by column chromatography. We also observed that eliminating silver from the reaction only diminished conversion (Table 2-5, entries 6-9 & 11).

2.4 Rhodium(III) catalyzed allylic C–H functionalization mechanism and kinetic studies

While we were working on the allylic C–H arylation of unsymmetrical disubstituted olefins, others in our lab were conducting experiments to support a mechanism proposal for allylic C–H amination.^{8–10} Kinetic studies, conducted by Daniel Salgueiro, using 1,3-diphenylpropene and benzyl carbamate indicated that the allylic C–H amination was first-order in rhodium and that the reaction was inhibited by the amine nucleophile. The observed inhibition was consistent with benzyl carbamate binding to the rhodium and pulling the catalyst off-cycle. Also, kinetic isotope experiments suggest the intermediacy of a π -allyl complex and an irreversible C–H cleavage step. All of these kinetic studies together establish that C–H cleavage is rate determining. Isolation and characterization of rhodium(III) π -allyl complex and subsequent stoichiometric studies suggest that allylic C–H amination proceeds through an allylic acetate intermediate. From these studies, we were able to propose a catalytic mechanism for allylic C–H amination via allylic acetate intermediate (**Figure 2-3**).

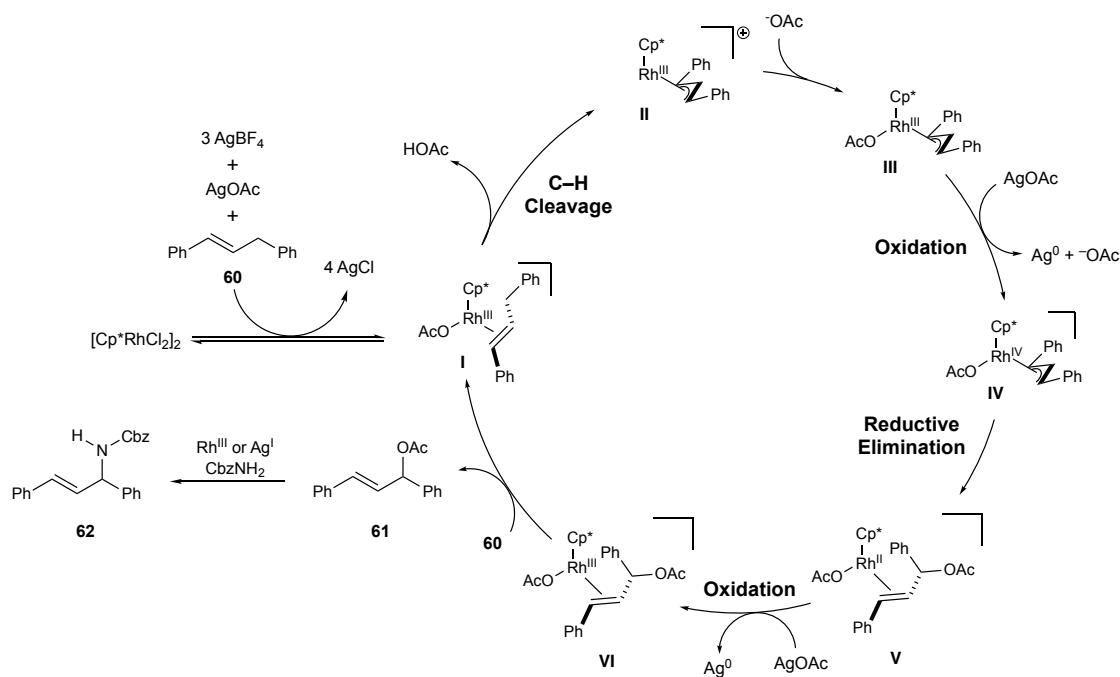


Figure 2-3. Proposed reaction mechanism for allylic C–H amination.

The rhodium(III) Cp^* precatalyst, $[RhCp^*Cl_2]_2$, reacts with silver, which abstracts all of the chlorides, and olefin **60** coordinates to form complex **I**. The newly formed complex **I** undergoes C–H cleavage via concerted metalation deprotonation (CMD) to afford complex **II** and acetic acid. Acetate can then coordinate to the empty coordination site on complex **II** providing complex **III**. Stoichiometric π -allyl studies conducted by Dr. Robert Harris suggest that complex **III** must be oxidized to rhodium(IV) complex **IV**. In the presence of nucleophile the rhodium(III) complex **III** does not react, but product is observed when nucleophile and oxidant are present. After a single electron oxidation, complex **IV** is formed which is in the correct oxidation state for reductive elimination to afford complex **V**. Now rhodium(II) complex **V** must be oxidized to complex **VI** via another one electron oxidation. Next, the complex undergoes a ligand exchange, which liberates allylic acetate **61** and reforms complex **I** completing the catalytic cycle. Lastly, allylic acetate **61** participates in a Lewis acid-catalyzed nucleophilic substitution reaction providing allylic amine **62**.

We observed that AgOAc and $[\text{RhCp}^*\text{Cl}_2]_2$ both promote the conversion of allylic acetate **61** to allylic amine **62**. Computational studies conducted by Baik and co-workers in collaboration with our group suggests a $\text{S}_{\text{N}}1$ mechanistic pathway is the most plausible.

We hypothesize that allylic C–H arylation with *N*-substituted indole nucleophiles proceeds via the same mechanistic pathway proposed in **Figure 2-3**. The proposed mechanism suggests that the presence of allylic acetate **53** in the reaction is not because of a side reaction, but it is actually the product of the catalytic cycle. Consumption of the allylic acetate relies on the efficiency of the Lewis acid catalysed $\text{S}_{\text{N}}1$ reaction with the nucleophile, thus exclusivity for the desired product meant that we were efficiently catalysing the allylic C–H acetoxylation and the subsequent substitution reaction. Based on this catalytic cycle, we can propose a reaction coordinate diagram for the Lewis acid catalysed $\text{S}_{\text{N}}1$ reaction for both nucleophile cases, electron-donating and electron-withdrawing group on nitrogen. The reaction coordinate diagram should allow us to successfully explain the regioselectivity differences between electron-donating verses electron-withdrawing groups.

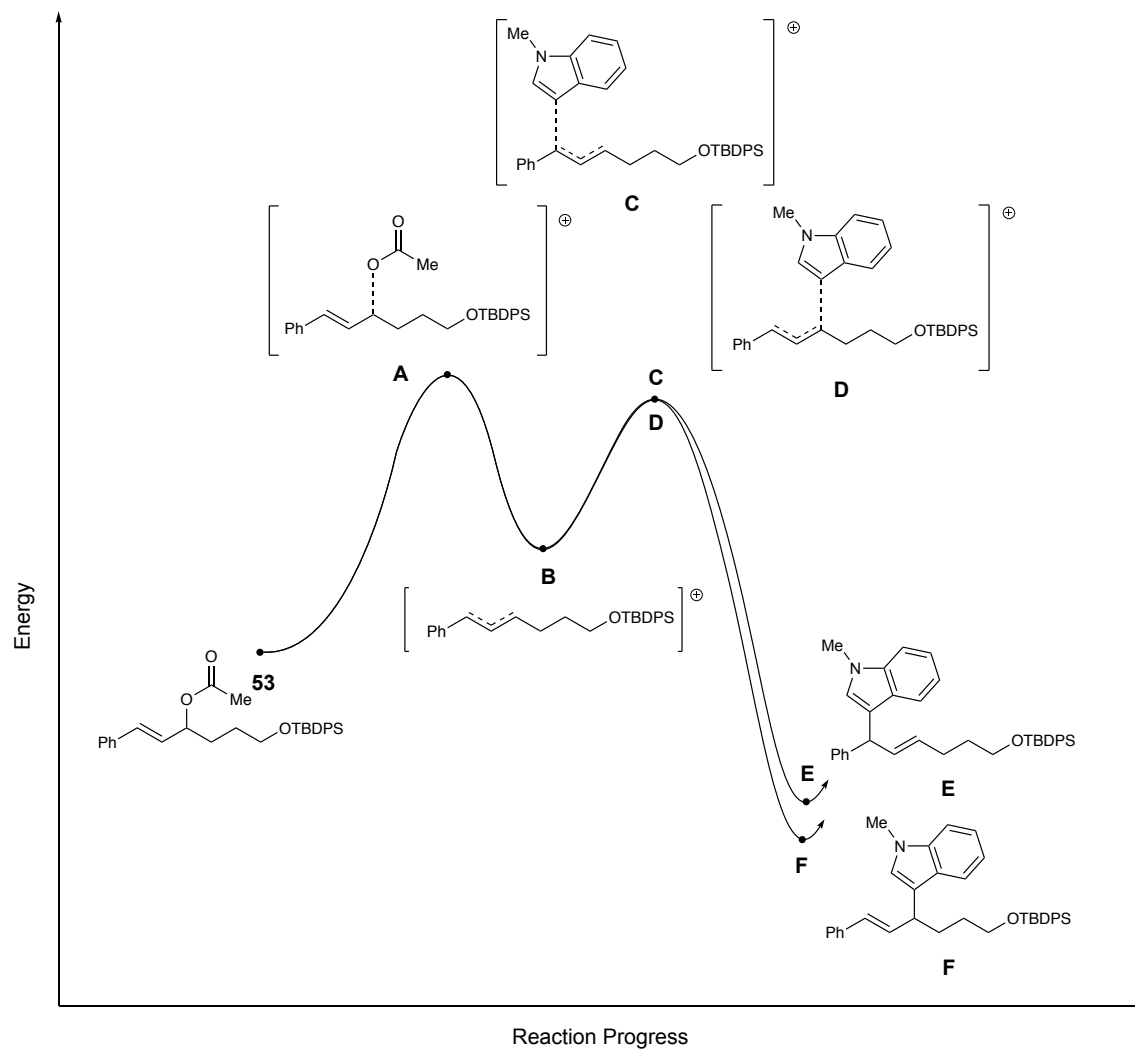


Figure 2-4. Proposed reaction coordinate diagram for S_N1 reaction of allylic acetate **53 with N-methyl indole.**

Firstly, we investigate the reaction coordinate diagram for the S_N1 reaction of allylic acetate **53** with the N-methyl indole nucleophile (Figure 2-4). Allylic acetate **53** undergoes dissociation of acetate, which is a sufficient leaving group, via transition state **A** to afford carbocation **B**. The carbocation character is delocalized over three carbons which provides the opportunity for nucleophilic attack at either the benzylic carbon or the carbon which would result in the conjugated product. When carbocation intermediate, **B**, is attacked by the N-methyl nucleophile, the reaction

can proceed via transition state **C** or **D**. The transition state determines which regioisomer will be produced. In the case of electron-donating groups on the indole nitrogen of the nucleophile, like N-methyl indole, we observe a 1.0:1.0 regiomer ratios. These ratios suggest an unselective reaction thus there is no energy difference between the **C** and **D**. The electron rich N-methyl indole is highly reactive and likely proceeds through an early transition state. Thus, the transition states, **C** and **D** closely resemble carbocation intermediate **B**, explaining why they are similar in energy. Once the reaction conditions provide enough energy to overcome the activation barrier product **E** and **F** can be produced without discrimination for a specific regioisomer, since there is no energy difference between **C** and **D**. In the case of the olefin products, we hypothesize that the conjugated isomer **F** would be the most stable and major product because the resulting alkene is in conjugation with the phenyl ring. This reaction coordinate diagram depicts N-methyl indole reaction with allylic acetate **53** but we hypothesize this general diagram would be true for all of the nucleophiles with electron-donating nitrogen groups. We are aware that there will be slight variation in the energies of the transition states corresponding to **C** and **D** because the different electron-donating nitrogen groups on the indole nucleophiles give varying regioselectivities (2.0:1.0 to 1.0:1.0 r.r.).

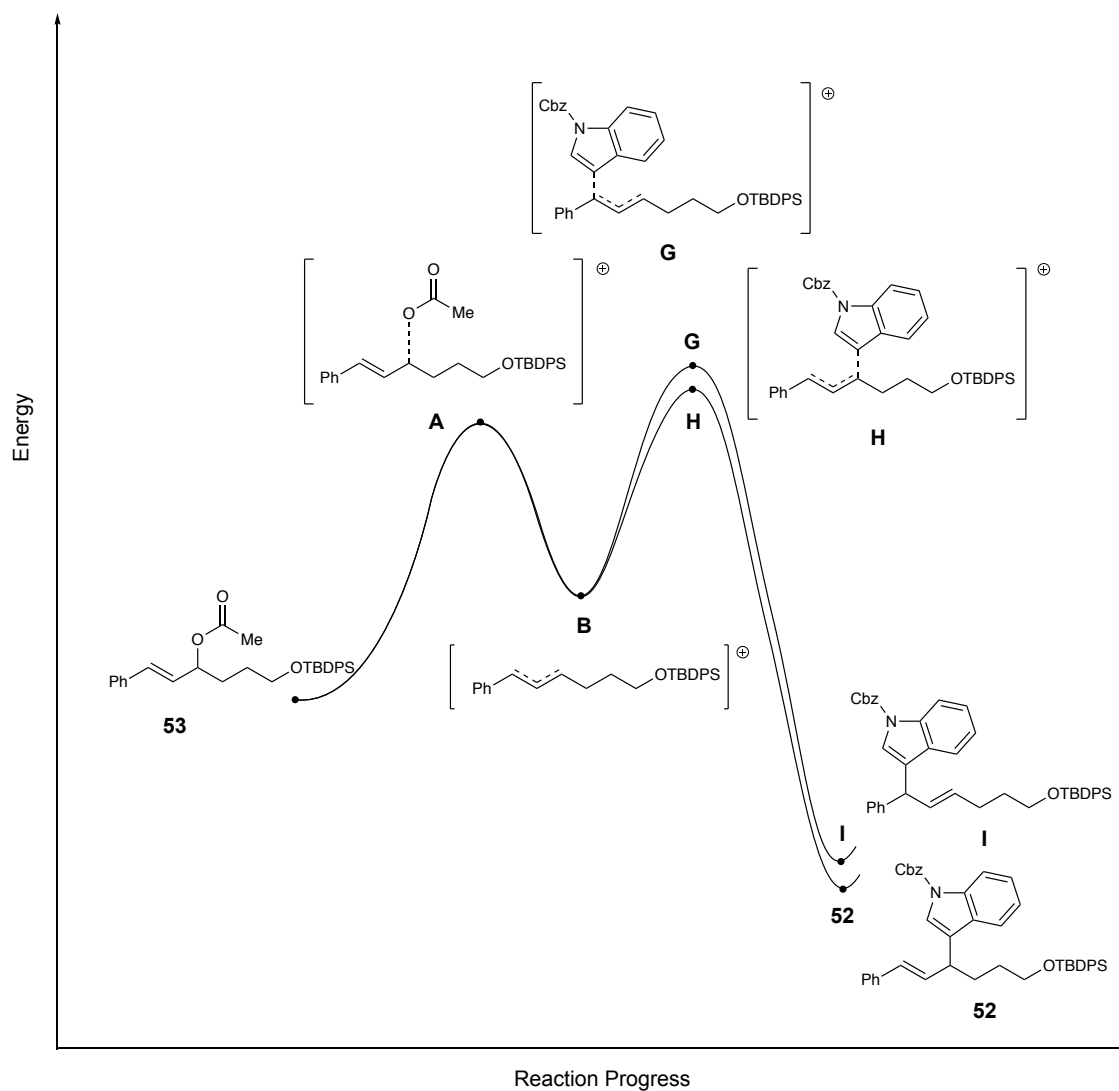


Figure 2-5. Proposed reaction coordinate diagram for S_N1 reaction of allylic acetate **53 with N-Cbz indole.**

Secondly, for the case of electron-withdrawing nitrogen protecting groups on the indole nucleophile, like N-Cbz indole, we propose a reaction coordinate diagram that starts in a similar manner. Allylic acetate **53** undergoes the same steps to afford carbocation intermediate **B**, then we propose a similar mechanism. However, the electron deficient indole is less nucleophilic than the previously described case, and thus the reaction proceeds through a later transition state. Transition states **G** and **H** have a large energy difference because they more closely resemble the products, this

is described as a late transition state. The bonds forming between the *N*-Cbz indole nucleophile and the carbocation are very close to a normal bond lengths and the alkene character is starting to localize where the olefin will appear in the respective product so we begin to see an energy difference similar to the products, **I** and **52**. Thus, the selectivity for the conjugated isomer **52** is due to the energy difference between **G** and **H**. Our hypothesis is that this would be generally true for all electron-withdrawing nitrogen groups. This is one argument for the observed regioselectivity for electron-donating verses electron-withdrawing nitrogen groups on the indole nucleophile, we would need to conduct computational studies to support this hypothesis and provide activation energies. The transition state argument suggests that no changes in reaction conditions or catalyst would change the regioselectivity, since it solely relies on the nucleophilicity of the indole nucleophile interacting with carbocation **B**.

2.5 Conclusion

In conclusion, we explored the effects of the nitrogen protecting groups on the regioselectivity of allylic C-H arylation with indole nucleophiles. We developed a regioselective allylic C-H arylation of unsymmetrical disubstituted olefin with *N*-Cbz indole and investigated a small nucleophile scope. Based on the proposed reaction mechanism, we decided that continuing the investigation of complementary regioselectivity with *N*-Bn indole was not a productive. We could continue investigating the regioselective allylic C-H arylation with *N*-Cbz indole but it would not provide any significant intellectual advances. We decided to halt the project with *N*-substituted indole nucleophiles in order to focus our efforts towards the discovery of an allylic C-H functionalization which proceeds via new mechanistic pathway. We targeted a mechanism in which the product is product is formed directly via a reductive elimination from the metal. This would

provide the foundation for the development of a regioselective and enantioselective allylic C–H functionalization.

After we made the decision to halt our allylic C–H arylation project, Glorius and co-workers published an allylic C–H arylation with arenes and heteroarenes.¹⁰ The conditions utilized in this publication are very similar to our optimized conditions for allylic C–H arylation with *N*-Cbz indole, the only difference is the use of AgBF₄ as a halide scavenger instead of AgSbF₆. The substrate scope did include *N*-Me indole but no other substituted indoles were explored. This publication confirmed the significance of an allylic C–H arylation technology.

2.6 Experimental Procedures

General Information

All reactions were carried out under nitrogen atmosphere with anhydrous solvents in oven- or flame-dried glassware using standard Schlenk technique, unless otherwise stated. Anhydrous tetrahydrofuran (THF) was obtained by passage through activated alumina using a *Glass Contours* solvent purification system. 1,2-dichloroethane (DCE), was distilled over calcium hydride (CaH_2) and stored over activated molecular sieves. Solvents for workup, extraction, and column chromatography were used as received from commercial suppliers without further purification. The *N*-protected indole substrates were synthesized via literature precedent or were commercially available. All other chemicals were purchased from Millipore Sigma, Strem Chemicals, Oakwood Chemicals, Alfa Aesar, or Combi-Blocks and used as received without further purification, unless otherwise stated.

^1H and ^{13}C nuclear magnetic resonance (NMR) spectra were recorded on a Varian Inova 600 spectrometer (600 MHz ^1H , 151 MHz ^{13}C), a Bruker 600 spectrometer (600 MHz ^1H , 151 MHz ^{13}C), a Varian Inova 500 spectrometer (500 MHz ^1H , 126 MHz ^{13}C), and a Varian Inova 400 spectrometer (400 MHz ^1H , 126 MHz ^{13}C) at room temperature in CDCl_3 (neutralized and dried over K_2CO_3 and activated molecular sieves) with internal CHCl_3 as the reference (7.26 ppm for ^1H , 77.16 ppm for ^{13}C), unless otherwise stated. Chemical shifts (δ values) were reported in parts per million (ppm) and coupling constants (J values) in Hz. Multiplicity was indicated using the following abbreviations: s = singlet, d = doublet, t = triplet, q = quartet, qn = quintet, m = multiplet, br = broad. Analytical thin layer chromatography (TLC) was performed on precoated glass-backed Silicycle SiliaPure® 0.25 mm silica gel 60 plates and visualized with UV light, ethanolic *p*-anisaldehyde, ethanolic bromocresol green, or aqueous potassium permanganate (KMnO_4). Flash column chromatography was performed using Silicycle SiliaFlash® F60 silica gel (40-63 μm) on a Biotage Isolera One system.

Preparatory TLC was performed on precoated glass-backed Silicycle SiliaPure® 1.0 mm silica gel 60 plates. We acknowledge the use of shared instrumentation provided by grants from the NSF.

General Procedure A: Exploration of *N*-protected indoles as nucleophiles

Oven dried 4 mL vial with Teflon septum cap with Teflon stir bar were cycled into an N₂ filled glovebox. AgSbF₆ (6.29 mg, 0.0183 mmol, 8 mol%) and AgOAc (80.3 mg, 0.481 mmol, 2.1 equiv) were weighed out into the oven dried 4 mL vial in an N₂ filled glovebox. [RhCp*Cl₂]₂ (2.83 mg, 0.00458 mmol, 2 mol%) was weighed out into a separate oven dried 7 mL vial in N₂ filled glovebox. The vials were sealed with a Teflon septum caps, removed from glovebox and placed under an atmosphere of N₂. To the 7 mL vial containing [RhCp*Cl₂]₂, 0.4 mL of anhydrous 1,2-DCE was added. In a separate oven dried 7 mL vial with stir bar and Teflon septum cap, (*E*)-*tert*-butyldiphenyl((6-phenylhex-5-en-1-yl)oxy)silane (100 mg, 0.241 mmol, 1 equiv) was weighed out into vial. The vial was sealed and evacuated/backfilled with N₂ three times. 0.4 mL of anhydrous 1,2-DCE was added to the vial. In another separate oven dried 7 mL vial with stir bar and Teflon septum cap, *N*-protected Indole (x mg, 0.0482 mmol, 2 equiv) was weighed out into vial. The vial was sealed and evacuated/backfilled with N₂ three times. 0.4 mL of anhydrous 1,2-DCE was added to the vial. To the vial containing AgSbF₆ and AgOAc, 0.4 mL of the [RhCp*Cl₂]₂ solution was added. Then 0.4 mL of the (*E*)-*tert*-butyldiphenyl((6-phenylhex-5-en-1-yl)oxy)silane solution was added. Then 0.4 mL of the *N*-protected indole solution was added. The vial was placed in an aluminium heating block set at 40 °C for 24 hours. The reaction was allowed to cool for 5 minutes. 1,4-dinitrobenzene (10.13 mg, 0.0603 mmol, 0.25 equiv) was weighed out into a 4 mL vial and 0.4 mL of 1,2-DCE was added. To the cooled reaction, 0.4 mL of the 1,4-dinitrobenzene solution was added. The reaction was stirred for 5 minutes. The reaction was filtered with 14 mL of ethyl acetate through a plug of celite into a 50 mL RBF. The solution was concentrated under reduced pressure.

The yield of product was determined by H^1 NMR of the crude reaction mixture using 1,4-dinitrobenzene as an internal standard.

General Procedure B: Optimization for regioselective *N*-Cbz indole addition

Oven dried 4 mL vial with Teflon septum cap with Teflon stir bar were cycled into an N_2 filled glovebox. $AgSbF_6$ (6.29 mg, 0.0183 mmol, 8 mol%) and oxidant (0.481 mmol, 2.1 equiv) were weighed out into the oven dried 4 mL vial in an N_2 filled glovebox. $[RhCp^*Cl_2]_2$ (2.83 mg, 0.00458 mmol, 2 mol%) was weighed out into a separate oven dried 7 mL vial in N_2 filled glovebox. The vials were sealed with a Teflon septum caps, removed from glovebox and placed under an atmosphere of N_2 . To the 7 mL vial containing $[RhCp^*Cl_2]_2$, 0.4 mL of anhydrous 1,2-DCE was added. In a separate oven dried 7 mL vial with stir bar and Teflon septum cap, (*E*)-*tert*-butyldiphenyl((6-phenylhex-5-en-1-yl)oxy)silane (100 mg, 0.241 mmol, 1 equiv) was weighed out into vial. The vial was sealed and evacuated/backfilled with N_2 three times. 0.4 mL of anhydrous 1,2-DCE was added to the vial. In another separate oven dried 7 mL vial with stir bar and Teflon septum cap, *N*-Cbz Indole was weighed out into vial. The vial was sealed and evacuated/backfilled with N_2 three times. 0.4 mL of anhydrous 1,2-DCE was added to the vial. To the vial containing $AgSbF_6$ and oxidant, 0.4 mL of the $[RhCp^*Cl_2]_2$ solution was added. Then 0.4 mL of the (*E*)-*tert*-butyldiphenyl((6-phenylhex-5-en-1-yl)oxy)silane solution was added. Then 0.4 mL of the *N*-Cbz indole solution was added. The vial was placed in an aluminium heating block set at 40 °C, 60 °C or off (rt) for 24 or 48 hours. The reaction was allowed to cool for 5 minutes. 1,4-dinitrobenzene (10.13 mg, 0.0603 mmol, 0.25 equiv) was weighed out into a 4 mL vial and 0.4 mL of 1,2-DCE was added. To the cooled reaction, 0.4 mL of the 1,4-dinitrobenzene solution was added. The reaction was stirred for 5 minutes. The reaction was filtered with 14 mL of ethyl acetate through a plug of

celite into a 50 mL RBF. The solution was concentrated under reduced pressure. The yield of product was determined by ^1H NMR of the crude reaction mixture using 1,4-dinitrobenzene as an internal standard.

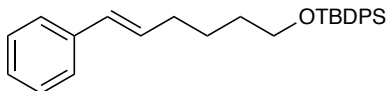
General Procedure C: Allylic C–H Arylation with *N*-Cbz indole

Inside an N_2 filled glovebox, to an oven dried 4 mL vial equipped with a magnetic stir bar was added $[\text{RhCp}^*\text{Cl}_2]_2$ (0.002 mmol, 2 mol%), AgSbF_6 (0.008 mmol, 8 mol%) and AgOAc (0.21 mmol, 2.1 equiv). The reaction vial was fitted with a septum cap and removed from the N_2 filled glovebox. In a separate oven dried vial fitted with septum cap, under N_2 atmosphere, a 0.2M solution of (*E*)-*tert*-butyldiphenyl((6-phenylhex-5-en-1-yl)oxy)silane was prepared in 1,2-dichloroethane. An aliquot of the solution (0.25 mL, 0.1 mmol, 1 equiv) was transferred to the vial containing the solid reagents. In a separate oven dried vial fitted with septum cap, under N_2 atmosphere, a 0.4M solution of the protected indole was prepared in 1,2-dichloroethane. An aliquot of the solution (0.25 mL, 0.2 mmol, 2 equiv) was transferred to the vial containing the solid reagents. The reaction was heated in an aluminium heating block set at 60 °C and stirred for 24 hours. The reaction was allowed to cool to room temperature, filtered with 10 mL of dichloromethane through a plug of celite, and concentrated under reduced pressure. The reaction was purified by flash column chromatography (0-10% EtOAc/hexanes) to afford the title compound.

General Procedure D: Condition Screening for Regioselective and Benzylic Site-Selective *N*-Bn Indole Addition

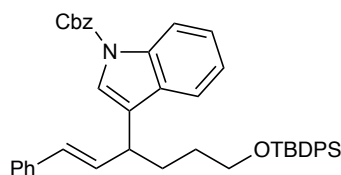
Oven dried 7 mL vials with Teflon septum caps and Teflon stir bars were cycled into an N_2 filled glovebox. AgSbF_6 or alternate silver salt (0.0212 mmol, 8.8 mol%) and oxidant (0.513 mmol, 2.1 equiv) were weighed out into the oven dried 7 mL vial in an N_2 filled glovebox. Next, rhodium

source ([Rh]) (0.00964 mmol, 4 mol%) was weighed out into a separate oven dried 7 mL vial in N₂ filled glovebox. The vials were sealed with a Teflon septum caps, removed from glovebox and placed under an atmosphere of N₂. To the 7 mL vial containing rhodium source, 0.4 mL of anhydrous 1,2-DCE to make a 0.01 M solution. In a separate oven dried 7 mL vial with stir bar and Teflon septum cap that was evacuated/backfilled with N₂ three times, a 0.6 M solution of (*E*)-*tert*-butyldiphenyl((6-phenylhex-5-en-1-yl)oxy)silane in 1,2-DCE was prepared. In a separate oven dried 7 mL vial with stir bar and Teflon septum cap that was evacuated/backfilled with N₂ three times, a 1.2 M solution of 1-benzyl-1*H*-indole in 1,2-DCE was prepared. To the vial containing silver salt and oxidant, 0.4 mL of the [RhCp*Cl₂]₂ (0.00482 mmol) solution was added. Then 0.4 mL of the (*E*)-*tert*-butyldiphenyl((6-phenylhex-5-en-1-yl)oxy)silane (0.241 mmol) solution was added. Then 0.4 mL of the 1-benzyl-1*H*-indole (0.482 mmol) solution was added. The vial was placed in an aluminium heating block set at 60 °C or 40 °C for 24-72 hours. The reaction was allowed to cool for 5 minutes. For reactions where conversion was monitored: The reaction was filtered with ethyl acetate (14 mL) through a plug of celite and concentrated under reduced pressure, then the product and starting material ratios were determined by H¹ NMR. For reactions monitored for yield: A 0.15 M solution of 1,4-dinitrobenzene (0.0602 mmol) in 1,2-DCE was prepared in a separate vial. To the cooled reaction, 0.4 mL of the 1,4-dinitrobenzene solution was added. The reaction was stirred for 5 minutes. The reaction was filtered with ethyl acetate (14 mL) through a plug of celite into a 50 mL RBF. The solution was concentrated under reduced pressure. Yield of the two regioisomers and starting material were determined by H¹ NMR of the crude reaction mixture using 1,4-dinitrobenzene as an internal standard.



(*E*)-*tert*-butyldiphenyl((6-phenylhex-5-en-1-yl)oxy)silane (**50**): Oven dried schlenck flask was charged with Cp₂ZrCl(H) (2.04 g, 5.9 mmol) in

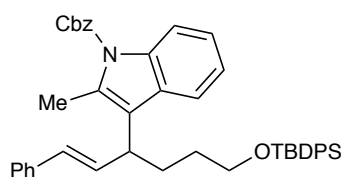
an N₂ filled glovebox and sealed with a rubber septum. The reaction flask was removed from glovebox, placed under an atmosphere of N₂ and anhydrous DCM (6 mL) was added. The suspension was cooled to 0 °C. In a separate 7 mL vial, *tert*-butyl(hex-5-yn-1-yloxy)diphenylsilane (2.07 g, 6.1 mmol) was dissolved in DCM (2 mL). The solution of *tert*-butyl(hex-5-yn-1-yloxy)diphenylsilane was slowly added to the reaction suspension at 0 °C. The reaction was allowed to come to room temperature for 1 hour. The solvent was removed *in vacuo* and the residue was dissolved in THF (7 mL). In a separate round bottom flask, ZnCl₂ (0.945 g, 6.9 mmol) was weighed into a round bottom flask in an N₂ filled glovebox. The round bottom flask was sealed with a septum, removed from the glovebox and placed under a balloon of N₂. The ZnCl₂ was dissolved in THF (6 mL) and added to the reaction via syringe. In a separate round bottom flask, Pd(PPh₃)₄ (0.350g, 0.3 mmol) was weighed into a round bottom flask in an N₂ filled glovebox. The round bottom flask was sealed with a septum, removed from the glovebox and placed under a balloon of N₂. The Pd(PPh₃)₄ was dissolved in THF (6 mL) then iodobenzene (0.33 mL, 3 mmol) was added. The suspension was then added to the reaction via syringe. The reaction was allowed to stir for 18 hours at room temperature under a balloon of N₂. The reaction was quenched with a saturated solution NH₄Cl and extracted with ethyl acetate (60 mL x 3). The combined organic extracts were dried over Na₂SO₄ and concentrated under reduced pressure. The crude product was purified by flash column chromatography on silica gel (100% hexanes → 7% toluene) afforded the desired product (0.826 g, 67% yield). Synthesis was adapted from published literature procedure providing the product.^{26,27} **¹H NMR** (500 MHz, CDCl₃) δ 7.67 (dd, *J* = 8.0, 1.5 Hz, 4H), 7.35 (m, 10H), 7.21 – 7.17 (m, 1H), 6.35 (d, *J* = 15.8 Hz, 1H), 6.20 (dt, *J* = 15.8, 6.9 Hz, 1H), 3.68 (t, *J* = 6.2 Hz, 2H), 2.20 (qd, *J* = 7.2, 1.3 Hz, 2H), 1.67 – 1.52 (m, 4H), 1.05 (s, 9H).

Allylic C–H Arylation *N*-Cbz Indole Scope

benzyl (E)-3-(6-((tert-butylidiphenylsilyl)oxy)-1-phenylhex-1-en-3-yl)-1H-indole-1-

carboxylate (52): Prepared according to **General Procedure C** using

benzyl 1H-indole-1-carboxylate (0.0503 g, 0.2 mmol, 2.0 equiv), (*E*)-*tert*-butyldiphenyl((6-phenylhex-5-en-1-yl)oxy)silane (0.0415 g, 0.1 mmol, 1.0 equiv), [RhCp*Cl₂]₂ (0.0012 g, 0.002 mmol, 2 mol%), AgSbF₆ (0.0028 g, 0.008 mmol, 8 mol%) and AgOAc (0.0350 g, 0.21 mmol, 2.1 equiv). Purified by flash column chromatography (0-10% EtOAc/hexanes) to afford the title compound as a single regioisomer (44.9 mg, 68%). ¹H NMR (500 MHz, Chloroform-*d*) δ 7.69 – 7.62 (m, 4H), 7.58 (d, *J* = 7.8 Hz, 1H), 7.51 (s, 2H), 7.48 – 7.37 (m, 7H), 7.37 – 7.31 (m, 7H), 7.29 (t, *J* = 7.6 Hz, 2H), 7.21 (q, *J* = 6.9 Hz, 2H), 6.47 (d, *J* = 15.8 Hz, 1H), 6.30 (dd, *J* = 15.8, 7.9 Hz, 1H), 5.46 (s, 2H), 3.71 (t, *J* = 6.2 Hz, 2H), 3.65 (q, *J* = 7.4 Hz, 2H), 2.13 – 1.99 (m, 1H), 1.92 (ddtd, *J* = 14.6, 9.8, 5.7, 2.9 Hz, 1H), 1.77 – 1.60 (m, 2H), 1.05 (s, 9H).

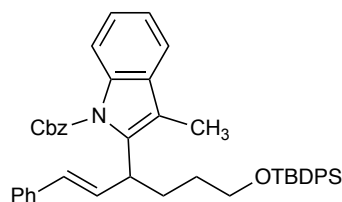


benzyl (E)-3-(6-((tert-butylidiphenylsilyl)oxy)-1-phenylhex-1-en-3-yl)-2-methyl-1H-

indole-1-carboxylate (54): Prepared according to **General Procedure C**

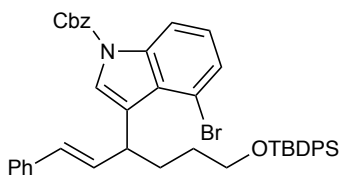
using *benzyl 2-methyl-1H-indole-1-carboxylate* (0.0531 g, 0.2 mmol, 2.0 equiv), (*E*)-*tert*-butyldiphenyl((6-phenylhex-5-en-1-yl)oxy)silane (0.0415 g, 0.1 mmol, 1.0 equiv), [RhCp*Cl₂]₂ (0.0012 g, 0.002 mmol, 2 mol%), AgSbF₆ (0.0028 g, 0.008 mmol, 8 mol%) and AgOAc (0.0350 g, 0.21 mmol, 2.1 equiv). Purified by flash column chromatography (0-10% EtOAc/hexanes) to afford the title compound as a single regioisomer (35.5 mg, 52%). ¹H NMR (500 MHz, Chloroform-*d*) δ 8.14 (d, *J* = 8.3 Hz, 1H), 7.62 (dd, *J* = 16.0, 6.6 Hz, 4H), 7.53 (dd, *J* = 16.9, 7.4 Hz, 3H), 7.46 – 7.36 (m, 6H), 7.36 – 7.29 (m, 6H), 7.28 (d, *J* = 7.4 Hz, 2H), 7.24 – 7.12 (m, 4H),

6.53 (dd, $J = 15.9, 6.1$ Hz, 1H), 6.38 (d, $J = 17.2$ Hz, 1H), 5.47 (s, 2H), 3.71 (m, 1H), 3.64 (t, $J = 6.3$ Hz, 2H), 2.53 (s, 3H), 2.15 – 1.99 (m, 2H), 1.62 – 1.40 (m, 2H), 1.02 (s, 9H).



benzyl (E)-2-(6-((tert-butylidiphenylsilyl)oxy)-1-phenylhex-1-en-3-yl)-3-methyl-1H-indole-1-carboxylate (55): Prepared according to **General Procedure C**

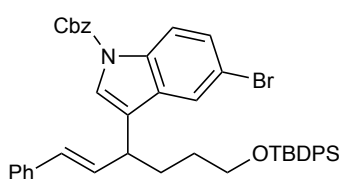
using benzyl 3-methyl-1H-indole-1-carboxylate (0.0531 g, 0.2 mmol, 2.0 equiv), (*E*)-*tert*-butyldiphenyl((6-phenylhex-5-en-1-yl)oxy)silane (0.0415 g, 0.1 mmol, 1.0 equiv), [RhCp*Cl₂]₂ (0.0012 g, 0.002 mmol, 2 mol%), AgSbF₆ (0.0028 g, 0.008 mmol, 8 mol%) and AgOAc (0.0350 g, 0.21 mmol, 2.1 equiv). Purified by flash column chromatography (0-10% EtOAc/hexanes) to afford the title compound as a single regioisomer (11.6mg, 17%). ¹H NMR (500 MHz, Chloroform-*d*): ¹H NMR (500 MHz, Chloroform-*d*) δ 8.03 – 8.00 (m, 1H), 7.63 (tt, $J = 7.9, 1.4$ Hz, 4H), 7.47 – 7.41 (m, 3H), 7.40 – 7.36 (m, 3H), 7.36 – 7.30 (m, 8H), 7.27 (dd, $J = 4.4, 1.0$ Hz, 5H), 7.25 – 7.22 (m, 2H), 7.21 – 7.17 (m, 1H), 6.54 – 6.44 (dd, $J = 16.0, 16.4$ Hz 1H), 6.31 (d, $J = 16.0$ Hz, 1H), 5.42 (d, $J = 2.5$ Hz, 2H), 3.63 (t, $J = 6.3$ Hz, 2H), 2.25 (s, 3H), 2.10 – 1.97 (m, 2H), 1.66 – 1.57 (m, 1H), 1.48 (ddt, $J = 11.0, 7.7, 3.6$ Hz, 1H), 1.03 (s, 9H).



benzyl (E)-4-bromo-3-(6-((tert-butylidiphenylsilyl)oxy)-1-phenylhex-1-en-3-yl)-1H-indole-1-carboxylate (56): Prepared according to **General**

Procedure C using benzyl 5-bromo-1H-indole-1-carboxylate (0.0658 g, 0.2 mmol, 2 equiv), (*E*)-*tert*-butyldiphenyl((6-phenylhex-5-en-1-yl)oxy)silane (0.0415 g, 0.1 mmol, 1 equiv), [RhCp*Cl₂]₂ (0.002 mmol, 2 mol%), AgSbF₆ (0.008 mmol, 8 mol%) and AgOAc (0.21 mmol, 2.1 equiv). Purified by flash column chromatography (0-10% EtOAc/hexanes) to

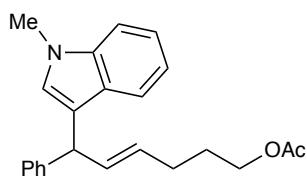
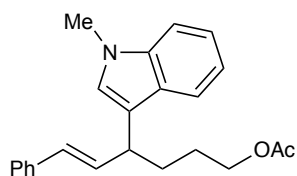
afford the title compound as a single regioisomer (31.7 mg, 43%). **¹H NMR** (500 MHz, Chloroform-*d*): δ 8.06 (s, 1H), 7.74 – 7.61 (m, 6H), 7.49 (dt, $J = 6.3, 1.6$ Hz, 2H), 7.41 (m, 8H), 7.36 – 7.27 (m, 8H), 7.21 (ddq, $J = 8.6, 6.3, 1.4$ Hz, 1H), 6.42 (d, $J = 15.2$ Hz, 1H), 6.24 (ddt, $J = 15.9, 7.9, 1.5$ Hz, 1H), 5.44 (s, 2H), 3.69 (t, $J = 6.2$ Hz, 2H), 3.57 (q, $J = 8.2$ Hz, 1H), 1.99 (m, 1H), 1.94 – 1.84 (m, 1H), 1.71 – 1.56 (m, 2H), 1.04 (s, 9H).



benzyl (E)-5-bromo-3-(6-((tert-butyl)diphenylsilyl)oxy)-1-phenylhex-1-en-3-yl)-

1H-indole-1-carboxylate (57): Prepared according to **General**

Procedure C using benzyl 4-bromo-1*H*-indole-1-carboxylate (0.0658 g, 0.2 mmol, 2 equiv), *E*-*tert*-butyldiphenyl((6-phenylhex-5-en-1-yl)oxy)silane (0.0415 g, 0.1 mmol, 1 equiv), [RhCp*Cl₂]₂ (0.002 mmol, 2 mol%), AgSbF₆ (0.008 mmol, 8 mol%) and AgOAc (0.21 mmol, 2.1 equiv). Purified by flash column chromatography (0-10% EtOAc/hexanes) to afford **57** as a single regioisomer (25.8 mg, 35%). **¹H NMR** (500 MHz, Chloroform-*d*): δ 8.23 (d, $J = 7.2$ Hz, 1H), 7.71 – 7.59 (m, 4H), 7.53 – 7.45 (m, 3H), 7.44 – 7.36 (m, 6H), 7.36 – 7.27 (m, 8H), 7.21 (ddt, $J = 7.7, 6.5, 1.4$ Hz, 1H), 7.14 (t, $J = 8.1$ Hz, 1H), 6.43 (d, $J = 15.9$ Hz, 1H), 6.38 (dd, $J = 15.9, 6.8$ Hz, 1H), 5.45 (s, 2H), 4.44 (q, $J = 7.1$ Hz, 1H), 3.71 (t, $J = 6.3$ Hz, 2H), 2.08 – 1.98 (m, 1H), 1.88 – 1.67 (m, 3H), 1.04 (d, $J = 1.3$ Hz, 9H).



(E)-4-(1-methyl-1H-indol-3-yl)-6-phenylhex-5-en-1-yl acetate (Me-a-OAc) and (E)-6-(1-methyl-1H-indol-3-yl)-6-phenylhex-4-en-1-yl acetate (Me-b-OAc):

Prepared according to **General Procedure C** using 1-methyl-1*H*-indole (0.0531 g, 0.2 mmol, 2.0 equiv), *E*-6-phenylhex-5-en-1-yl acetate (0.0262 g, 0.1 mmol, 1.0 equiv), [RhCp*Cl₂]₂ (0.002 mmol,

2 mol%), AgSbF₆ (0.008 mmol, 8 mol%) and AgOAc (0.21 mmol, 2.1 equiv). Purified by flash column chromatography (0-10% EtOAc/hexanes) to afford **Me-a-OAc** and **Me-b-OAc** as a mixture of regioisomers (15.2 mg, 25%). *A portion of each regioisomer could be isolated purely by subsequent flash column chromatography and was used for structural determination.

(E)-4-(1-methyl-1H-indol-3-yl)-6-phenylhex-5-en-1-yl acetate (**Me-a-OAc**)

¹H NMR (399 MHz, Chloroform-*d*): δ 7.65 (dd, *J* = 7.94, 0.94 Hz, 1H), 7.32-7.31 (m, 2H), 7.31-7.27 (m, 3H), 7.24-1.17 (m, 2H), 7.08 (t, *J* = 7.9 Hz, 1H), 6.90 (s, 1H), 6.51 (d, *J* = 15.9 Hz, 1H), 6.38 (dd, *J* = 15.9, 7.9 Hz, 1H), 4.10 (q, *J* = 6.6 Hz, 1H), 3.77 (s, 3H), 2.03 (s, 3H), 1.97-1.84 (m, 2H), 1.81-1.66 (m, 4H), 1.64-1.59 (m, 2H), 1.52-1.48 (m, 1H)

1D NOE (599 MHz, Chloroform-*d*, Selective band center: 6.89 (ppm); width: 27.6 (Hz)): δ 6.89 (s), 3.76 (s)

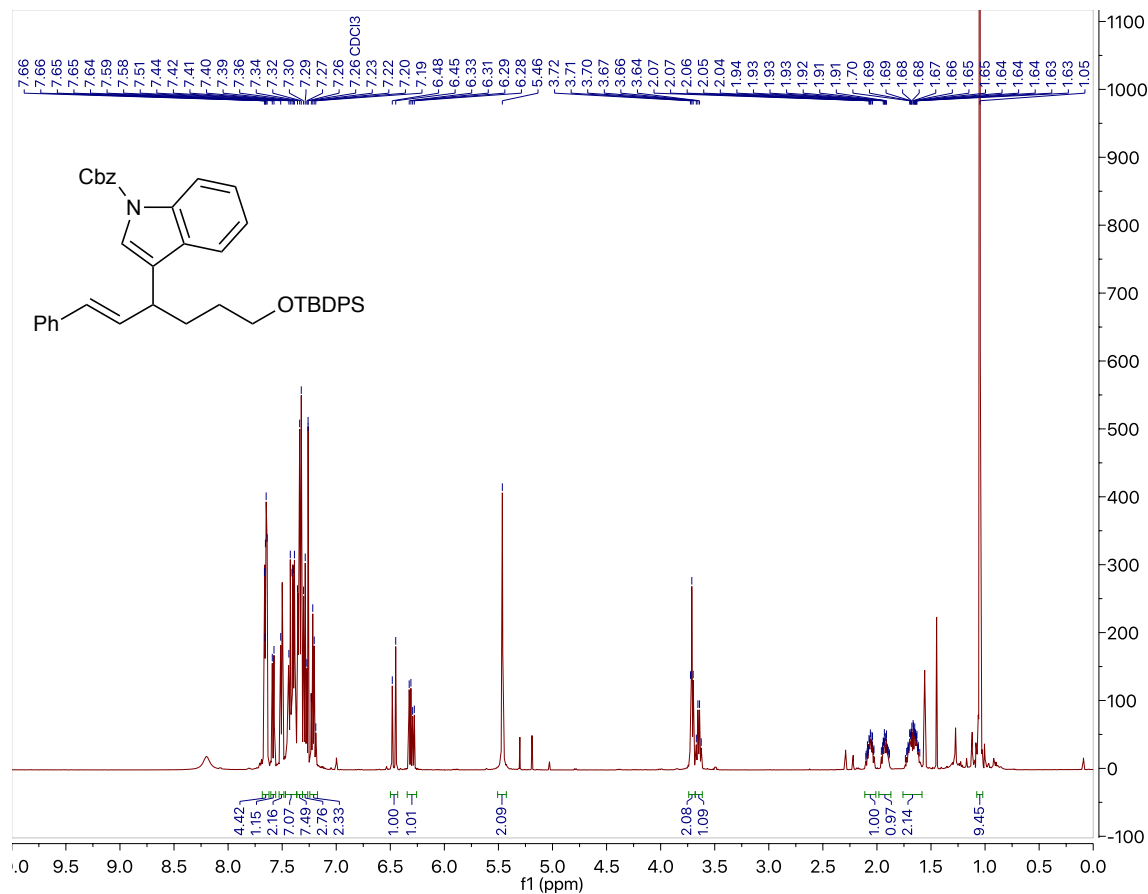
(E)-6-(1-methyl-1H-indol-3-yl)-6-phenylhex-4-en-1-yl acetate (**Me-b-OAc**)

¹H NMR (399 MHz, Chloroform-*d*): δ 7.37 (dt, *J* = 7.94, 0.94 Hz, 1H), 7.32-7.27 (m, 6H), 7.24-7.17 (m, 2H), 7.03-6.00 (m, 1H), 6.70 (s, 1H), 5.97 (dd, *J* = 15.2, 7.4 Hz, 1H), 5.49 (dt, *J* = 15.2, 1.2 Hz, 1H), 4.90 (d, *J* = 7.4 Hz, 1H), 3.74 (s, 3H), 2.17-2.12 (m, 2H), 2.03 (s, 3H), 1.76-1.69 (m, 3H), 1.32-1.25 (m, 3H)

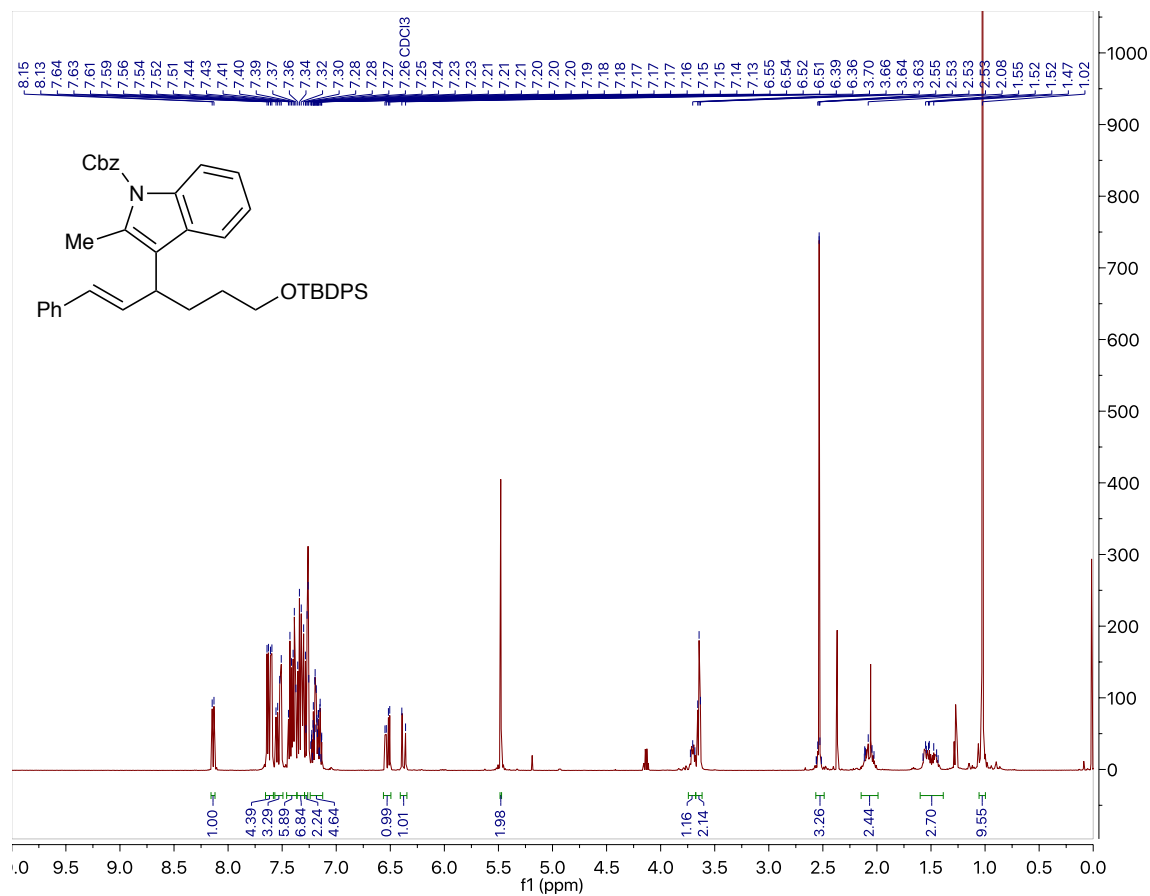
1D NOE (599 MHz, Chloroform-*d*, Selective band center: 6.70 (ppm); width: 16.2 (Hz)): δ 6.70 (s), 3.74 (s)

2.7 Spectral Data

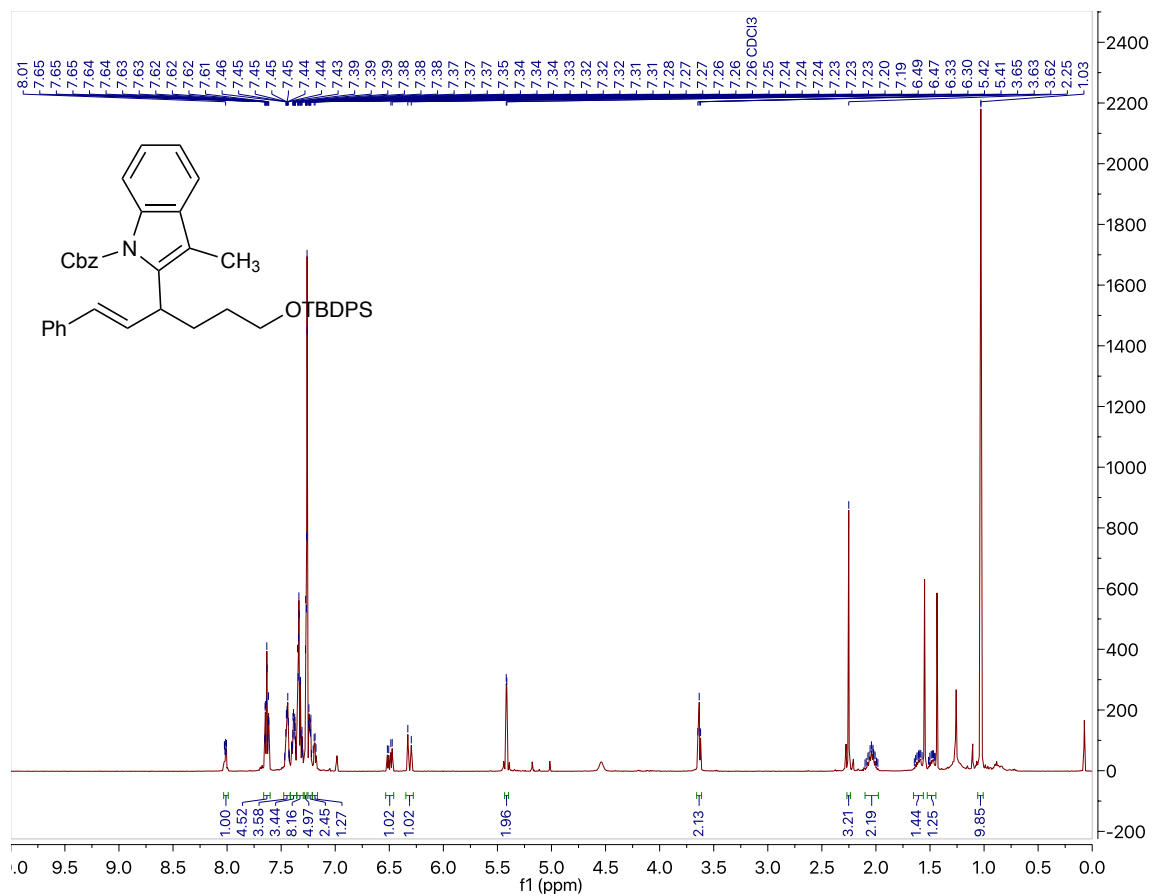
benzyl (E)-3-(6-((tert-butylidiphenylsilyl)oxy)-1-phenylhex-1-en-3-yl)-1H-indole-1-carboxylate (52)



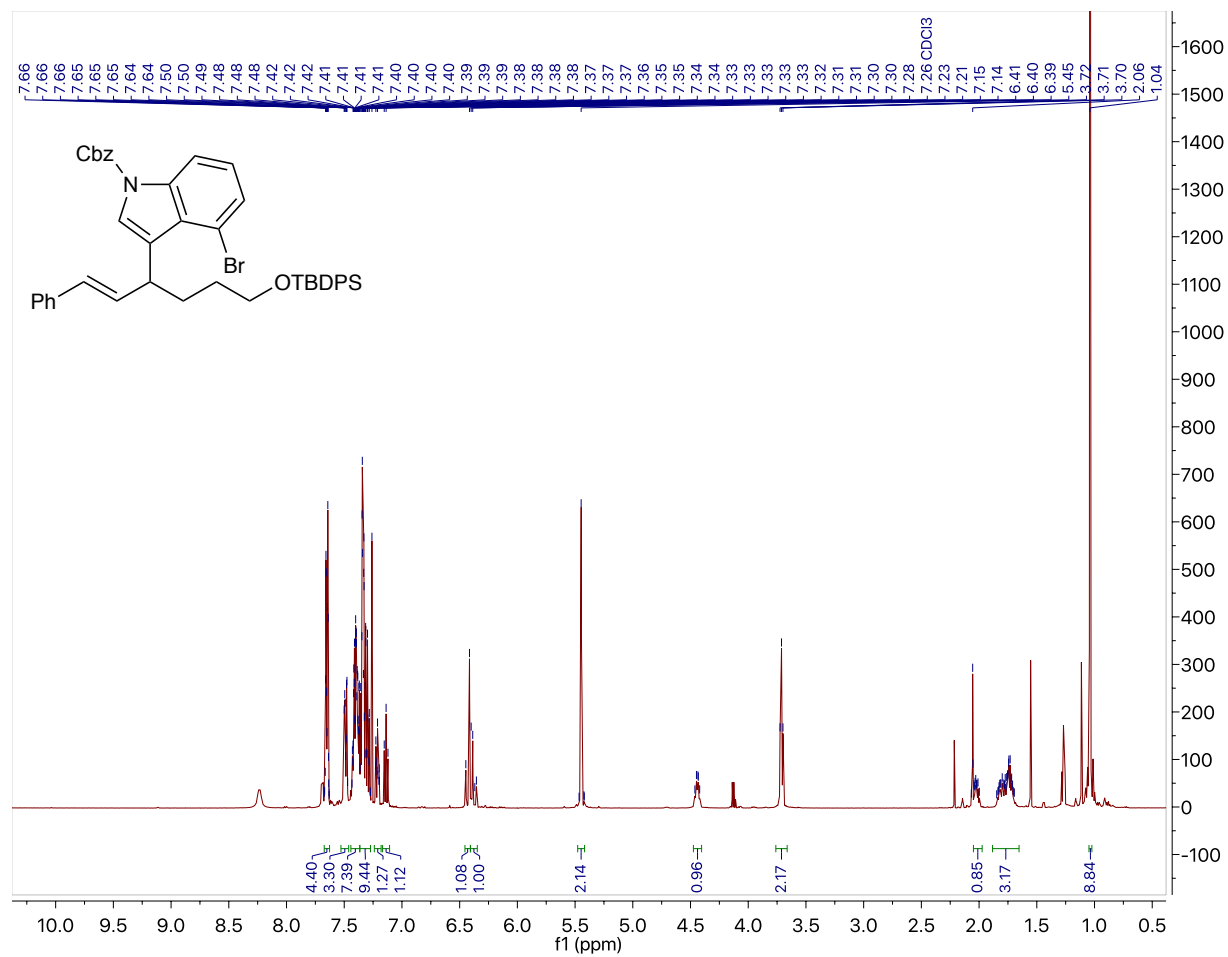
benzyl (E)-3-(6-((tert-butyl-diphenylsilyl)oxy)-1-phenylhex-1-en-3-yl)-2-methyl-1H-indole-1-carboxylate (54)



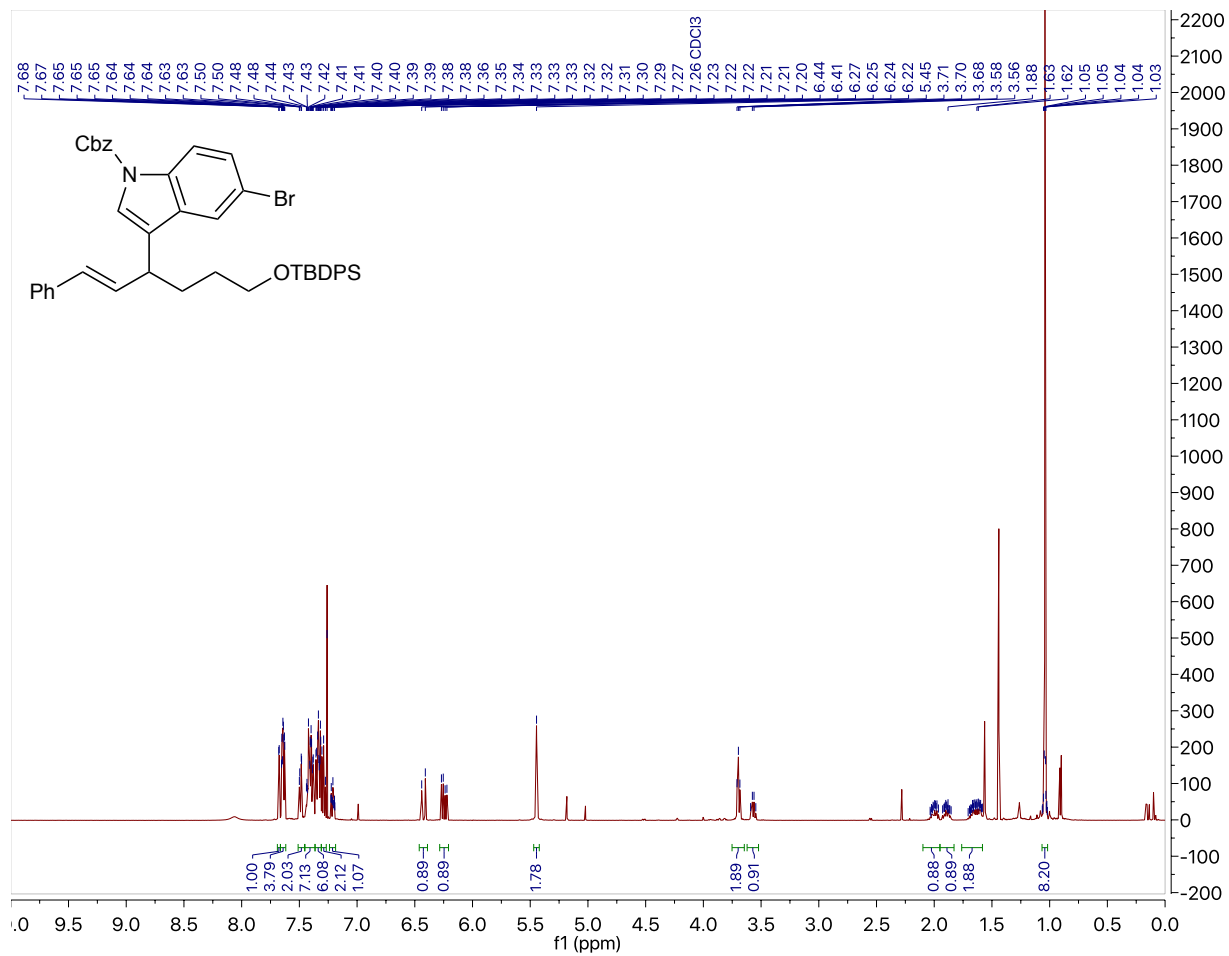
benzyl (E)-2-(6-((tert-butylidiphenylsilyl)oxy)-1-phenylhex-1-en-3-yl)-3-methyl-1H-indole-1-carboxylate (55)



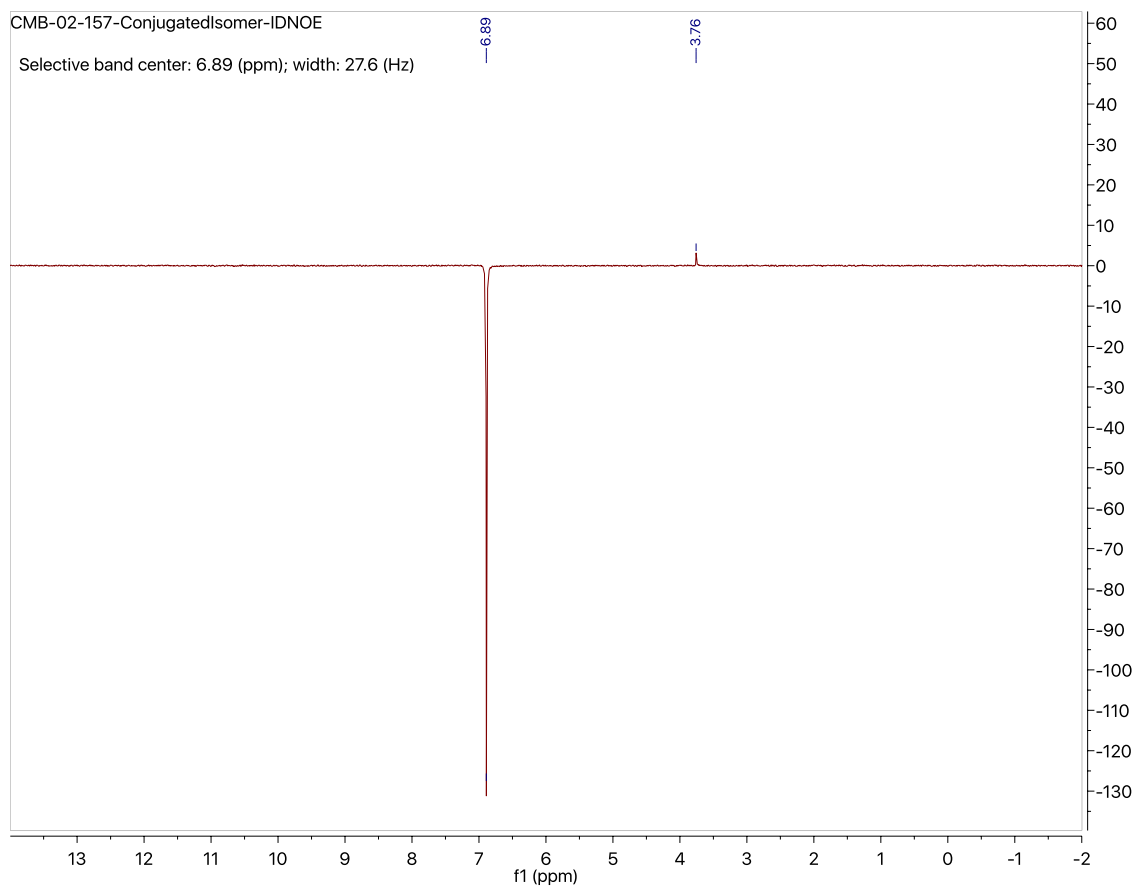
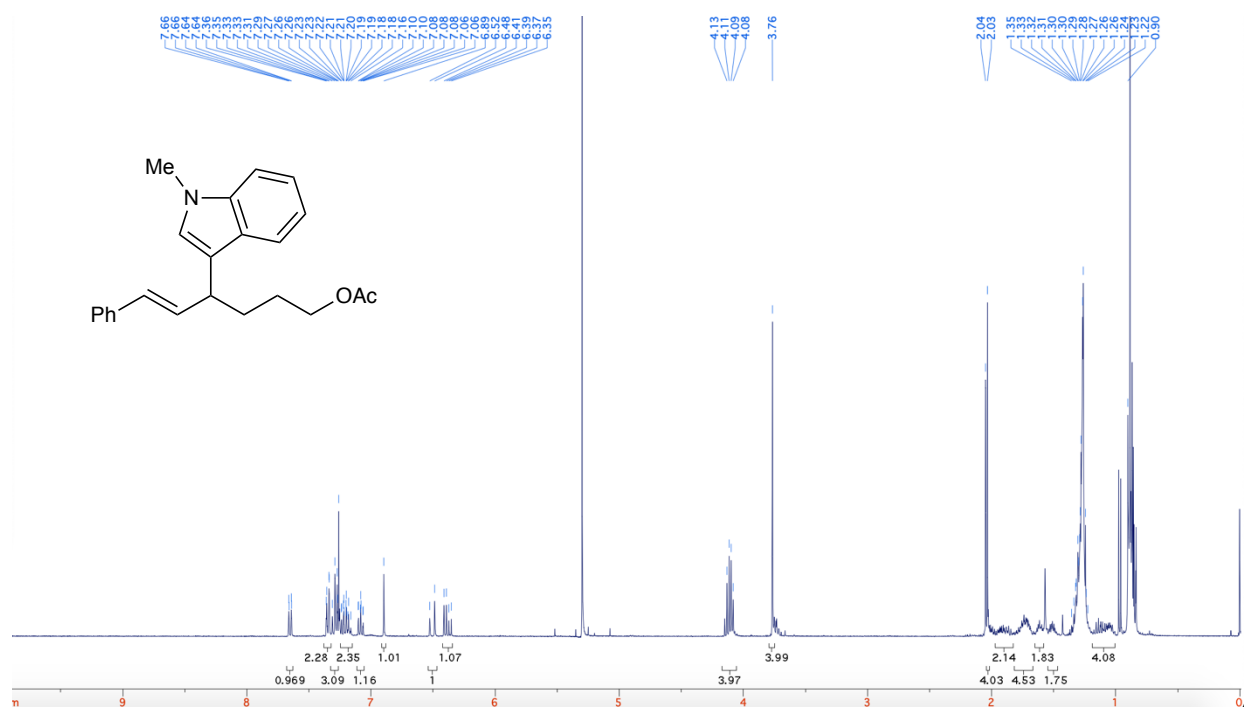
benzyl (E)-5-bromo-3-(6-((tert-butylidiphenylsilyl)oxy)-1-phenylhex-1-en-3-yl)-1H-indole-1-carboxylate (56)



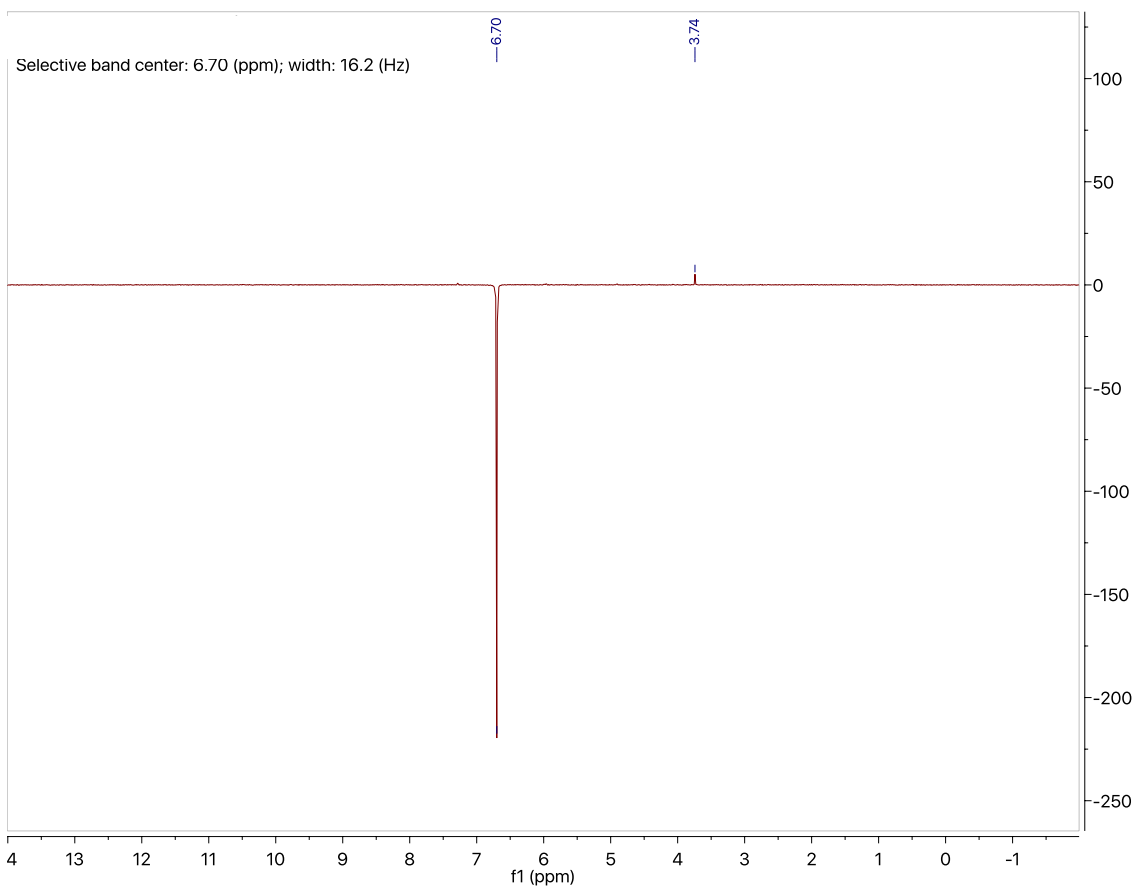
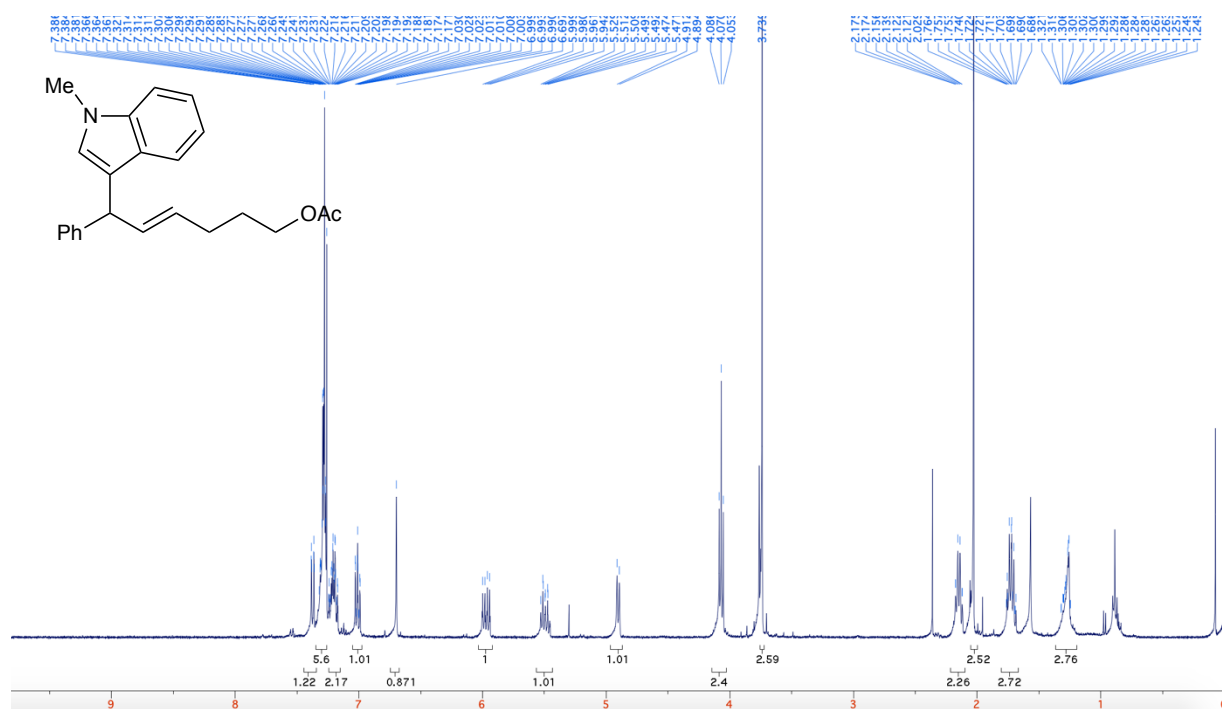
benzyl (E)-4-bromo-3-(6-((tert-butyl)diphenylsilyl)oxy)-1-phenylhex-1-en-3-yl)-1H-indole-1-carboxylate (57)



(E)-4-(1-methyl-1H-indol-3-yl)-6-phenylhex-5-en-1-yl acetate (**Me-a-OAc**)



(E)-6-(1-methyl-1H-indol-3-yl)-6-phenylhex-4-en-1-yl acetate (Me-b-OAc)



2.8 References

- (1) Bandini, M.; Melloni, A.; Umani-Ronchi, A. New Versatile Pd-Catalyzed Alkylation of Indoles via Nucleophilic Allylic Substitution: Controlling the Regioselectivity. *Organic Letters* **2004**, *6* (18), 3199–3202.
- (2) Liang, X.; Zhang, T. Y.; Zeng, X. Y.; Zheng, Y.; Wei, K.; Yang, Y. R. Ir-Catalyzed Asymmetric Total Synthesis of (-)-Communesin F. *Journal of the American Chemical Society* **2017**, *139* (9), 3364–3367.
- (3) Lin, T.-Y.; Wu, H.-H.; Feng, J.-J.; Zhang, J. Design and Enantioselective Synthesis of β -Vinyl Tryptamine Building Blocks for Construction of Privileged Chiral Indole Scaffolds *ACS Catalysis* **2017**, *7*, 4047–4053.
- (4) Knölker, H.-J.; Reddy, K. R. Isolation and Synthesis of Biologically Active Carbazole Alkaloids. *Chemical Reviews* **2002**, *102* (11), 4303–4428.
- (5) Kuehne, M. E.; Roland, D. M.; Hafter, R. Studies in Biomimetic Alkaloid Syntheses. 2. Synthesis of Vincadifformine from Tetrahydro-(8-carboline through a Secodine Intermediate *Journal of Organic Chemistry* **1978**, *43*, 3705–3710.
- (6) Marcum, J. S.; Roberts, C. C.; Manan, R. S.; Cervarich, T. N.; Meek, S. J. *Journal of the American Chemical Society* **2017**, *139*, 15580–15583.
- (7) Burman, J. S.; Harris, R. J.; B. Farr, C. M.; Bacsa, J.; Blakey, S. B. Rh(III) and Ir(III)Cp* Complexes Provide Complementary Regioselectivity Profiles in Intermolecular Allylic C–H Amidation Reactions. *ACS Catalysis* **2019**, *9* (6), 5474–5479.
- (8) Burman, J. S.; Blakey, S. B. Regioselective Intermolecular Allylic C–H Amination of Disubstituted Olefins via Rhodium/ π -Allyl Intermediates. *Angewandte Chemie International Edition* **2017**, *56* (44), 13666–13669.
- (9) Harris, R. J.; Park, J.; Nelson, T. A. F.; Iqbal, N.; Salgueiro, D. C.; Bacsa, J.; MacBeth, C. E.; Baik, M.-H.; Blakey, S. B. The Mechanism of Rhodium-Catalyzed Allylic C–H Amination. *Journal of the American Chemical Society* **2020**, *142* (12), 5842–5851.
- (10) Nelson, T. A. F.; Blakey, S. B. Intermolecular Allylic C–H Etherification of Internal Olefins. *Angewandte Chemie International Edition* **2018**, *57* (45), 14911–14915.

Chapter 3. Development of a Novel Chiral Indenyl Catalyst for Regio- and Enantioselective C–H Amidation of Unactivated Olefins

3.1 Introduction: Allylic C–H Amidation

During the development of allylic C–H arylation, our lab, in collaboration with the Baik group, discovered the reaction proceeds through an allylic acetate intermediate. The acetate then undergoes a Lewis acid catalyzed S_N1 reaction with the respective nucleophile. This discovery precludes the use of a chiral rhodium(III) catalyst because the formation of the allylic acetate can be catalyzed by the achiral silver salt or the rhodium(III) catalyst. Thus Jacob Burman and others in our group, including myself, began focusing our efforts toward the discovery of an allylic C–H functionalization where the bond forming step occurs via a reductive elimination from the metal center. The group researchers working on the amidation project proposed that an allylic C–H functionalization, like allylic C–H sulfamidation with tosyl azide, which proceeds through a nitrene intermediate would provide the ideal platform for a conceptual advance in allylic C–H functionalization (**Figure 3-1**).¹

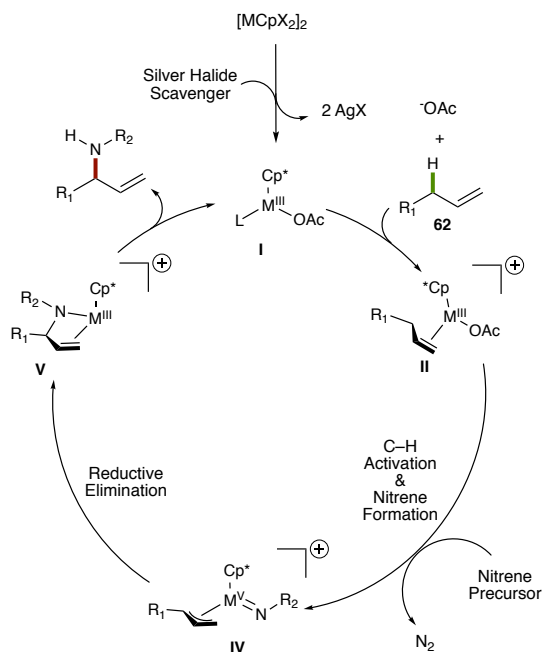


Figure 3-1. Proposed mechanism for allylic C–H amidation via nitrene intermediate.¹

Jacob Burman and co-workers successfully developed, alongside the groups of Rovis and Glorius, the regioselective allylic C–H amidation of unactivated terminal and 1,2-disubstituted olefins which presumably proceeds via reductive elimination from a rhodium(V) nitrene intermediate (**Figure 3-2**).²⁻⁴ We observed large functional group tolerance within the nucleophile scope on allyl benzene. We were able to incorporate aziridines, piperidines, heteroaromatics, strained cyclic systems and simple alkyl functionality with moderate to excellent regioselectivity for the branched regioisomer. The choice of metal catalyst, rhodium(III) versus iridium(III), was important for the efficient allylic C–H amidation of olefin substrates. We found that allyl benzene derivatives proceeded with greater efficacy and regioselectivity with rhodium(III) catalysts, whereas alkyl substituted and nitrogen rich olefins required iridium(III) catalysts to increase efficiency or effectively catalyze the reaction.

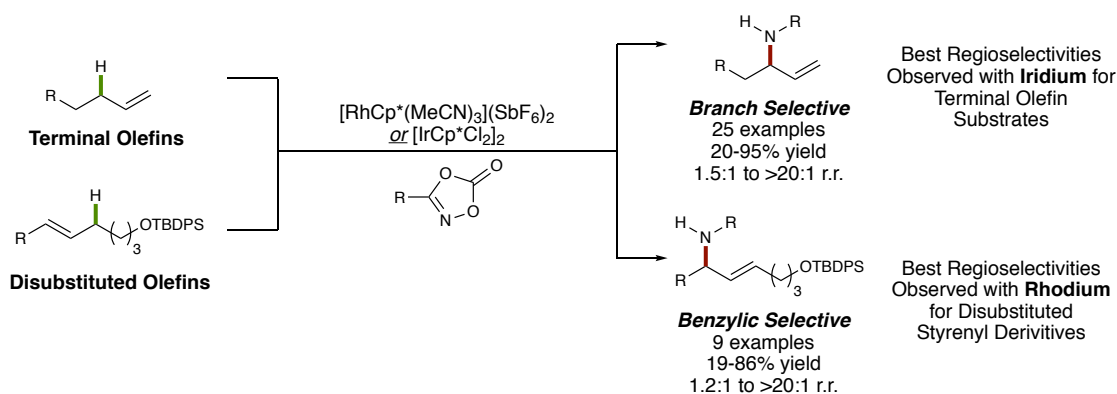


Figure 3-2. Rhodium(III) and iridium(III) catalyzed regioselective intermolecular allylic C–H amidation with dioxazolone reagents.

We successfully developed a novel allylic C–H amidation which provides complementary regioselectivities compared to our previously developed allylic C–H amidation, etherification and arylation. The branched or benzylic selective allylic C–H amidation produces allylic amides with a stereocenter but the use of an achiral catalyst provides a racemic reaction. The proposed mechanistic

pathway provides the opportunity for the development of a chiral catalyst for the enantioselective C–H amidation.

3.2 Chiral group IX catalysts for allylic C–H amidation

Our group, along with many others, has made significant advances in the selective functionalization of allylic C–H bonds. The challenge of stereoselectivity, however, remains largely unsolved. The field of asymmetric C–H functionalization as a whole has been dominated by transition metal catalysis utilizing privileged ligand classes for enantioinduction.⁵⁻¹¹ One class of privileged ligands that has found widespread utility in transition metal catalyzed C–H functionalization is the cyclopentadienyl (Cp) ligand scaffold. Recently, many groups, such as the Cramer, Waldmann, You, Rovis and Ward groups, have designed and developed chiral Cp ligands for asymmetric catalysis.⁵⁻¹¹

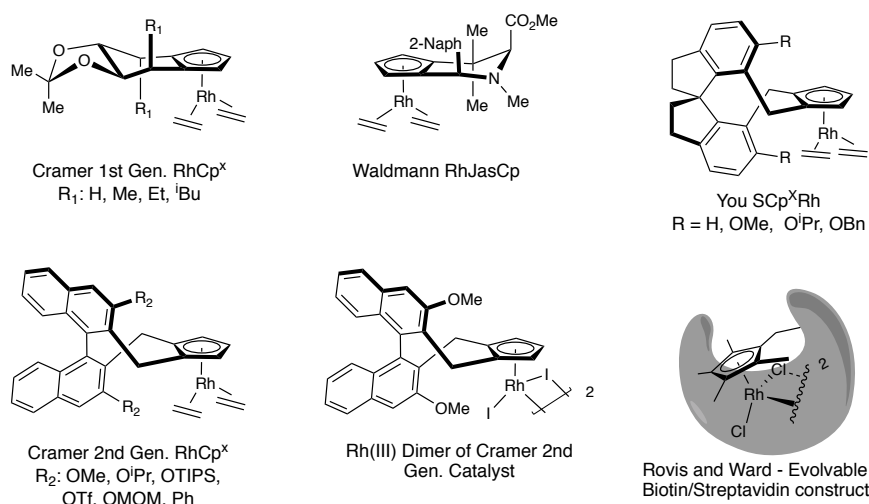


Figure 3-3. Rhodium(III) chiral Cp and Cp* catalysts for asymmetric induction

Chiral Cp variants developed by Cramer and co-workers have shown broad applicability in hydroarylations, allylations, carbene insertions, and Heck-type couplings via directed C–H functionalization. Cramer’s first-generation catalysts were derived from a chiral pool starting

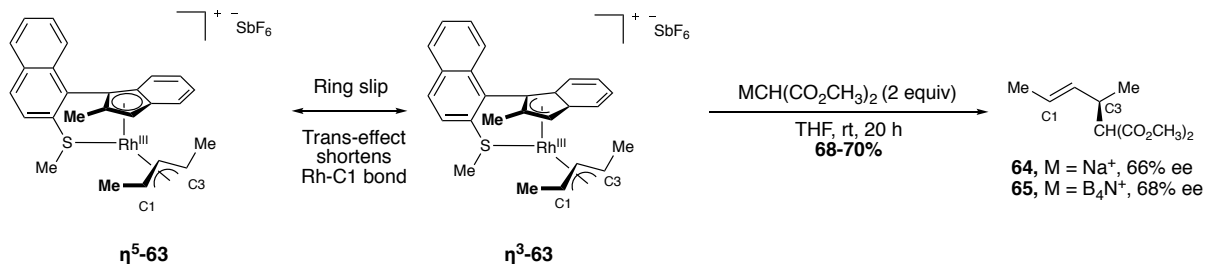
material, *D*-mannitol (**Figure 3-3**). The synthesis of these ligands is five steps but utilized thallium ethoxide, which is very toxic and safety precautions must be taken. Complementary to the first generation, the second-generation catalysts are derived from chiral binol. The synthesis of this new class of ligands is twelve steps, while requiring high temperatures (220 °C) and still including the use of thallium ethoxide. These catalysts have powerful synthetic utility while relying on steric blocking to afford stereoselective bond formation.

Another noteworthy approach to enantioselective C–H functionalization catalysis, involving the use of Cp or Cp* derivatives, is Rovis and Ward's discovery of an evolvable, engineered streptavidin docked with biotinylated Rh^{III}Cp* (**Figure 3-3**). This catalyst was utilized for the asymmetric synthesis of dihydroisoquinolones via the directed C–H functionalization of benzamides.⁹

Other approaches include amino acid derived ligands synthesized by Waldman and Antonchick and the planar chiral complex isolated by Perekalin (**Table 3-3**).¹⁰⁻¹¹ The enantioselective approaches pioneered by these groups have sparked both the investigation and discovery of chiral Cp derivatives for enantioselective C–H functionalization.

We propose that the field of chiral Cp-type ligand for asymmetric catalysis is still an area that has challenges to overcome and new reactivity modes to be discovered. We chose to remain in the field of group IX metal catalyzed allylic C–H functionalization via π -allyl intermediates, the recently developed allylic C–H amidation provides an excellent platform for a conceptual advance in chiral catalysis. The data strongly suggests that the C–N bond forming step is the result of the reductive elimination from a rhodium(V) or iridium(V) intermediate so we hypothesize that a novel chiral ligand would afford an enantioselective allylic C–H amidation.²

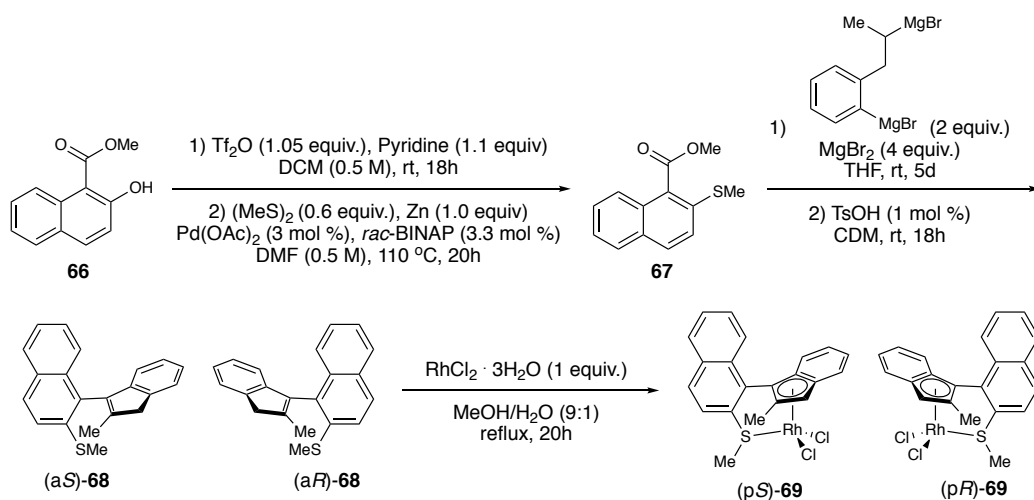
Scheme 3-1. Baker's discovery of an enantioselective allylic C–H alkylation utilizing asymmetric rhodium(III) π -allyl complexes.¹²



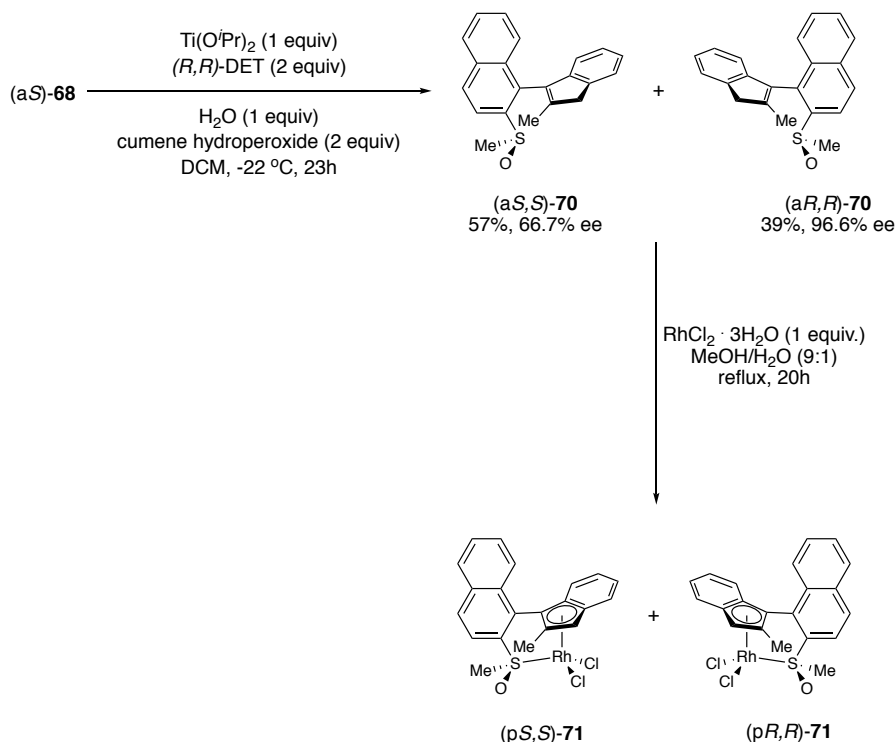
A recent publication from the Baker group described a stereoselective allylic C–H alkylation of (*E*)-2-pentene with the sodium salt of dimethyl malonate (**Scheme 3-1**).¹³⁻¹⁴ Baker utilized his rhodium(III) chiral indenyl sulfide complex (*pS*)-**63** to synthesize rhodium(III) indenyl π -allyl complex (*pS*)-**63**. Although he was unable to crystallize the π -allyl complex to determine the stereochemistry of the complex, in a previous publication Baker and co-workers were able to crystallize the rhodium(III) dichloride complex with the indenyl sulfide ligand.¹⁵ Baker and co-workers were able to assign the stereochemistry of the π -allyl complex by analogy with their previous publication and characterization using 2D NMR techniques coupled with density functional theory (DFT) calculations provided evidence for the π -allyl structure shown in **Scheme 3-1**. Baker observed coupling of the carbons on the five membered ring of the indene to the rhodium nucleus. This coupling suggests that the carbons on the five-membered ring of the indene are in close proximity to the metal center. Indenyl ligands, like the Baker ligand, are known to ring-slip from an η^5 -coordination towards an η^3 -coordination, based on the electronic ligand environment around the metal center (**Scheme 3-1**).¹⁶⁻¹⁹ In some most cases, the indenyl ligand undergoes a degree of distortion, where the benzo portion of the ligand lifts slightly off the metal but not fully. In most cases, the ring-slip from η^5 - towards η^3 -coordination can facilitate an associative mechanism for ligand exchange.¹⁸ The observed η^5 -coordination distortion in Baker's

ligand provides an element of asymmetry in the π -allyl ligand which provides a chiral environment for the allylic C–H alkylation. Exposing the enantioenriched π -allyl complex **63** to the sodium salt of dimethyl malonate affords **64** in moderate yield and enantioselectivity (68% yield, 66% ee). The stoichiometric results presented by Baker provided evidence that a chiral indenyl ligand may provide an asymmetric π -allyl complex and afford enantioenriched allylic products upon exposure to a suitable nucleophile.

Scheme 3-4. Baker's synthesis and structure of planar chiral bidentate indenyl-sulfinyl complexes of rhodium(III).¹⁴⁻¹⁵



Scheme 3-5. Baker's oxidation of (pS)-70 for chiral resolution protocol.



The synthesis and enantioenrichment of indenyl catalyst (*pS*)-69 is laborious and necessitates multiple chiral resolutions. The synthesis of enantiopure ligand **68** begins with the four step sequence to furnish racemic ligand, including the use of a di-Grignard reagent, subsequently followed by an asymmetric sulfoxidation with titanium(IV) isopropoxide and (*R,R*)-tartrate. The asymmetric sulfoxidation afforded the diastereomers (*aR,R*)-70 and (*aS,R*)-70 in 57% and 39% yield, respectively, and with moderate to excellent enantioselectivities ((*aR,R*)-70, 66.7% ee and (*aS,R*)-70, 96.6% ee). Once the two diastereomers were obtained, a recrystallization and subsequent deoxygenation afforded (*aS*)-68 in >98% ee. Accessing (*aR*)-68 required significantly more chiral resolution steps. Firstly, the asymmetric sulfoxidation with (*R,R*)-tartrate provided a lower enantiopurity (66.7% ee) for the (*aR,R*)-70 because of mismatched substrate and catalyst pair. In order to afford high levels of enantiopurity, deoxygenation of (*aR,R*)-70, oxidation via Kagan

sulfoxidation with (*S,S*)-tartrate, and another deoxygenation was necessitated. After (*aR*)-**68** and (*aS*)-**68** were obtained, complexation with rhodium trichloride provided (*pR,R*)-**69** and (*pS,S*)-**69**, respectively. The synthesis of the Baker chiral indenyl ligand is not efficient or modular, due to the multiple redox steps, difficult chiral resolutions, and long linear synthetic sequences.

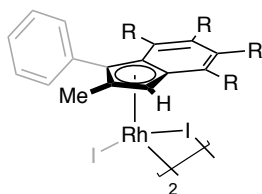


Figure 3-5. Simplified asymmetric rhodium(III) complex with simplified ligand structure.

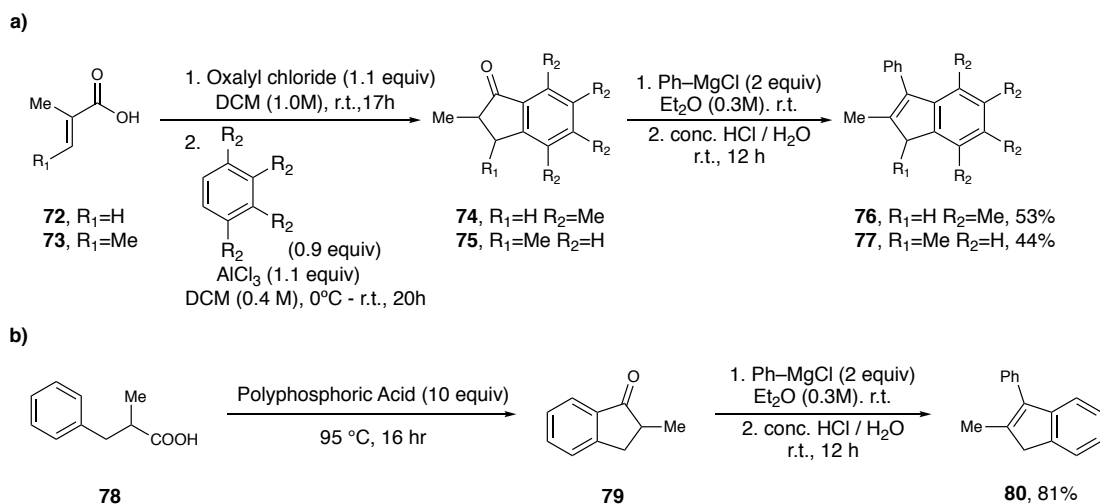
We hypothesized that the simplified indenyl ligand structure in **Figure 3-5** would afford catalytically active complexes, while still providing a chiral environment for stereoselective product formation. By stripping off some of the molecular complexity of the Baker complex **70**, we could simplify the synthesis of the rhodium(III) complex and provide the opportunity for a modular synthesis.

3.3 Development of Catalyst for enantioselective allylic C–H amidation

We recognized that known 2-methyl-3-phenylindene (**80**) presents as a viable ligand, by providing simplified planar chirality and ease of synthesis. The ligand is accessible via a two-step modular synthesis starting from 2-methylindanone and phenyl magnesium bromide (**Scheme 3-6**). More derivatives of this ligand scaffold can be achieved by utilizing various 2-methylindanones, such as 2,3-dimethylindanone, 2,4,5,6,7-pentamethylindanone, and 2,3,4,5,6,7-hexamethylindanone (**Scheme 3-6**). We hypothesized that additional methyl groups incorporated into the indene scaffold would enhance reactivity similar to Cp variants, as outlined by Rovis.²⁰ The methyl groups increase electron density on the metal center, providing greater π -backbonding, making the resulting

complexes more easily oxidized. In our seminal publication outlining allylic C–H amination and racemic allylic C–H amidation, we found that rhodium(III) Cp was not an effective catalyst but rhodium(III) Cp* was an efficient catalyst. This suggests that the allylic C–H functionalization benefits from the increased electron density on the metal. These observations led us to design and synthesize a library of indenyl ligands with varying methyl substitution.

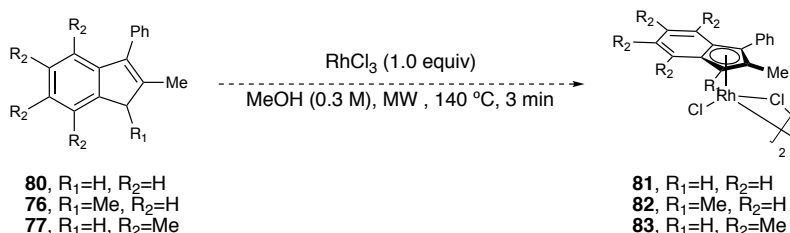
Scheme 3-6. Synthesis of substituted indenyl ligands.



In order to synthesize this library of catalysts, we first synthesized each indanone precursor (74, 75 and 77). Indanone 74 and 75 were derived from α,β -unsaturated carboxylic acid 72 or 73 (Scheme 3-6a). The carboxylic acid was converted to the acid chloride with oxalyl chloride, followed by Friedel-Crafts acylation and subsequent Nazarov cyclization afforded indanone 74 and 75. While 2-methyl-3-phenyl indanone (80) can be synthesized via the method in Scheme 3-6b, Christopher Poff found that we could eliminate a step by utilizing commercially available 78 in a polyphosphoric acid mediated cyclization. This change reduced the step-count and provided a more efficient and scalable reaction. After a Grignard reaction with phenylmagnesium bromide and alcohol dehydration, indenyl ligands 76, 77, and 80 were isolated in moderate to excellent yield (76, 53%

yield, **77**, 44% yield, and **80**, 81% yield). The addition of phenyl magnesium bromide to each respective indanone afforded a tertiary alcohol intermediate, which consequently eliminates upon the introduction of hydrochloric acid. Reaction progress was monitored by thin layer chromatography, since the tertiary alcohols and indene products (**76-77**, **80**) were stable on silica gel. The indene products are especially non-polar, and purification of these products by chromatography on silica gel required the use of hexane, toluene, or a mixture of these two solvents as the mobile phase..

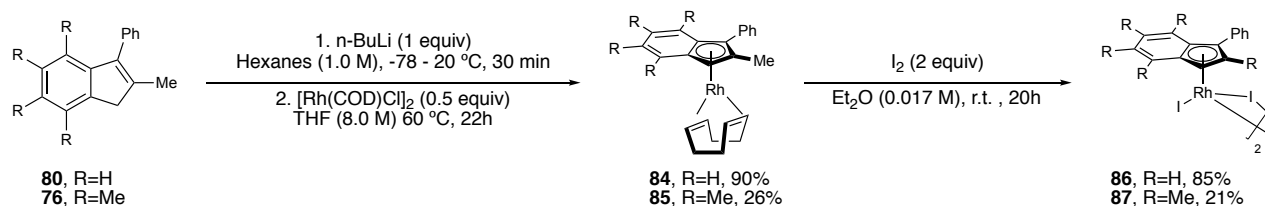
Scheme 3-7. Proposed complexation of indene ligands 76-77 and 80 with rhodium(III) chloride.



Once a small library of ligands were synthesized, we explored complexation with rhodium(III) chloride to afford the rhodium(III) indenyl chloride dimers (**Scheme 3-7**). These complexes were desired for comparison to the rhodium(III) pentamethylcyclopentadienyl (Cp*) dichloride catalyst prevalent in C–H functionalization literature. We were able to synthesize complex **82**, by modification of the rhodium(III) Cp* synthesis, but complexes **81** and **83** were never observed under these conditions (**Scheme 3-7**). While this synthetic route enabled quick access to racemic catalyst, we could not resolve the resulting dimer **81** by any chiral methods available to our lab due to the complex's limited solubility in organic solvents. In researching other methods of accessing rhodium(III) indenyl dichloride dimers, we discovered methodology which afforded rhodium(III) indenyl diiodide dimers via a rhodium(I) cyclooctadienyl (COD) intermediate (**Scheme 3-8**). This discovery provided advances from our previous synthesis; firstly, the rhodium(I) COD

intermediate provides an alternate complex for chiral resolution and secondly, the rhodium(III) dibromide or dichloride dimers could be synthesized using different oxidants. Thus, we set out to synthesize complexes **85** and **86** via this method.

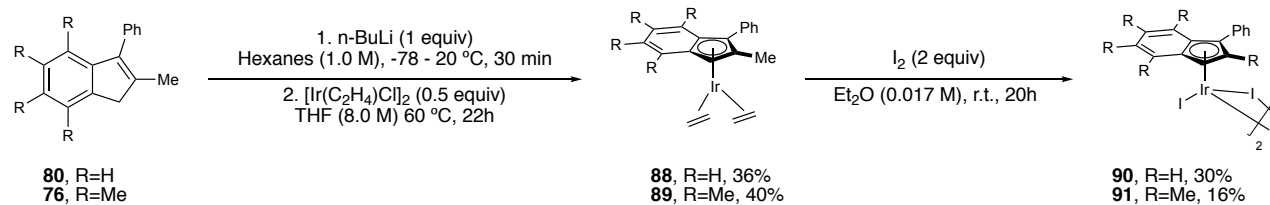
Scheme 3-8. Complexation of indene ligands **78 and **75** via rhodium(I) cyclooctadiene ([Rh(COD)Cl]₂).**



Each ligand underwent complexation with [Rh(I)(COD)Cl]₂ to afford a racemic mixture of planar chiral COD complexes **84** and **85** in modest to excellent yields (26%-90%) (**Scheme 3-8**). In initial studies, the indene ligand was deprotonated with *n*-BuLi to provide the necessary organolithium for the ligand exchange. The reaction yields were variable with *n*-BuLi, therefore Christopher Poff screened several bases and found that KO^{*t*}Bu allowed for scalable reactions and synthetically useful yields. Alongside the rhodium(III) dimers, we wanted to explore the reactivity of iridium(III) dimers as catalyst for allylic C–H amidation due to their documented complementary reactivity.² We synthesized iridium(III) indenyl diiodide dimers **86** and **87** by a similar sequence of steps (**Scheme 3-9**). The major change occurred because the iridium(I) indenyl COD monomers were not stable to isolation or purification, so the iridium(I) indenyl bisethylene monomers **88** and **89** were synthesized instead.

Scheme 3-9. Complexation of indene ligands **80** and **76** via iridium(I) bisethylene

($[\text{Ir}(\text{C}_2\text{H}_4)\text{Cl}]_2$).



Next we began exploring the chiral resolution of the rhodium(I) COD (**84-85**) and iridium(I) bisethylene (**88-89**) monomers. The racemic COD or bisethylene complexes were subjected to chiral HPLC column to determine if separation was achievable on chiracel AD-H, OD-H, OJ-H and AS-H. After a screening all chiral columns, we found that the enantiomers of monomer **84** were separable on both a chiracel AD-H and OD-H column and monomers **85** and **88-89** were separable on the OD-H column only. At the time of this discovery, we only had access to a chiral semi-preparatory AD-H column and thus we proceeded to resolve the Rh(I) COD monomer **84**. Using 1% iso-propanol in hexanes as the mobile phase, we were able to resolve 100 mg of monomer **84** via multiple 10-15 mg injections. In order to determine that the isolated monomer was enantiomerically pure, we would not collect the fractions that were a mixture and would run each isolated batch of monomer on the analytical chiral HPLC to determine the enantiomeric ratio. It was discovered that instead of waiting for each run to complete, we were able to stagger each run to get more material resolved at a given time. With minimal loss from transferring and isolating the enantiomers, enough enantiopure monomers, the first enantiomer that eluted off the column (*en1-86*) and the second enantiomer that eluted off the column (*en2-86*), were present to begin oxidation to the diiodide dimer precatalyst. All of the other monomers were separated by the same procedure on either the AD-H or OD-H column, depending on degree of separation.

The rhodium(I) COD monomers and iridium(I) bisethylene monomers were oxidized to the corresponding rhodium(III) or iridium(III) indenyl diiodide dimers directly after chiral resolution.

Each individual enantiomer was oxidized separately to the rhodium(III) or iridium(III) diiodide dimer with iodine at room temperature (**Scheme 3-8** and **3-9**). The rhodium(III) and iridium(III) diiodide dimers precipitated out of solution and were isolated by filtration using a Büchner funnel with filter paper. The solid diiodide dimers were rinsed thoroughly with diethyl ether to remove excess iodine and dried to remove residual diethyl ether. The rhodium(III) dimers **86** and **87** were dark maroon in color, while the iridium(III) diiodide dimers **90** and **91** were brown/black. All of the dimers had minimal solubility in dichloromethane (DCM) but were completely soluble in dimethylsulfoxide (DMSO).

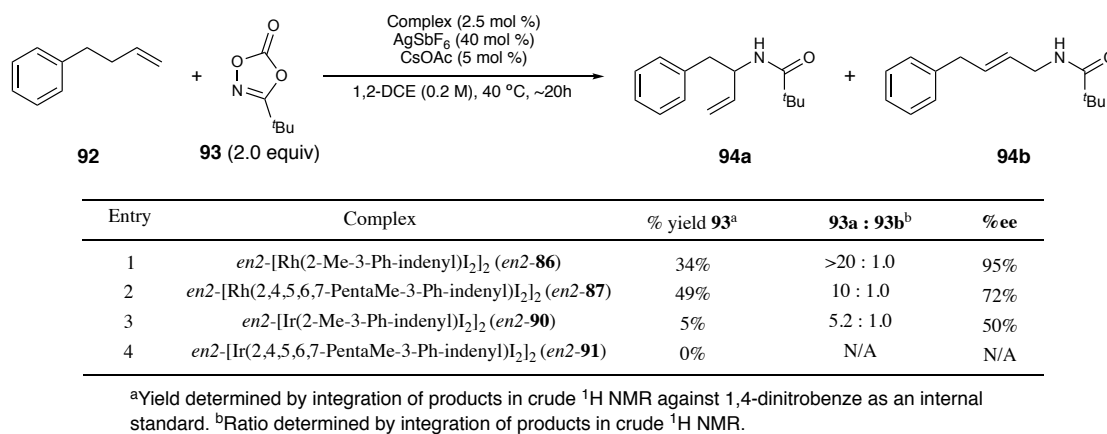


Figure 3-6. Allylic C–H amidation with novel rhodium(III) and iridium(III) planar chiral indenyl complexes.

Once the enantiopure rhodium(III) and iridium(III) indenyl diiodide dimers were obtained, we were able to test the complexes for efficiency, regioselectivity and enantioselectivity in allylic C–H amidation. 4-phenylbutene and *t*-butyl dioxazolone were used as the test reaction because with racemic Cp* catalysts there was moderate reactivity with rhodium and iridium and the olefin was commercially accessible (**Figure 3-6**). Complex *en2*-**86** afforded a modest yield (34%) and excellent e.r. (95% ee), while complex *en2*-**87** provided an increase in yield (45%) and only modest enantioselectivity (72% ee). The iridium(III) complex *en2*-**90** was not as efficient or selective (5%,

50% ee) and complex *en2-91* was not an effective catalyst. Since we are seeking to develop an enantioselective allylic C–H amidation, we decided to move forward with rhodium(III) complex **86**.

3.4 Determining Catalyst and Substrate Stereochemistry

Christopher Poff was able to determine the stereochemistry of the rhodium(III) indenyl diiodide complex by isolating and characterizing the corresponding π -allyl complex. We hypothesize that once the facial selectivity for indene coordination occurs, the ligand does not dissociate from the metal center. This is supported by the high levels of enantioinduction in the allylic C–H amidation and absence of free ligand in reaction workup. We were able to isolate rhodium(III) indenyl π -allyl complex **95** by subjecting the enantiopure rhodium(III) diiodide dimer *en1-86* to AgSbF_6 , CsOAc and 2-pentene (**Figure 3-7a**). The π -allyl complex was purified by column chromatography and isolated in moderate yield (32% yield). In previous allylic C–H functionalization projects, we have observed that many of the Cp^* and indenyl π -allyl complexes are stable on silica gel. After isolation of the π -allyl complex **95**, single x-ray crystals were obtained via vapor diffusion of pentane into chloroform. The x-ray crystallographic data revealed that the selected enantiomer of the catalyst afforded the (*S*)- π -allyl complex **95**. We assigned the stereochemistry of rhodium(III) indenyl diiodide dimer *en1-86* as (*S,S*) by x-ray crystallographical analysis. We must assume that the indenyl ligand does not switch facial coordination when forming the π -allyl complex. Now that we have assigned the stereochemistry of the rhodium(III) indenyl complex (***S,S*-86**), Christopher Poff then proceeded to determine the stereochemistry of the amide products.

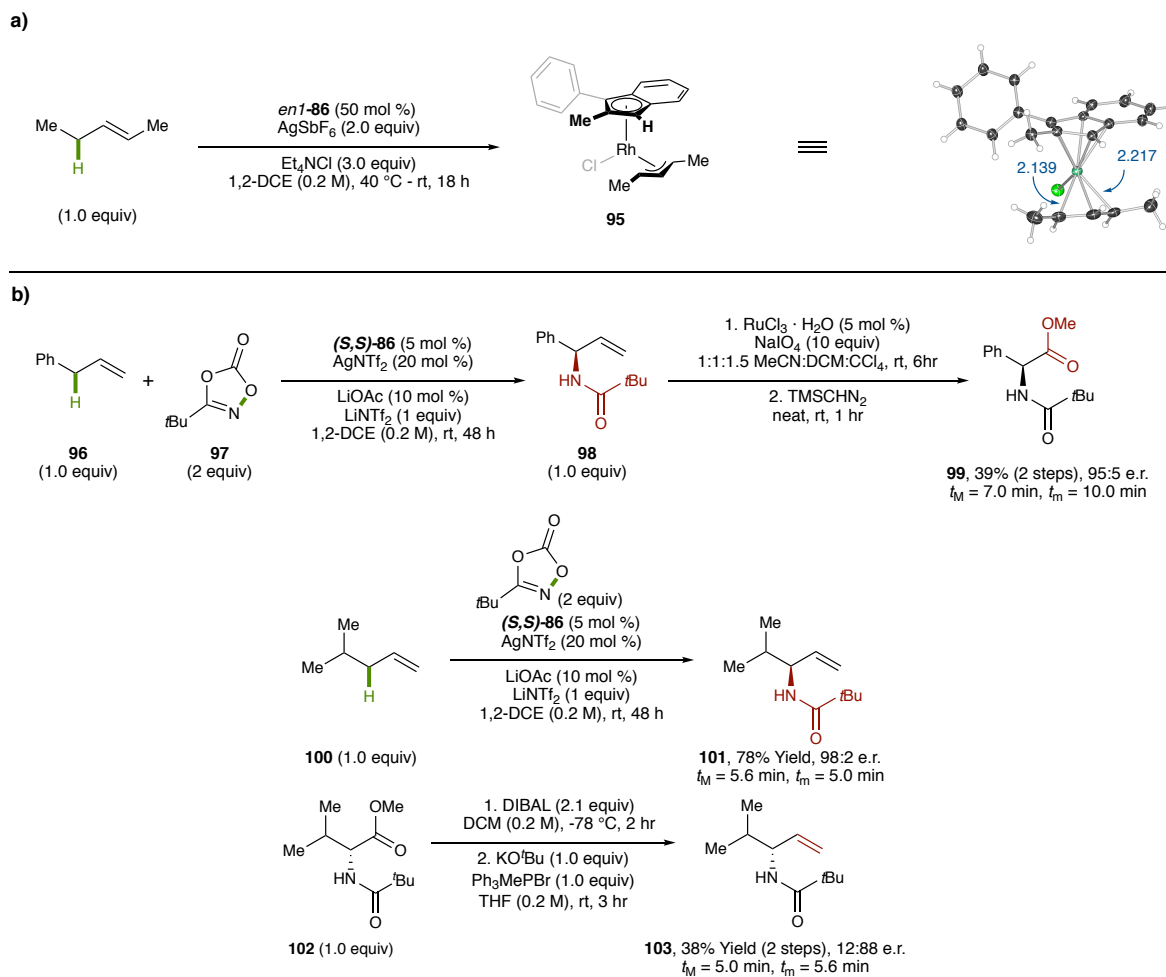


Figure 3-7. Stereochemical assignment of rhodium(III) complex **86 and stereochemical determination of aryl and alkyl amide products.**

The stereochemistry of the amide products was determined by comparison to natural or unnatural amino acids (**Figure 3-7b**). Christopher Poff analyzed alkyl and aryl substituted olefins so each class of product was represented and assumptions could be made for the remainder of the substrates. First, allyl benzene **96** was subjected to allylic C–H amidation conditions with *(S,S)-86* as the precatalyst to afford amide **98** (78% yield). It was observed that methyl pivaloyl-*D*-valinate (**98**), the amino acid derivative we chose to target, was not detectable by the UV-Vis detector on the chiral HPLC. As a result, methyl pivaloyl-*D*-valinate (**99**), synthesized according to the published

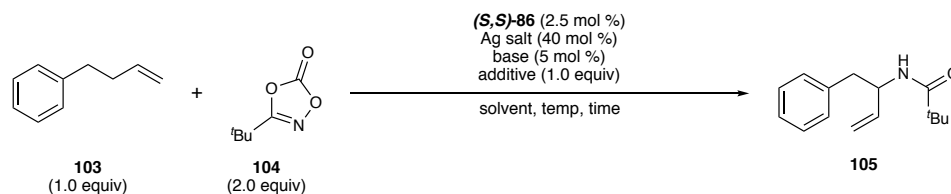
procedure, was subjected to a DIBAL reduction and subsequent Wittig reaction to afford allylic C–H amidation product. Since the stereochemistry of the valine starting material is known, we can conclude that we synthesized the (*R*)-enantiomer of amide **98**. Once the retention time of the (*R*)-enantiomer on our chiral HPLC column is known, we gain the ability to compare the retention time to the chiral HPLC trace of the amide produced from the catalytic reaction. This method of stereochemical analysis determined that (***S,S***)-**86** catalyzed allylic C–H amidation of 4-methylpentene gives the (*S*)-enantiomer of amide **101**. All other olefin substrates that proceed through a similar alkyl substituted π -allyl complex were assigned stereochemistry by analogy. However, we were not able to use this analogy for substrates proceeding through an aryl substituted π -allyl complex so we needed to establish the stereochemistry of a representative amide. Chris chose to analyze the allylic C–H amidation of allyl benzene with *tert*-butyl dioxazolone. Allylbenzene was subjected to allylic C–H amidation conditions with *tert*-butyl dioxazolone and (***S,S***)-**86**, oxidative cleavage of the olefin, and subsequent methylation to afford methyl ester **102**. This product is simply pivaloyl-protected phenyl-glycine methyl ester, meaning the retention times can be compared directly to determine the stereochemistry of the methyl ester **102** and amide **101**. Christopher Poff found that catalyst (***S,S***)-**86**, affords the (*R*)-enantiomer of amide **101**, all other substrates resembling allyl benzene were assigned stereochemistry by analogy.

3.5 Reaction development: rhodium(III) indenyl catalyzed allylic C–H amidation

We sought to find optimal reaction conditions for allylic C–H amidation using catalyst **86**. We initiated our studies utilizing the optimized conditions from our discovery of the racemic allylic amidation reaction.² With 2.5 mol % of racemic precatalyst (***S,S***)-**86**, CsOAc as a soluble carboxylate source to promote the concerted metalation-deprotonation (CMD) mechanism, and AgSbF₆ as a dual halide scavenger and oxidant in 1,2-dichloroethane (1,2-DCE) at 40 °C for 24 hours, 4-

phenylbutene (**103**) was successfully amidated in 26% yield with exceptional enantioselectivity (**Table 3-1, entry 1**, 94:6 e.r.). Substituting LiOAc for CsOAc, as our acetate source, provided a boost in enantioselectivity (96:4 e.r.) while maintaining a modest yield (**Table 3-1, entry 2**). Exploring fluorinated solvents, such as 1,1,1-trifluoroethanol (TFE) and 1,1,1,3,3,3-hexafluoro-2-propanol (HFIP), did not improve the yield of reaction (**Table 3-1, entry 3 & 4**). Limited solubility was observed for catalyst (**S,S**)-**86** in HFIP during reaction set-up which lead to difficulty reliably transferring reagents into the reaction flask. After a small silver salt screen, AgNTf₂ promoted a higher yield while maintaining enantioselectivity (**Table 3-1, entry 5**, 38%, 95:5 e.r.). We hypothesized that lithium cations might bind to the product and prohibit catalyst inhibition or arrest. Introduction of LiNTf₂ (1 equiv) as an additive, lowering the temperature (30 °C), and extending the reaction time (48 h) delivered modest increase in yield without affecting enantioselectivity (**Table 3-1, entry 6**, 50%, 95:5 e.r.). Doubling catalyst loading and only introducing enough halide scavenger for the four halides on the catalyst afforded the optimal reaction conditions for the regio- and enantioselective allylic C–H amidation (**Table 3-1, entry 10**, 68%, 95:5 e.r.).

Table 3-1. Optimization of enantioselective allylic C–H amidation.

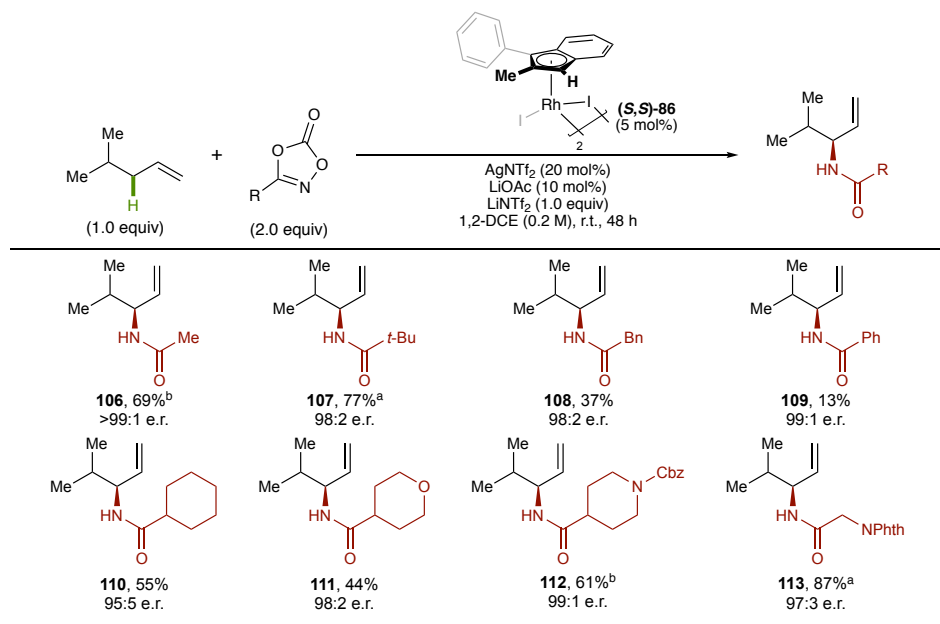


entry	Ag salt	base	additive	temp	time	solvent	% yield ^a	e.r. ^b
1	AgSbF ₆	CsOAc	—	40 °C	24 h	DCE	26	94 : 6
2	AgSbF ₆	LiOAc	—	40 °C	24 h	DCE	25	96 : 4
3	AgSbF ₆	LiOAc	—	40 °C	24 h	TFE	0	N/A
4	AgSbF ₆	LiOAc	—	40 °C	24 h	HFIP	26	96 : 4
5	AgNTf ₂	LiOAc	—	40 °C	24 h	DCE	38	95 : 5
7	AgNTf ₂	LiOAc	LiNTf ₂	30 °C	48 h	DCE	50	95 : 5
8	AgNTf ₂	LiOAc	LiNTf ₂	20 °C	48 h	DCE	52	96 : 4
9 ^c	AgNTf ₂	LiOAc	LiNTf ₂	20 °C	48 h	DCE	55	95 : 5
10 ^f	AgNTf ₂	LiOAc	LiNTf ₂	20 °C	48 h	DCE	68	95 : 5

^aYield determined by integration of products in crude ¹H NMR against 1,4-dinitrobenzene as an internal standard.

^bEnantiomeric ratio was determined by chiral HPLC on OD-H column in 5% isopropanol. ^c15 mol % AgNTf₂ and 20 mol % LiOAc. ^e5 mol % [Rh(2-methyl-3-phenylindene)I₂]₂. ^f5 mol % [Rh(2-methyl-3-phenylindene)I₂]₂ and 20 mol % AgNTf₂.

Amaan, Christopher and myself sought to explore functional group tolerance in relation to the dioxazolone reagent after establishing conditions for efficient regio- and enantioselective allylic C–H amidation. A simple feedstock olefin, 4-methyl-1-pentene, was selected and effectively amidated with a variety of functionalized dioxazolone reagents (**Figure 3-8**). Alkyl substituted dioxazolones, such as methyl, *tert*-butyl, cyclohexyl and benzyl dioxazolone, provided amide products **106-108** and **110** in moderate to good yields (37-77% yield) and excellent enantioselectivity (95:5 to >99:1 e.r.). The reaction conditions tolerated dioxazolones with both ether and carbamate functionality, affording amides **111** and **112** in 44% and 61% yield and 98:2 and 99:1 e.r. respectively. We desired to emphasize the utility of amino acid derived dioxazolones so we included a phthaloyl-glycine-derived dioxazolone, which afforded amide **113** in 87% yield and 97:3 e.r.. Only modest yield (13% yield) of amide **109** was achieved with phenyl dioxazolone, while maintaining high enantioselectivity (99:1 e.r.). The observed reduction in yield with aryl dioxazolones is consistent with data from previous racemic reactions with rhodium(III) Cp* and iridium(III) Cp* catalysts.²



Reactions were run on 0.10 mmol scale. Isolated yields are reported, and enantiomeric ratios were determined by chiral HPLC. ^aReaction ran by Christopher Poff. ^bReaction ran by Amaan Kazerouni.

Figure 3-8. Scope of dioxazolone substrates for enantioselective allylic C–H amidation of 4-methylpentene.

To exemplify the robustness of this reaction, we chose to explore the olefin scope utilizing an electron-rich dioxazolone, *tert*-butyl, and an electron-poor dioxazolone, *N*-phth-glycine (**Figure 3-9**). The amidation of hex-1-ene with *tert*-butyl dioxazolone afforded branched amide **114** in 51% yield and 98:2 e.r., while the *N*-phth-glycine amide product **115** was isolated in 81% yield and 93:7 e.r.. *N*-phthalimide hex-1-ene was an effective substrate for *tert*-butyl dioxazolone (**116**, 90% yield, 98:2 e.r.) and *N*-phth-glycine dioxazolone (**117**, 73% yield, 92:8 e.r.). An olefin containing a silyloxy substituent afforded *tert*-butyl amide **118** in 49% yield and 90:10 e.r., while isolation of *N*-phth-glycine amide **119** in 22% yield and 97:3 er. required elevated temperature. The reaction performed well on 4-phenylbut-1-ene with no olefin isomerization, providing amides **122** and **123** in good yields and excellent enantioselectivities (**122**, 57% yield, 98:2 e.r. and **123**, 45% yield, 95:5 e.r.). Branched amides **124** and **125** were isolated in 69% and 33% yield, respectively, and 93:7 e.r. when

allylbenzene was subjected to reaction conditions. Good enantioselectivities were seen when 1,3-diphenylpropene was subjected to reaction conditions (**126**, 24% yield, 96:4 e.r. and **127**, 44% yield, 79:21 e.r.). Amides **128** and **129**, arising from an unsymmetrical, internal olefin, were observed in moderate to excellent levels of regio- and stereoselectivity with *tert*-butyl dioxazolone (**128**, 23% yield, >20:1 r.r., 99:1 e.r.) and *N*-phth-glycine dioxazolone (**129**, 74% yield, 4:1 r.r., 98:2 e.r.).

Amidation of an olefin with a homoallylic stereocenter afforded amides **120** and **121** as exclusively one diastereomer (**120** and **121**, >20:1 d.r.). While the (*R,R*) pre-catalyst and homoallylic stereogenic substrate provide modest yields (**120**, 37% yield and **121**, 41% yield), the (*S,S*) pre-catalyst afforded no reaction under identical conditions. This result revealed that with the (*R,R*) pre-catalyst we have a matched scenario, but with the (*S,S*) pre-catalyst it is mismatched. We hypothesize that the synthesis of a wide-range of planar chiral indenyl catalysts will provide a solution to the match verses mismatch allylic C–H amidation.

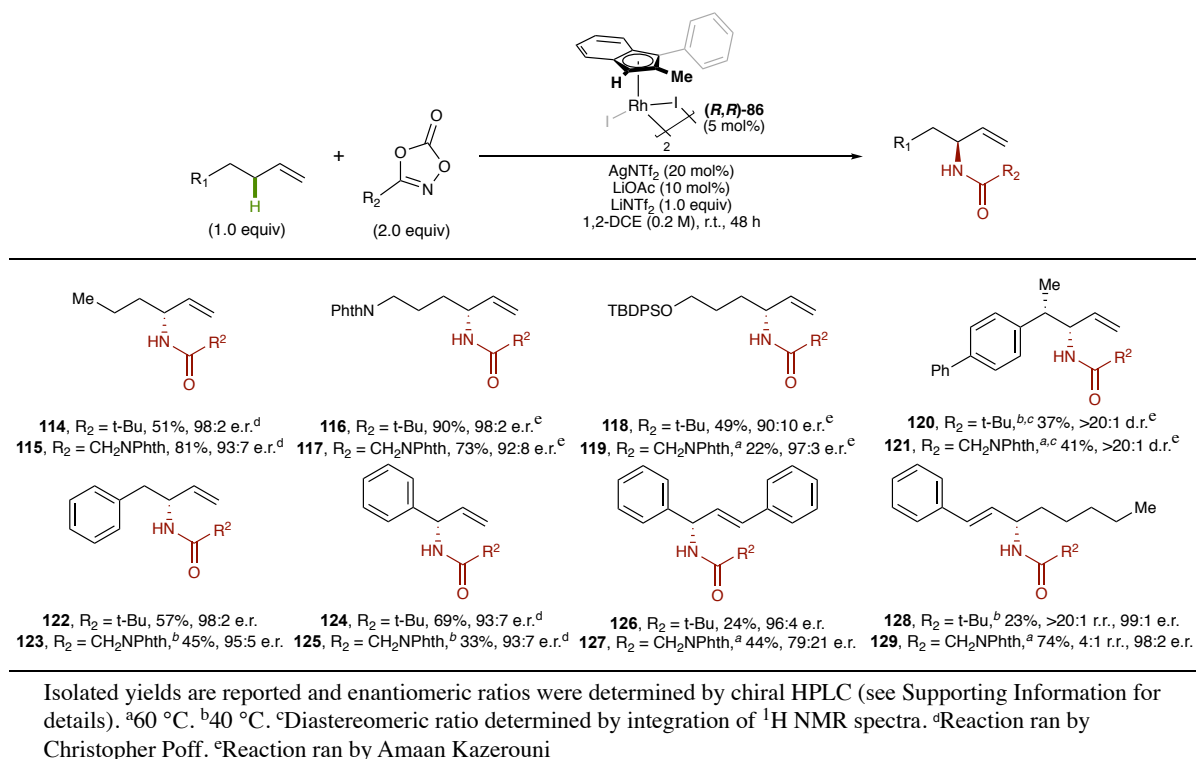


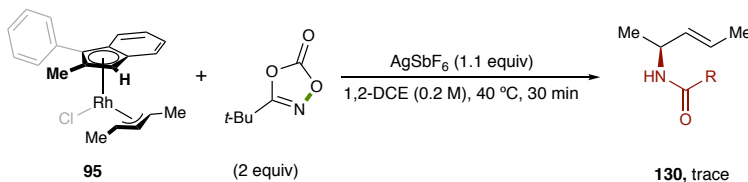
Figure 3-9. Scope of olefin substrates for enantioselective allylic C–H amidation with *tert*-butyl dioxazolone and *N*-phth-glycine dioxazolone.

In exploring the olefin scope for this reaction, we observed that at lower temperatures electron rich or Lewis basic dioxazolones performed more efficiently. This is supported by the *tert*-butyl dioxazolone results providing optimal yields at room temperature in **Table 3-1**. Conversely, less electron rich dioxazolones, such as *N*-Phth-glycine dioxazolone, required use of elevated temperatures to increase yield or, in the case of the silyloxy substrate, even provide the amide product. We postulate that more Lewis basic dioxazolones are able to coordinate to the catalyst and compete with π -allyl formation. The coordination of the dioxazolone, we hypothesize, leads to detrimental side reactions and catalyst arrest. We observed that lower reaction temperatures diminished the effects of the off-cycle pathways while allowing the productive reaction to proceed more efficiently.

3.6 Reaction Mechanism and Stoichiometric Studies

Our group and the Rovis group previously reported stoichiometric and kinetic studies for iridium(II) and rhodium(III) Cp* catalyzed allylic C–H amidation.² The isolation, characterization and subsequent reactions of both the iridium(III) and rhodium(III) Cp* π -allyl complexes suggests that they are intermediates in the catalytic cycle. When the iridium(III) and rhodium(III) Cp* π -allyl complexes were subjected to *tert*-butyl dioxazolone and AgSbF₆, as a halide scavenger, the regioselectivities mirrored the catalytic reactions. Christopher Poff conducted a similar experiment with (*S*)- π -allyl complex **95** and found that the stoichiometric reaction afforded the same regioisomer and major enantiomer of amide **130** as the catalytic reaction (**Scheme 3-10**). This observation supports the hypothesis that both the racemic and enantioselective allylic C–H amidations proceed via a metal(III) Cp* π -allyl complex, rather than through the direct insertion of a metallonitrene species into the allylic C–H bond. Moreover, the Rovis group's isotopic competition experiments revealed that C–H activation is irreversible and C–H cleavage may be involved in the rate-determining step of the reaction.

Scheme 3-10. Stoichiometric reaction with (*S,S*)-95** and 2-pentene.**



In collaboration with the Baik group, density functional theory (DFT) calculations were used to propose a tentative mechanism and determine the origin of regio- and enantioselectivity. We were able to calculate the complete energy profile for the reaction of allylbenzene and *tert*-butyl dioxazolone with (*R,R*)-[Rh(2-Me-3-Ph-Ind)₂]₂ (**(*R,R*)-85**) as the catalyst (**Figure 3-10**). The

coordination of the olefin, allylbenzene, to rhodium cationic complex **A** is reversible, allowing the olefin to bind to both faces of the catalyst without discrimination (**B** and **B'**). The allylic C–H activation step proceeds via a concerted-metalation-deprotonation (CMD) mechanism which has a 18.8 and 19.9 kcal/mol barrier, respectively. This high barrier suggests that the C–H activation step is rate-limiting. The chiral indenyl ligand favors the **B-TS** transition state, which positions the phenyl of the olefin substrate away from the phenyl substituent on the indenyl ligand. Positioning the two phenyl groups in close proximity, **B'-TS**, to each other leads to a barrier that is 1.1 kcal/mol higher in energy. The enantioselectivity of the reaction is determined when π -allyl complexes **C** and **C'** are formed because the subsequent steps retain the stereochemical information. Once dissociation of the acetic acid from complex **C** occurs, one equivalent of *tert*-butyl dioxazolone binds to the metal center.

The dioxazolone is able to bind in order to form two different conformations, **E** and **E''**. The *tert*-butyl group on the dioxazolone is positioned *syn* to the π -allyl portion of the complex in complex **E**, whereas in complex **E''** the *tert*-butyl group of the dioxazolone is *syn* to the phenyl group on the π -allyl. Due to the high energy of transition state **E''-TS**, the reaction proceeds to give complex **F** via CO₂ liberation instead of the thermodynamically favored **F''**. This step of the reaction is irreversible and under kinetic control. After forming imido complex **F**, a low energy reductive elimination occurs at the branched position of the π -allyl moiety via transition state **F-TS**¹. Experimentally, we observe exclusively the branched amide products which is in agreement with the large energy difference present between **E-TS** and **E''-TS** and subsequent formation of **F** instead of

F''. This suggests that while enantioselectivity is determined when the π -allyl is formed, the regioselectivity is set upon liberation of CO_2 from complex **E** giving rise to imido complex **F**.

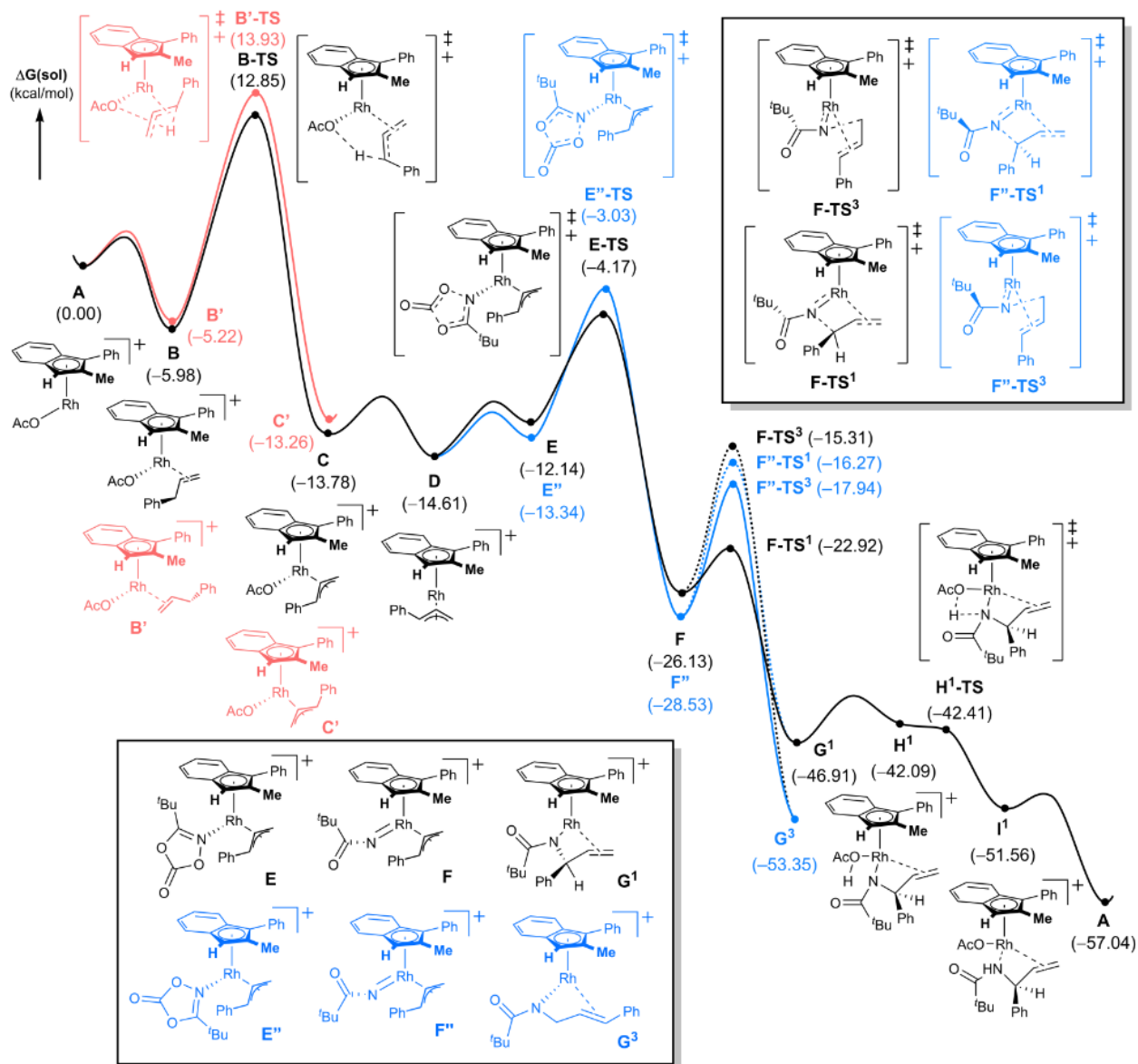


Figure 3-10. Complete energy profile diagram for the enantioselective allylic C–H amidation of allylbenzene and *tert*-butyl dioxazolone.

After combining all of the computational studies, experimental observations, and previously reported stoichiometric investigations, we propose the catalytic cycle in **Figure 3-10**. Firstly, the dimeric precatalyst **85** undergoes activation by AgNTf_2 and LiOAc to form complex **I**, which has an open coordination site. After olefin coordination, complex **II** is formed and is set-up for the enantiodetermining C–H activation step to form π -allyl complex **III**. Next, dioxazolone coordination to the metal center and subsequent CO_2 liberation affords imido complex **IV**, which can reductively eliminate to form the branched allylic C–N bond. Lastly, protodemetalation of complex **V** and coordination of acetate gives the desired product and regenerates the active catalyst, **I**

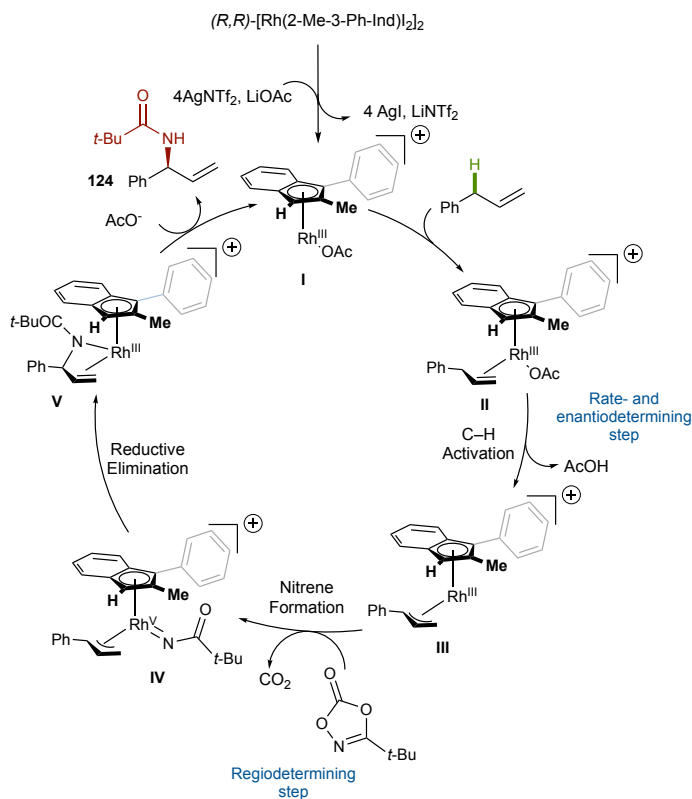


Figure 3-11. Proposed catalytic cycle for enantioselective allylic C–H amidation with planar chiral rhodium(III) indenyl complex **(R,R)-86**.

3.7 Conclusion and Future Directions

We have successfully designed a novel family of planar chiral group IX metal complexes for regio- and enantioselective allylic C–H amidation. We have disclosed an efficient synthesis of a small library of indenyl ligands from readily accessible starting materials. The enantioselective allylic C–H functionalization reaction displays large functional group tolerance in both the olefin and dioxazolone substrates while achieving high enantiomeric ratios in an array of allylic amide products. The reaction also allows quick introduction of molecular complexity to feedstock olefins, such as hexene and 2-methylpentene. Through stoichiometric studies and computational investigations, we were able to propose a catalytic cycle which includes a rate-determining C–H functionalization step, enantio-determining π -allyl forming step and regio-determining nitrenoid formation.

Our group is working to expand this new family of chiral indenyl catalysts to include other group IX metals and the addition of a wide array of functional groups on the indenyl ligand scaffold. We envision that this family of catalysts will have broad applicability to induce asymmetry in other reactions where Cp-variants are utilized. We would like to explore the catalysts utility in direct C–H functionalizations, where steric chiral Cp-variants are currently used. We also propose that derivatization of the ligand by incorporation of heteroatoms would alter the reactivity and electronic environment of the catalyst.

3.8 Experimental Procedures

General Information

All reactions were carried out under nitrogen atmosphere with anhydrous solvents in oven- or flame-dried glassware using standard Schlenk technique, unless otherwise stated. Anhydrous dichloromethane (DCM), diethyl ether (Et₂O), tetrahydrofuran (THF), and toluene were obtained by passage through activated alumina using a *Glass Contours* solvent purification system. 1,2-dichloroethane (DCE), 2,2,2-trifluoroethanol, 1,1,1,3,3,3-hexafluoroisopropanol (HFIP) were distilled over calcium hydride (CaH₂) and stored over activated molecular sieves. Solvents for workup, extraction, and column chromatography were used as received from commercial suppliers without further purification. 2-methyl-3-phenyl-1*H*-indene (2-Me-3-Ph-Ind), ((±)-[Rh(2-Me-3-Ph-Ind)(COD)]), (*S,S*)-[Rh(2-Me-3-Ph-Ind)I₂]₂, and (*R,R*)-[Rh(2-Me-3-Ph-Ind)I₂]₂ were stored and weighed in a nitrogen-filled glovebox. All other chemicals were purchased from Millipore Sigma, Strem Chemicals, Oakwood Chemicals, Alfa Aesar, or Combi-Blocks and used as received without further purification, unless otherwise stated.

¹H and ¹³C nuclear magnetic resonance (NMR) spectra were recorded on a Varian Inova 600 spectrometer (600 MHz ¹H, 151 MHz ¹³C), a Bruker 600 spectrometer (600 MHz ¹H, 151 MHz ¹³C), a Varian Inova 500 spectrometer (500 MHz ¹H, 126 MHz ¹³C), and a Varian Inova 400 spectrometer (400 MHz ¹H, 126 MHz ¹³C) at room temperature in CDCl₃ (neutralized and dried over K₂CO₃ and activated molecular sieves) with internal CHCl₃ as the reference (7.26 ppm for ¹H, 77.16 ppm for ¹³C), unless otherwise stated. Chemical shifts (δ values) were reported in parts per million (ppm) and coupling constants (*J* values) in Hz. Multiplicity was indicated using the following abbreviations: s = singlet, d = doublet, t = triplet, q = quartet, qn = quintet, m = multiplet, br = broad. High resolution mass spectra (HRMS) were obtained using a Thermo Electron Corporation Finigan LTQFTMS (at the Mass Spectrometry Facility, Emory University). High Pressure Liquid

Chromatography (HPLC) was performed on an Agilent 1100 series HPLC utilizing CHIRALPAK AD-H, AS-H, OD-H and OJ-H 4.6 x 150 mm analytical columns and a 4.6 x 250 mm Whelk column by Regis Technologies. Analytical thin layer chromatography (TLC) was performed on precoated glass-backed Silicycle SiliaPure® 0.25 mm silica gel 60 plates and visualized with UV light, ethanolic *p*-anisaldehyde, ethanolic bromocresol green, or aqueous potassium permanganate (KMnO₄). Flash column chromatography was performed using Silicycle SiliaFlash® F60 silica gel (40-63 μm) on a Biotage Isolera One system. Preparatory TLC was performed on precoated glass-backed Silicycle SiliaPure® 1.0 mm silica gel 60 plates. We acknowledge the use of shared instrumentation provided by grants from the NIH and the NSF.

General Procedure A: Optimization of Enantioselective Allylic C–H Amidation

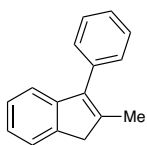
In a nitrogen-filled glovebox, base, silver salt, additive, and [Rh(2-Me-3-Ph-Ind)₂]₂ ((*R,R*) or (*S,S*), as indicated) were added to an oven-dried 4-mL vial equipped with a magnetic stir-bar and a teflon-septum screw cap. The vial was capped and brought out of the glovebox. 4-phenylbutene (0.015 mL, 0.10 mmol, 1.0 equiv) was added as a stock solution in DCE (0.25 mL), followed by *t*-Bu dioxazolone (0.0286 g, 0.20 mmol, 2.0 equiv) as a stock solution in DCE (0.25 mL). The reaction was stirred at the indicated temperature under a balloon of nitrogen for the time indicated. A solution of 1,4-dinitrobenzene (0.25 equiv) in dichloromethane was added as an internal standard. The reaction was filtered through a pipette containing celite with EtOAc (8 mL) and the filtrate was concentrated under reduced pressure. Product yield was determined by integration against 1,4-dinitrobenzene in the crude ¹H NMR spectra. Crude purification by preparatory thin layer chromatography on silica gel provided product for analysis by chiral normal phase HPLC on OD-H column in 5% isopropanol in hexanes.

General Procedure B: Enantioselective Allylic C–H Amidation of Unactivated Olefins

In a nitrogen-filled glovebox, LiOAc (0.0006 g, 0.010 mmol, 0.10 equiv), AgNTf₂ (0.0078 g, 0.020 mmol, 0.20 equiv), LiNTf₂ (0.0290 g, 0.10 mmol, 1.0 equiv), and [Rh(2-Me-3-Ph-Ind)I₂]₂ (0.0056 g, 0.05 mmol, 0.005 equiv, ((*R,R*) or (*S,S*), as indicated) were added to an oven-dried 4-mL vial equipped with a magnetic stir-bar and a teflon-septum screw cap. The vial was capped and brought out of the glovebox. The olefin (0.10 mmol, 1.0 equiv) was added as a stock solution in DCE (0.25 mL), followed by the dioxazolone (0.20 mmol, 2 equiv) as a stock solution in DCE (0.25 mL). The reaction was stirred at room temperature (unless otherwise indicated) under a balloon of nitrogen for 48 hours. The reaction was filtered through a pipette containing celite with EtOAc (10 mL) and the filtrate was concentrated under reduced pressure. Purification by flash chromatography on silica gel provided the amide products.

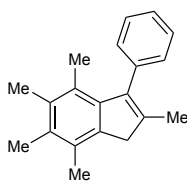
Catalyst Preparation

Synthesis of Indenyl ligands



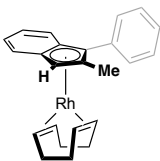
A 250 mL flame dried 3-neck round bottom flask equipped with a stir bar and reflux condenser under nitrogen was placed into a 0 °C ice/water bath. 2-methylindan-1-one¹ (1.32 g, 9.01 mmol, 1.0 equiv) was dissolved in anhydrous THF (40.0 mL) and added to the round bottom flask. After 5 minutes, phenylmagnesium bromide (3.27 g, 18.0 mmol, 2.0 equiv) was added. The ice bath was removed and the reaction allowed to warm to room temperature. The reaction was heated to reflux and allowed to stir while refluxing for 16 hours. The reaction was cooled to room temperature and quenched with DI water (20 mL). Concentrated HCl (20 mL) and Et₂O (20 mL) were added and the reaction was allowed to stir open to air for 16 hours. The layers were separated, and the aqueous layer extracted 3x with Et₂O (20 mL). The organic layers were combined and washed with NaHCO₃ (3x 50 mL), DI water (1x 50 mL) and brine (1x 50 mL).

The organic extract was dried over MgSO_4 , filtered, and the filtrate was concentrated under reduced pressure. Purification by flash chromatography (100% hexanes) afforded 2-methyl-3-phenyl-1*H*-indene (**1**) (1.50 g, 81% yield) as a white solid. $^1\text{H NMR}$ (CDCl_3 , 500 MHz) δ 7.51 – 7.41 (m, 4H), 7.40 – 7.35 (m, 1H), 7.26 – 7.24 (m, 1H), 7.16 – 7.20 (m, 1H), 3.48 (s, 1H), 2.17 (s, 2H) ppm.



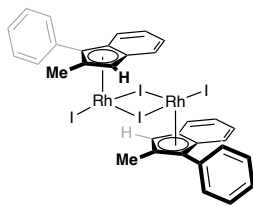
A 100 mL flame dried 3-neck round bottom flask equipped with a stir bar and reflux condenser under nitrogen was placed into a 0 °C ice/water bath. 2,4,5,6,7-pentamethylindan-1-one¹ (0.517 g, 1.97 mmol, 1.0 equiv) was dissolved in anhydrous THF (8 mL) and added to the round bottom flask. After 5 minutes, phenylmagnesium bromide (0.8M in THF, 6.2 mL, 4.94 mmol, 2.0 equiv) was added. The ice bath was removed and the reaction allowed to warm to room temperature. The reaction was heated to reflux and allowed to stir while refluxing for 15 hours. The reaction was cooled to room temperature and quenched with DI water (3 mL). Concentrated HCl (20 mL) and Et_2O (20 mL) were added and the reaction was allowed to stir open to air for 7 hours. The layers were separated, and the aqueous layer extracted 3x with Et_2O (20 mL). The organic layers were combined and washed with NaHCO_3 (3x 20 mL), DI water (1x 20 mL) and brine (1x 20 mL). The organic extract was dried over MgSO_4 , filtered, and the filtrate was concentrated under reduced pressure. Purification by flash chromatography (100% hexanes – 10% ether in hexanes) afforded 2-methyl-3-phenyl-1*H*-indene (**xx**) (343.5 g, 53% yield) as a white solid. $^1\text{H NMR}$ (CDCl_3 , 399 MHz) δ 7.38 (t, $J = 7.5$ Hz, 1H), 7.31 (t, $J = 7.4$ Hz, 0H), 7.21 (d, $J = 7.4$ Hz, 1H), 3.31 (s, 1H), 2.29 (s, 2H), 2.25 (s, 2H), 2.16 (s, 2H), 1.88 (s, 2H), 1.79 (s, 2H) ppm.

Synthesis and Resolution of rhodium and iridium indenyl catalysts **84**, **85**, **89**, and **90**



In a nitrogen-filled glovebox, 2-methyl-3-phenyl-1*H*-indene (0.0580 g, 0.281 mmol, 1.1 equiv), [Rh(COD)Cl₂] (0.0756 g, 0.153 mmol, 0.6 equiv), and potassium *tert*-butoxide (0.0430 g, 0.383 mmol, 1.5 equiv) were added to an oven-dried 4 mL vial equipped with a magnetic stir bar. A Teflon-septum screw cap was added and the vial was brought out of the glovebox. THF (2.0 mL) was added to the vial and the reaction stirred at room temperature under a balloon of nitrogen for 16 hours. The reaction was filtered through a pipette containing celite with hexanes (6 mL) and the filtrate was concentrated under reduced pressure. Purification by flash chromatography on silica gel with hexanes provided (±)-1,5-cyclooctadiene(±)-2-methyl-3-phenylinden-1*H*-yl)rhodium(I) ((±)-[Rh(2-Me-3-Ph-Ind)(COD)]) [(±)-**2**] (0.0960 g, 90% yield) as a yellow oil. ¹H NMR (CDCl₃, 600 MHz) δ 7.46 – 7.39 (m, 4H), 7.29 (tt, *J* = 6.0, 2.8 Hz, 1H), 7.27 – 7.24 (m, 2H), 7.07 – 7.01 (m, 2H), 5.01 (s, 1H), 3.86 (td, *J* = 7.4, 3.4 Hz, 2H), 3.62 (tt, *J* = 7.3, 3.0 Hz, 2H), 2.50 (d, *J* = 1.5 Hz, 3H), 1.97 – 1.83 (m, 4H), 1.79 – 1.67 (m, 4H) ppm. ¹³C NMR (CDCl₃, 151 MHz) δ 135.12, 129.28, 128.38, 126.15, 122.50, 121.80, 119.21, 117.32, 112.32 (d, *J*_{C-Rh} = 2.2 Hz), 111.60 (d, *J*_{C-Rh} = 2.7 Hz), 107.79 (d, *J*_{C-Rh} = 5.0 Hz), 95.47 (d, *J*_{C-Rh} = 3.6 Hz), 76.55 (d, *J*_{C-Rh} = 4.7 Hz), 71.98, 71.89, 69.11, 69.02, 31.43, 31.33, 14.80 ppm. HRMS (+APCI) calculated for C₂₄H₂₅Rh[M]⁺ 416.10058, found 416.10045.

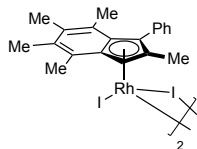
Chiral Resolution – Semi-prep HPLC (Chiracel, ODH, 0% IPA) – (*S*)-[Rh(2-Me-3-Ph-Ind)(COD)] *t* = 16.2 min. (*R*)-[Rh(2-Me-3-Ph-Ind)(COD)] *t* = 26.9 min.



To a 20 mL scintillation vial containing (*S*)-[Rh(2-Me-3-Ph-Ind)(COD)] (0.0515 g, 0.124 mmol, 2.0 equiv) and a stir bar, iodine (0.0785 g, 0.309 mmol, 5.0 equiv) was added and the vial was sealed with a rubber septum. Anhydrous Et₂O (5.0 mL) was added and the reaction stirred for 24 hours under a balloon of nitrogen. The reaction was filtered through a Büchner funnel and washed with Et₂O (50 mL, or until

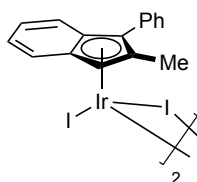
the filtrate is clear). The product was collected and dried the filtered material to afford (*S,S*)-(2-methyl-3-phenylinden-1*H*-yl)rhodium(III) diiodide dimer ((*S,S*)-[Rh(2-Me-3-Ph-Ind)I₂]₂) [**(*S,S*)-83**] as a black solid (0.0593 g, 85% yield). **¹H NMR** (DMSO-*d*₆, 600 MHz) δ 7.87 – 7.84 (m, 4H), 7.69 (dt, *J* = 8.5, 1.1 Hz, 2H), 7.63 – 7.56 (m, 2H), 7.51 – 7.48 (m, 6H), 7.44 – 7.41 (m, 2H), 6.46 (s, 2H), 2.25 (s, 6H) ppm. **¹³C NMR** (DMSO-*d*₆, 151 MHz) δ 133.55, 132.42, 130.89, 129.20, 128.86, 128.41, 127.72, 125.49, 111.39 (d, *J*_{C-Rh} = 5.5 Hz), 107.32 (d, *J*_{C-Rh} = 3.6 Hz), 103.61 (d, *J*_{C-Rh} = 4.7 Hz), 94.84 (d, *J*_{C-Rh} = 6.0 Hz), 77.87 (d, *J*_{C-Rh} = 7.1 Hz), 13.61 ppm. **HRMS** (+APCI) calculated for C₃₂H₂₆I₃Rh₂ [M - I]⁺ 996.72731, found 996.7258.

(*R,R*)-[Rh(2-Me-3-Ph-Ind)I₂]₂ [**(*R,R*)-85**] was prepared using the above procedure starting from (*R*)-[Rh(2-Me-3-Ph-Ind)(COD)].



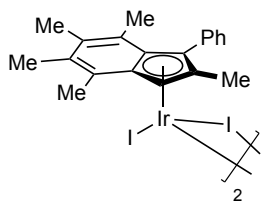
In a nitrogen-filled glovebox, 2,4,5,6,7-pentamethyl-3-phenyl-1*H*-indene (0.0446 g, 0.170 mmol, 1.0 equiv) was added to an oven-dried 4 mL vial equipped with a magnetic stir bar. A Teflon-septum screw cap was added and the vial was brought out of the glovebox. Hexanes (2.0 mL) was added to the vial and the reaction was cooled to -78 °C and *n*-butyl lithium (2.13M in THF, 0.08 mL, 0.17 mmol, 1.0 equiv) was added. The reaction was allowed to warm to room temperature and stirred under a balloon of nitrogen for 2 hours. The contents of the reaction flask was then transferred into a 4 mL vial containing [Rh(COD)Cl₂] (0.0419 g, 0.085 mmol, 0.5 equiv). The reaction was allowed to stir at room temperature for 16 hours. The reaction was filtered through a pipette containing celite with hexanes (6 mL) and the filtrate was concentrated under reduced pressure. Purification by flash chromatography on silica gel with hexanes provided (±)-1,5-cyclooctadiene(η⁵-2,4,5,6,7-pentamethyl-3-phenylinden-1*H*-yl)rhodium(I) ((±)-[Rh(2-Me-3-Ph-Ind)(COD)]) [**(±)-84**] as a yellow oil. Chiral Resolution – Semi-prep HPLC (Chiracel, ODH, 0% IPA) – (±)-[Rh(2,4,5,6,7-PentaMe-3-Ph-Ind)(COD)]. To a 20 mL

scintillation vial containing *en2*-[Rh(2,4,5,6,7-PentaMe-3-Ph-Ind)(COD)] (0.0102 g, 0.024 mmol, 1.0 equiv) and a stir bar, iodine (0.009 g, 0.037 mmol, 1.5 equiv) was added and the vial was sealed with a rubber septum. Anhydrous Et₂O (0.85 mL) was added and the reaction stirred for 24 hours under a balloon of nitrogen. The reaction was filtered through a Büchner funnel and washed with Et₂O (20 mL, or until the filtrate is clear). The product was collected and dried the filtered material to afford *en2*-(2,4,5,6,7-pentamethyl-3-phenylinden-1*H*-yl)rhodium(III) diiodide dimer (*en2*-[Rh(2,4,5,6,7-PentaMe-3-Ph-Ind)I₂]₂) [**en2-86**] as a black solid (0.0031 g, 21% yield).



In a nitrogen-filled glovebox, 2-methyl-3-phenyl-1*H*-indene (0.0432 g, 0.209 mmol, 2.0 equiv) was added to an oven-dried 4 mL vial equipped with a magnetic stir bar. A Teflon-septum screw cap was added and the vial was brought out of the glovebox. THF (0.7 mL) was added to the vial and the reaction was cooled to -78 °C and *n*-butyl lithium (1.0 M in THF, 0.17 mL, 0.17 mmol, 1.64 equiv) was added. The reaction was allowed to warm to room temperature and stirred under a balloon of nitrogen for 2 hours. The contents of the reaction flask was then transferred into a 4 mL vial containing [Ir(C₂H₄)Cl₂] (0.041 g, 0.071 mmol, 0.34 equiv). The reaction was allowed to stir at room temperature for 16 hours. The reaction was filtered through a pipette containing celite with hexanes (6 mL) and the filtrate was concentrated under reduced pressure. Purification by flash chromatography on silica gel with hexanes provided (±)-bisethylene-(η⁵-2,-methyl-3-phenylinden-1*H*-yl)iridium(I) ((±)-[Ir(2-Me-3-Ph-Ind)(COD)]) [**(±)-87**] as a yellow oil. Chiral Resolution – Semi-prep HPLC (Chiracel, ODH, 0% IPA) – (±)-[Ir(2-Me-3-Ph-Ind)(COD)]. Next, *en2*-[Ir(2-Me-3-Ph-Ind)(COD)] was taken forward into the next reaction separately. To a 20 mL scintillation vial containing *en2*-[Ir(2-PentaMe-3-Ph-Ind)(C₂H₄)] (0.009 g, 0.021 mmol, 1.0 equiv) and a stir bar, iodine (0.010 g, 0.041 mmol, 2.0 equiv) was added and the vial was sealed with a rubber septum. Anhydrous Et₂O (1.0 mL) was added and the reaction stirred for

24 hours under a balloon of nitrogen. The reaction was filtered through a Büchner funnel and washed with Et₂O (20 mL, or until the filtrate is clear). Product was collected and dried the filtered material to afford *en2*-(2-methyl-3-phenylinden-1*H*-yl)rhodium(III) diiodide dimer (*en2*-[Rh(2-Me-3-Ph-Ind)I₂]₂) [**en2-89**] as a red solid (0.0081 g, 30% yield)

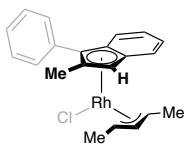


In a nitrogen-filled glovebox, 2,4,5,6,7-methyl-3-phenyl-1*H*-indene (0.0685 g, 0.255 mmol, 2.0 equiv) was added to an oven-dried 4 mL vial equipped with a magnetic stir bar. A Teflon-septum screw cap was added and the vial was brought out of the glovebox. THF (0.7 mL) was added to the vial and the reaction was cooled to -78 °C and *n*-butyl lithium (1.0 M in THF, 0.21 mL, 0.21 mmol, 1.1 equiv) was added. The reaction was allowed to warm to room temperature and stirred under a balloon of nitrogen for 2 hours. The contents of the reaction flask was then transferred into a 4 mL vial containing [Ir(C₂H₄)Cl₂]^x (0.034 g, 0.060 mmol, 0.5 equiv). The reaction was allowed to stir at room temperature for 16 hours. The reaction was filtered through a pipette containing celite with hexanes (6 mL) and the filtrate was concentrated under reduced pressure. Purification by flash chromatography on silica gel with hexanes provided (±)-bisethylene-(η⁵-2,4,5,6,7-pentamethyl-3-phenylinden-1*H*-yl)iridium(I) ((±)-[Ir(2,4,5,6,7-PentaMe-3-Ph-Ind)(COD)]) [**(±)-88**] as a yellow oil. Chiral Resolution – Semi-prep HPLC (Chiracel, ODH, 0% IPA) – (±)-[Ir(2,4,5,6,7-PentaMe-3-Ph-Ind)(COD)]. Next, *en2*-[Ir(2,4,5,6,7-PentaMe-3-Ph-Ind)(COD)] was taken forward into the next reaction separately. To a 20 mL scintillation vial containing *en2*-[Ir(2,4,5,6,7-PentaMe-3-Ph-Ind)(C₂H₄)] (0.0122 g, 0.024 mmol, 1.0 equiv) and a stir bar, iodine (0.011 g, 0.043 mmol, 1.8 equiv) was added and the vial was sealed with a rubber septum. Anhydrous Et₂O (1.1 mL) was added and the reaction stirred for 24 hours under a balloon of nitrogen. The reaction was filtered through a Büchner funnel and washed with Et₂O (20 mL, or until the filtrate is clear). Product was collected

and dried the filtered material to afford *en*2-(2,4,5,6,7-pentamethyl-3-phenylinden-1*H*-yl)rhodium(III) diiodide dimer (*en*2-[Rh(2,4,5,6,7-PentaMe-3-Ph-Ind)I₂]₂) [**en2-90**] as a red solid (0.0028 g, 16% yield)

Determination of Stereochemistry

Catalyst Stereochemistry – π -Allyl Complex



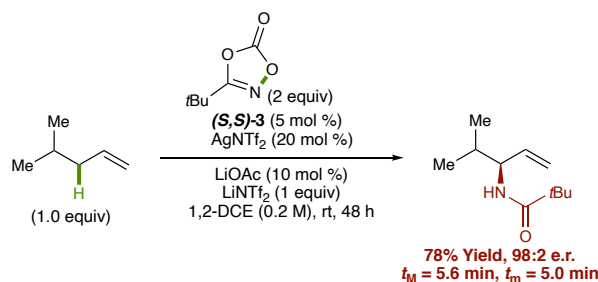
Experiment conducted by Christopher Poff. In a nitrogen filled glove box, (*S,S*)-[Rh(2-Me-3-Ph-Ind)I₂]₂ (0.0121 g, 0.0108 mmol, 0.5 equiv), silver hexafluoroantimonate (0.0148 g, 0.0431 mmol, 2.0 equiv), and cesium acetate (0.007 mg, 0.0360 mmol, 1.7 equiv) were added to a 7 mL vial equipped with a stir bar. The vial was sealed with a teflon cap and removed from the box. To the reaction vial was added 1,2-dichloroethane (2.0 mL) and 2-pentene (0.066 mL, 0.0413 mmol, 2.0 equiv). The vial was placed into a 40 °C heating block and allowed to stir under a balloon of nitrogen for 16 hours. A solution of tetraethylammonium chloride (0.0114 g, 0.0688 mmol, 3.2 equiv) in 1,2-dichloroethane (3.0 mL) was prepared and sonicated for 30 minutes. The reaction vial was cooled to room temperature and the solution of tetraethylammonium chloride in 1,2-dichloroethane was added. The reaction continued to stir at room temperature for 2 hours. The reaction was filtered through celite eluting with excess dichloromethane and the filtrate concentrated in vacuo. The crude material was purified on silica (25:75 EtOAc/hexanes) to provide (*E*)-(η⁵-*S*-2-methyl-3-phenylinden-1*H*-yl)(η³-pent-3-enyl)rhodium(III) chloride (0.0028 g, 32 % yield) as a red solid. Single crystals suitable for X-Ray were obtained by vapor diffusion of pentane into chloroform. ¹H NMR (CDCl₃, 600 MHz) δ 7.78 – 7.74 (m, 2H), 7.52 – 7.47 (m, 2H), 7.45 – 7.37 (m, 4H), 7.14 – 7.11 (m, 2H), 5.08 (s, 1H), 4.68 (td, *J* = 10.2, 1.9 Hz, 1H), 3.46 – 3.39 (m, 1H), 3.38 – 3.32 (m, 1H), 2.04 (d, *J* = 1.5 Hz, 3H), 1.52 (d, *J* = 6.9 Hz, 3H), 1.29 (d, *J* = 6.4 Hz, 3H) ppm. ¹³C NMR (CDCl₃, 151 MHz, Chloroform-*d*) δ 131.78, 130.57, 128.76, 128.35, 128.10,

127.57, 122.66, 121.06, 111.59, 111.14 (d, , $J_{C-Rh} = 3.6$ Hz), 108.45 (d, , $J_{C-Rh} = 7.0$), 90.53 (d, , $J_{C-Rh} = 6.2$ Hz), 79.27 (d, , $J_{C-Rh} = 9.0$ Hz), 74.99 (d, , $J_{C-Rh} = 11.6$ Hz), 32.08, 22.85, 19.71, 19.46, 14.27, 12.12 ppm. **HRMS** (+APCI) calculated for $C_{21}H_{22}Rh$ $[M - Cl]^+$ 377.07711, found 377.07680.

Stereochemical assignment of the indene ring in the π -allyl complex was used to assume stereochemistry of the $[Rh(2-Me-3-Ph-Ind)_2]_2$ starting material.

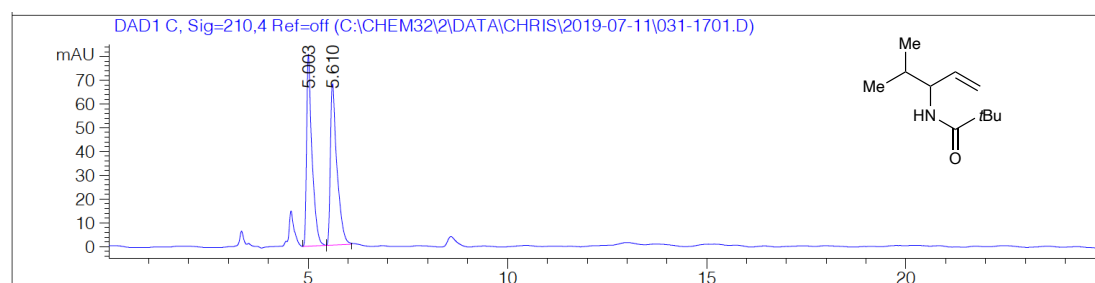
Product Stereochemistry – Experiments conducted by Christopher Poff.

Stereochemistry of *N*-(4-methylpent-1-en-3-yl)pivalamide was assigned by converting methyl pivaloyl-*D*-valinate² to the corresponding olefin product by reduction to the aldehyde and subsequent Wittig reaction. HPLC data was then compared to the reaction HPLC data for the same substrate, shown below. All substrates with alkyl substituents at the homoallylic position were assigned by analogy.



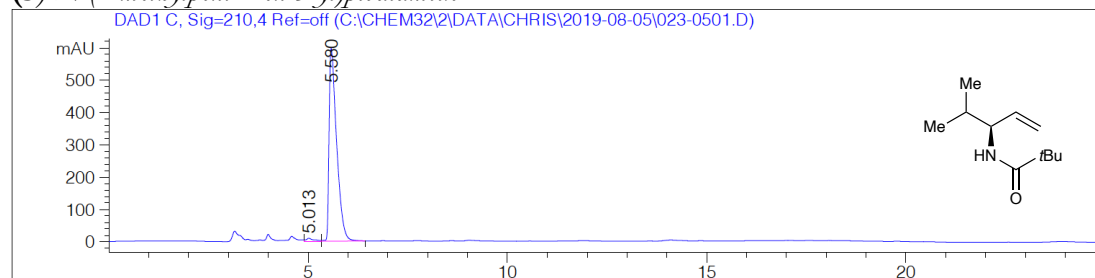
(S)-*N*-(4-methylpent-1-en-3-yl)acetamide : See **Dioxazolone Scope** for full experimental. HPLC (OJ-H column, 10% 2-propanol in Hexanes, 1 mL/min) $t_M = 5.6$ min, $t_m = 5.0$ min, 98:2 e.r.

(±)-*N*-(4-methylpent-1-en-3-yl)pivalamide



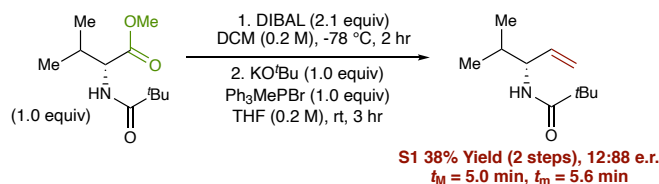
Signal 1: DAD1 C, Sig=210,4 Ref=off

Peak #	RetTime [min]	Type	Width [min]	Area [mAU*s]	Height [mAU]	Area %
1	5.003	VV	0.1348	767.14093	80.80962	50.2210
2	5.610	VB	0.1585	760.38782	67.99258	49.7790
Totals :				1527.52875	148.80220	

(S)-N-(4-methylpent-1-en-3-yl)pivalamide

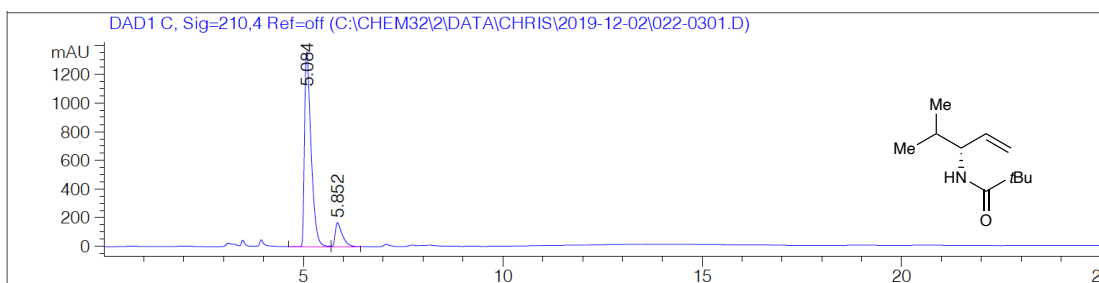
Signal 2: DAD1 C, Sig=210,4 Ref=off

Peak #	RetTime [min]	Type	Width [min]	Area [mAU*s]	Height [mAU]	Area %
1	5.013	VV	0.1808	126.23240	9.27309	1.6162
2	5.580	VB	0.1861	7684.32129	597.17950	98.3838
Totals :				7810.55369	606.45259	



(R)-N-(4-methylpent-1-en-3-yl)pivalamide: To an oven-dried 7 mL vial equipped with a stir bar was added methyl pivaloyl-*D*-valinate² (0.0741 g, 0.344 mmol, 1.0 equiv) and the atmosphere was exchanged with N₂. The solid was dissolved in DCM (2.0 mL) and cooled to -78 °C in an acetone/dry ice bath. DIBAL-H (0.720 mL, 0.723 mmol, 2.1 equiv) was added to the reaction vial over 20 minutes via syringe pump and the reaction allowed to stir at -78 °C for 2 hours. The reaction was quenched with DI H₂O (4 mL) and allowed to come to room temperature. A white solid was filtered away by passing the reaction through a cotton plug before the layers were separated and the organic layer was washed with brine (4 mL), dried over MgSO₄, filtered, and concentrated *in vacuo*. The Wittig reagent was prepared by adding

methyltriphenylphosphonium bromide (0.123 g, 0.344 mmol, 1.0 equiv) and potassium *tert*-butoxide (0.0386 g, 0.344 mmol, 1.0 equiv) to a flame dried 7 mL vial equipped with a stir bar. The vial was sealed, and the atmosphere exchanged with N₂ before the addition of anhydrous THF (2.0 mL). The vial was stirred at room temperature for 5 minutes. The crude aldehyde was dissolved in anhydrous THF (2.0 mL) and added dropwise to the vial containing the yellow Wittig reagent. The reaction stirred at room temperature until the yellow color had changed to white (3 hours). The reaction was concentrated *in vacuo* and purified on silica gel (10-50% EtOAc in hexanes) to afford (**S1**) (0.0239 g, 38% yield, 2 steps) as a white solid. ¹H NMR (CDCl₃, 400 MHz) δ 5.76 (ddd, *J* = 17.0, 10.6, 5.5 Hz, 1H), 5.54 (s, 1H), 5.15 – 5.05 (m, 2H), 4.35 (dtt, *J* = 8.9, 5.5, 1.6 Hz, 1H), 1.81 (qnd, *J* = 6.9, 5.6 Hz, 1H), 1.22 (s, 9H), 0.90 (d, *J* = 6.9 Hz, 3H), 0.88 (d, *J* = 7.0 Hz, 3H). HPLC (OJ-H column, 10% 2-propanol in Hexanes, 1 mL/min) *t*_M = 5.0 min, *t*_m = 5.9 min, 88:11 e.r.



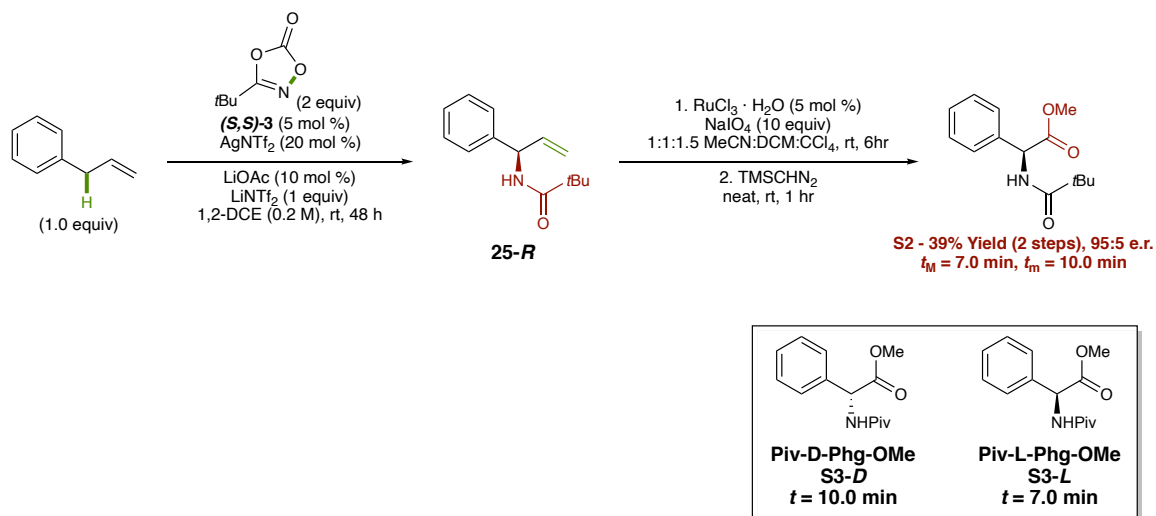
Signal 1: DAD1 C, Sig=210,4 Ref=off

Peak #	RetTime [min]	Type	Width [min]	Area [mAU*s]	Height [mAU]	Area %
1	5.084	VV	0.1704	1.56517e4	1359.12085	88.3109
2	5.852	VB	0.1806	2071.69434	167.13620	11.6891

Totals : 1.77234e4 1526.25705

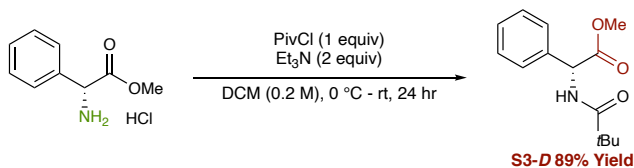
Stereochemistry of *N*-(1-phenylallyl)pivalamide assigned by converting the amidated product of the reaction between allyl benzene and *tert*-butyl dioxazolone to its *N*-pivaloyl phenylglycine methyl ester derivative by oxidative cleavage of the olefin and methyl protection of the resulting carboxylic acid. Comparison to the HPLC traces of *N*-pivaloyl-*D*-phenylglycine methyl ester and *N*-pivaloyl-*L*-phenylglycine methyl ester, formed from their enantiopure amino acid precursors, allowed for final

stereochemical assignment. All substrates with aryl substituents at the homoallylic position are assigned by analogy.



N-pivaloyl-*L*-phenylglycine methyl ester : (**xx-R**) was prepared using the same procedure as (**xx**) utilizing the (*S,S*)-[Rh(2-Me-3-Ph-Ind)₂]₂ catalyst in place of the (*R,R*)-[Rh(2-Me-3-Ph-Ind)₂]₂ catalyst. To a 7 mL oven dried vial equipped with stir bar was added sodium periodate (0.1310 g, 1.15 mmol, 10.0 equiv) and ruthenium(III) chloride hydrate (0.2460 mg, 0.00575 mmol, 5 mol %), the vial was sealed, and atmosphere exchanged with N₂. (**xx-R**) (0.0360 mg, 0.166 mmol) was dissolved in CCl₄ (1.44 mL) and 1.0 mL of the (**xx-R**) solution (0.0250 mg, 0.115 mmol, 1.0 equiv), MeCN (1.0 mL), and DCM (1.0 mL) were added to the reaction vial and the reaction stirred at room temperature for 4 hours. The reaction was poured into a 1:1 DCM:DI H₂O mixture (10 mL). The organic layer was separated, and the aqueous layer extracted 3x with DCM (5 mL). The combined organic layers were dried over MgSO₄, filtered, and concentrated *in vacuo*. To the crude carboxylic acid was added (diazomethyl)trimethylsilane (0.1310 g, 1.15 mmol, 10.0 equiv) and the reaction stirred at room temperature for 1 hour. The reaction was concentrated *in vacuo* and then purified on silica gel (10-50% EtOAc in Hexanes) to afford the product (0.0112 g, 39% yield) as a white solid. ¹H NMR (CDCl₃,

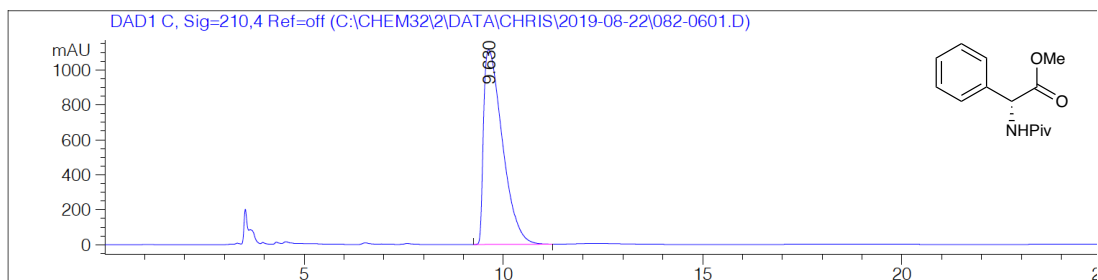
500 MHz) δ 7.40 – 7.27 (m, 5H), 6.61 (d, J = 6.7 Hz, 1H), 5.53 (d, J = 6.8 Hz, 1H), 3.73 (s, 3H), 1.22 (s, 9H). **HPLC** (AS-H column, 5% 2-propanol in Hexanes, 1 mL/min) t_M = 7.0 min, t_m = 10.0 min, 94:6 e.r.



N-pivaloyl-D-phenylglycine methyl ester (HPLC Standards): To a 20 mL flame dried round bottom flask equipped with a stir bar, added methyl-(*S*)-2-amino-2-phenylacetate hydrochloride (0.5041 g, 2.50 mmol, 1.0 equiv) sealed with a rubber septum exchanged the atmosphere with N₂. Added DCM (8.0 mL) and placed into a 0 °C ice/water bath for 30 minutes before the addition of Et₃N (0.0073 L, 5.00 mmol, 2.0 equiv) and pivaloyl chloride (0.000308 L, 2.50 mmol, 1.0 equiv). The reaction was allowed to stir for 24 hours and warmed to room temperature. The reaction was poured into a separatory funnel containing EtOAc (40 mL) and DI H₂O (40 mL). The organic layer was separated, and the aqueous layer extracted with EtOAc (3x15 mL). The combined organic layers were dried over MgSO₄, filtered, and concentrated *in vacuo*. Purification on silica gel (10-50% EtOAc in hexanes) afforded the product (0.5532 g, 89% yield, single enantiomer) as a white solid. **¹H NMR** (CDCl₃, 500 MHz) δ 7.41 – 7.29 (m, 5H), 6.61 (d, J = 6.7 Hz, 1H), 5.53 (d, J = 6.8 Hz, 1H), 3.73 (s, 3H), 1.22 (s, 9H). **HPLC** (AS-H column, 5% 2-propanol in Hexanes, 1 mL/min) t = 7.0 min.

N-pivaloyl-L-phenylglycine methyl ester HPLC standard prepared according to the same procedure utilizing methyl-(*R*)-2-amino-2-phenylacetate hydrochloride as the starting material. **¹H NMR** (CDCl₃, 500

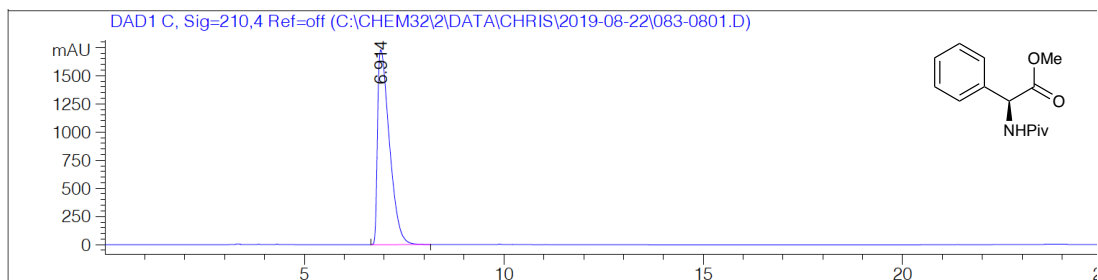
MHz) δ 7.41 – 7.29 (m, 5H), 6.61 (d, $J = 6.7$ Hz, 1H), 5.53 (d, $J = 6.8$ Hz, 1H), 3.73 (s, 3H), 1.22 (s, 9H). **HPLC** (AS-H column, 5% 2-propanol in Hexanes, 1 mL/min) $t = 9.6$ min.



Signal 1: DAD1 C, Sig=210,4 Ref=off

Peak #	RetTime [min]	Type	Width [min]	Area [mAU*s]	Height [mAU]	Area %
1	9.630	BB	0.5104	3.66984e4	1113.71863	100.0000

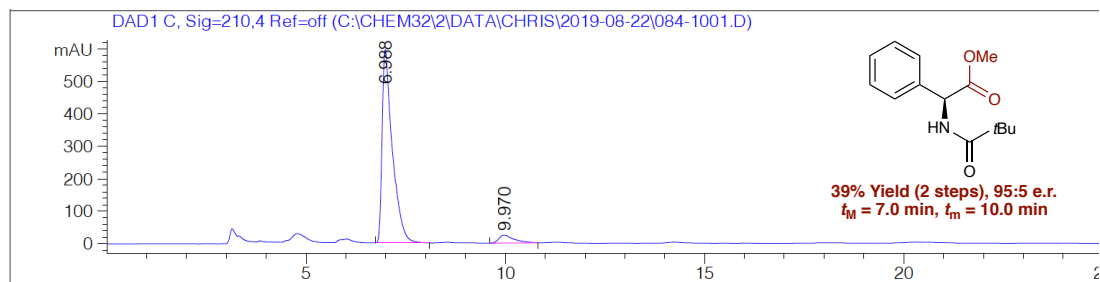
Totals : 3.66984e4 1113.71863



Signal 1: DAD1 C, Sig=210,4 Ref=off

Peak #	RetTime [min]	Type	Width [min]	Area [mAU*s]	Height [mAU]	Area %
1	6.914	BB	0.3150	3.60334e4	1730.04883	100.0000

Totals : 3.60334e4 1730.04883



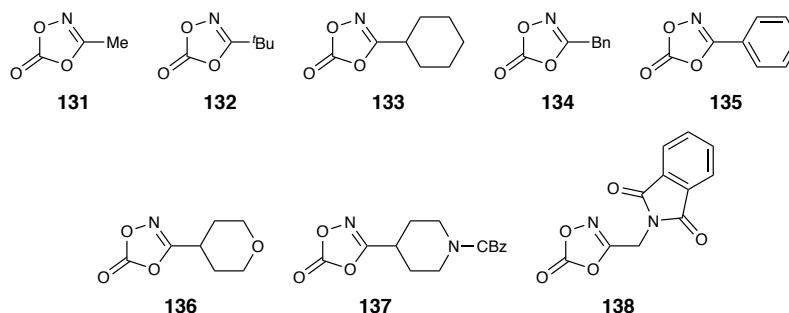
Signal 1: DAD1 C, Sig=210,4 Ref=off

Peak #	RetTime [min]	Type	Width [min]	Area [mAU*s]	Height [mAU]	Area %
1	6.988	BB	0.2569	1.06587e4	595.19495	94.4866
2	9.970	BB	0.3668	621.94397	24.28669	5.5134

Totals : 1.12806e4 619.48164

Preparation of Substrates

DIOXAZOLONE SUBSTRATES

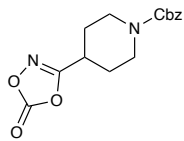


131, 132, 133, 134, 135, and 136 were synthesized according to previously reported procedures.³

General Procedure C for preparation of new dioxazolones

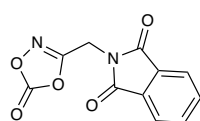
1,1'-carbonyldiimidazole (CDI) (1.25 equiv) was added to an oven-dried 15 mL vial equipped with a magnetic stir-bar and Teflon-septum screw cap, the vial was evacuated and backfilled with nitrogen (3x). MeCN (0.25 M), and the carboxylic acid (1 equiv) was added. The resulting suspension was stirred at room temperature for 3 hours. The cap was opened and hydroxylamine hydrochloride ($\text{NH}_2\text{OH}\cdot\text{HCl}$) (1.25 equiv) was added. The vial was quickly resealed, and the reaction was stirred at room temperature for 18 hours. The cap was opened and CDI (1.5 equiv) was added. The vial was

quickly resealed, and the reaction was stirred at room temperature for 3 hours. The reaction was quenched with aqueous hydrochloric acid (HCl) (1 N, 7 mL) and allowed to stir at room temperature for 10 minutes. The mixture was diluted with DCM (15 mL), the layers were separated, and the aqueous layer was extracted 3x with DCM (15 mL). The combined organic extracts were washed with brine (30 mL), dried over anhydrous Na₂SO₄, filtered, and concentrated under reduced pressure.



Experiment conducted by Amaan Kazerouni. *Benzyl 4-(5-oxo-1,4,2-dioxazol-3-yl)piperidine-1-carboxylate (137)*: Prepared according to **General Procedure C** from 1-((benzyloxy)carbonyl)piperidine-4-carboxylic acid (1.0 equiv). Purified by filtration

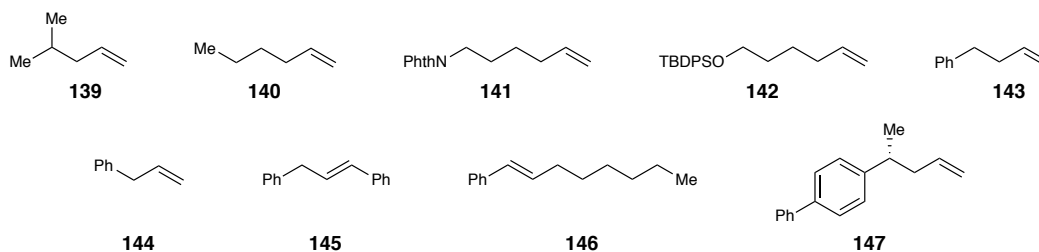
through a plug of silica gel with DCM. **¹H NMR** (CDCl₃, 500 MHz) δ 7.43 – 7.31 (m, 5H), 5.14 (s, 2H), 4.20 (s, 2H), 3.00 (s, 2H), 2.87 (tt, *J* = 11.1, 3.9 Hz, 1H), 2.06 – 1.97 (m, 2H), 1.83 – 1.66 (m, 2H) ppm. **¹³C{¹H} NMR** (CDCl₃, 151 MHz) δ 167.92, 155.13, 153.96, 136.56, 128.69, 128.32, 128.13, 67.57, 42.83, 33.05, 27.20 ppm. **HRMS** (+NSI) calculated for C₁₆H₂₀N₂NaO₆ [M+Na+MeOH]⁺ 359.1219 and C₁₅H₁₆N₂NaO₅ [M+Na]⁺ 327.0957, found 359.1214 and 327.0953.



2-((5-oxo-1,4,2-dioxazol-3-yl)methyl)isoindoline-1,3-dione (138): Prepared according to **General Procedure C** from *N*-phthaloylglycine (1.0 equiv). Purified by layered

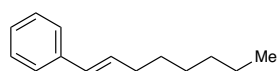
recrystallization from DCM and cold hexanes. **¹H NMR** (CDCl₃, 600 MHz, Chloroform-*d*) δ 7.96 – 7.92 (m, 2H), 7.84 – 7.79 (m, 2H), 4.89 (s, 2H) ppm. **¹³C{¹H} NMR** (151 MHz, CDCl₃) δ 166.59, 161.47, 153.25, 135.02, 131.63, 124.28, 31.79 ppm. **HRMS** (+NSI) calculated for C₁₁H₇N₂O₅ [M + H]⁺ calculated for 247.03495, found 247.0485.

ALKENE SUBSTRATES



139, **140**, **143**, and **144** were purchased commercially from Millipore Sigma and used from the bottle.

141⁴, **142**⁵, **145**⁶, and **146**⁷ were synthesized according to previously reported procedures.

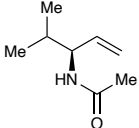


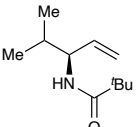
(E)-*oct-1-en-1-ylbenzene* (**146**)⁸: In a nitrogen-filled glovebox, Pd(PPh₃)₄ (0.142 g, 0.120 mmol, 0.05 equiv) was added to an oven-dried 10-mL round bottom flask equipped with a magnetic stir-bar and a septum. The round bottom flask was sealed with septum and brought out of the glovebox. The flask was placed under N₂ atmosphere and dimethoxyethane (2.5 mL) was added. *(E)*-4,4,5,5-tetramethyl-2-(*oct-1-en-1-yl*)-1,3,2-dioxaborolane (1.0 mL, 3.68 mmol, 1.5 equiv), saturated K₂CO₃ (3.0 mL, 2M, 6.86 mmol, 2.8 equiv), and iodobenzene (275 μ L, 2.45 mmol, 1.0 equiv) were added to the flask. The reaction was stirred at 90 °C under a balloon of nitrogen for 19 hours. The reaction was quenched with brine, extracted 3x with Et₂O (20 mL), the organic extracts were combined, dried over MgSO₄, filtered and concentrated under reduced pressure. Purified by flash chromatography on silica gel (100% Hexanes) to provide **146** (0.1683 g, 37% yield) as a clear, colorless oil. ¹H NMR (CDCl₃, 600 MHz) δ 7.35 (d, *J* = 8.0 Hz, 2H), 7.30 (t, *J* = 7.4 Hz, 2H), 7.19 (td, *J* = 7.5, 1.2 Hz, 1H), 6.38 (dd, *J* = 15.8, 1.4 Hz, 1H), 6.24 (dtd, *J* = 15.4, 6.9, 1.1 Hz, 1H), 2.21 (tdd, *J* = 7.1, 5.8, 1.4 Hz, 2H), 1.47 (qnd, *J* = 8.0, 7.5, 1.2 Hz, 2H), 1.39 – 1.26 (m, 6H), 0.90 (td, *J* = 6.9, 1.4 Hz, 3H) ppm.

Characterization of Enantioselective Allylic C–H Amidation Products

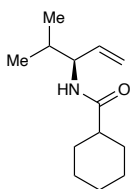
All racemic runs were carried out with the designated alkene and dioxazolone, utilizing $[\text{IrCp}^*\text{Cl}_2]_2$ as the catalyst under previously reported conditions.³

DIOXAZOLONE SCOPE


 Experiment conducted by Amaan Kazerouni. *(S)*-*N*-(4-methylpent-1-en-3-yl)acetamide (**106**): Prepared according to **General Procedure B** using 4-methylpentene (0.0127 mL, 0.10 mmol, 1.0 equiv), 3-methyl-1,4,2-dioxazol-5-one (0.0202 g, 0.20 mmol, 2.0 equiv), LiOAc (0.0006 g, 0.010 mmol, 0.10 equiv), AgNTf₂ (0.0078 g, 0.020 mmol, 0.20 equiv), LiNTf₂ (0.0290 g, 0.10 mmol, 1.0 equiv), and *(S,S)*-[Rh(2-Me-3-Ph-Ind)₂]₂ (0.0056 g, 0.005 mmol, 0.05 equiv) in DCE (0.5 mL) at room temperature for 48 hours. Purified by flash chromatography on silica gel (90-100% EtOAc in Hexanes) to provide **106** (0.0098 g, 69% yield, >99:1 e.r.) as a yellow oil. ¹H NMR (CDCl₃, 600 MHz) δ 5.74 (ddd, *J* = 17.5, 10.2, 5.9 Hz, 1H), 5.41 (s, 1H), 5.17 – 5.11 (m, 2H), 4.34 (dtt, *J* = 9.1, 5.9, 1.6 Hz, 1H), 2.02 (s, 3H), 1.80 (qnd, *J* = 6.9, 5.7 Hz, 1H), 0.91 (d, *J* = 4.8 Hz, 3H), 0.90 (d, *J* = 4.9 Hz, 3H) ppm. ¹³C{¹H} NMR (CDCl₃, 151 MHz) δ 169.43, 136.67, 115.62, 56.58, 32.01, 23.52, 18.64, 18.19 ppm. HRMS (+APCI) calculated for C₈H₁₆NO [M+H]⁺ 142.12264, found 142.12267. HPLC (AD-H column, 1% 2-propanol in Hexanes, 1 mL/min) *t*_M = 19.1 min, *t*_m = 22.8 min, >99:1 e.r.

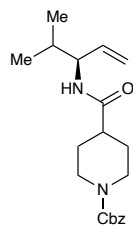

 Experiment conducted by Christopher Poff. *(S)*-*N*-(4-methylpent-1-en-3-yl)pivalamide (**107**): Prepared according to **General Procedure B** using 4-methylpentene (0.0253 mL, 0.20 mmol, 1.0 equiv), 3-(*tert*-butyl)-1,4,2-dioxazol-5-one (**6**) (0.0573 g, 0.40 mmol, 2.0 equiv), LiOAc (0.0012 g, 0.020 mmol, 0.10 equiv), AgNTf₂ (0.0155 g, 0.040 mmol, 0.20 equiv), LiNTf₂ (0.0574 g, 0.20 mmol, 1.0 equiv), and *(S,S)*-[Rh(2-Me-3-Ph-Ind)₂]₂ (0.0112 g, 0.01 mmol, 0.05 equiv) in DCE (0.5 mL) at room temperature for 48 hours. Purified by flash chromatography on silica

gel (10-50% EtOAc in Hexanes) to provide **107** (0.0285 g, 78% yield, 98:2 e.r.) as a white solid. **¹H NMR** (CDCl₃, 600 MHz) δ 5.77 (ddd, *J* = 17.1, 10.6, 5.6 Hz, 1H), 5.54 (s, 1H), 5.13 – 5.07 (m, 2H), 4.38 – 4.32 (m, 1H), 1.82 (qnd, *J* = 6.9, 5.6 Hz, 1H), 1.22 (s, 9H), 0.90 (d, *J* = 6.8 Hz, 3H), 0.89 (d, *J* = 6.8 Hz, 3H) ppm. **¹³C{¹H} NMR** (CDCl₃, 151 MHz) δ 177.66, 137.13, 115.15, 55.86, 38.92, 32.10, 27.71, 18.80, 17.98 ppm. **HRMS** (+APCI) calculated for C₁₁H₂₂NO [M+H]⁺ 184.16926, found 184.16959. **HPLC** (OJ-H column, 10% 2-propanol in Hexanes, 1 mL/min) *t*_M = 5.6 min, *t*_m = 5.0 min, 98:2 e.r.

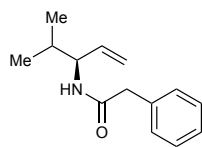


(S)-*N*-(4-methylpent-1-en-3-yl)cyclohexanecarboxamide (**110**): Prepared according to **General**

Procedure B using 4-methylpent-1-ene (0.0127 mL, 0.10 mmol, 1.0 equiv), 3-cyclohexyl-1,4,2-dioxazol-5-one (**S5**) (0.0338 g, 0.20 mmol, 2.0 equiv), LiOAc (0.0006 g, 0.010 mmol, 0.10 equiv), AgNTf₂ (0.0078 g, 0.020 mmol, 0.20 equiv), LiNTf₂ (0.0290 g, 0.10 mmol, 1.0 equiv), and (*S,S*)-[Rh(2-Me-3-Ph-Ind)I₂]₂ (0.0056 g, 0.005 mmol, 0.05 equiv) in DCE (0.5 mL) at room temperature for 48 hours. Purified by flash chromatography on silica gel (10-30% EtOAc in Hexanes) to provide **110** (0.0114 g, 55% yield, 94:6 e.r.) as a white solid. **¹H NMR** (CDCl₃, 500 MHz) δ 5.75 (ddd, *J* = 17.7, 10.0, 5.6 Hz, 1H), 5.34 (d, *J* = 9.2 Hz, 1H), 5.14 – 5.08 (m, 2H), 4.36 (dtt, *J* = 8.9, 5.6, 1.6 Hz, 1H), 2.12 (tt, *J* = 11.7, 3.5 Hz, 1H), 1.88 (ddd, *J* = 12.7, 3.6, 1.7 Hz, 2H), 1.85 – 1.77 (m, 3H), 1.67 (dtd, *J* = 9.5, 3.2, 1.6 Hz, 1H), 1.46 (qd, *J* = 12.1, 3.2 Hz, 2H), 1.34 – 1.18 (m, 3H), 0.90 (d, *J* = 8.3 Hz, 3H), 0.88 (d, *J* = 8.4 Hz, 3H) ppm. **¹³C{¹H} NMR** (CDCl₃, 126 MHz) δ 175.5, 137.2, 115.4, 55.9, 46.0, 32.2, 30.2, 30.0, 26.96, 25.93, 25.92, 18.9, 18.2 ppm. **HRMS** (+APCI) calculated for C₁₃H₂₄NO [M+H]⁺ 210.1858, found 210.1848. **HPLC** (AS-H column, 5% 2-propanol in Hexanes, 1 mL/min) *t*_M = 13.8 min, *t*_m = 10.4 min, 94:6 e.r.

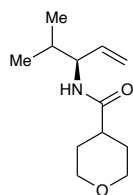


Experiment conducted by Amaan Kazerouni. *Benzyl (S)-4-((4-methylpent-1-en-3-yl)carbamoyl)piperidine-1-carboxylate (112)*: Prepared according to **General Procedure B** using 4-methylpent-1-ene (0.0127 mL, 0.10 mmol, 1.0 equiv), benzyl 4-(5-oxo-1,4,2-dioxazol-3-yl)piperidine-1-carboxylate (0.0610 g, 0.20 mmol, 2.0 equiv), LiOAc (0.0006 g, 0.010 mmol, 0.10 equiv), AgNTf₂ (0.0078 g, 0.020 mmol, 0.20 equiv), LiNTf₂ (0.0290 g, 0.10 mmol, 1.0 equiv), and (*S,S*)-[Rh(2-Me-3-Ph-Ind)₂]₂ (0.0056 g, 0.005 mmol, 0.05 equiv) in DCE (0.5 mL) at room temperature for 48 hours. Purified by flash chromatography on silica gel (30-50% EtOAc in Hexanes) to provide **112** (0.0210 g, 61% yield, 99:1 e.r.) as a white solid. **¹H NMR** (CDCl₃, 600MHz) δ 7.40 – 7.30 (m, 5H), 5.74 (ddd, *J* = 16.8, 10.5, 5.8 Hz, 1H), 5.41 (d, *J* = 9.1 Hz, 1H), 5.16 – 5.07 (m, 4H), 4.38 – 4.31 (m, 1H), 4.29 – 4.15 (m, 2H), 2.97 – 2.71 (m, 2H), 2.29 (ddt, *J* = 11.6, 7.5, 3.7 Hz, 1H), 1.88 – 1.78 (m, 2H) 1.80 (dq, *J* = 13.6, 6.7 Hz, 1H), 1.72 – 1.63 (s, 2H), 0.90 (d, *J* = 6.7 Hz, 3H), 0.88 (d, *J* = 6.8 Hz, 3H) ppm. **¹³C{¹H} NMR** (CDCl₃, 126 MHz) δ 173.63, 155.34, 136.85, 136.81, 128.63, 128.15, 128.02, 115.76, 67.31, 56.31, 43.61, 43.58, 32.18, 29.84, 28.98, 28.78, 18.86, 18.23 ppm. **HRMS** (+APCI) calculated for C₂₀H₂₉N₂O₃ [M+H]⁺ 345.2178, found 345.2165. **HPLC** (AS-H column, 10% 2-propanol in hexanes, 1mL/min) *t*_M = 20.1 min, *t*_m = 14.0 min, 99:1 e.r.



(S)-N-(4-methylpent-1-en-3-yl)-2-phenylacetamide (108): Prepared according to **General Procedure B** using 4-methylpentene (0.0127 mL, 0.10 mmol, 1.0 equiv), 3-benzyl-1,4,2-dioxazol-5-one 0.0354 g, 0.20 mmol, 2.0 equiv), LiOAc (0.0006 g, 0.010 mmol, 0.10 equiv), AgNTf₂ (0.0078 g, 0.020 mmol, 0.20 equiv), LiNTf₂ (0.0290 g, 0.10 mmol, 1.0 equiv) and (*S,S*)-[Rh(2-Me-3-Ph-Ind)₂]₂ (0.0056 g, 0.005 mmol, 0.05 equiv) in DCE (0.5 mL) at room temperature for 48 hours. Purified by flash chromatography on silica gel (20-50% EtOAc in Hexanes) to provide **108** (0.080 g, 37% yield, 99:1 e.r.) as a white solid. **¹H NMR** (CDCl₃, 400 MHz) δ 7.41 – 7.35 (m, 2H), 7.34 – 7.27 (m, 3H), 5.66 (ddd, *J* = 17.2, 10.5, 5.5 Hz, 1H), 5.05 (dq, *J* = 10.5, 1.5 Hz,

1H), 4.95 (dq, $J = 17.2, 1.5$ Hz, 1H), 4.33 (dtd, $J = 9.2, 5.5, 1.5$ Hz, 1H), 1.70 (dt, $J = 13.6, 6.8$ Hz, 1H), 0.79 (d, $J = 6.8$ Hz, 3H), 0.73 (d, $J = 6.9$ Hz, 3H) ppm. $^{13}\text{C}\{^1\text{H}\}$ NMR (CDCl₃, 126 MHz) δ 170.41, 136.72, 135.20, 129.58, 129.24, 127.60, 115.39, 56.38, 44.25, 32.10, 18.74, 17.90 ppm. **HRMS** (+APCI) calculated for C₁₄H₂₀NO [M+H]⁺ 218.15394, found 218.15361. **HPLC** (AD-H column, 5% 2-propanol in Hexanes, 1 mL/min) $t_M = 12.4$ min, $t_m = 10.1$ min, 99:1 e.r.

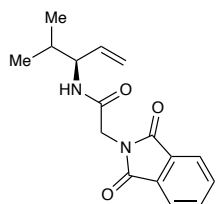


(*S*)-*N*-(4-methylpent-1-en-3-yl)tetrahydro-2H-pyran-4-carboxamide (**111**): Prepared according to

General Procedure B using 4-methylpentene (0.0127 mL, 0.10 mmol, 1.0 equiv), 3-

(tetrahydro-2H-pyran-4-yl)-1,4,2-dioxazol-5-one (0.0342 g, 0.20 mmol, 2.0 equiv),

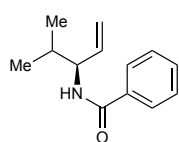
LiOAc (0.0006 g, 0.010 mmol, 0.10 equiv), AgNTf₂ (0.0078 g, 0.020 mmol, 0.20 equiv), LiNTf₂ (0.0290 g, 0.10 mmol, 1.0 equiv) and (*S,S*)-[Rh(2-Me-3-Ph-Ind)I₂]₂ (0.0056 g, 0.005 mmol, 0.05 equiv) in DCE (0.5 mL) at room temperature for 48 hours. Purified by flash chromatography on silica gel (20-50% EtOAc in Hexanes) to provide **111** (0.093 g, 44% yield, 98:2 e.r.) as a white solid. ^1H NMR (CDCl₃, 600 MHz) δ 5.76 (ddd, $J = 17.1, 10.5, 5.8$ Hz, 1H), 5.36 (d, $J = 8.7$ Hz, 1H), 5.16 – 5.10 (m, 2H), 4.37 (dtd, $J = 9.0, 5.7, 1.6$ Hz, 1H), 4.03 (ddd, $J = 11.4, 4.0, 2.3$ Hz, 2H), 3.43 (tt, $J = 11.5, 2.4$ Hz, 2H), 2.38 (tt, $J = 11.3, 4.3$ Hz, 1H), 1.90 – 1.73 (m, 5H), 0.91 (d, $J = 6.8$ Hz, 3H), 0.89 (d, $J = 6.9$ Hz, 3H) ppm. $^{13}\text{C}\{^1\text{H}\}$ NMR (CDCl₃, 151 MHz) δ 173.68, 136.91, 115.69, 67.44, 56.22, 42.72, 32.20, 29.53, 18.87, 18.22 ppm. **HRMS** (+APCI) calculated for C₁₂H₂₂NO₂ [M+H]⁺ 212.16451, found 212.16413 ppm. **HPLC** (OD-H column, 5% 2-propanol in Hexanes, 1 mL/min) $t_M = 14.7$ min, $t_m = 10.4$ min, 98:2 e.r.



Experiment conducted by Christopher Poffi. (*S*)-2-(1,3-dioxoisindolin-2-yl)-*N*-(4-methylpent-1-en-3-yl)acetamide (**113**): Prepared according to **General Procedure**

B using 4-methylpentene (0.0127 mL, 0.10 mmol, 1.0 equiv), 2-((5-oxo-1,4,2-

dioxazol-3-yl)methyl)isoindoline-1,3-dione (**S10**) (0.0492 g, 0.20 mmol, 2.0 equiv), LiOAc (0.0006 g, 0.010 mmol, 0.10 equiv), AgNTf₂ (0.0078 g, 0.020 mmol, 0.20 equiv), LiNTf₂ (0.0290 g, 0.10 mmol, 1.0 equiv), and (*S,S*)-[Rh(2-Me-3-Ph-Ind)I₂]₂ (0.0056 g, 0.005 mmol, 0.05 equiv) in DCE (0.5 mL) at room temperature for 48 hours. Purified by flash chromatography on silica gel (20-50% EtOAc in Hexanes) to provide **113** (0.0250 g, 87% yield, 97:3 e.r.) as a white solid. **¹H NMR** (CDCl₃, 600 MHz) δ 7.89 (dd, *J* = 5.4, 3.1 Hz, 2H), 7.75 (dd, *J* = 5.5, 3.0 Hz, 2H), 5.74 (ddd, *J* = 17.2, 10.5, 5.9 Hz, 1H), 5.66 (d, *J* = 9.1 Hz, 1H), 5.20 – 5.13 (m, 2H), 4.37 (s, 2H), 4.35 (ddt, *J* = 9.0, 5.8, 1.6 Hz, 1H), 1.88 – 1.78 (m, 1H), 0.91 (d, *J* = 6.8 Hz, 3H), 0.90 (d, *J* = 6.9 Hz, 3H) ppm. **¹³C NMR** (CDCl₃, 151 MHz, CDCl₃) δ 167.79, 165.45, 136.07, 134.28, 132.01, 123.68, 116.17, 57.04, 41.18, 32.03, 18.68, 18.08 ppm. **HRMS** (+APCI) calculated for C₁₆H₁₉NO₃ [M+H]⁺ 287.13902, found 287.13889. **HPLC** (OJ)-H column, 10% 2-propanol in Hexanes, 1 mL/min) *t*_M = 20.2 min, *t*_m = 17.9 min, 97:3 e.r.

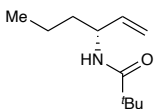


(*S*)-*N*-(4-methylpent-1-en-3-yl)benzamide (**109**): Prepared according to **General**

Procedure B using 4-methylpentene (0.0127 mL, 0.10 mmol, 1.0 equiv), 3-phenyl-1,4,2-dioxazol-5-one (0.0326 g, 0.20 mmol, 2.0 equiv), LiOAc (0.0006 g, 0.010 mmol, 0.10 equiv), AgNTf₂ (0.0078 g, 0.020 mmol, 0.20 equiv), LiNTf₂ (0.0290 g, 0.10 mmol, 1.0 equiv) and (*S,S*)-[Rh(2-Me-3-Ph-Ind)I₂]₂ (0.0056 g, 0.005 mmol, 0.05 equiv) in DCE (0.5 mL) at room temperature for 48 hours. Purified by flash chromatography on silica gel (10-50% EtOAc in Hexanes) to provide **109** (0.0026 g, 13% yield, 99:1 e.r.) as a white solid. **¹H NMR** (CDCl₃, 600 MHz) δ 7.80 – 7.77 (m, 2H), 7.53 – 7.49 (m, 1H), 7.47 – 7.43 (m, 2H), 6.02 (d, *J* = 7.4 Hz, 1H), 5.85 (ddd, *J* = 17.1, 10.5, 5.8 Hz, 1H), 5.23 (dt, *J* = 17.2, 1.5 Hz, 1H), 5.19 (dt, *J* = 10.5, 1.4 Hz, 1H), 4.58 (dtt, *J* = 8.8, 5.7, 1.5 Hz, 1H), 1.94 (qnd, *J* = 6.9, 5.7 Hz, 1H), 0.99 (d, *J* = 3.9 Hz, 3H), 0.98 (d, *J* = 4.0 Hz, 3H). **¹³C{¹H} NMR** (CDCl₃, 151 MHz) δ 167.06, 136.81, 135.10, 131.58, 128.77, 126.97, 116.02, 57.02, 32.41, 18.95, 18.39.

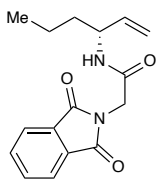
HRMS (+APCI) calculated for $C_{13}H_{18}NO$ $[M+H]^+$ 204.13854, found 204.13854. **HPLC** (AS-H column, 5% 2-propanol in Hexanes, 1 mL/min) $t_M = 21.5$ min, $t_m = 17.6$ min, 99:1 e.r.

ALKENE SCOPE



Experiment conducted by Christopher Poff. *(R)*-*N*-(hex-1-en-3-yl)pivalamide (**114**):

Prepared according to **General Procedure B** using hex-1-ene (0.0084 g, 0.10 mmol, 1.0 equiv), 3-(*tert*-butyl)-1,4,2-dioxazol-5-one (0.0286 g, 0.20 mmol, 2.0 equiv), (*R,R*)-[Rh(2-Me-3-Ph-Ind) I_2] I_2 (0.0056 g, 0.005 mmol, 0.05 equiv), LiOAc (0.0006 g, 0.010 mmol, 0.10 equiv), AgNTf $_2$ (0.0078 g, 0.020 mmol, 0.20 equiv), and LiNTf $_2$ (0.0290 g, 0.10 mmol, 1.0 equiv) in DCE (0.5 mL) at room temperature for 48 hours. Purified by flash chromatography on silica gel (10-30% EtOAc in Hexanes) to provide **114** (0.0297 g, 90% yield, 98:2 e.r.) as a white solid. 1H NMR (CDCl $_3$, 500 MHz) δ 5.82 – 5.73 (m, 1H), 5.45 (s, 1H), 5.15 – 5.05 (m, 2H), 4.50 – 4.42 (m, 1H), 1.58 – 1.50 (m, 1H), 1.50 – 1.40 (m, 1H), 1.40 – 1.30 (m, 2H), 1.22 (s, 9H), 0.95 – 0.91 (m, 3H) ppm. ^{13}C NMR (CDCl $_3$, 126 MHz) δ 177.77, 139.00, 114.43, 50.78, 38.89, 37.24, 27.81, 19.14, 14.04 ppm. **HRMS** (+APCI) calculated for $C_{11}H_{22}NO$ $[M+H]^+$ 184.16959, found 184.16954. **HPLC** (WHELK column, 1% 2-propanol in Hexanes, 1 mL/min) $t_M = 18.4$ min, $t_m = 16.1$ min, 98:2 e.r.



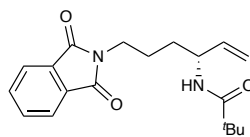
Experiment conducted by Christopher Poff. *(R)*-2-(1,3-dioxoisindolin-2-yl)-*N*-(hex-1-en-

3-yl)acetamide (**115**): Prepared according to **General Procedure B** using hex-1-ene

(0.0084 g, 0.10 mmol, 1.0 equiv), 2-((5-oxo-1,4,2-dioxazol-3-yl)methyl)isoindoline-1,3-

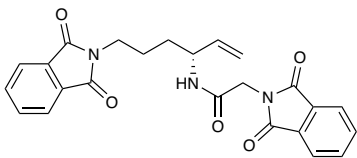
dione (0.0492 g, 0.20 mmol, 2.0 equiv), (*R,R*)-[Rh(2-Me-3-Ph-Ind) I_2] I_2 (0.0056 g, 0.005 mmol, 0.05 equiv), LiOAc (0.0006 g, 0.010 mmol, 0.10 equiv), AgNTf $_2$ (0.0078 g, 0.020 mmol, 0.20 equiv), and LiNTf $_2$ (0.0290 g, 0.10 mmol, 1.0 equiv) in DCE (0.5 mL) at room temperature for 48 hours. Purified by flash chromatography on silica gel (10-30% EtOAc in Hexanes) to provide **115** (0.0297 g, 90%

yield, 93:7 e.r.) as a white solid. $^1\text{H NMR}$ (CDCl_3 , 600 MHz) δ 7.92 – 7.85 (m, 2H), 7.78 – 7.71 (m, 2H), 5.75 (ddd, $J = 17.2, 10.4, 5.7$ Hz, 1H), 5.59 (d, $J = 8.3$ Hz, 1H), 5.21 – 5.07 (m, 2H), 4.47 (dq, $J = 7.3, 5.9, 1.6$ Hz, 1H), 4.35 (s, 2H), 1.56 – 1.45 (m, 2H), 1.40 – 1.30 (m, 2H), 0.92 (t, $J = 7.3$ Hz, 3H) ppm. $^{13}\text{C NMR}$ (CDCl_3 , 151 MHz) δ 167.93, 165.44, 137.96, 134.40, 134.34, 132.21, 132.18, 123.81, 115.43, 51.78, 41.18, 41.12, 37.03, 19.06, 13.95 ppm. **HRMS** (+APCI) calculated for $\text{C}_{16}\text{H}_{19}\text{N}_2\text{O}_3$ $[\text{M}+\text{H}]^+$ 287.13902, found 287.13888. **HPLC** (AD-H column, 5% 2-propanol in Hexanes, 1 mL/min) $t_{\text{M}} = 29.1$ min, $t_{\text{m}} = 31.6$ min, 93:7 e.r.



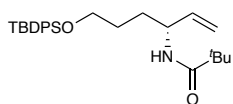
Experiment conducted by Amaan Kazerouni. *(R)*-*N*-(6-(1,3-dioxoisindolin-2-yl)hex-1-en-3-yl)pivalamide (**116**): Prepared according to **General Procedure B** using 2-(hex-5-en-1-yl)isoindoline-1,3-dione (0.0230 g, 0.10 mmol, 1.0 equiv),

3-(*tert*-butyl)-1,4,2-dioxazol-5-one (0.0286 g, 0.20 mmol, 2.0 equiv), (*R,R*)-[Rh(2-Me-3-Ph-Ind) I_2] $_2$ (0.0056 g, 0.005 mmol, 0.05 equiv), LiOAc (0.0006 g, 0.010 mmol, 0.10 equiv), AgNTf $_2$ (0.0078 g, 0.020 mmol, 0.20 equiv), and LiNTf $_2$ (0.0290 g, 0.10 mmol, 1.0 equiv) in DCE (0.5 mL) at room temperature for 48 hours. Purified by flash chromatography on silica gel (10-30% EtOAc in Hexanes) to provide **116** (0.0297 g, 90% yield, 98:2 e.r.) as a white solid. $^1\text{H NMR}$ (CDCl_3 , 600 MHz) δ 7.83 (dd, $J = 5.4, 3.0$ Hz, 2H), 7.71 (dd, $J = 5.5, 2.9$ Hz, 2H), 5.74 (ddd, $J = 17.3, 10.4, 5.5$ Hz, 1H), 5.58 (d, $J = 8.6$ Hz, 1H), 5.16 – 5.05 (m, 2H), 4.55 – 4.46 (m, 1H), 3.70 (t, $J = 7.0$ Hz, 2H), 1.75 – 1.66 (m, 2H), 1.67 – 1.58 (m, 1H), 1.56 – 1.47 (m, 1H), 1.20 (s, 9H) ppm. $^{13}\text{C NMR}$ (CDCl_3 , 126 MHz) δ 178.00, 168.55, 138.40, 134.09, 132.24, 123.37, 115.08, 50.68, 38.90, 37.84, 32.06, 27.75, 25.21 ppm. **HRMS** (+APCI) calculated for $\text{C}_{19}\text{H}_{25}\text{N}_2\text{O}_3$ $[\text{M}+\text{H}]^+$ 329.1865, found 329.1859. **HPLC** (AS-H column, 1% 2-propanol in Hexanes, 1 mL/min) $t_{\text{M}} = 13.1$ min, $t_{\text{m}} = 18.3$ min, 98:2 e.r.



Experiment conducted by Amaan Kazerouni. *(R)*-2-(1,3-dioxoisindolin-2-yl)-*N*-(6-(1,3-dioxoisindolin-2-yl)hex-1-en-3-yl)acetamide (**117**): Prepared according to **General Procedure B** using 2-(hex-5-en-1-

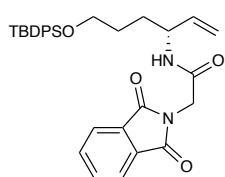
yl)isindoline-1,3-dione (0.0230 g, 0.10 mmol, 1.0 equiv), 2-((5-oxo-1,4,2-dioxazol-3-yl)methyl)isindoline-1,3-dione (0.0492 g, 0.20 mmol, 2.0 equiv), *(R,R)*-[Rh(2-Me-3-Ph-Ind)₂]₂ (0.0056 g, 0.005 mmol, 0.05 equiv), LiOAc (0.0006 g, 0.010 mmol, 0.10 equiv), AgNTf₂ (0.0078 g, 0.020 mmol, 0.20 equiv), and LiNTf₂ (0.0290 g, 0.10 mmol, 1.0 equiv) in DCE (0.5 mL) at room temperature for 48 hours. Purified by flash chromatography on silica gel (50-66% EtOAc in Hexanes) to provide **117** (0.0313 g, 73% yield, 92:8 e.r.) as a white solid. ¹H NMR (CDCl₃, 600 MHz) δ 7.85 (dd, *J* = 5.5, 3.1 Hz, 2H), 7.78 (dd, *J* = 5.4, 3.1 Hz, 2H), 7.71 (dd, *J* = 5.5, 3.0 Hz, 2H), 7.70 (dd, *J* = 5.5, 3.0 Hz, 2H), 6.17 (d, *J* = 8.5 Hz, 1H), 5.72 (ddd, *J* = 17.2, 10.4, 5.6 Hz, 1H), 5.25 – 5.05 (m, 2H), 4.56 – 4.48 (m, 1H), 4.38 (s, 2H), 3.71 (t, *J* = 7.0 Hz, 2H), 1.75 (qn, *J* = 7.3 Hz, 2H), 1.67 – 1.58 (m, 1H), 1.57 – 1.48 (m, 1H) ppm. ¹³C{¹H} NMR (CDCl₃, 151 MHz) δ 168.69, 167.99, 165.80, 137.53, 134.30, 134.13, 132.21, 132.14, 123.73, 123.40, 115.76, 51.93, 41.15, 37.71, 31.40, 25.46 ppm. HRMS (+APCI) calculated for C₂₄H₂₂N₃O₅ [M+H]⁺ 432.1559, found 432.1552. HPLC (AD-H column, 15% 2-propanol in Hexanes, 1.5 mL/min) *t*_M = 25.2 min, *t*_m = 28.7 min, 92:8 e.r.



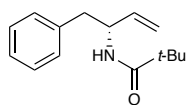
Experiment conducted by Amaan Kazerouni. *(R)*-*N*-(6-((*tert*-butyldiphenylsilyl)oxy)hex-1-en-3-yl)pivalamide (**118**): Prepared according to **General**

Procedure B using *tert*-butyl(hex-5-en-1-yloxy)diphenylsilane (0.0339 g, 0.10 mmol, 1.0 equiv), 3-(*tert*-butyl)-1,4,2-dioxazol-5-one (0.0286 g, 0.20 mmol, 2.0 equiv), *(R,R)*-[Rh(2-Me-3-Ph-Ind)₂]₂ (0.0056 g, 0.005 mmol, 0.05 equiv) LiOAc (0.0006 g, 0.010 mmol, 0.10 equiv), AgNTf₂ (0.0078 g, 0.020 mmol, 0.20 equiv), and LiNTf₂ (0.0290 g, 0.10 mmol, 1.0 equiv) in DCE (0.5 mL) at room temperature for 48 hours. Purified by flash chromatography on silica gel (10-30% EtOAc in Hexanes) to provide **118**

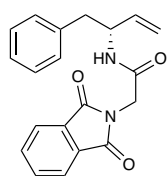
(0.0215 g, 49% yield, 90:10 e.r.) as a white solid. **¹H NMR** (CDCl₃, 600 MHz) δ 7.65 (dt, *J* = 6.6, 1.5 Hz, 4H), 7.45 – 7.34 (m, 6H), 5.76 (ddd, *J* = 17.2, 10.4, 5.3 Hz, 1H), 5.46 (d, *J* = 7.8 Hz, 1H), 5.16 – 5.06 (m, 2H), 4.50 – 4.41 (m, 1H), 3.73 – 3.62 (m, 2H), 1.74 – 1.64 (m, 2H), 1.61 – 1.48 (m, 2H), 1.20 (s, 9H), 1.05 (s, 9H) ppm. **¹³C{¹H} NMR** (CDCl₃, 151 MHz) δ 177.66, 138.70, 135.55, 133.95, 133.91, 129.60, 127.64, 114.47, 63.51, 50.66, 38.74, 31.22, 28.89, 27.65, 26.89, 19.23 ppm. **HRMS** (+APCI) calculated for C₂₇H₄₀NO₂Si [M+H]⁺ 438.2828, found 438.2820. **HPLC** (AS-H column, 1% 2-propanol in Hexanes, 1 mL/min) *t*_M = 5.2 min, *t*_m = 4.5 min, 90:10 e.r.



Experiment conducted by Amaan Kazerouni. *(R)*-*N*-(6-((*tert*-butyldiphenylsilyl)oxy)hex-1-en-3-yl)-2-(1,3-dioxoisindolin-2-yl)acetamide (**119**): Prepared according to **General Procedure B** using *tert*-butyl(hex-5-en-1-yloxy)diphenylsilane (0.0339 g, 0.10 mmol, 1.0 equiv), 2-((5-oxo-1,4,2-dioxazol-3-yl)methyl)isoindoline-1,3-dione (0.0492 g, 0.20 mmol, 2.0 equiv), (*R,R*)-[Rh(2-Me-3-Ph-Ind)₂]₂ (0.0056 g, 0.005 mmol, 0.05 equiv), LiOAc (0.0006 g, 0.010 mmol, 0.10 equiv), AgNTf₂ (0.0078 g, 0.020 mmol, 0.20 equiv), and LiNTf₂ (0.0290 g, 0.10 mmol, 1.0 equiv) in DCE (0.5 mL) at 60 °C for 48 hours. Purified by flash chromatography on silica gel (10-50% EtOAc in Hexanes) to provide **119** (0.0184 g, 34% yield, 97:3 e.r.) as an off-white solid. **¹H NMR** (CDCl₃, 600 MHz) δ 7.87 (dd, *J* = 5.5, 3.0 Hz, 2H), 7.73 (dd, *J* = 5.5, 3.0 Hz, 2H), 7.68 – 7.63 (m, 4H), 7.47 – 7.35 (m, 6H), 5.74 (ddd, *J* = 17.2, 10.4, 5.6 Hz, 1H), 5.67 (d, *J* = 8.2 Hz, 1H), 5.20 – 5.10 (m, 2H), 4.49 – 4.41 (m, 1H), 4.29 (d, *J* = 2.1 Hz, 1H), 4.29 (d, *J* = 2.1 Hz, 1H), 3.68 (qd, *J* = 6.0, 3.0 Hz, 2H), 1.75 – 1.66 (m, 2H), 1.63 – 1.57 (m, 2H), 1.04 (s, 9H) ppm. **¹³C NMR** (CDCl₃, 151 MHz) δ 167.89, 165.47, 137.83, 135.70, 134.36, 134.03, 132.19, 129.77, 127.82, 123.78, 115.57, 63.57, 51.85, 41.11, 31.15, 28.78, 27.05, 19.38. **HRMS** (+APCI) calculated for C₃₂H₃₇N₂O₄Si [M+H]⁺ 541.2523, found 541.2509. **HPLC** (AS-H column, 5% 2-propanol in Hexanes, 1 mL/min) *t*_M = 56.2 min, *t*_m = 41.2 min, 97:3 e.r.

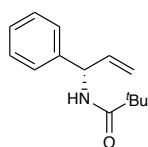


(R)-*N*-(1-phenylbut-3-en-2-yl)pivalamide (**122**): Prepared according to **General Procedure B** using 4-phenylbutene (0.0127 mL, 0.10 mmol, 1.0 equiv), 3-(*tert*-butyl)-1,4,2-dioxazol-5-one (0.0338 g, 0.20 mmol, 2.0 equiv), (*R,R*)-[Rh(2-Me-3-Ph-Ind)₂]₂ (0.0056 g, 0.005 mmol, 0.05 equiv), LiOAc (0.0006 g, 0.010 mmol, 0.10 equiv), AgNTf₂ (0.0078 g, 0.020 mmol, 0.20 equiv), and LiNTf₂ (0.0290 g, 0.10 mmol, 1.0 equiv) in DCE (0.5 mL) at room temperature for 48 hours. Purified by flash chromatography on silica gel (10-25% EtOAc in Hexanes) to provide **122** (0.0132 g, 57% yield, 98:2 e.r.) as a white solid. ¹H NMR (CDCl₃, 600 MHz) δ 7.30 – 7.27 (m, 2H), 7.24 – 7.20 (m, 1H), 7.19 – 7.15 (m, 2H), 5.85 (ddd, *J* = 17.2, 10.5, 5.2 Hz, 1H), 5.46 (d, *J* = 8.2 Hz, 1H), 5.12 – 5.05 (m, 2H), 4.78 (dtdt, *J* = 8.4, 6.8, 5.2, 1.7 Hz, 1H), 2.92 (dd, *J* = 13.7, 6.6 Hz, 1H), 2.83 (dd, *J* = 13.7, 6.8 Hz, 1H), 1.12 (s, 9H) ppm. ¹³C NMR (CDCl₃, 151 MHz) δ 177.71, 138.05, 137.35, 129.65, 128.50, 126.77, 114.91, 51.55, 41.03, 38.86, 27.65 ppm. HRMS (+APCI) calculated for C₁₅H₂₂NO [M+H]⁺ 232.16959, found 232.16947. HPLC (OD-H column, 5% 2-propanol in Hexanes, 1 mL/min) *t*_M = 8.4 min, *t*_m = 7.6 min, 98:2 e.r.



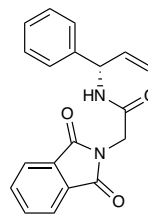
(R)-2-(1,3-dioxoisindolin-2-yl)-*N*-(1-phenylbut-3-en-2-yl)acetamide (**123**): Prepared according to **General Procedure B** using 4-phenyl-1-butene (0.015 mL, 0.10 mmol, 1.0 equiv), 2-((5-oxo-1,4,2-dioxazol-3-yl)methyl)isoindoline-1,3-dione (0.0492 g, 0.20 mmol, 2.0 equiv), (*R,R*)-[Rh(2-Me-3-Ph-Ind)₂]₂ (0.0056 g, 0.005 mmol, 0.05 equiv), LiOAc (0.0006 g, 0.010 mmol, 0.10 equiv), AgNTf₂ (0.0078 g, 0.020 mmol, 0.20 equiv), and LiNTf₂ (0.0290 g, 0.10 mmol, 1.0 equiv) in DCE (0.5 mL) at 40 °C for 48 hours. Purified by flash chromatography on silica gel (30-50% EtOAc in Hexanes) to provide **123** (0.0151 g, 45% yield, 95:5 e.r.) as a white solid. ¹H NMR (CDCl₃, 600 MHz) δ 7.87 (dd, *J* = 5.4, 3.0 Hz, 2H), 7.75 (dd, *J* = 5.4, 3.0 Hz, 2H), 7.21 – 7.15 (m, 2H), 7.16 – 7.10 (m, 3H), 5.80 (ddd, *J* = 17.3, 10.4, 5.4 Hz, 1H), 5.71 (d, *J* = 8.4 Hz, 1H), 5.15 –

5.09 (m, 2H), 4.80 – 4.72 (m, 1H), 4.29 (s, 2H), 2.88 (dd, $J = 6.5, 1.7$ Hz, 2H) ppm. $^{13}\text{C}\{^1\text{H}\}$ NMR (CDCl₃, 151 MHz) δ 167.79, 165.50, 136.90, 136.79, 134.40, 132.09, 129.62, 128.49, 126.77, 123.79, 115.87, 52.42, 41.17, 40.76 ppm. HRMS (+APCI) calculated for C₂₀H₁₉N₂O₃ [M+H]⁺ 335.13902, found 335.13887. HPLC (AD-H column, 10% 2-propanol in Hexanes, 1 mL/min) $t_M = 18.4$ min, $t_m = 21.7$ min, 95:5 e.r.



Experiment conducted by Amaan Kazerouni. (*S*)-*N*-(1-phenylallyl)pivalamide (**124**):

Prepared according to **General Procedure B** using allyl benzene (0.0132 mL, 0.10 mmol, 1.0 equiv), 3-(*tert*-butyl)-1,4,2-dioxazol-5-one (0.0286 g, 0.20 mmol, 2.0 equiv), LiOAc (0.0006 g, 0.010 mmol, 0.10 equiv), AgNTf₂ (0.0078 g, 0.020 mmol, 0.20 equiv), LiNTf₂ (0.0290 g, 0.10 mmol, 1.0 equiv), and (*R,R*)-[Rh(2-Me-3-Ph-Ind)I₂]₂ (0.0056 g, 0.200 mmol, 0.005 equiv) in DCE (0.5 mL) at room temperature for 48 hours. Purified by flash chromatography on silica gel (10-30% EtOAc in Hexanes) to provide **124** (0.0150 g, 69% yield, 93:7 e.r.) as a colorless solid. ^1H NMR (CDCl₃, 600 MHz) δ 7.37 – 7.33 (m, 2H), 7.30 – 7.27 (m, 3H), 6.02 (ddd, $J = 17.1, 10.4, 5.3$ Hz, 1H), 5.85 (s, 1H), 5.62 (dd, $J = 7.9, 5.5$ Hz, 1H), 5.29 – 5.13 (m, 2H), 1.23 (s, 9H). ^{13}C NMR (CDCl₃, 151 MHz) δ 173.37, 140.84, 137.50, 128.78, 127.61, 127.11, 115.68, 54.78, 38.79, 27.61 ppm. HRMS (+APCI) calculated for C₁₄H₂₀NO [M+H]⁺ 218.15339, found 218.15394. HPLC (OJ-H column, 10% 2-propanol in Hexanes, 1 mL/min) $t_M = 9.1$ min, $t_m = 8.1$ min, 93:7 e.r.

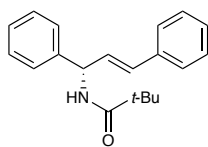


Experiment conducted by Amaan Kazerouni. (*S*)-2-(1,3-dioxoisindolin-2-yl)-*N*-(1-

phenylallyl)acetamide (**125**): Prepared according to **General Procedure B** using allyl benzene (0.0132 mL, 0.10 mmol, 1.0 equiv), 2-((5-oxo-1,4,2-dioxazol-3-yl)methyl)isindoline-1,3-dione 0.0492 g, 0.20 mmol, 2.0 equiv), (*R,R*)-[Rh(2-Me-3-Ph-

Ind)I₂]₂ (0.0056 g, 0.005 mmol, 0.05 equiv), LiOAc (0.0006 g, 0.010 mmol, 0.10 equiv), AgNTf₂ (0.0078

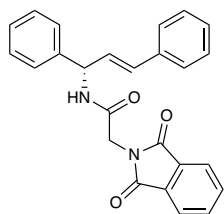
g, 0.020 mmol, 0.20 equiv), and LiNTf₂ (0.0290 g, 0.10 mmol, 1.0 equiv) in DCE (0.5 mL) at 60 °C for 48 hours. Purified by flash chromatography on silica gel (10-50% EtOAc in Hexanes) to provide **125** (0.0105 g, 33% yield, 93:7 e.r.) as a white solid. **¹H NMR** (CDCl₃, 600 MHz) δ 7.88 (dd, *J* = 5.4, 3.0 Hz, 2H), 7.74 (dd, *J* = 5.5, 3.0 Hz, 2H), 7.38 – 7.33 (m, 2H), 7.31 – 7.27 (m, 3H), 6.04 (d, *J* = 8.2 Hz, 1H), 6.00 (ddd, *J* = 17.1, 10.4, 5.3 Hz, 1H), 5.66 – 5.59 (m, 1H), 5.30 – 5.23 (m, 2H), 4.40 (d, *J* = 16.0 Hz, 1H), 4.36 (d, *J* = 16.0 Hz, 1H) ppm. **¹³C NMR** (CDCl₃, 151 MHz) δ 167.78, 165.15, 139.89, 136.54, 134.28, 132.01, 128.87, 127.90, 127.27, 123.68, 116.44, 55.59, 40.99 ppm. **HRMS** (+APCI) calculated for C₁₉H₁₇N₂O₃ [M+H]⁺ 321.1239, found 321.1229. **HPLC** (OD-H column, 3% 2-propanol in Hexanes, 1 mL/min) *t*_M = 22.5 min, *t*_m = 19.0 min, 93:7 e.r.



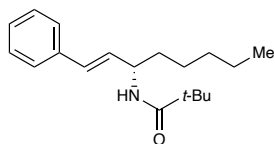
(*S,E*)-*N*-(1,3-diphenylallyl)pivalamide (**126**): Prepared according to **General**

Procedure B using (*E*)-prop-1-ene-1,3-diyl dibenzene (0.0194 g, 0.10 mmol, 1.0 equiv), 3-(*tert*-butyl)-1,4,2-dioxazol-5-one (0.0286 g, 0.20 mmol, 2.0 equiv), (*R,R*)-

[Rh(2-Me-3-Ph-Ind)I₂]₂ (0.0056 g, 0.005 mmol, 0.05 equiv), LiOAc (0.0006 g, 0.010 mmol, 0.10 equiv), AgNTf₂ (0.0078 g, 0.020 mmol, 0.20 equiv), and LiNTf₂ (0.0290 g, 0.10 mmol, 1.0 equiv) in DCE (0.5 mL) at 40 °C for 48 hours. Purified by flash chromatography on silica gel (5-30% EtOAc in Hexanes) to provide **126** (0.0065 g, 22% yield, 98:2 e.r.) as a white solid. **¹H NMR** (CDCl₃, 600 MHz) δ 7.37 (t, *J* = 7.2 Hz, 4H), 7.34 – 7.28 (m, 5H), 7.26 – 7.22 (m, 1H), 6.51 (dd, *J* = 16.0, 1.5 Hz, 1H), 6.35 (dd, *J* = 15.9, 6.1 Hz, 1H), 5.98 (d, *J* = 8.0 Hz, 1H), 5.80 (ddd, *J* = 8.0, 6.2, 1.3 Hz, 1H), 1.25 (s, 9H). **¹³C{¹H} NMR** (CDCl₃, 151 MHz) δ 177.49, 141.27, 136.62, 131.62, 129.23, 128.96, 128.71, 127.94, 127.75, 127.15, 126.69, 54.63, 38.98, 27.78. **HRMS** (+APCI) calculated for C₂₀H₂₄NO [M+H]⁺ 294.18524, found 294.185123. **HPLC** (AD-H column, 5% 2-propanol in Hexanes, 1 mL/min) *t*_M = 16.2 min, *t*_m = 13.8 min, 98:2 e.r.

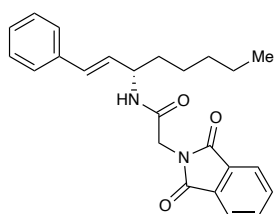


(S,E)-2-(1,3-dioxoisindolin-2-yl)-*N*-(1,3-diphenylallyl)acetamide (**127**): Prepared according to **General Procedure B** using (*E*)-prop-1-ene-1,3-diyl dibenzene (0.0194 mg, 0.10 mmol, 1.0 equiv), 2-((5-oxo-1,4,2-dioxazol-3-yl)methyl)isindoline-1,3-dione (0.0492 g, 0.20 mmol, 2.0 equiv), (*R,R*)-[Rh(2-Me-3-Ph-Ind)₂]₂ (0.0056 g, 0.005 mmol, 0.05 equiv), LiOAc (0.0006 g, 0.010 mmol, 0.10 equiv), AgNTf₂ (0.0078 g, 0.020 mmol, 0.20 equiv), and LiNTf₂ (0.0290 g, 0.10 mmol, 1.0 equiv) in DCE (0.5 mL) at 60 °C for 48 hours. Purified by flash chromatography on silica gel (20-50% EtOAc in Hexanes) to provide **127** (0.0175 g, 44% yield, 79:21 e.r.) as a white solid. ¹H NMR (CDCl₃, 600 MHz) δ 7.87 (dd, *J* = 5.4, 3.0 Hz, 2H), 7.73 (dd, *J* = 5.4, 3.0 Hz, 2H), 7.38 – 7.32 (m, 6H), 7.30 (t, *J* = 7.5 Hz, 3H), 7.23 (t, *J* = 7.3 Hz, 1H), 6.56 (dd, *J* = 15.9, 1.5 Hz, 1H), 6.32 (dd, *J* = 15.9, 6.0 Hz, 1H), 6.22 (d, *J* = 8.1 Hz, 1H), 5.80 (ddd, *J* = 7.8, 6.0, 1.5 Hz, 1H), 4.40 (s, 2H) ppm. ¹³C{¹H} NMR (CDCl₃, 151 MHz) δ 167.92, 165.32, 140.35, 136.44, 134.39, 132.14, 132.05, 129.04, 128.70, 128.22, 128.00, 127.33, 126.76, 123.81, 55.42, 41.17 ppm. HRMS (+APCI) calculated for C₂₅H₂₁N₂O₃ [M+H]⁺ 397.15467, found 397.15448. HPLC (AD-H column, 8% 2-propanol in Hexanes, 1.5 mL/min) *t*_M = 40.0 min, *t*_m = 45.0 min, 79:21 e.r.



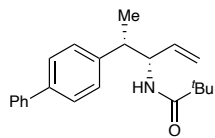
(S,E)-*N*-(1-phenyloct-1-en-3-yl)pivalamide (**128**): Prepared according to **General Procedure B** using (*E*)-oct-1-en-1-ylbenzene (0.0188 g, 0.10 mmol, 1 equiv), 3-(*tert*-butyl)-1,4,2-dioxazol-5-one (0.0286 g, 0.20 mmol, 2 equiv), (*R,R*)-[Rh(2-Me-3-Ph-Ind)₂]₂ (0.0056 g, 0.005 mmol, 0.05 equiv), LiOAc (0.0006 g, 0.010 mmol, 0.10 equiv), AgNTf₂ (0.0078 g, 0.020 mmol, 0.20 equiv), and LiNTf₂ (0.0290 g, 0.10 mmol, 1 equiv) in DCE (0.5 mL) at 40 °C for 48 hours. Purified by flash chromatography on silica gel (15-50% EtOAc in Hexanes) [silica gel pipette column] to provide **128** (0.0065 g, 23% yield, 99:1 e.r.) as a white solid. ¹H NMR (CDCl₃, 600 MHz) δ 7.35 (d, *J* = 7.2 Hz, 2H), 7.30 (t, *J* = 7.7 Hz, 2H), 7.24 – 7.21 (m, 1H), 6.49 (dd,

$J = 16.0, 1.4$ Hz, 1H), 6.11 (dd, $J = 15.9, 6.3$ Hz, 1H), 5.54 (d, $J = 8.5$ Hz, 1H), 4.61 (dddd, $J = 14.0, 8.0, 6.5, 1.5$ Hz, 1H), 1.69 – 1.53 (m, 3H), 1.41 – 1.27 (m, 8H), 1.23 (s, 9H). $^{13}\text{C}\{^1\text{H}\}$ NMR (CDCl_3 , 151 MHz) δ 177.68, 136.99, 130.49, 130.37, 128.67, 127.66, 126.52, 50.78, 38.93, 35.40, 31.75, 27.83, 25.67, 22.69, 14.15. **HRMS** (+APCI) calculated for $\text{C}_{19}\text{H}_{30}\text{NO}$ $[\text{M}+\text{H}]^+$ 288.23219, found 288.232. **HPLC** (AS-H column, 5% 2-propanol in Hexanes, 1 mL/min) $t_{\text{M}} = 5.0$ min, $t_{\text{m}} = 6.7$ min, 99:1 e.r.



(*S,E*)-2-(1,3-dioxoisindolin-2-yl)-*N*-(1-phenyloct-1-en-3-yl)acetamide **(129)**:

Prepared according to **General Procedure B** using (*E*)-oct-1-en-1-ylbenzene (0.0188 g, 0.10 mmol, 1.0 equiv), 2-((5-oxo-1,4,2-dioxazol-3-yl)methyl)isindoline-1,3-dione (0.0492 g, 0.20 mmol, 2.0 equiv), (*R,R*)-[Rh(2-Me-3-Ph-Ind) I_2] $_2$ (0.0056 g, 0.005 mmol, 0.05 equiv), LiOAc (0.0006 g, 0.010 mmol, 0.10 equiv), AgNTf $_2$ (0.0078 g, 0.020 mmol, 0.20 equiv), and LiNTf $_2$ (0.0290 g, 0.10 mmol, 1.0 equiv) in DCE (0.5 mL) at 60 °C for 48 hours. Purified by flash chromatography on silica gel (15-50% EtOAc in Hexanes) [silica gel pipette column] to provide **129** (0.0287 g, 74% yield, 98:2 e.r.) as a white solid and as an inseparable mixture of regioisomers (3.5:1). ^1H NMR (CDCl_3 , 600 MHz) δ 7.87 (td, $J = 5.6, 3.0$ Hz, 2H), 7.73 (dd, $J = 5.5, 3.0$ Hz, 2H), 7.36 – 7.32 (m, 2H), 7.32 – 7.27 (m, 2H), 7.24 – 7.20 (m, 1H), 6.52 (dd, $J = 15.9, 1.4$ Hz, 1H), 6.07 (dd, $J = 15.9, 6.4$ Hz, 1H), 5.78 (d, $J = 8.5$ Hz, 1H), 5.66 (dtd, $J = 17.4, 6.4, 3.5$ Hz, 0H), 5.61 – 5.53 (m, 1H), 4.66 – 4.55 (m, 1H), 4.36 (s, 2H), 2.05 (q, $J = 7.1$ Hz, 1H), 1.68 – 1.55 (m, 3H), 1.42 – 1.32 (m, 3H), 1.31 – 1.24 (m, 8H), 0.91 – 0.83 (m, 4H). $^{13}\text{C}\{^1\text{H}\}$ NMR (CDCl_3 , 151 MHz) δ 167.91, 167.89, 165.41, 165.09, 141.02, 136.74, 134.37, 134.35, 133.87, 132.16, 131.07, 129.37, 128.82, 128.65, 128.50, 127.75, 127.67, 127.12, 126.58, 123.78, 123.76, 55.28, 51.78, 41.22, 41.11, 35.24, 32.35, 31.67, 31.53, 28.84, 25.59, 22.64, 22.61, 14.18, 14.13. **HRMS** (+APCI) calculated for $\text{C}_{24}\text{H}_{27}\text{N}_2\text{O}_3$ $[\text{M}+\text{H}]^+$ 391.20162, found 391.20136. **HPLC** (AS-H column, 10% 2-propanol in Hexanes, 1 mL/min) $t_{\text{M}} = 28.0$ min, $t_{\text{m}} = 36.0$ min, 98:2 e.r.

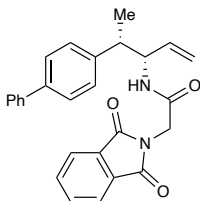


Experiment conducted by Amaan Kazerouni. *N-((3S,4S)-4-([1,1'-biphenyl]-4-yl)pent-*

1-en-3-yl)pivalamide (120): Prepared according to **General Procedure B** using (*R*)-

4-(pent-4-en-2-yl)-1,1'-biphenyl (0.0220 g, 0.10 mmol, 1.0 equiv), 3-(*tert*-butyl)-

1,4,2-dioxazol-5-one (0.0286 g, 0.20 mmol, 2.0 equiv), (*R,R*)-[Rh(2-Me-3-Ph-Ind)₂]₂ (0.0056 g, 0.005 mmol, 0.05 equiv), LiOAc (0.0006 g, 0.010 mmol, 0.10 equiv), AgNTf₂ (0.0078 g, 0.020 mmol, 0.20 equiv), and LiNTf₂ (0.0290 g, 0.10 mmol, 1.0 equiv) in DCE (0.5 mL) at 40 °C for 48 hours. Purified by flash chromatography on silica gel (5-30% EtOAc in Hexanes) to provide **120** (0.0120 g, 37% yield, >20:1 d.r.) as a white solid. **¹H NMR** (CDCl₃, 600 MHz) δ 7.59 (d, *J* = 8.0 Hz, 1H), 7.55 (d, *J* = 8.3 Hz, 1H), 7.44 (t, *J* = 7.8 Hz, 1H), 7.37 – 7.32 (m, 1H), 7.24 (dd, *J* = 8.2, 2.4 Hz, 2H), 5.70 (ddd, *J* = 16.8, 10.4, 6.1 Hz, 1H), 5.50 (d, *J* = 8.8 Hz, 1H), 5.15 – 5.04 (m, 1H), 4.75 – 4.66 (m, 1H), 3.03 (q, *J* = 6.9 Hz, 1H), 1.35 (d, *J* = 7.2 Hz, 2H), 1.19 (s, 2H) ppm. **¹³C NMR** (CDCl₃, 126 MHz) δ 177.53, 141.48, 140.90, 139.83, 135.58, 128.92, 128.87, 127.38, 127.13, 127.10, 116.42, 55.82, 43.57, 39.00, 27.77, 18.00 ppm. **HRMS** (+APCI) calculated for C₂₂H₂₈NO [M+H]⁺ 322.2171, found 322.2167.



Experiment conducted by Amaan Kazerouni. *N-((3S,4S)-4-([1,1'-biphenyl]-4-yl)pent-*

1-en-3-yl)-2-(1,3-dioxoisindolin-2-yl)acetamide (121): Prepared according to **General**

Procedure B using (*R*)-4-(pent-4-en-2-yl)-1,1'-biphenyl (0.0220 g, 0.10 mmol, 1.0

equiv), 2-((5-oxo-1,4,2-dioxazol-3-yl)methyl)isindoline-1,3-dione (0.0492 g, 0.20 mmol, 2.0 equiv), (*R,R*)-[Rh(2-Me-3-Ph-Ind)₂]₂ (0.0056 g, 0.005 mmol, 0.05 equiv), LiOAc (0.0006 g, 0.010 mmol, 0.10 equiv), AgNTf₂ (0.0078 g, 0.020 mmol, 0.20 equiv), and LiNTf₂ (0.0290 g, 0.10 mmol, 1.0 equiv) in DCE (0.5 mL) at 60 °C for 48 hours. Purified by flash chromatography on silica gel (20-50% EtOAc in Hexanes) to provide **121** (0.0290 g, 41% yield, >20:1 d.r.) as a white solid. **¹H NMR** (CDCl₃, 600 MHz) δ 7.85 (dd, *J* = 5.4, 3.0 Hz, 2H), 7.67 (dd, *J* = 5.4, 3.0 Hz, 2H), 7.50 – 7.47 (m, 2H), 7.44 – 7.37

(m, 4H), 7.36 – 7.32 (m, 1H), 7.19 (d, $J = 8.2$ Hz, 2H), 5.68 (ddd, $J = 17.0, 10.5, 6.3$ Hz, 1H), 5.59 (d, $J = 9.0$ Hz, 1H), 5.20 – 5.09 (m, 2H), 4.76 – 4.65 (m, 1H), 4.37 (d, $J = 16.1$ Hz, 1H), 4.31 (d, $J = 16.0$ Hz, 1H), 3.05 (q, $J = 7.1$ Hz, 1H), 1.34 (d, $J = 7.2$ Hz, 3H) ppm. $^{13}\text{C NMR}$ (CDCl_3 , 151 MHz) δ 167.82, 165.37, 140.77, 140.71, 139.85, 134.42, 134.29, 132.04, 128.89, 128.85, 127.37, 127.12, 127.11, 123.79, 117.48, 56.48, 43.24, 41.30, 17.89 ppm. **HRMS** (+APCI) calculated for $\text{C}_{27}\text{H}_{25}\text{N}_2\text{O}_3$ $[\text{M}+\text{H}]^+$ 425.1865, found 425.1869.

X-Ray Crystallographic Data – Experiment and crystalization conducted by Christopher Poff.

Experimental

Single orange plate-shaped crystals of CCDC 196624 (CDPoff-0035-0071) were recrystallised from a mixture of pentane and CHCl_3 by vapor diffusion. A suitable crystal $0.50 \times 0.14 \times 0.09$ mm^3 was selected and mounted on a loop with paratone oil on an XtaLAB Synergy-S diffractometer. The crystal was kept at $T = 100.0(2)$ K during data collection. The structure was solved with the **ShelXT** (Sheldrick, 2015) structure solution program using the Intrinsic Phasing solution method and by using **Olex2** (Dolomanov et al., 2009) as the graphical interface. The model was refined with version 2018/3 of **ShelXL** (Sheldrick, 2015) using Least Squares minimisation.

Crystal Data. $\text{C}_{21}\text{H}_{22}\text{ClRh}$, $M_r = 412.74$, monoclinic, $P2_1$ (No. 4), $a = 6.9777(6)$ Å, $b = 17.2222(15)$ Å, $c = 7.2610(10)$ Å, $\beta = 98.216(10)^\circ$, $\alpha = \gamma = 90^\circ$, $V = 863.60(16)$ Å³, $T = 100.0(2)$ K, $Z = 2$, $Z' = 1$, $\mu(\text{MoK}\alpha) = 1.140$ mm^{-1} , 15658 reflections measured, 5214 unique ($R_{int} = 0.0562$) which were used in all calculations. The final wR_2 was 0.0946 (all data) and R_1 was 0.0422 ($I > 2\sigma(I)$).

Compound	CCDC 1966524 (CDPoff-0035-0071)
Formula	C ₂₁ H ₂₂ ClRh
$D_{calc.}/\text{g cm}^{-3}$	1.587
μ/mm^{-1}	1.140
Formula Weight	412.74
Colour	orange
Shape	plate
Size/ mm^3	0.50×0.14×0.09
T/K	100.0(2)
Crystal System	monoclinic
Flack Parameter	-0.02(3)
Hooft Parameter	-0.01(2)
Space Group	$P2_1$
$a/\text{\AA}$	6.9777(6)
$b/\text{\AA}$	17.2222(15)
$c/\text{\AA}$	7.2610(10)
$\alpha/^\circ$	90
$\beta/^\circ$	98.216(10)
$\gamma/^\circ$	90
$V/\text{\AA}^3$	863.60(16)
Z	2
Z'	1
Wavelength/ \AA	0.71073
Radiation type	MoK α
$\theta_{min}/^\circ$	2.365
$\theta_{max}/^\circ$	30.506
Measured Refl.	15658
Independent Refl.	5214
Reflections with $I > 2\sigma(I)$	4605
R_{int}	0.0562
Parameters	260
Restraints	168
Largest Peak	1.105
Deepest Hole	-1.289
GooF	1.019
wR_2 (all data)	0.0946
wR_2	0.0920
R_1 (all data)	0.0500
R_1	0.0422

Structure Quality Indicators

Reflections:	d min (Mo)	0.70	I/ σ	15.7	Rint	5.62%	complete 100% (IUCr)	100%		
Refinement:	Shift	-0.009	Max Peak	1.1	Min Peak	-1.3	Goof	1.019	Flack	-0.02(3)

An orange plate-shaped crystal with dimensions $0.50 \times 0.14 \times 0.09 \text{ mm}^3$ was mounted on a loop with paratone oil. Data were collected using an XtaLAB Synergy, Dualflex, HyPix diffractometer equipped with an Oxford Cryosystems low-temperature device operating at $T = 100.0(2) \text{ K}$.

Data were measured using ω scans using MoK α radiation. The total number of runs and images was based on the strategy calculation from the program **CrysAlisPro** (Rigaku, V1.171.40.53, 2019). The maximum resolution that was achieved was $\theta = 30.506^\circ$ (0.70 \AA).

The diffraction pattern was indexed and the unit cell was refined using **CrysAlisPro** (Rigaku, V1.171.40.53, 2019) on 7723 reflections, 49% of the observed reflections.

Data reduction, scaling and absorption corrections were performed using **CrysAlisPro** (Rigaku, V1.171.40.53, 2019). The final completeness is 100.00 % out to 30.506° in θ . A numerical absorption correction based on Gaussian integration over a multifaceted crystal model was performed using **CrysAlisPro** (Rigaku, V1.171.40.53, 2019). An empirical absorption correction using spherical harmonics as implemented in SCALE3 ABSPACK was also applied. The absorption coefficient μ of this material is 1.140 mm^{-1} at this wavelength ($\lambda = 0.711 \text{ \AA}$) and the minimum and maximum transmissions are 0.441 and 1.000.

The structure was solved and the space group $P2_1$ (# 4) determined by the **ShelXT** (Sheldrick, 2015) structure solution program using Intrinsic Phasing and refined by Least Squares using version 2018/3 of **ShelXL** (Sheldrick, 2015). All non-hydrogen atoms were refined anisotropically. Most Hydrogen atom positions were calculated geometrically and refined using the riding model. Hydrogen atom positions for the allyl group were located and refined freely.

There is a single molecule in the asymmetric unit, which is represented by the reported sum formula. In other words: Z is 2 and Z' is 1.

The Flack parameter was refined to -0.02(3). Determination of absolute structure using Bayesian statistics on Bijvoet differences using the Olex2 results in -0.01(2). Note: The Flack parameter is used to determine chirality of the crystal studied, the value should be near 0, a value of 1 means that the stereochemistry is wrong and the model should be inverted. A value of 0.5 means that the crystal consists of a racemic mixture of the two enantiomers.

Images of the Crystal on the Diffractometer



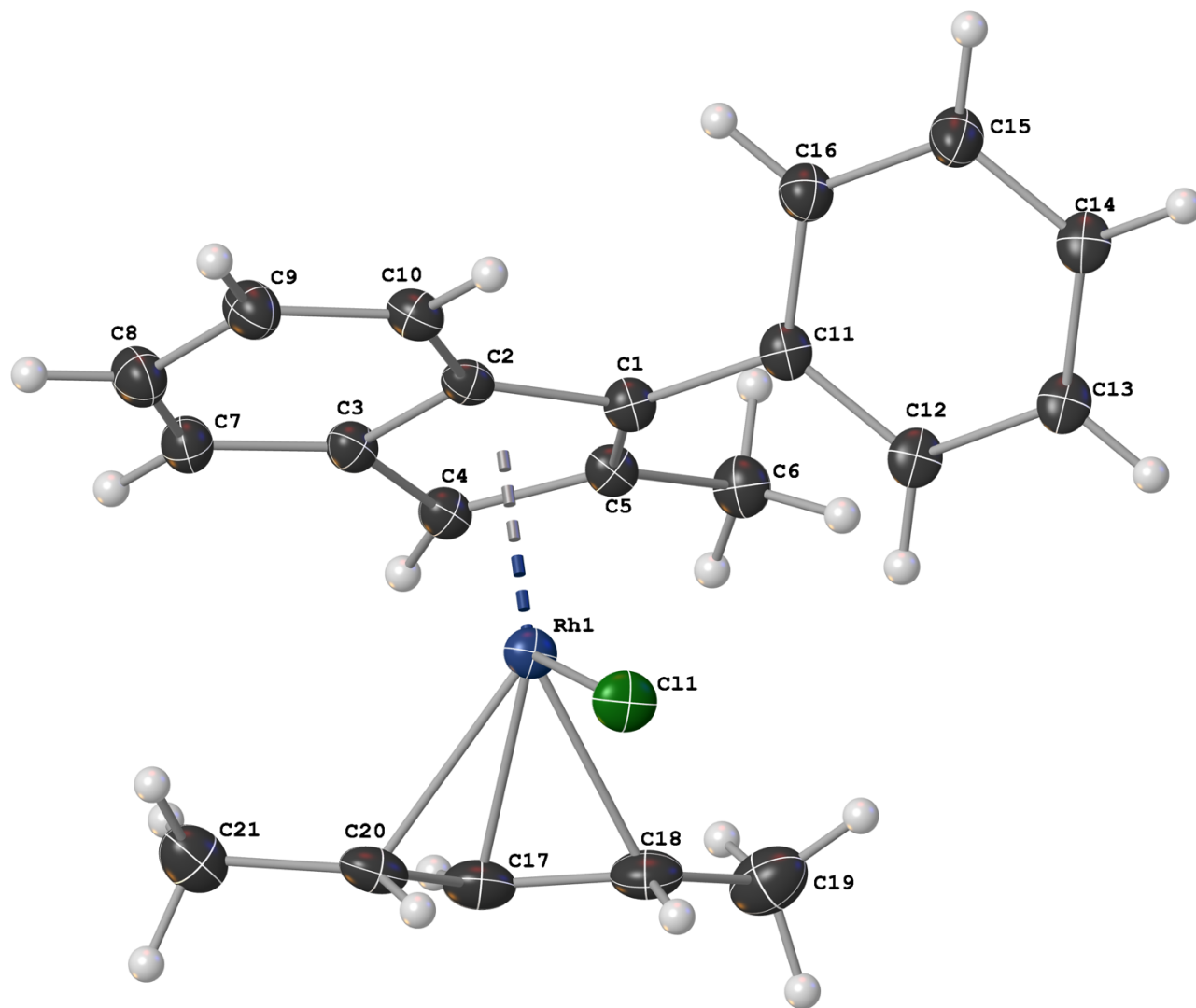
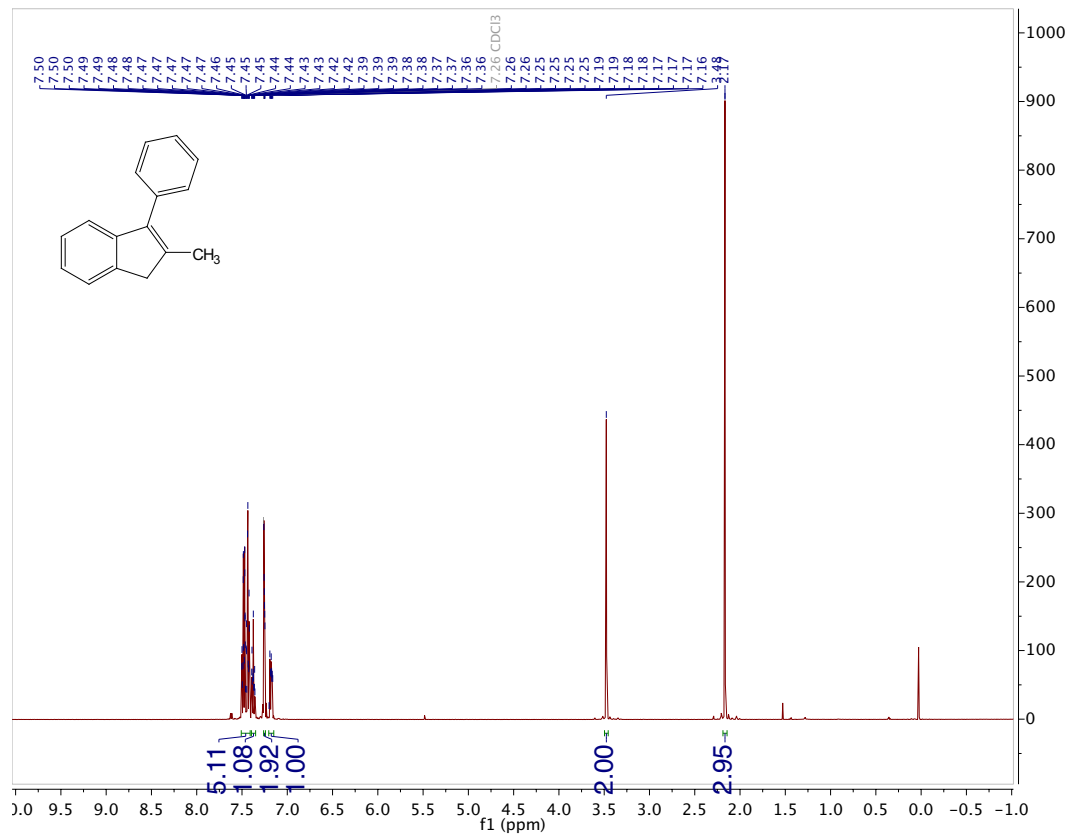


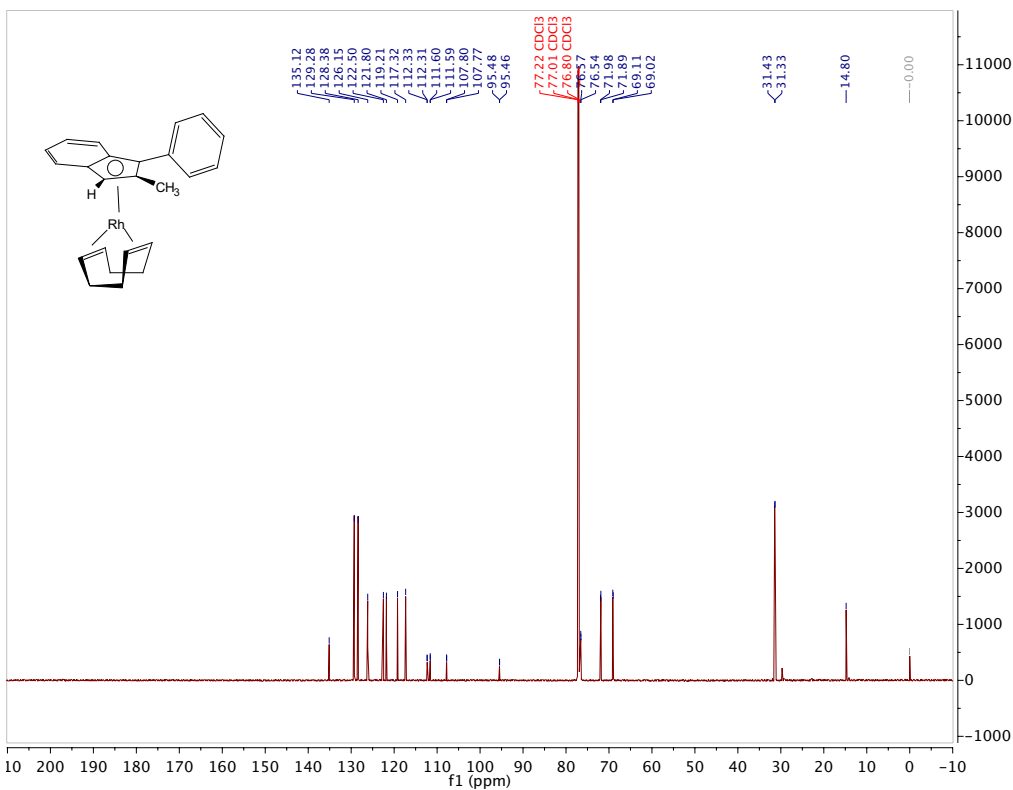
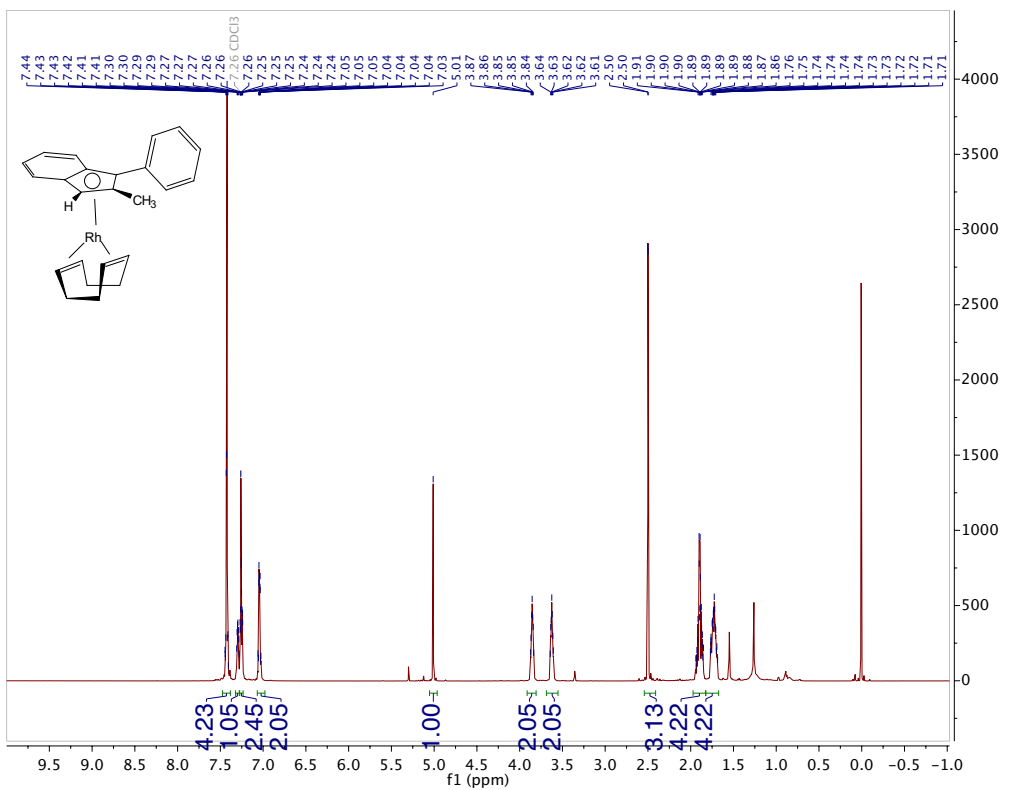
Figure S1: Crystal Structure for **CCDC 1966524** (CDPoff-0035-0071)

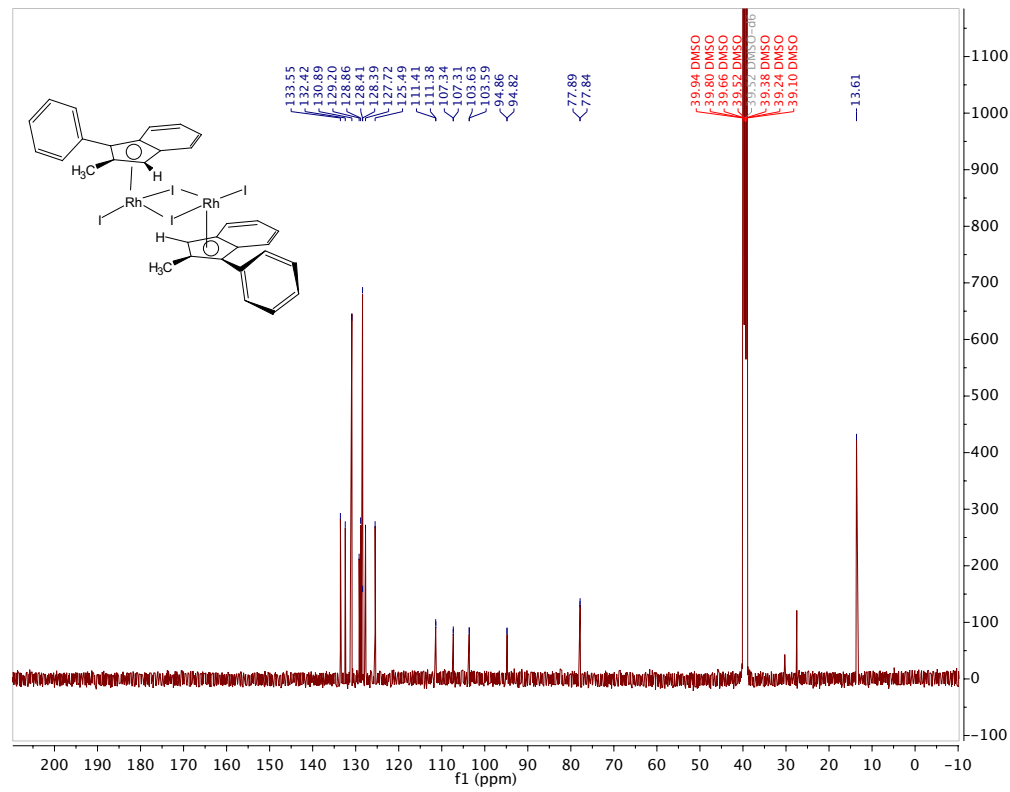
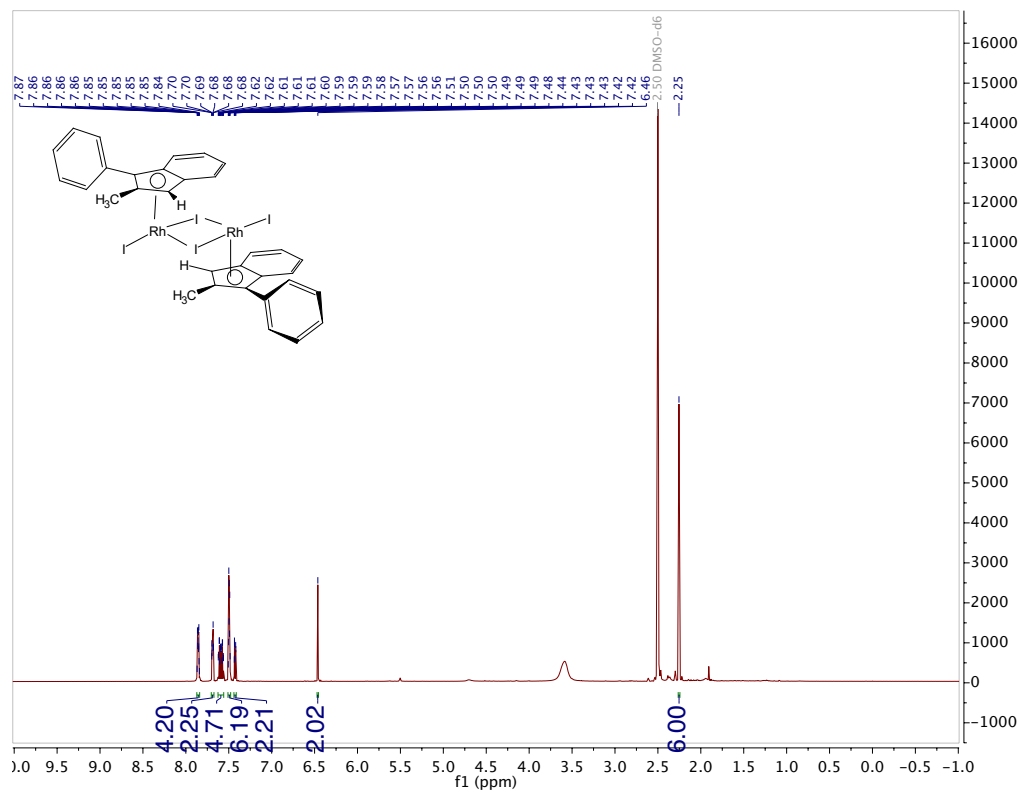
3.9 Spectral Data

2-Methyl-3-phenyl-1H-indene

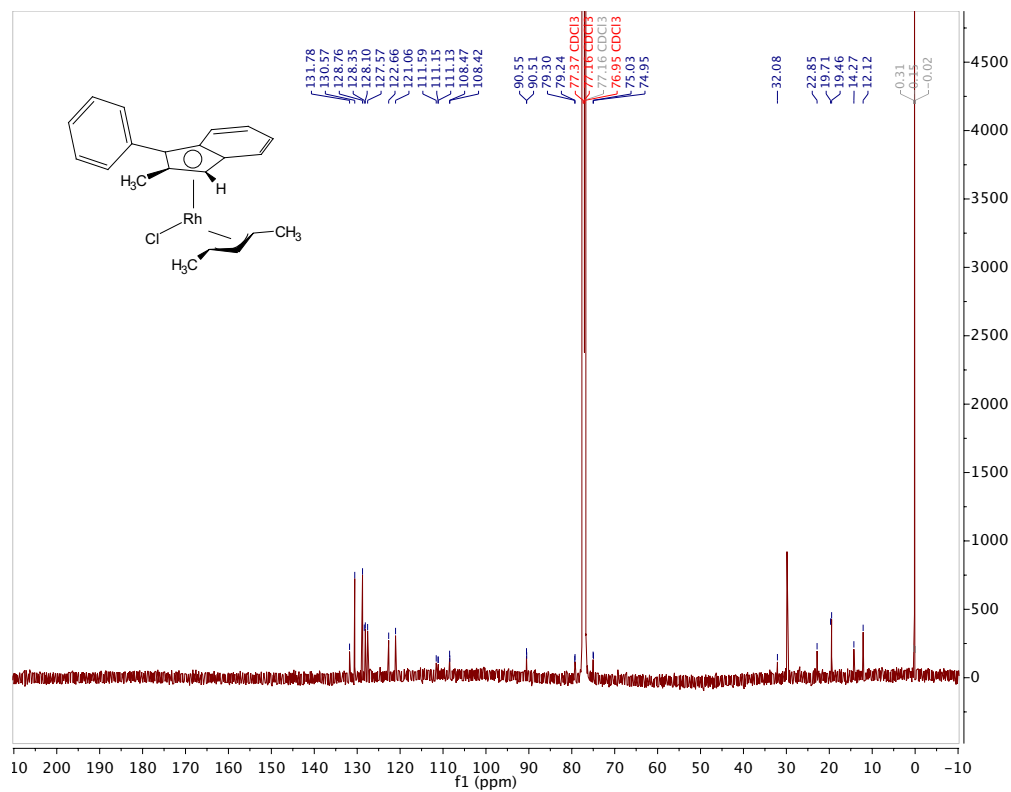
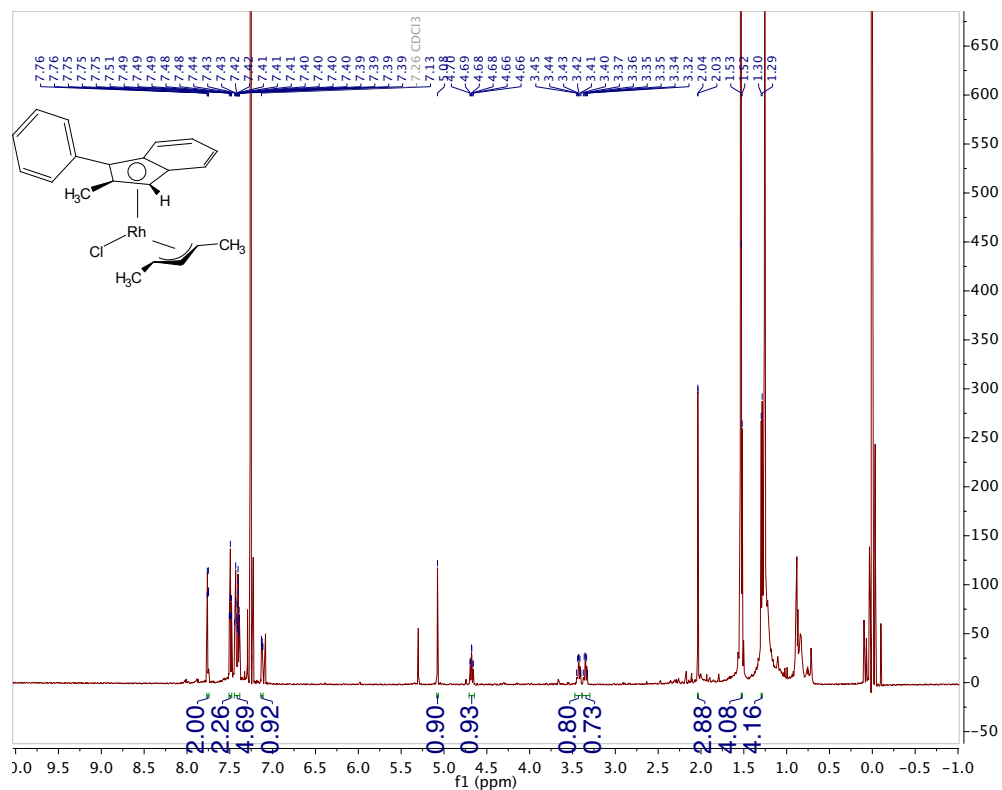


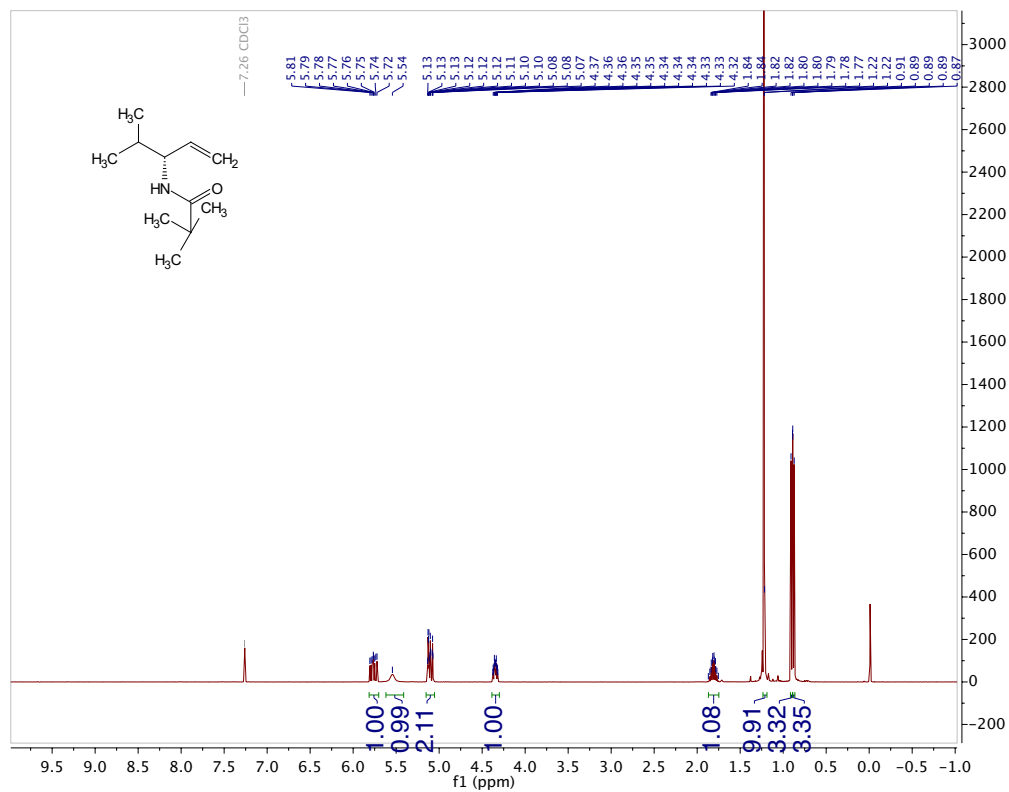
(±)-1,5-cyclooctadiene(η^5 -2-methyl-3-phenylinden-1H-yl)rhodium(I)

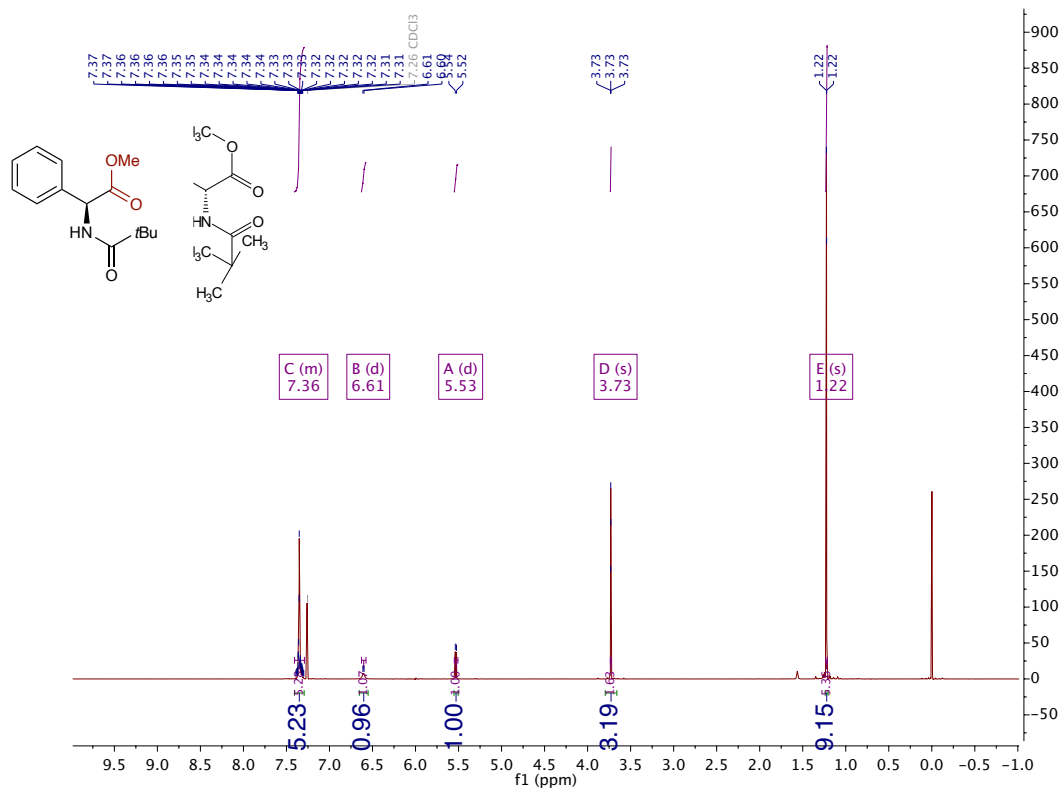


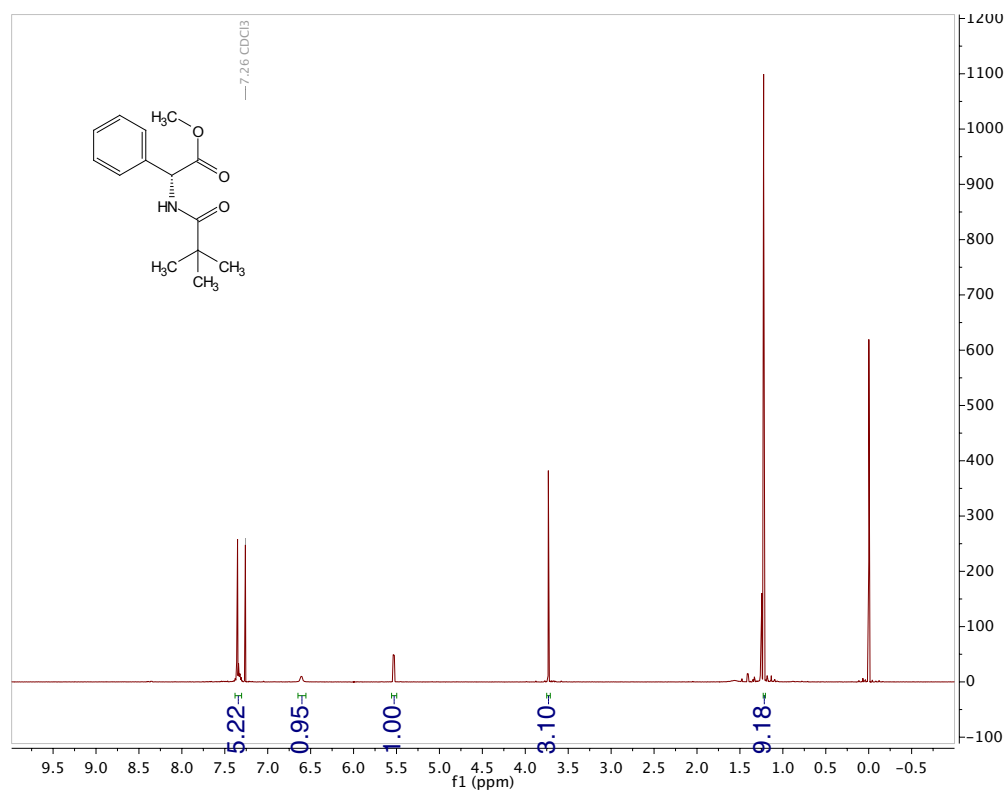
(S,S) -[Rh(2-Me-3-Ph-Ind) I_2] $_2$ 

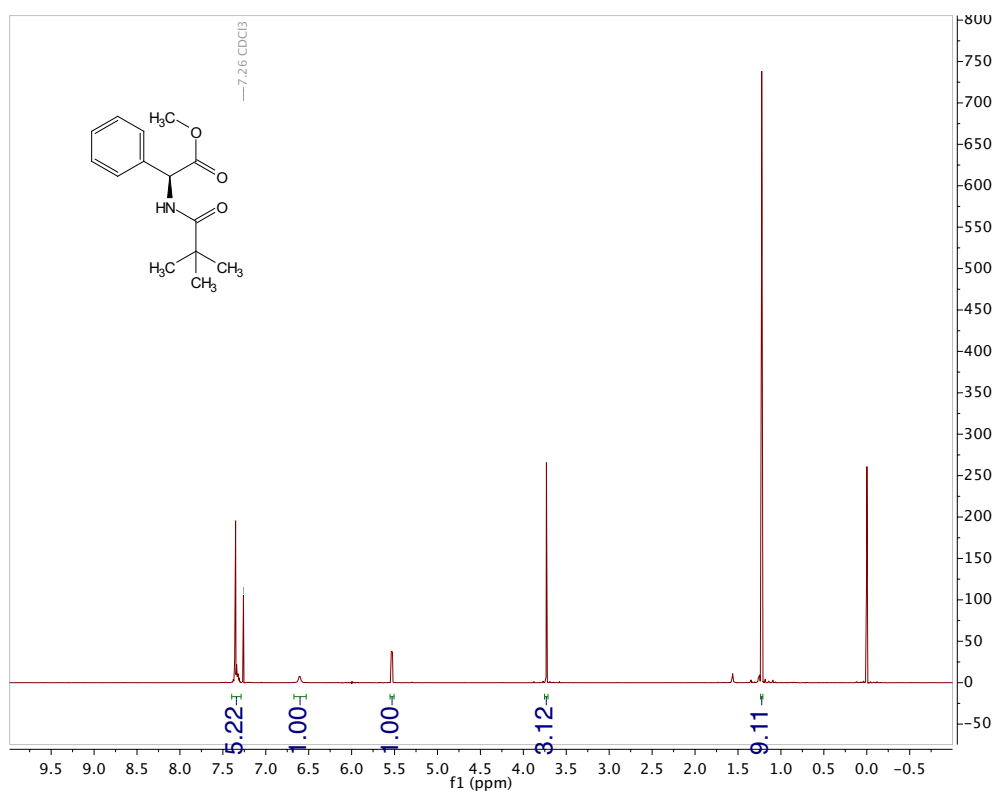
(E)-(η^5 -*S*-2-methyl-3-phenylinden-1*H*-yl)(η^3 -pent-3-enyl)rhodium(III) chloride

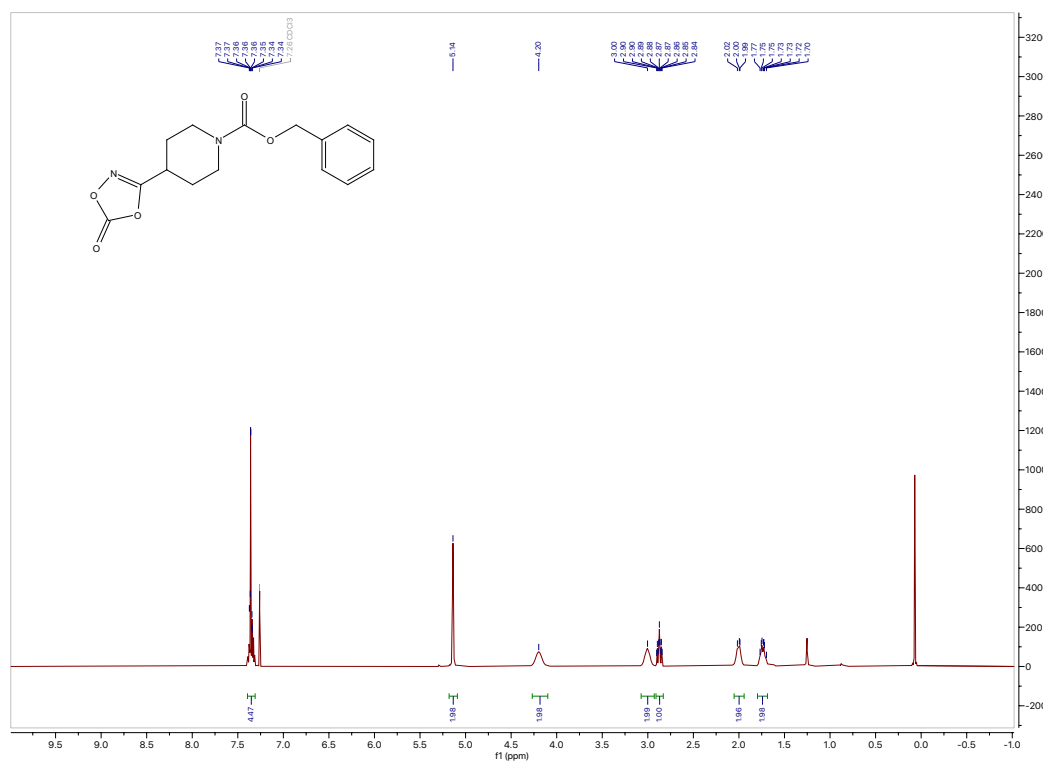


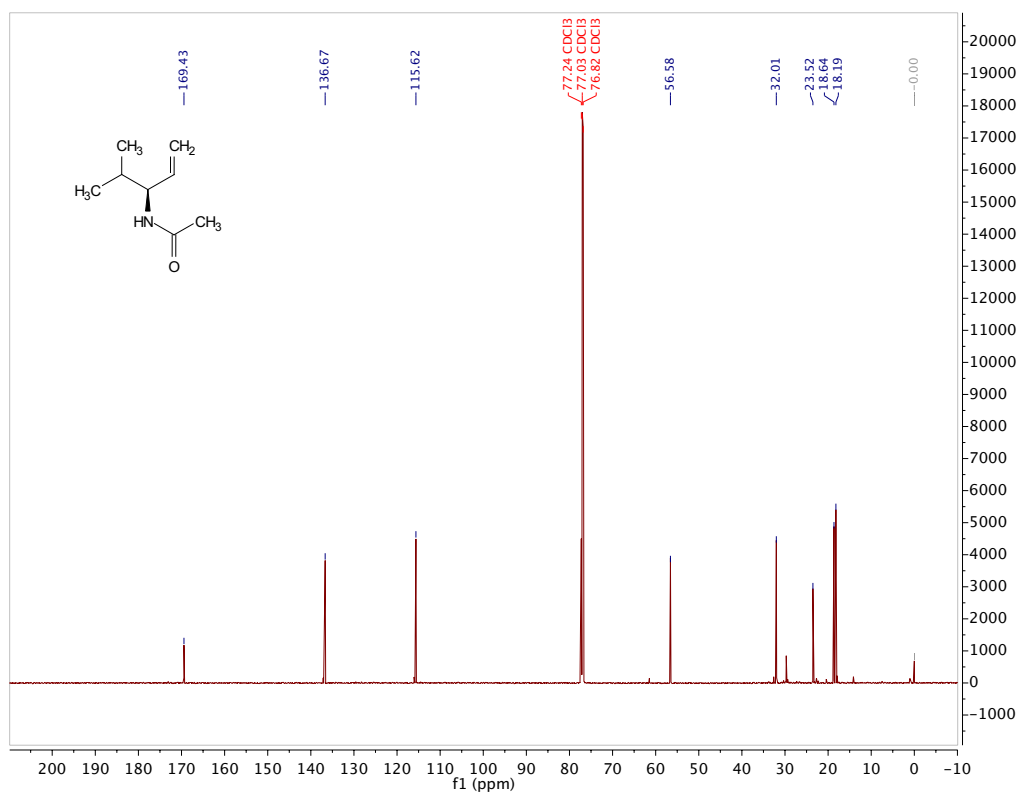
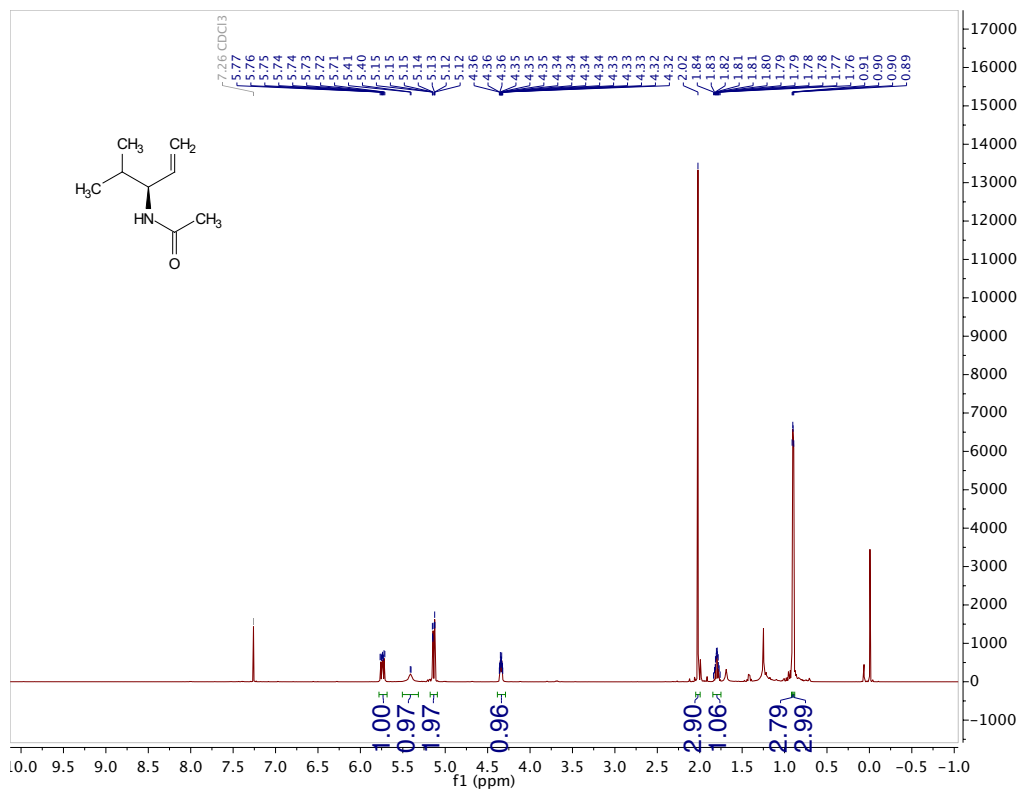
(R)-N-(4-methylpent-1-en-3-yl)pivalamide

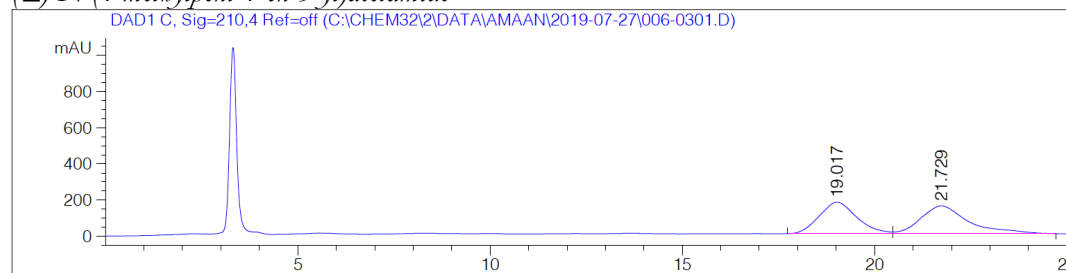
N-pivaloyl-L-phenylglycine methyl ester

N-pivaloyl-D-phenylglycine methyl ester

N-pivaloyl-L-phenylglycine methyl ester

Benzyl 4-(5-oxo-1,4,2-dioxazol-3-yl)piperidine-1-carboxylate

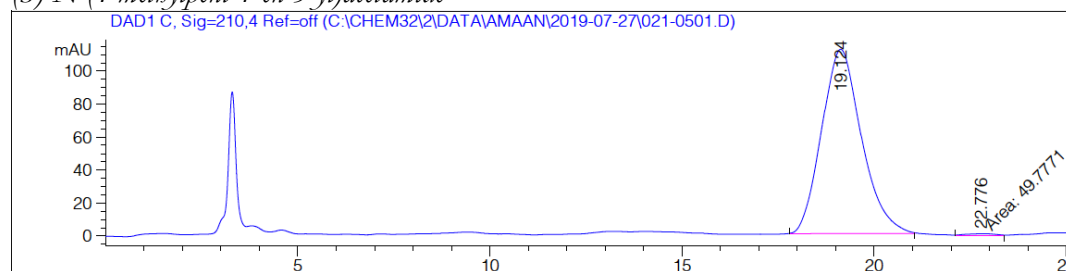
(S)-N-(4-methylpent-1-en-3-yl)acetamide

(±)-N-(4-methylpent-1-en-3-yl)acetamide

Signal 1: DAD1 C, Sig=210,4 Ref=off

Peak #	RetTime [min]	Type	Width [min]	Area [mAU*s]	Height [mAU]	Area %
1	19.017	BV	0.9845	1.18197e4	174.45068	47.1135
2	21.729	VB	1.1997	1.32681e4	154.53239	52.8865

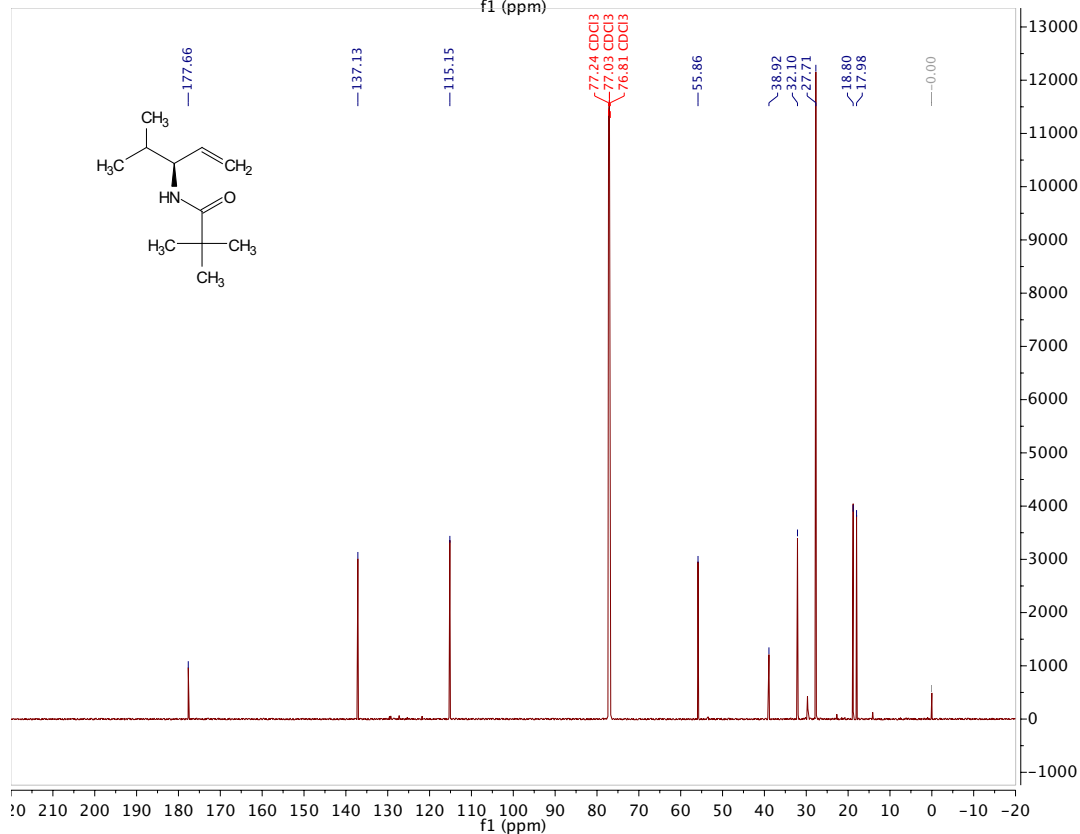
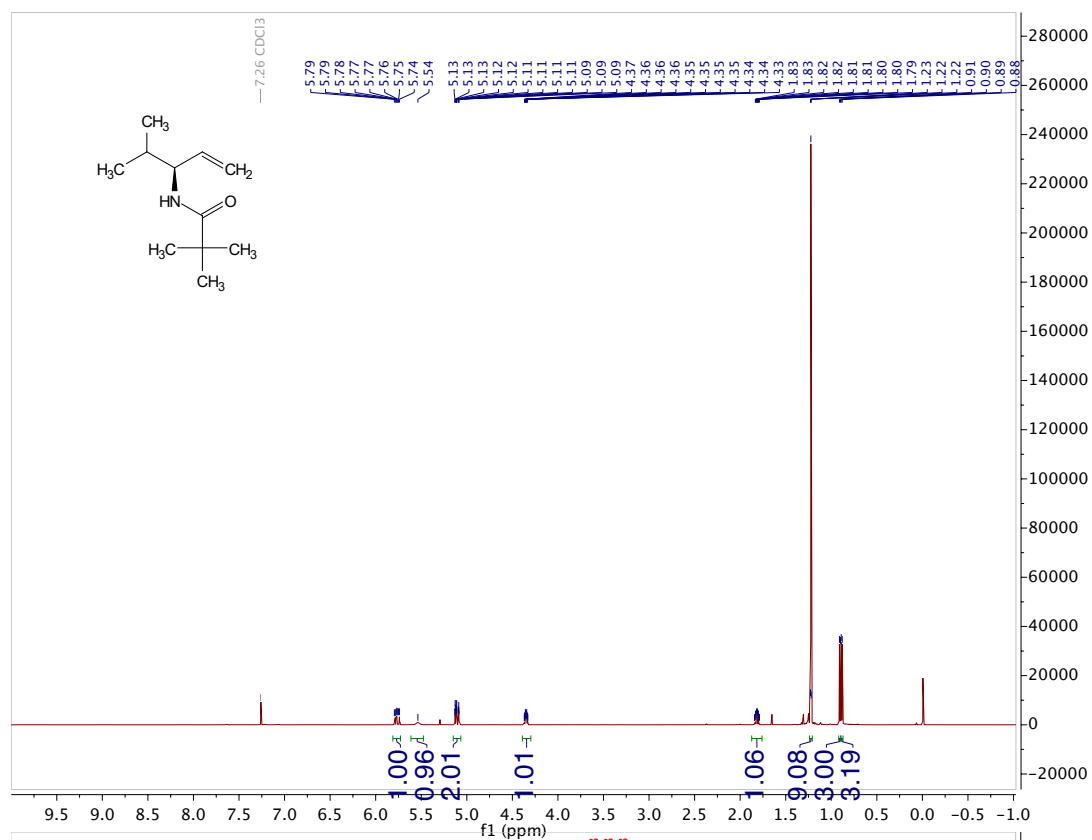
Totals : 2.50878e4 328.98308

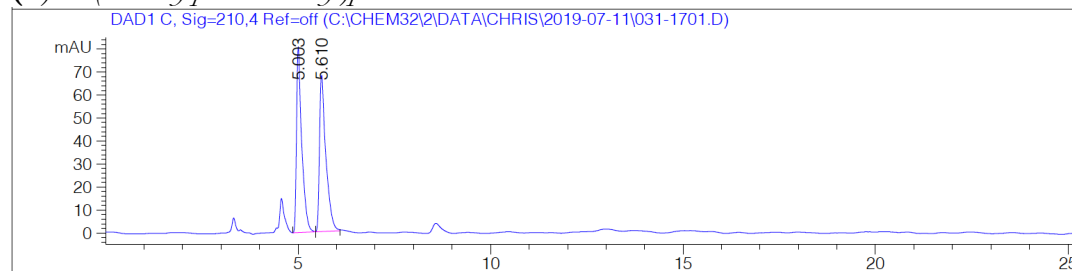
(S)-N-(4-methylpent-1-en-3-yl)acetamide

Signal 1: DAD1 C, Sig=210,4 Ref=off

Peak #	RetTime [min]	Type	Width [min]	Area [mAU*s]	Height [mAU]	Area %
1	19.124	BB	1.0659	8066.80420	111.78791	99.3867
2	22.776	MM	0.8456	49.77714	9.81139e-1	0.6133

Totals : 8116.58134 112.76905

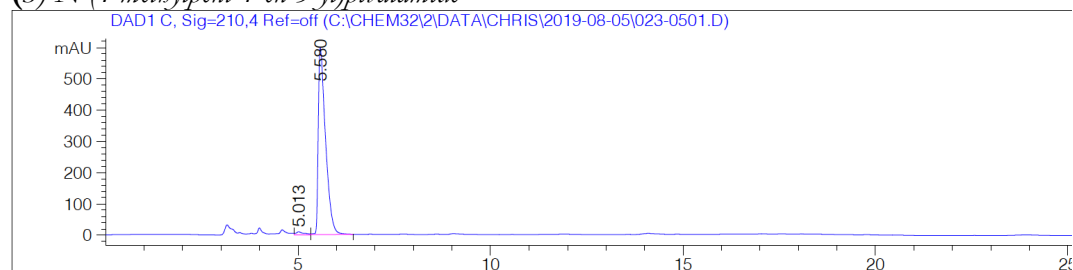
(S)-*N*-(4-methylpent-1-en-3-yl)pivalamide

(±)-N-(4-methylpent-1-en-3-yl)pivalamide

Signal 1: DAD1 C, Sig=210,4 Ref=off

Peak #	RetTime [min]	Type	Width [min]	Area [mAU*s]	Height [mAU]	Area %
1	5.003	VV	0.1348	767.14093	80.80962	50.2210
2	5.610	VB	0.1585	760.38782	67.99258	49.7790

Totals : 1527.52875 148.80220

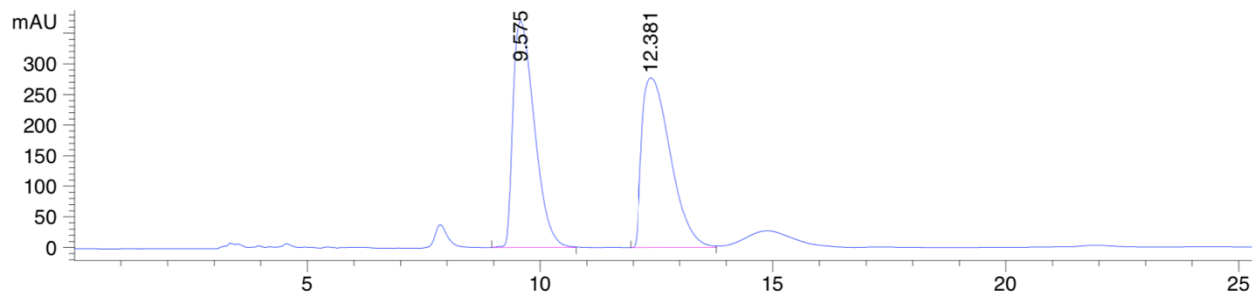
(S)-N-(4-methylpent-1-en-3-yl)pivalamide

Signal 2: DAD1 C, Sig=210,4 Ref=off

Peak #	RetTime [min]	Type	Width [min]	Area [mAU*s]	Height [mAU]	Area %
1	5.013	VV	0.1808	126.23240	9.27309	1.6162
2	5.580	VB	0.1861	7684.32129	597.17950	98.3838

Totals : 7810.55369 606.45259

(±)-N-(4-methylpent-1-en-3-yl)cyclohexanecarboxamide

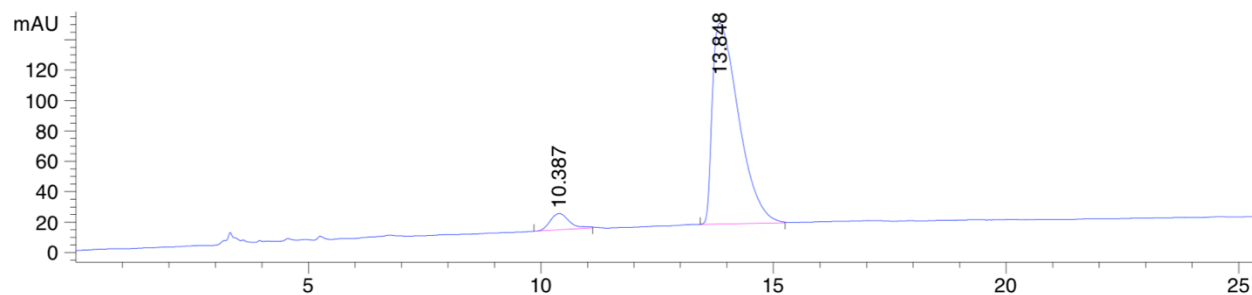


Signal 1: DAD1 C, Sig=210,4 Ref=off

Peak #	RetTime [min]	Type	Width [min]	Area [mAU*s]	Height [mAU]	Area %
1	9.575	BB	0.5100	1.18481e4	369.55115	49.9258
2	12.381	BB	0.6799	1.18833e4	277.32910	50.0742

Totals : 2.37314e4 646.88025

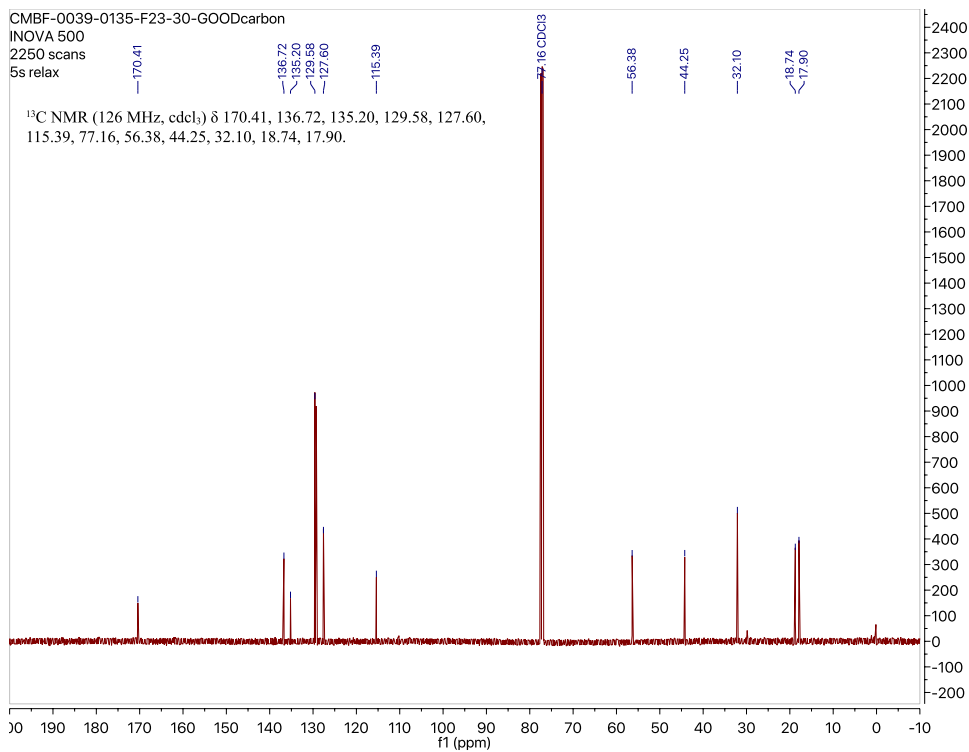
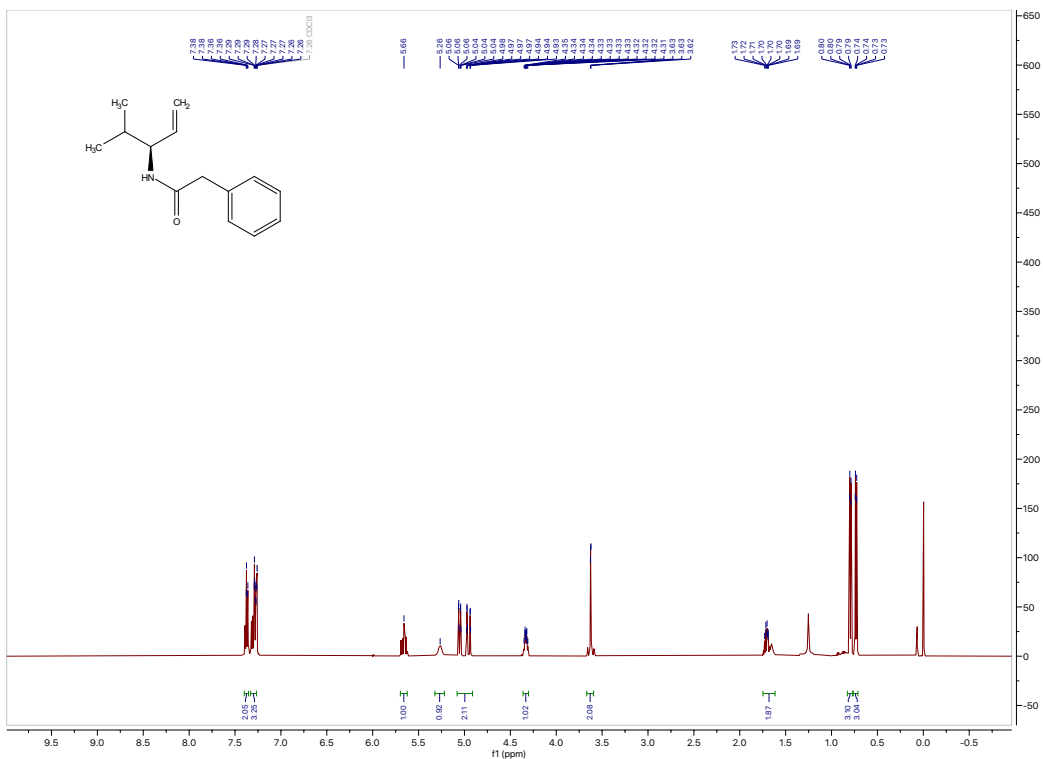
(S)-N-(4-methylpent-1-en-3-yl)cyclohexanecarboxamide

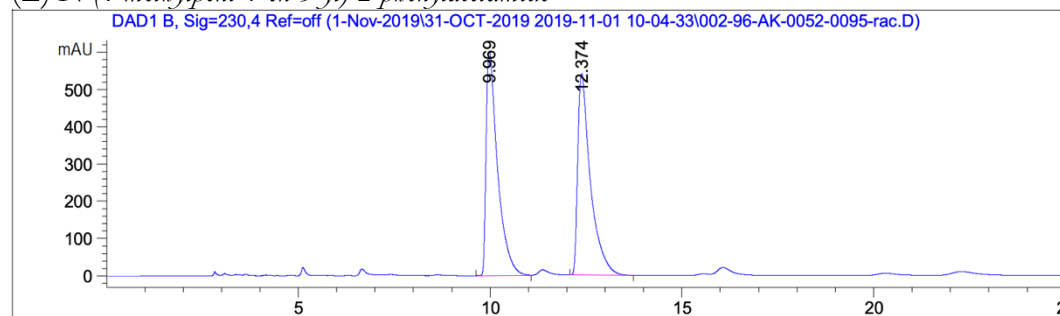


Signal 1: DAD1 C, Sig=210,4 Ref=off

Peak #	RetTime [min]	Type	Width [min]	Area [mAU*s]	Height [mAU]	Area %
1	10.387	BB	0.4364	308.14096	10.75106	5.6265
2	13.848	BB	0.6063	5168.50635	132.14665	94.3735

Totals : 5476.64731 142.89771

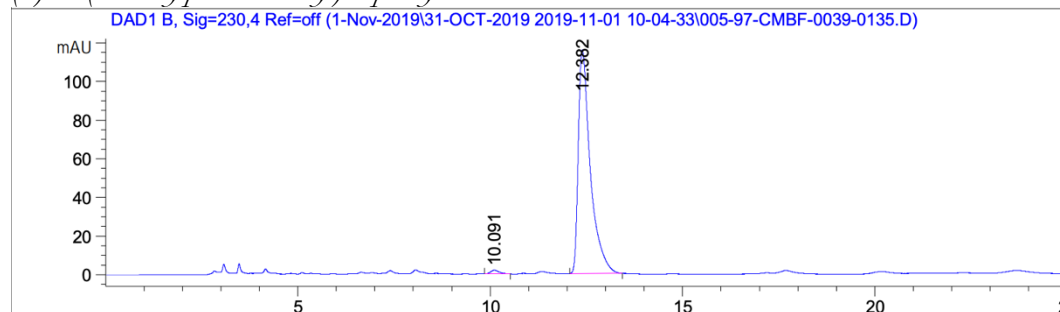
(S)-N-(4-methylpent-1-en-3-yl)-2-phenylacetamide

(±)-N-(4-methylpent-1-en-3-yl)-2-phenylacetamide

Signal 2: DAD1 B, Sig=230,4 Ref=off

Peak #	RetTime [min]	Type	Width [min]	Area [mAU*s]	Height [mAU]	Area %
1	9.969	BB	0.2953	1.24203e4	601.79449	50.0175
2	12.374	BB	0.3257	1.24116e4	539.88324	49.9825

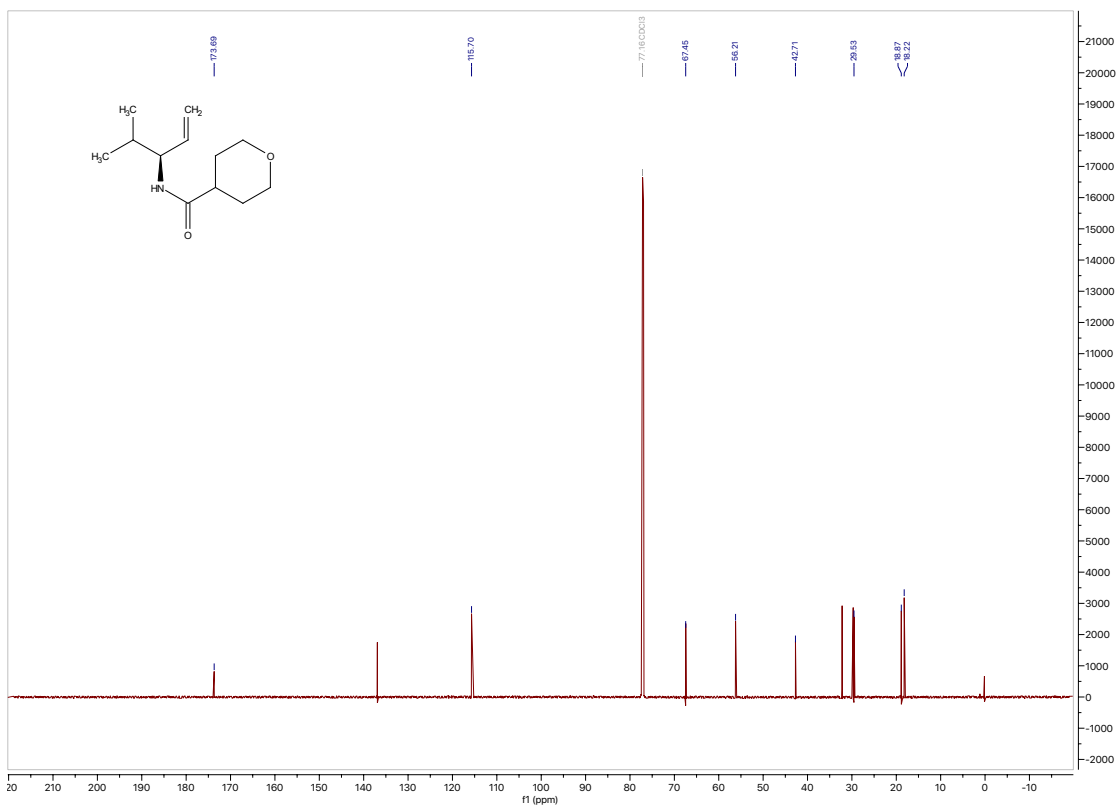
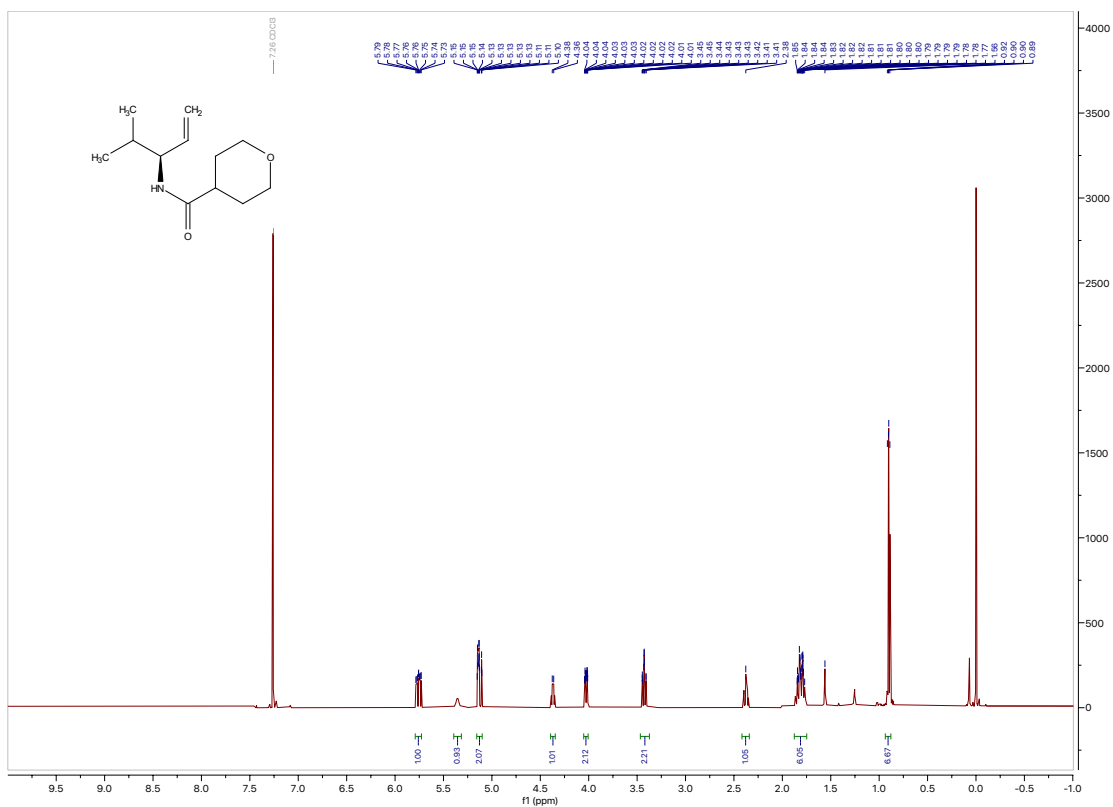
Totals : 2.48319e4 1141.67773

(S)-N-(4-methylpent-1-en-3-yl)-2-phenylacetamide

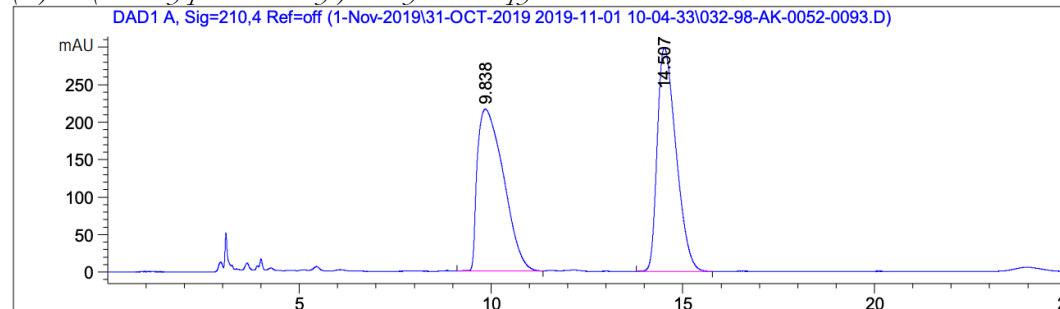
Signal 2: DAD1 B, Sig=230,4 Ref=off

Peak #	RetTime [min]	Type	Width [min]	Area [mAU*s]	Height [mAU]	Area %
1	10.091	BB	0.1825	29.42900	1.91270	1.1574
2	12.382	BB	0.3081	2513.15894	115.86034	98.8426

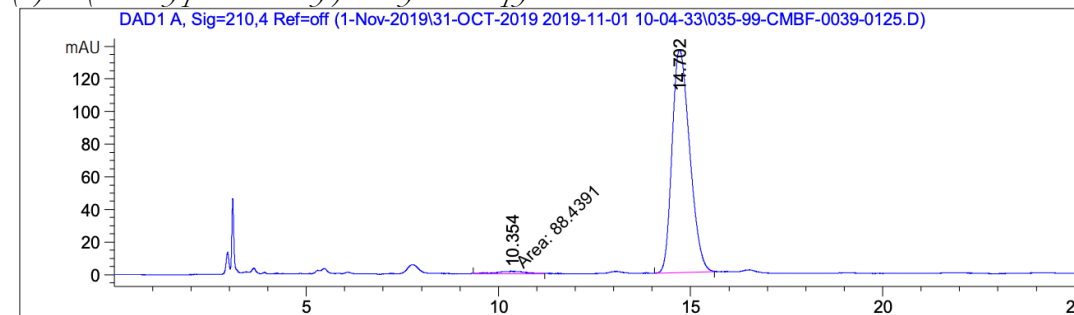
Totals : 2542.58794 117.77304

(S)-N-(4-methylpent-1-en-3-yl)tetrahydro-2H-pyran-4-carboxamide

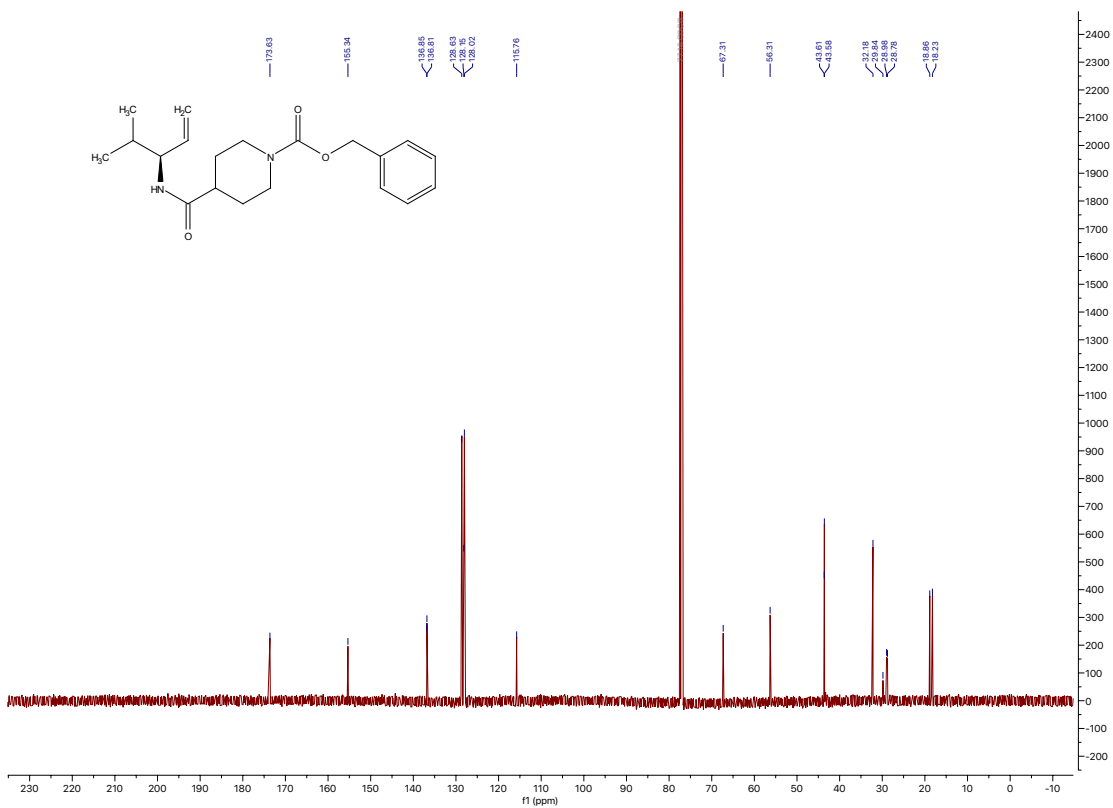
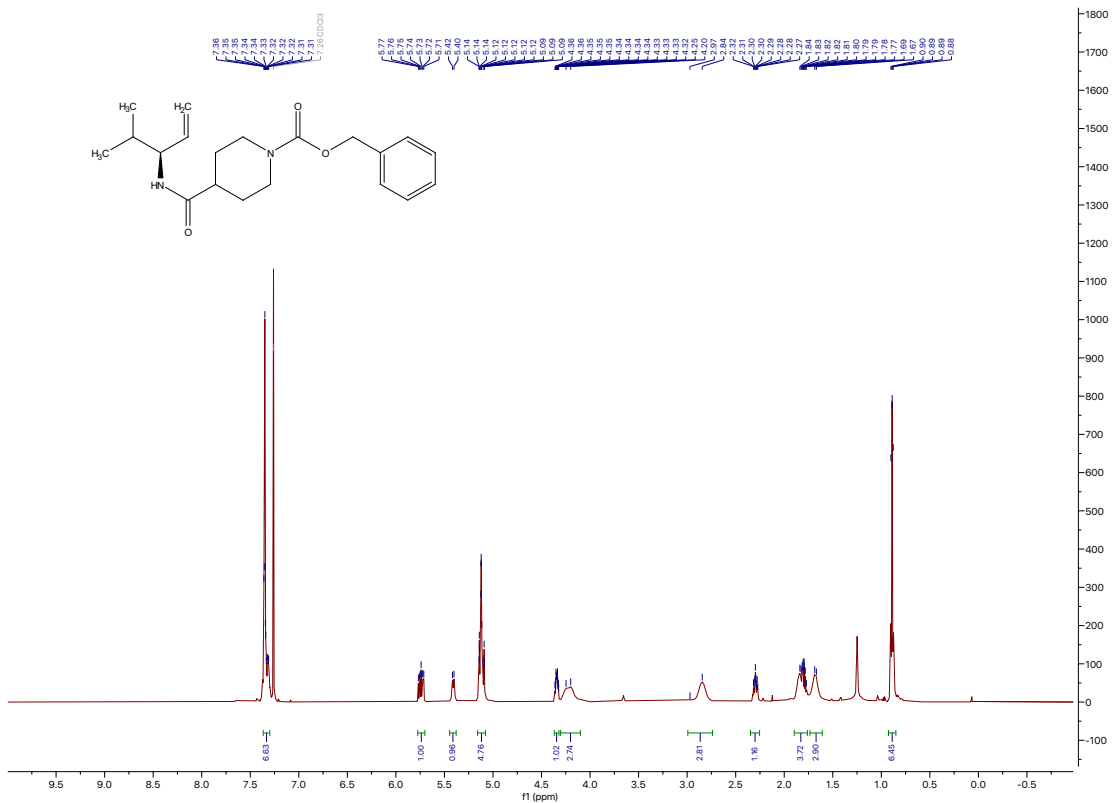
(±)-N-(4-methylpent-1-en-3-yl)tetrahydro-2H-pyran-4-carboxamide



(S)-N-(4-methylpent-1-en-3-yl)tetrahydro-2H-pyran-4-carboxamide

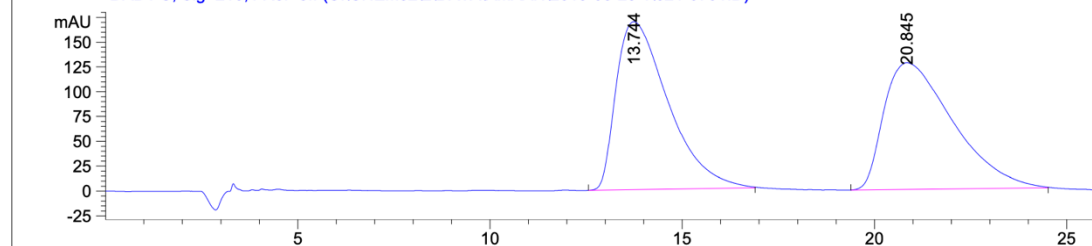


Benzyl (S)-4-((4-methylpent-1-en-3-yl)carbamoyl)piperidine-1-carboxylate



Benzyl (±)-4-((4-methylpent-1-en-3-yl)carbamoyl)piperidine-1-carboxylate

DAD1 C, Sig=210,4 Ref=off (C:\CHEM32\2\DATA\MAAN\2019-08-29 1\021-0701.D)



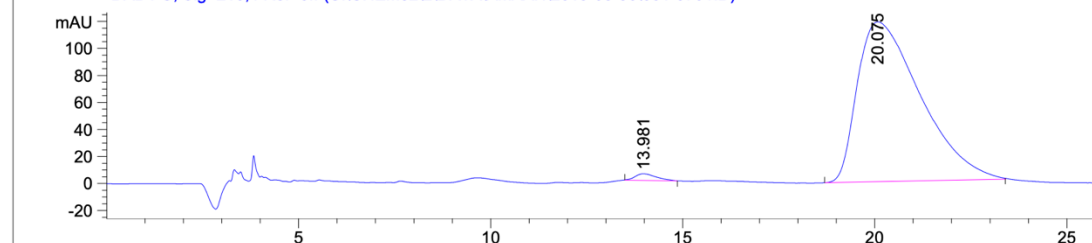
Signal 1: DAD1 C, Sig=210,4 Ref=off

Peak #	RetTime [min]	Type	Width [min]	Area [mAU*s]	Height [mAU]	Area %
1	13.744	BB	1.4529	1.59141e4	169.26764	50.0525
2	20.845	BB	1.8050	1.58808e4	127.50879	49.9475

Totals : 3.17949e4 296.77643

Benzyl (S)-4-((4-methylpent-1-en-3-yl)carbamoyl)piperidine-1-carboxylate

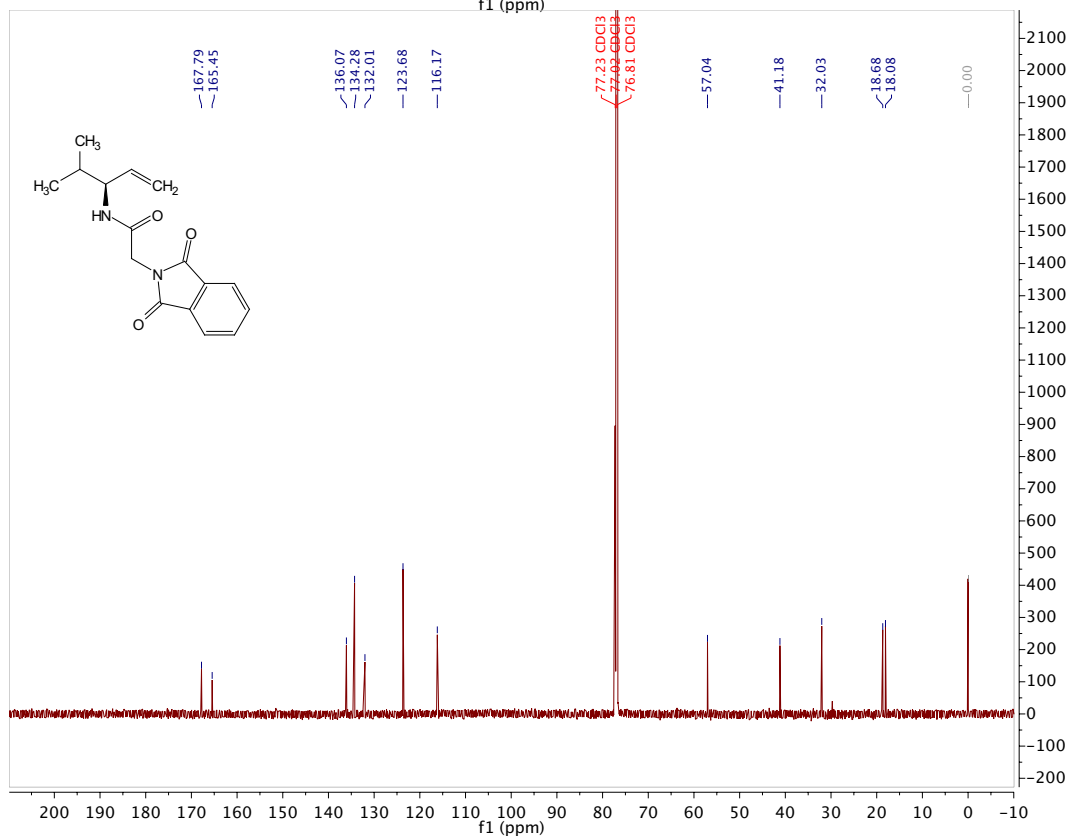
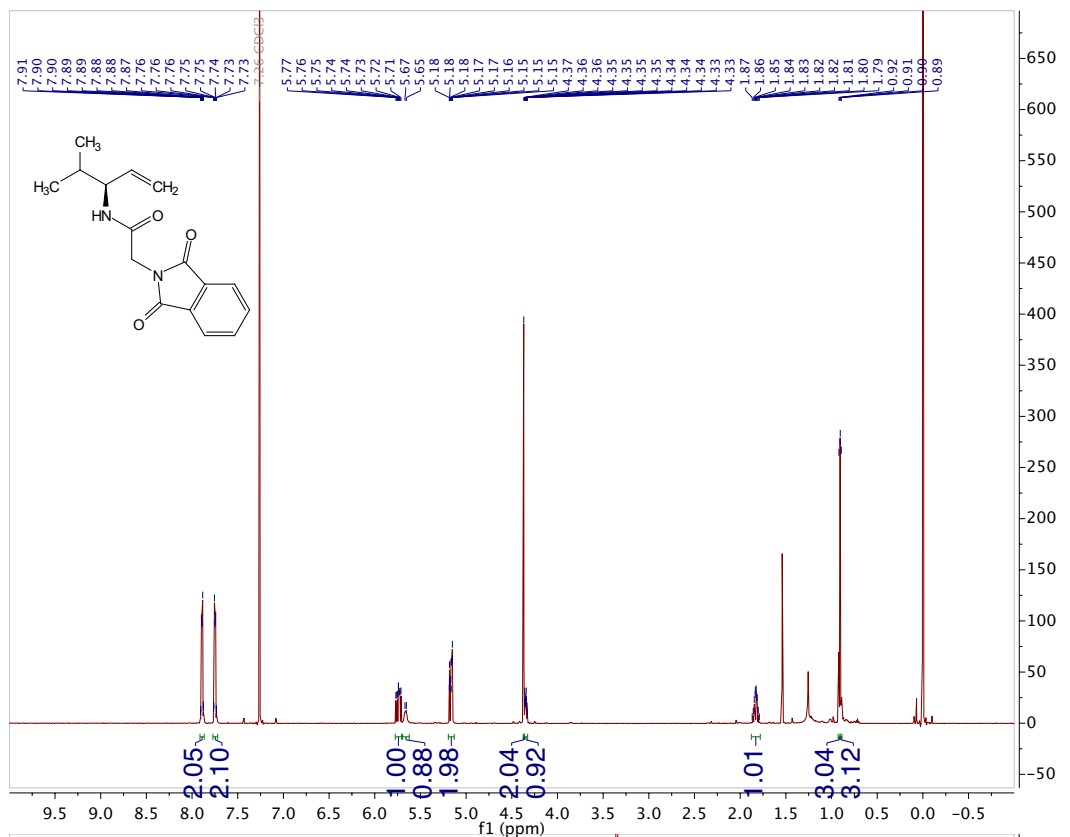
DAD1 C, Sig=210,4 Ref=off (C:\CHEM32\2\DATA\MAAN\2019-08-30\061-0701.D)



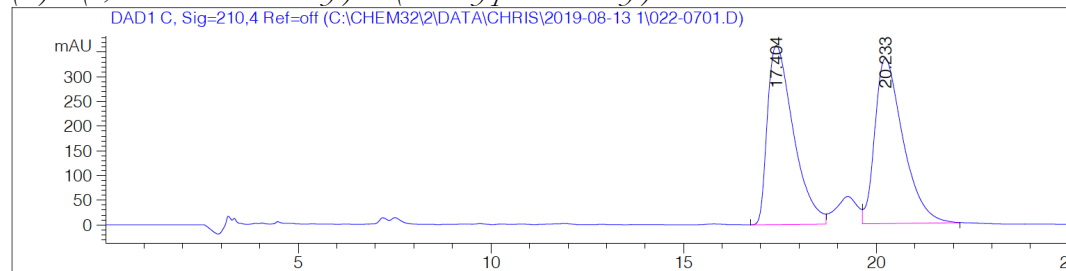
Signal 1: DAD1 C, Sig=210,4 Ref=off

Peak #	RetTime [min]	Type	Width [min]	Area [mAU*s]	Height [mAU]	Area %
1	13.981	BB	0.5363	191.27362	4.95513	1.3938
2	20.075	BB	1.5830	1.35318e4	118.25837	98.6062

Totals : 1.37231e4 123.21350

(S)-2-(1,3-dioxisoindolin-2-yl)-N-(4-methylpent-1-en-3-yl)acetamide

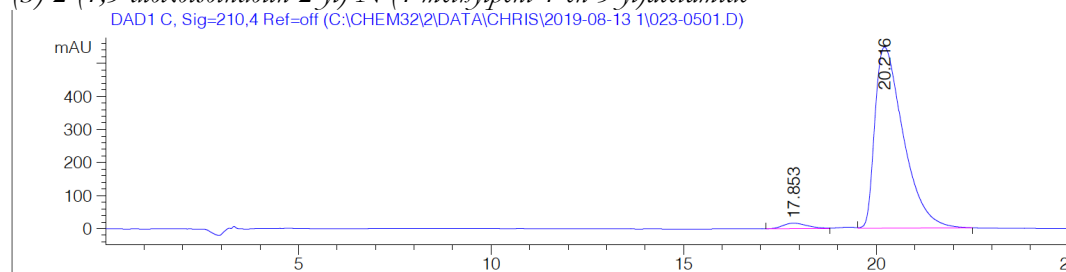
(±)-2-(1,3-dioxisoindolin-2-yl)-N-(4-methylpent-1-en-3-yl)acetamide



Peak #	RetTime [min]	Type	Width [min]	Area [mAU*s]	Height [mAU]	Area %
1	17.404	BV	0.7204	1.70021e4	362.99741	49.9559
2	20.233	VB	0.7666	1.70322e4	334.19327	50.0441

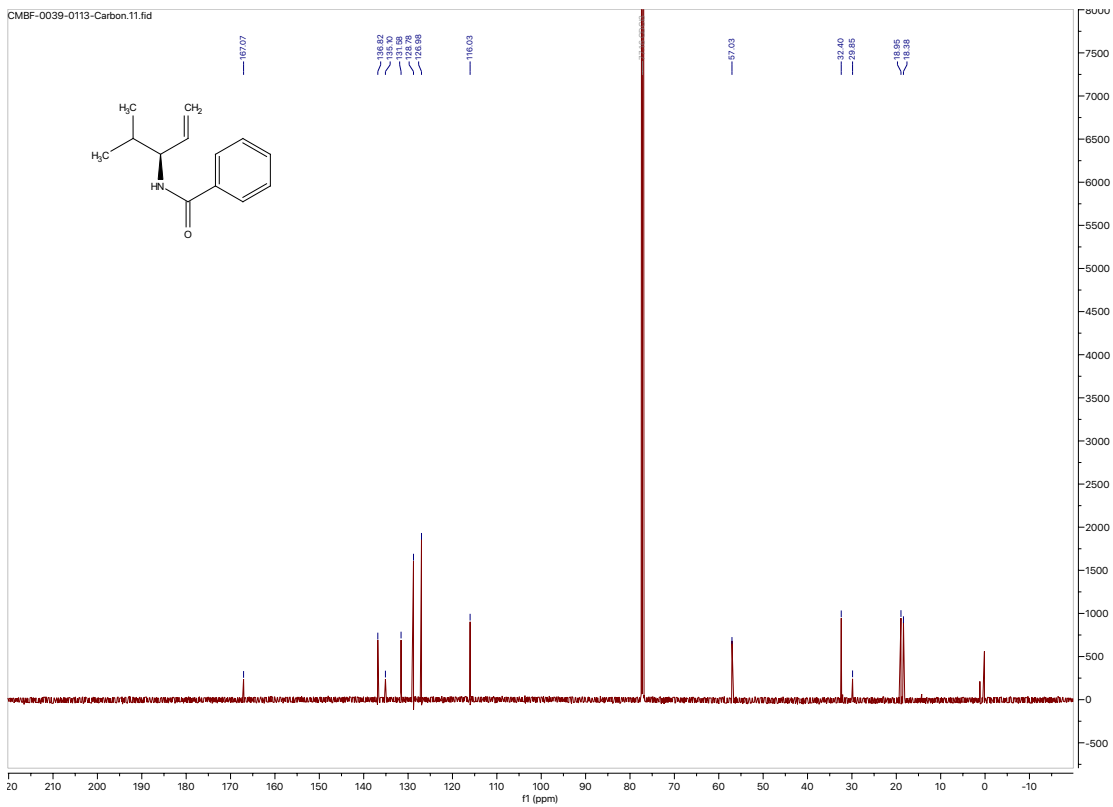
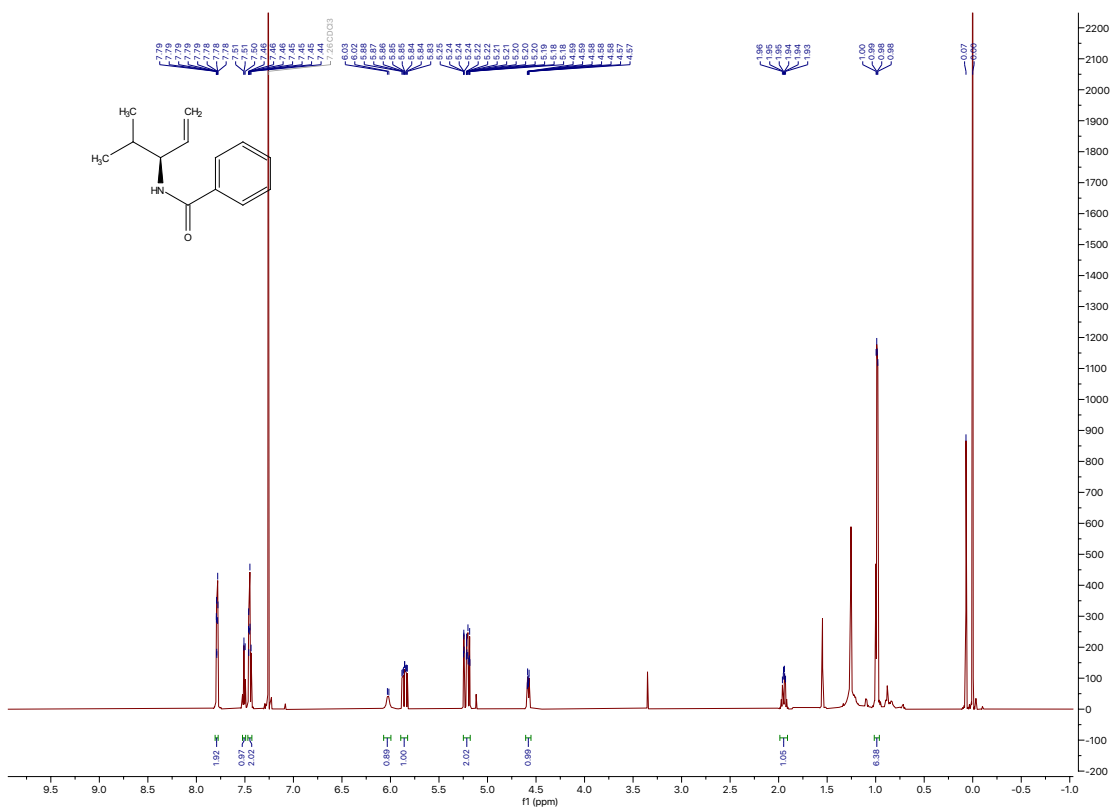
Totals : 3.40343e4 697.19067

(S)-2-(1,3-dioxisoindolin-2-yl)-N-(4-methylpent-1-en-3-yl)acetamide



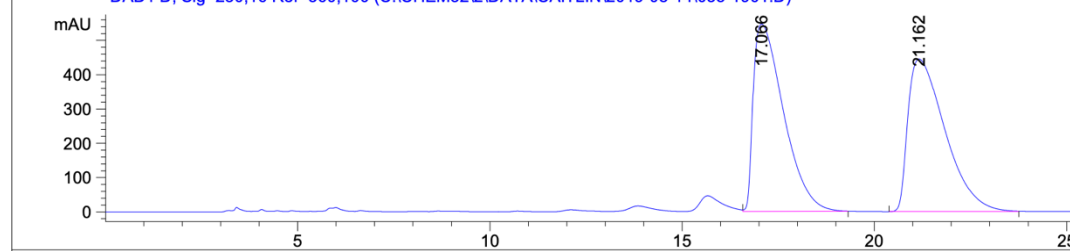
Peak #	RetTime [min]	Type	Width [min]	Area [mAU*s]	Height [mAU]	Area %
1	17.853	BV	0.6325	740.67694	16.66547	2.5624
2	20.216	VB	0.7857	2.81644e4	547.89539	97.4376

Totals : 2.89050e4 564.56085

(S)-N-(4-methylpent-1-en-3-yl)benzamide

(±)-N-(4-methylpent-1-en-3-yl)benzamide

DAD1 D, Sig=230,16 Ref=360,100 (C:\CHEM32\DATA\CAITLIN\2019-08-14\035-1901.D)



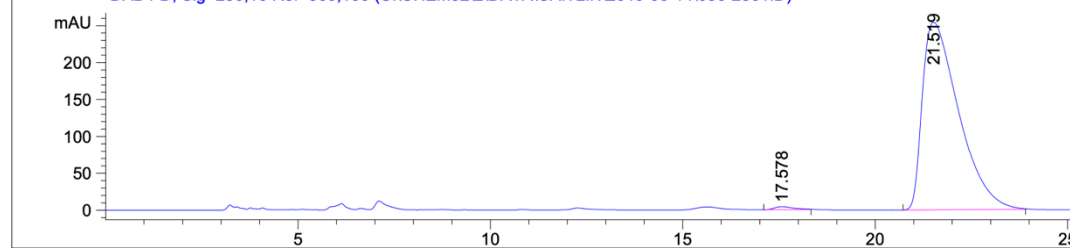
Signal 3: DAD1 D, Sig=230,16 Ref=360,100

Peak #	RetTime [min]	Type	Width [min]	Area [mAU*s]	Height [mAU]	Area %
1	17.066	VB	0.8521	2.98950e4	546.56543	50.0149
2	21.162	BB	1.0538	2.98772e4	444.71542	49.9851

Totals : 5.97723e4 991.28085

(S)-N-(4-methylpent-1-en-3-yl)benzamide

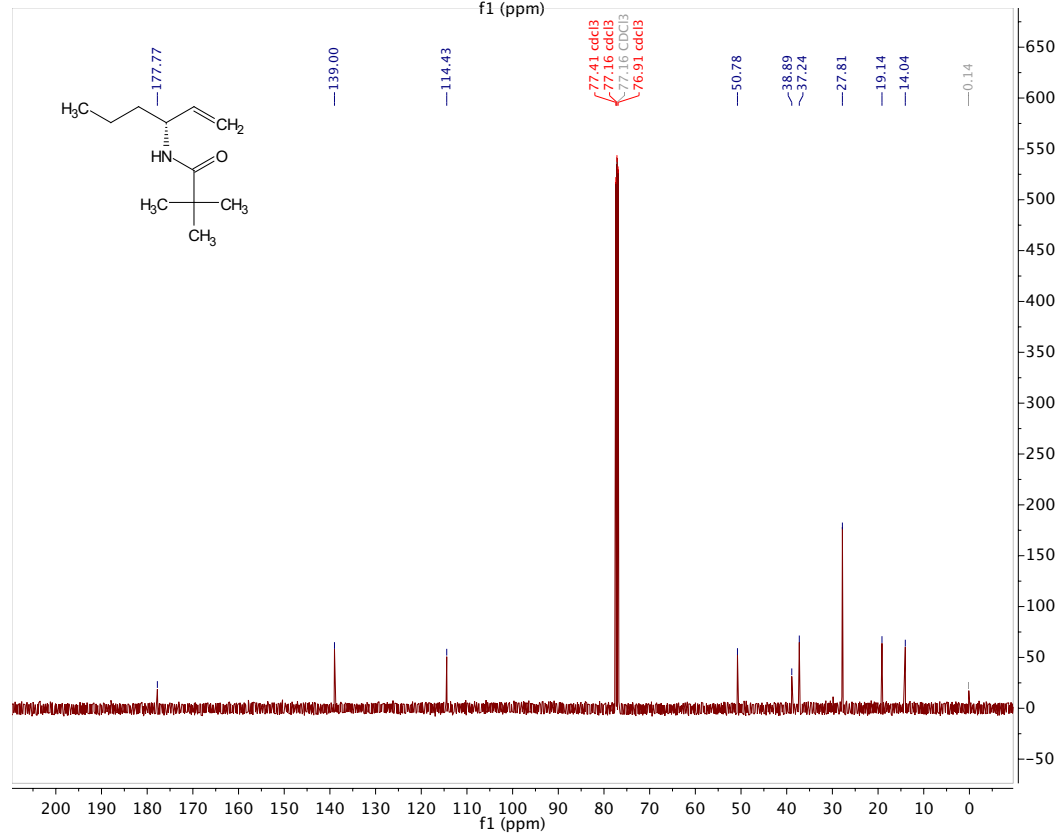
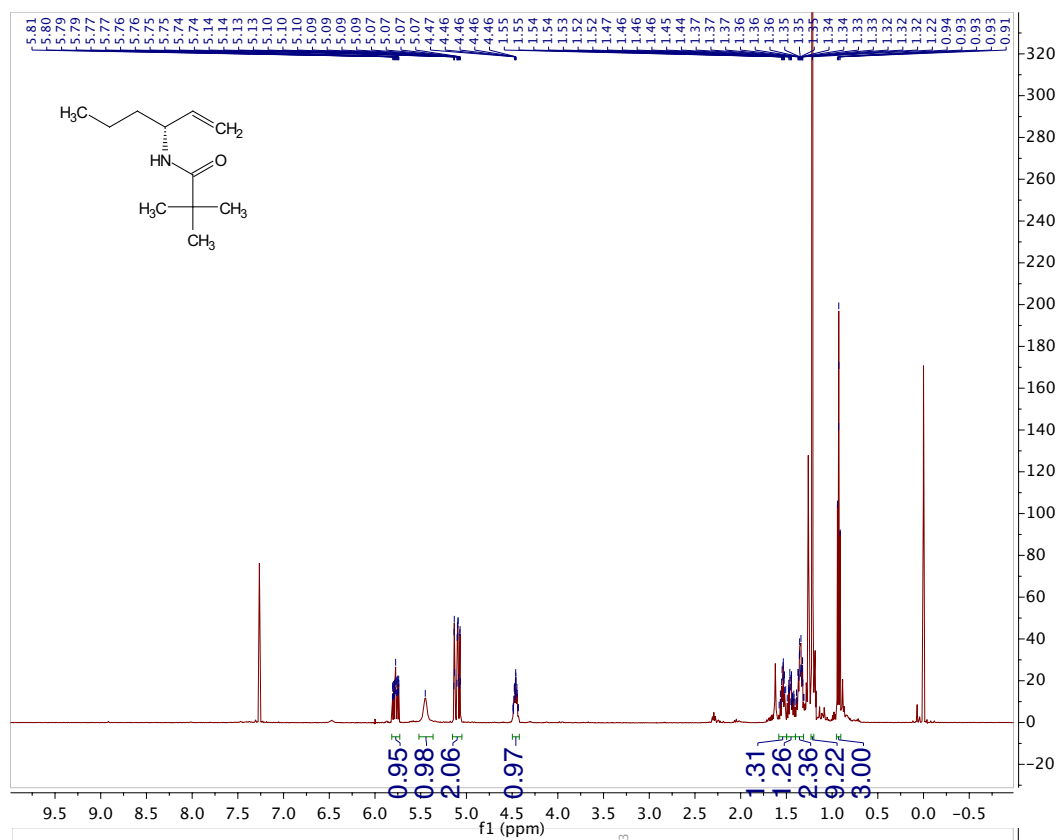
DAD1 D, Sig=230,16 Ref=360,100 (C:\CHEM32\DATA\CAITLIN\2019-08-14\036-2301.D)

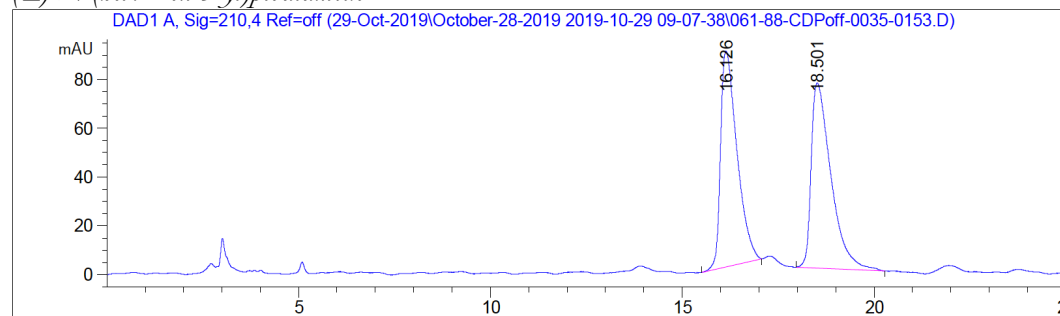


Signal 3: DAD1 D, Sig=230,16 Ref=360,100

Peak #	RetTime [min]	Type	Width [min]	Area [mAU*s]	Height [mAU]	Area %
1	17.578	BB	0.4992	142.68413	4.14934	0.8498
2	21.519	BB	1.0024	1.66485e4	254.08482	99.1502

Totals : 1.67912e4 258.23416

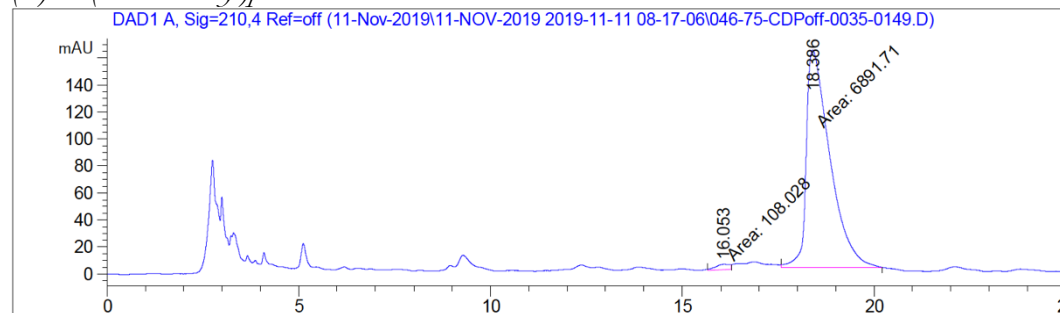
(R)-N-(hex-1-en-3-yl)pivalamide

(±)-N-(hex-1-en-3-yl)pivalamide

Signal 1: DAD1 A, Sig=210,4 Ref=off

Peak #	RetTime [min]	Type	Width [min]	Area [mAU*s]	Height [mAU]	Area %
1	16.126	BB	0.3726	2631.26929	88.56808	49.1456
2	18.501	BB	0.4307	2722.75781	75.95327	50.8544

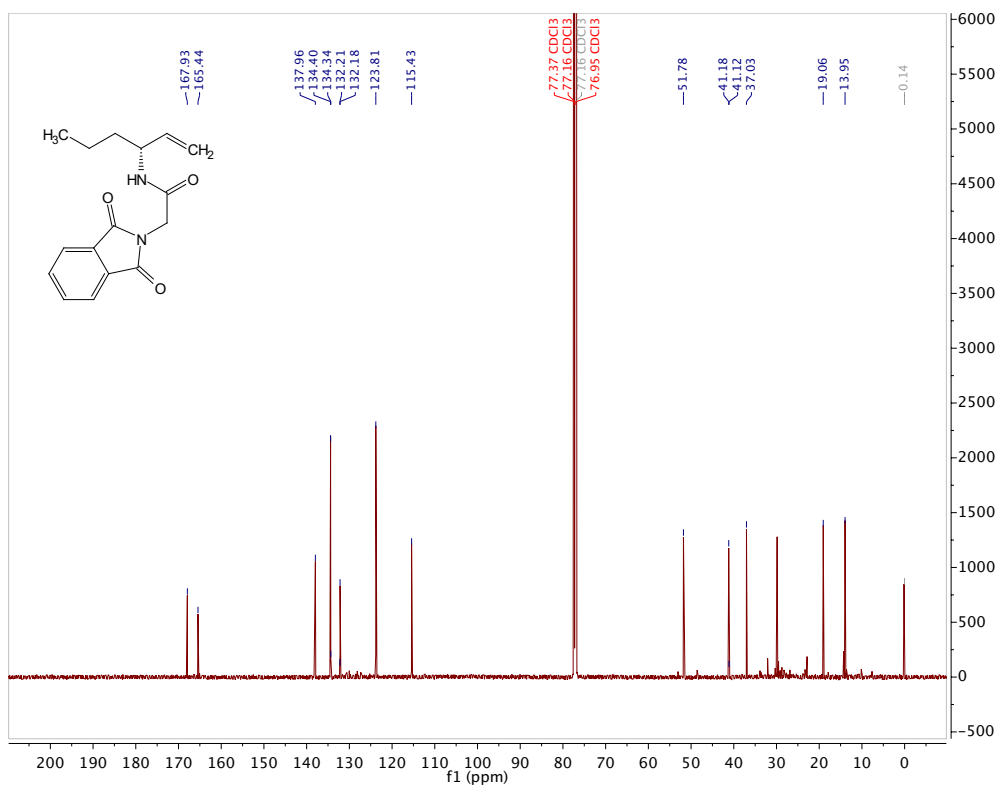
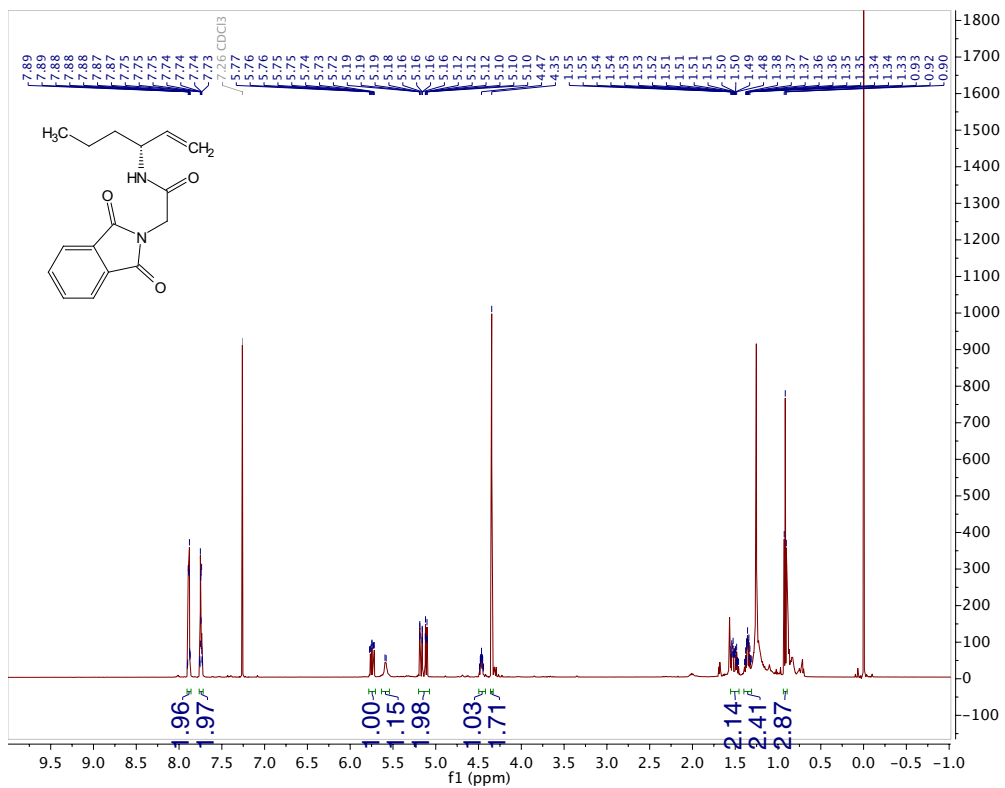
Totals : 5354.02710 164.52135

(R)-N-(hex-1-en-3-yl)pivalamide

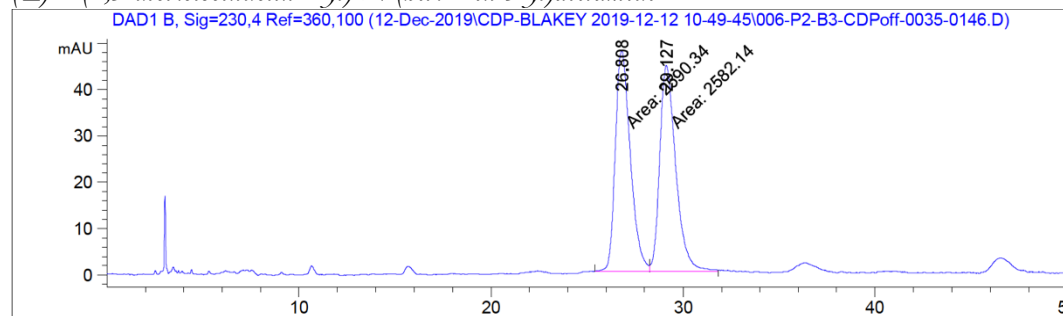
Signal 1: DAD1 A, Sig=210,4 Ref=off

Peak #	RetTime [min]	Type	Width [min]	Area [mAU*s]	Height [mAU]	Area %
1	16.053	MM	0.4373	108.02784	4.11707	1.5433
2	18.386	MM	0.7130	6891.71094	161.10773	98.4567

Totals : 6999.73878 165.22480

(R)-2-(1,3-dioxoisindolin-2-yl)-*N*-(hex-1-en-3-yl)acetamide

(±)-2-(1,3-dioxoisindolin-2-yl)-N-(hex-1-en-3-yl)acetamide

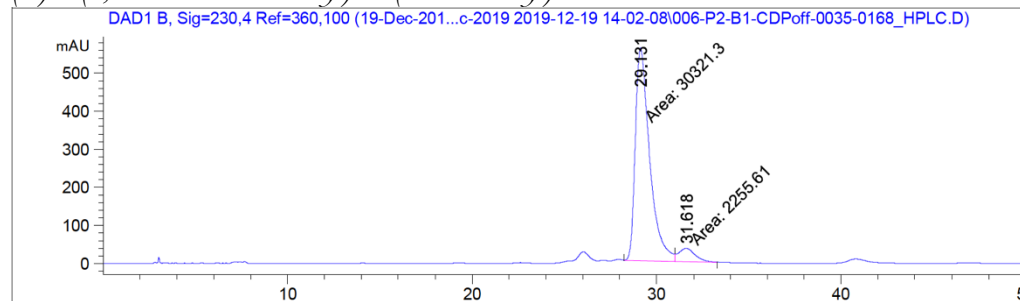


Signal 2: DAD1 B, Sig=230,4 Ref=360,100

Peak #	RetTime [min]	Type	Width [min]	Area [mAU*s]	Height [mAU]	Area %
1	26.808	MF	0.9051	2590.33911	47.69818	50.0793
2	29.127	FM	0.9676	2582.13672	44.47890	49.9207

Totals : 5172.47583 92.17709

(R)-2-(1,3-dioxoisindolin-2-yl)-N-(hex-1-en-3-yl)acetamide

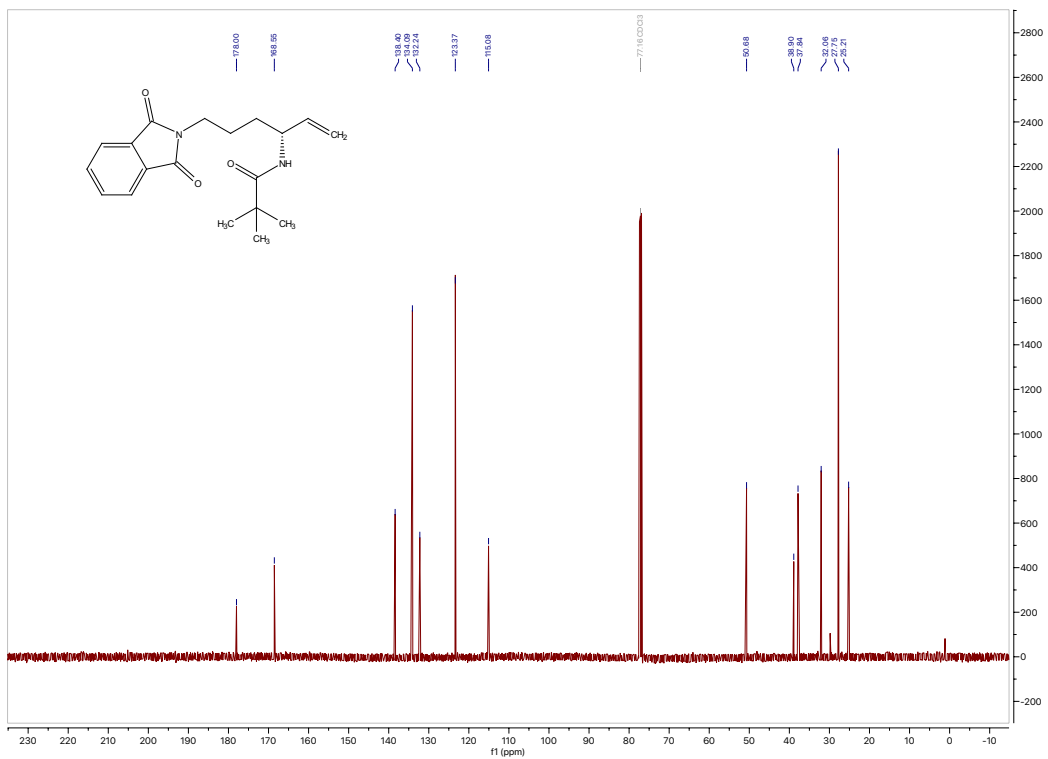
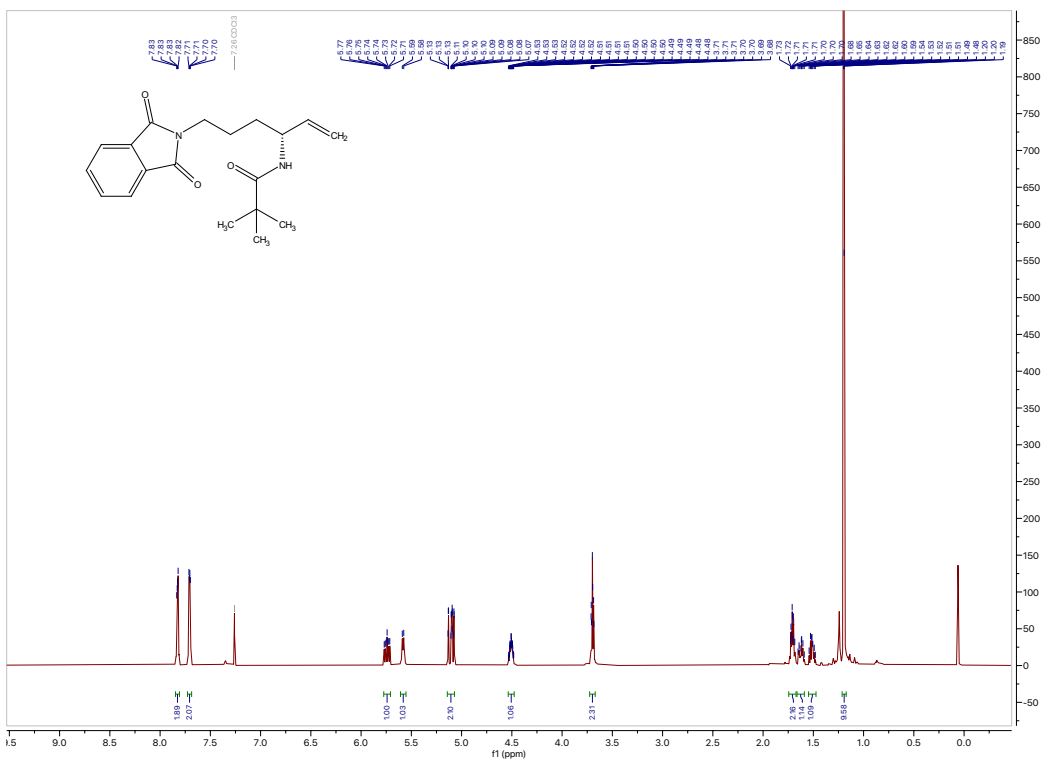


Signal 2: DAD1 B, Sig=230,4 Ref=360,100

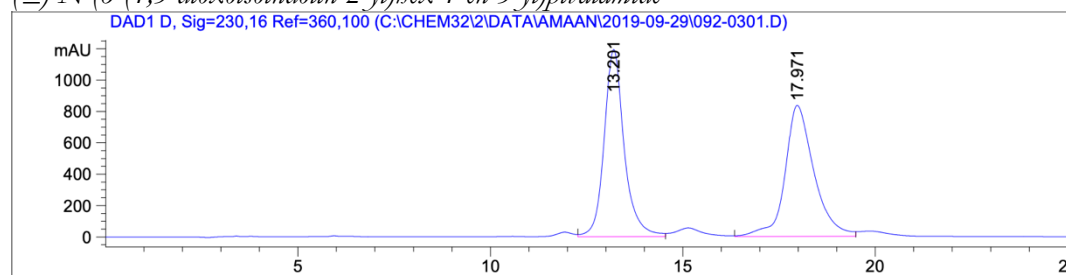
Peak #	RetTime [min]	Type	Width [min]	Area [mAU*s]	Height [mAU]	Area %
1	29.131	MF	0.9020	3.03213e4	560.25873	93.0761
2	31.618	FM	1.0542	2255.60840	35.66072	6.9239

Totals : 3.25769e4 595.91945

(R)-N-(6-(1,3-dioxisoindolin-2-yl)hex-1-en-3-yl)pivalamide



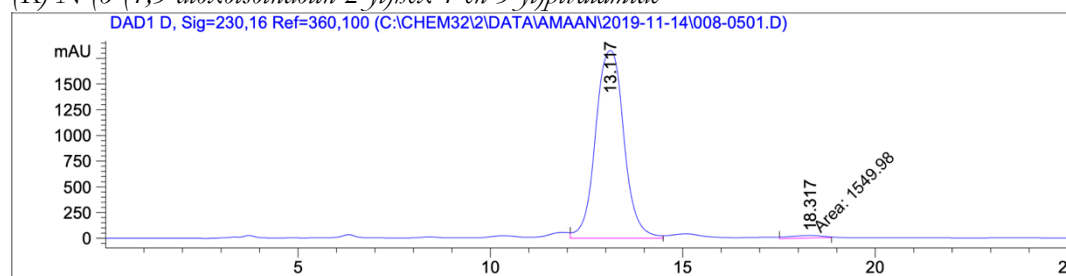
(±)-N-(6-(1,3-dioxisoindolin-2-yl)hex-1-en-3-yl)pivalamide



Peak #	RetTime [min]	Type	Width [min]	Area [mAU*s]	Height [mAU]	Area %
1	13.201	VV	0.5408	4.32601e4	1193.61682	49.6816
2	17.971	BV	0.7675	4.38145e4	835.98889	50.3184

Totals : 8.70746e4 2029.60571

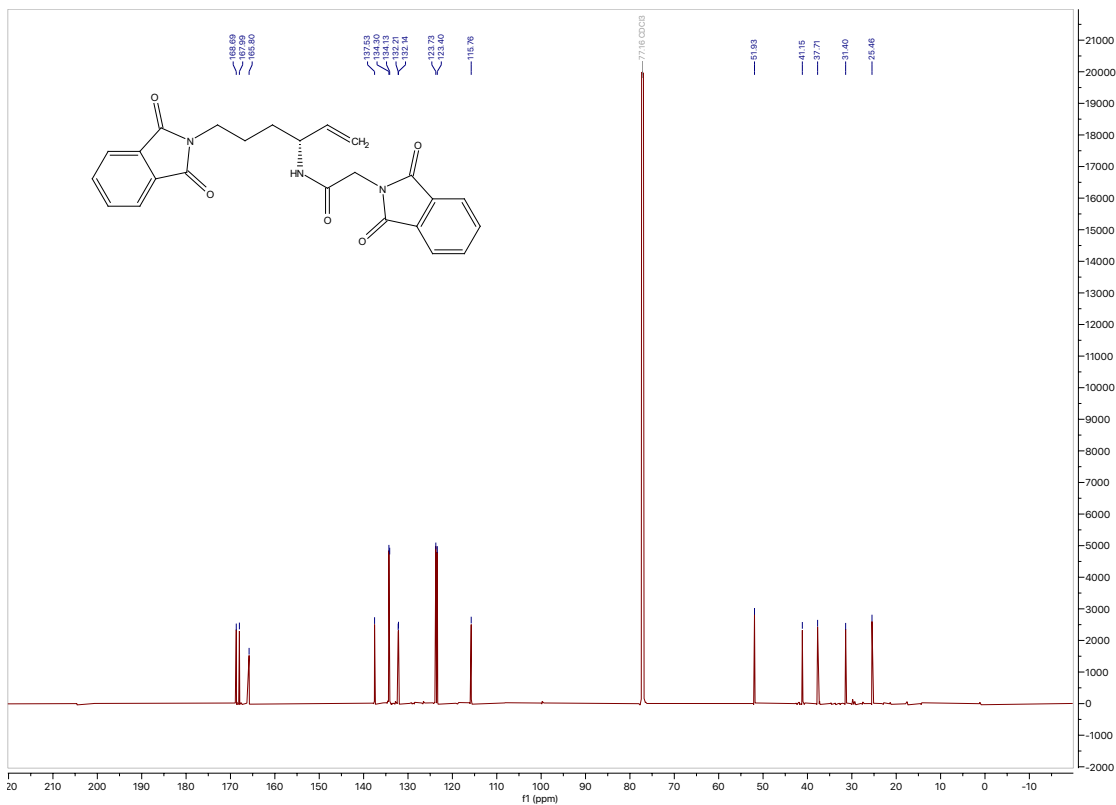
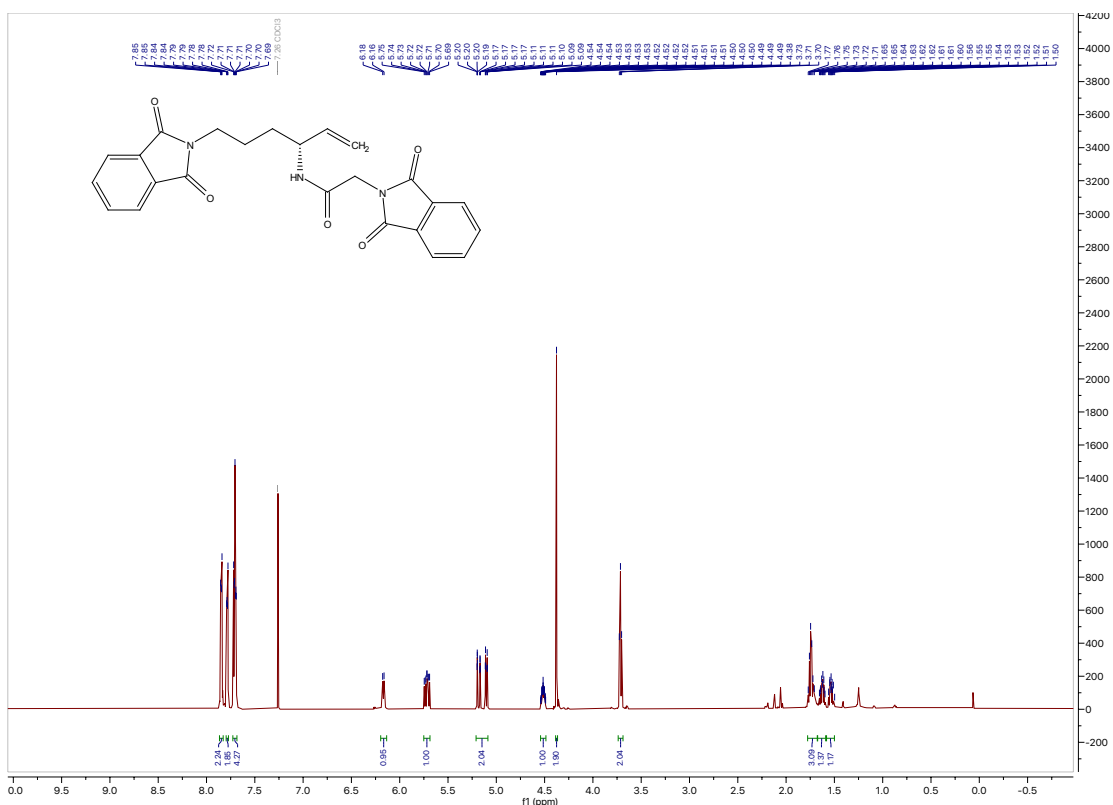
(R)-N-(6-(1,3-dioxisoindolin-2-yl)hex-1-en-3-yl)pivalamide



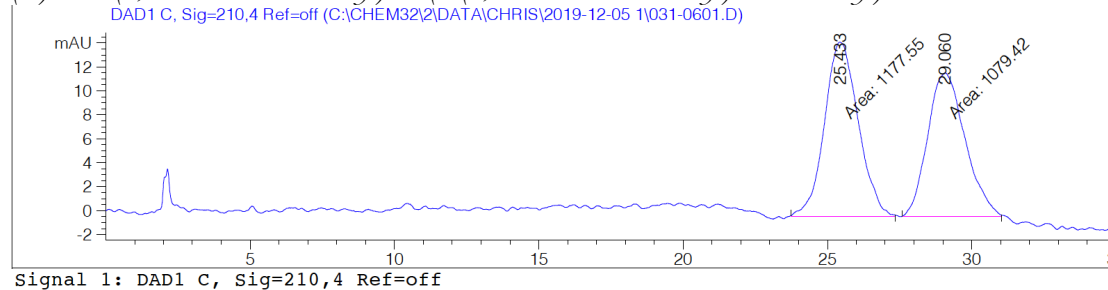
Peak #	RetTime [min]	Type	Width [min]	Area [mAU*s]	Height [mAU]	Area %
1	13.117	VV	0.8071	9.34638e4	1826.09387	98.3687
2	18.317	MM	1.0358	1549.98071	24.93963	1.6313

Totals : 9.50138e4 1851.03350

(R)-2-N-(1,3-dioxoisindolin-2-yl)-N-(6-(1,3-dioxoisindolin-2-yl)hex-1-en-3-yl)acetamide



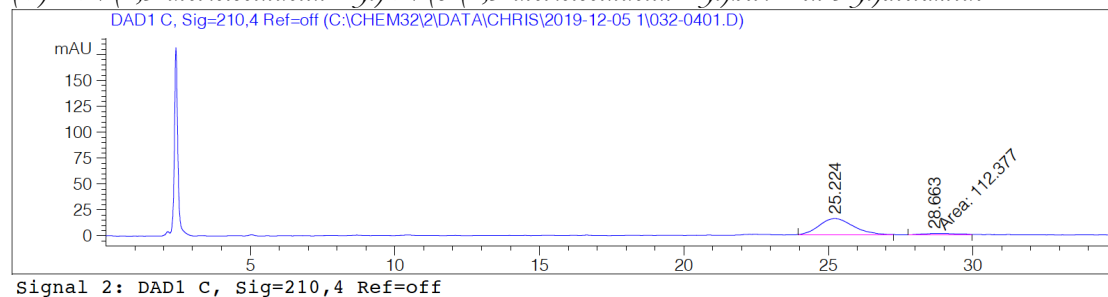
(±)-2-N-(1,3-dioxoisindolin-2-yl)-N-(6-(1,3-dioxoisindolin-2-yl)hex-1-en-3-yl)acetamide



Peak #	RetTime [min]	Type	Width [min]	Area [mAU*s]	Height [mAU]	Area %
1	25.433	MM	1.3514	1177.55273	14.52247	52.1740
2	29.060	MM	1.4997	1079.41809	11.99581	47.8260

Totals : 2256.97083 26.51828

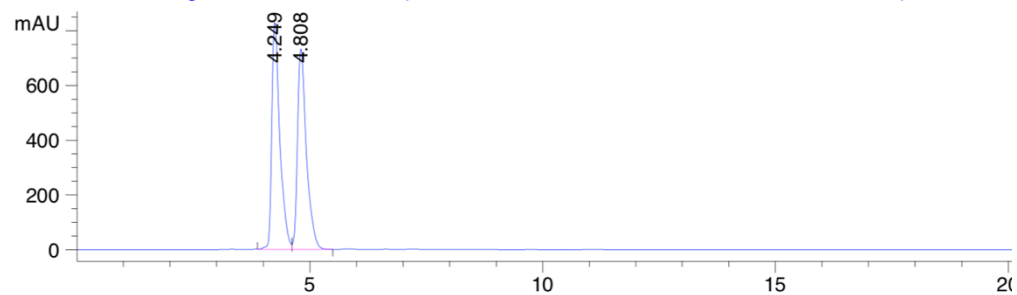
(R)-2-N-(1,3-dioxoisindolin-2-yl)-N-(6-(1,3-dioxoisindolin-2-yl)hex-1-en-3-yl)acetamide



Peak #	RetTime [min]	Type	Width [min]	Area [mAU*s]	Height [mAU]	Area %
1	25.224	BB	1.0140	1269.50793	15.49218	91.8678
2	28.663	MM	1.3726	112.37718	1.36449	8.1322

Totals : 1381.88512 16.85667

(±)-N-(6-((tert-butyl)diphenylsilyloxy)hex-1-en-3-yl)pivalamide

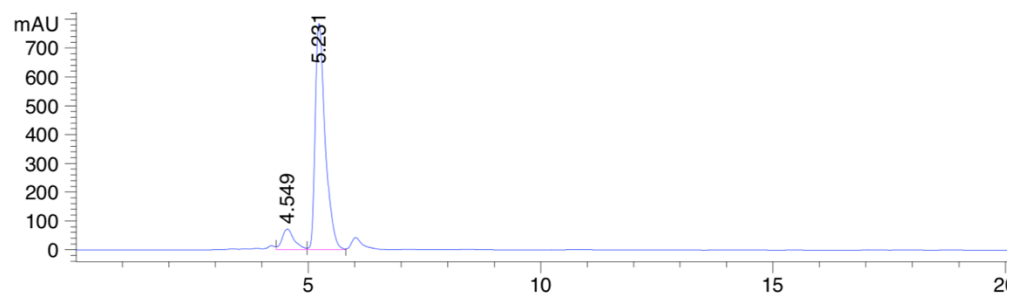


Signal 1: DAD1 D, Sig=230,16 Ref=360,100

Peak #	RetTime [min]	Type	Width [min]	Area [mAU*s]	Height [mAU]	Area %
1	4.249	BV	0.1793	1.00245e4	827.66113	50.5216
2	4.808	VB	0.2003	9817.56543	732.81635	49.4784

Totals : 1.98421e4 1560.47748

(R)-N-(6-((tert-butyl)diphenylsilyloxy)hex-1-en-3-yl)pivalamide

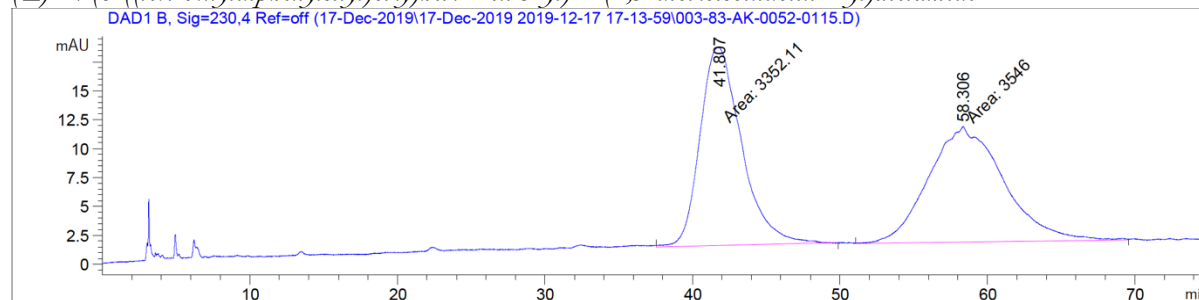


Signal 1: DAD1 D, Sig=230,16 Ref=360,100

Peak #	RetTime [min]	Type	Width [min]	Area [mAU*s]	Height [mAU]	Area %
1	4.549	VV	0.2670	1279.76208	71.44872	9.8542
2	5.231	VV	0.2262	1.17072e4	784.25903	90.1458

Totals : 1.29870e4 855.70775

(±)-N-(6-((tert-butylidiphenylsilyl)oxy)hex-1-en-3-yl)-2-(1,3-dioxisoindolin-2-yl)acetamide

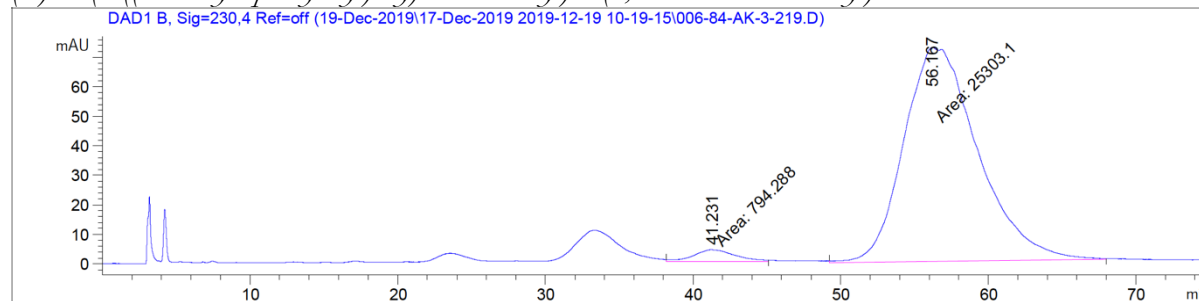


Signal 2: DAD1 B, Sig=230,4 Ref=off

Peak #	RetTime [min]	Type	Width [min]	Area [mAU*s]	Height [mAU]	Area %
1	41.807	MM	3.2564	3352.10791	17.15645	48.5946
2	58.306	MM	5.9019	3545.99854	10.01379	51.4054

Totals : 6898.10645 27.17023

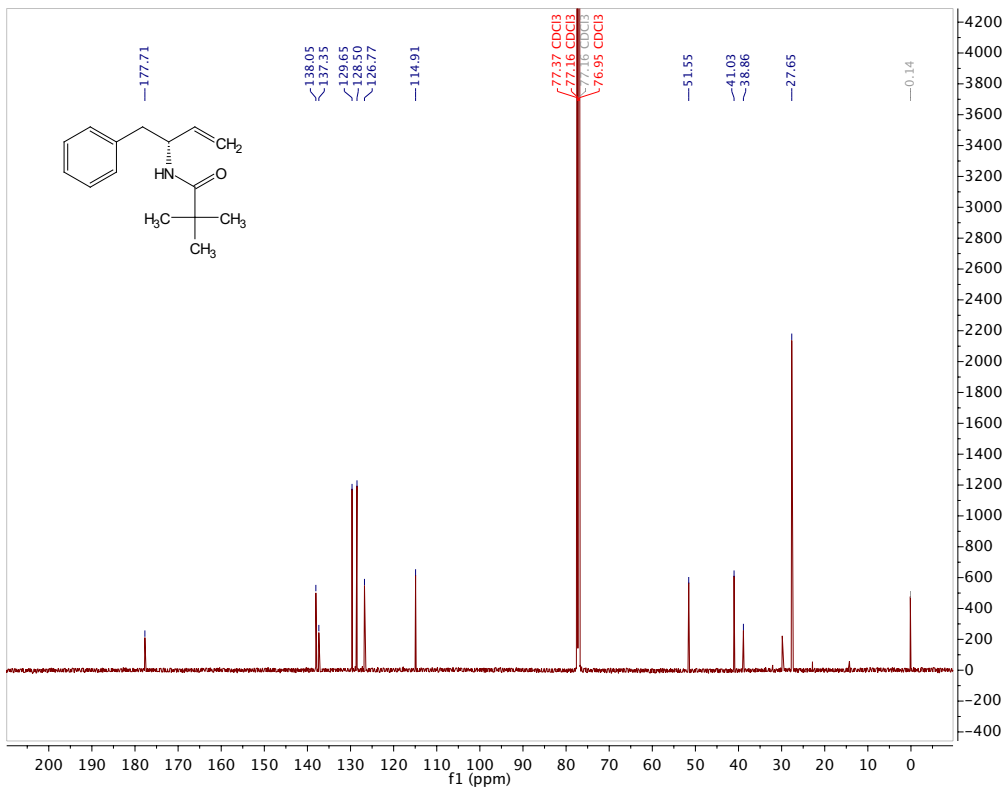
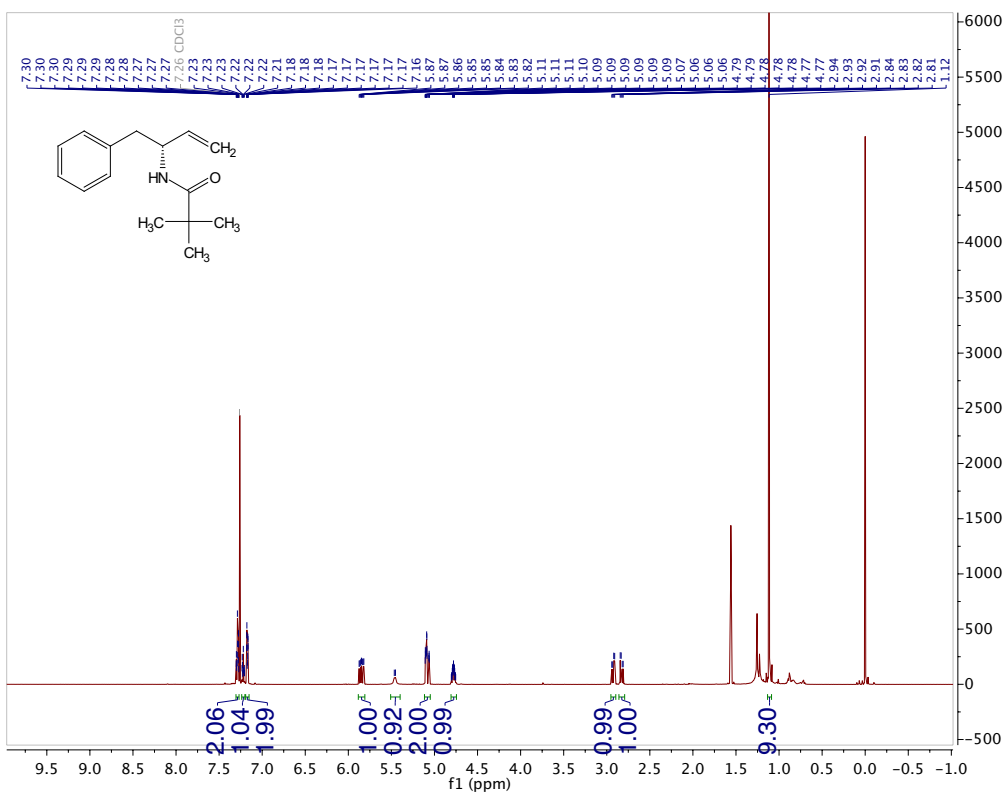
(R)-N-(6-((tert-butylidiphenylsilyl)oxy)hex-1-en-3-yl)-2-(1,3-dioxisoindolin-2-yl)acetamide

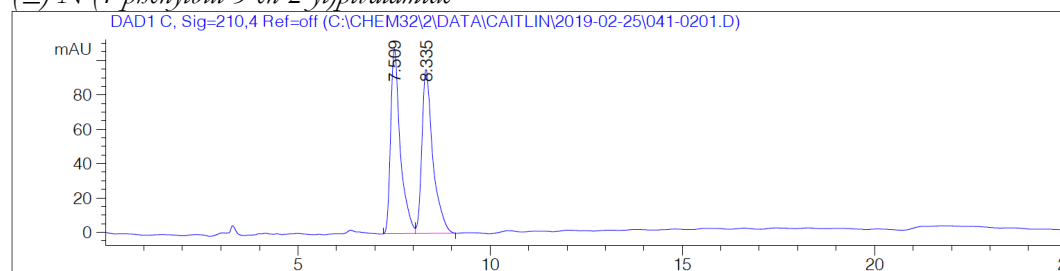


Signal 2: DAD1 B, Sig=230,4 Ref=off

Peak #	RetTime [min]	Type	Width [min]	Area [mAU*s]	Height [mAU]	Area %
1	41.231	MM	3.2846	794.28815	4.03041	3.0436
2	56.167	MM	5.8123	2.53031e4	72.55560	96.9564

Totals : 2.60974e4 76.58601

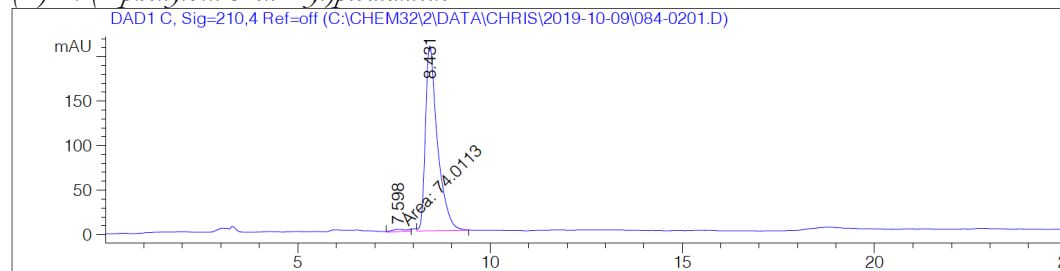
(R)-N-(1-phenylbut-3-en-2-yl)pivalamide

(±)-N-(1-phenylbut-3-en-2-yl)pivalamide

Signal 1: DAD1 C, Sig=210,4 Ref=off

Peak #	RetTime [min]	Type	Width [min]	Area [mAU*s]	Height [mAU]	Area %
1	7.509	BV	0.2528	1852.07629	107.60557	49.7381
2	8.335	VB	0.2887	1871.58264	95.46971	50.2619

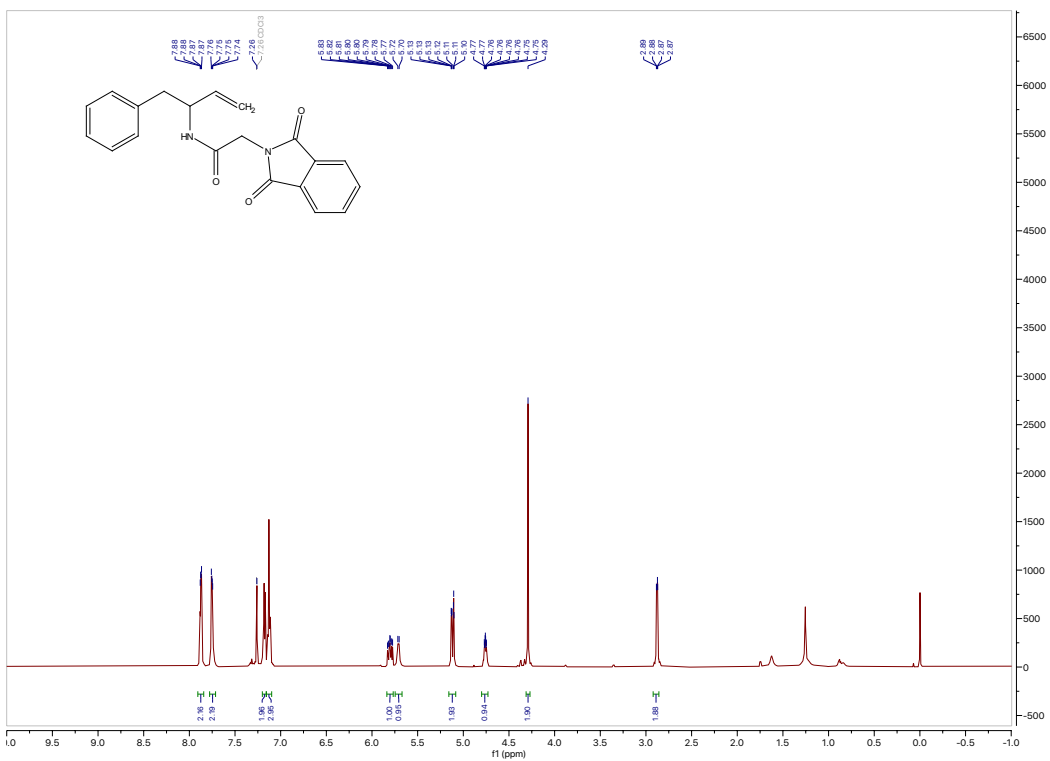
Totals : 3723.65894 203.07528

(R)-N-(1-phenylbut-3-en-2-yl)pivalamide

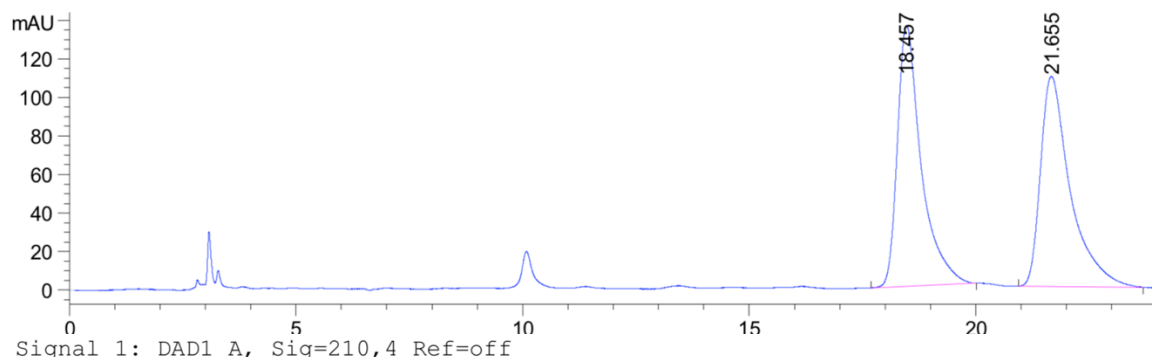
Signal 2: DAD1 C, Sig=210,4 Ref=off

Peak #	RetTime [min]	Type	Width [min]	Area [mAU*s]	Height [mAU]	Area %
1	7.598	MM	0.4611	74.01132	2.67536	1.6245
2	8.431	VB	0.3117	4481.90283	207.74052	98.3755

Totals : 4555.91415 210.41588

(R)-2-(1,3-dioxoisindolin-2-yl)-N-(1-phenylbut-3-en-2-yl)acetamide

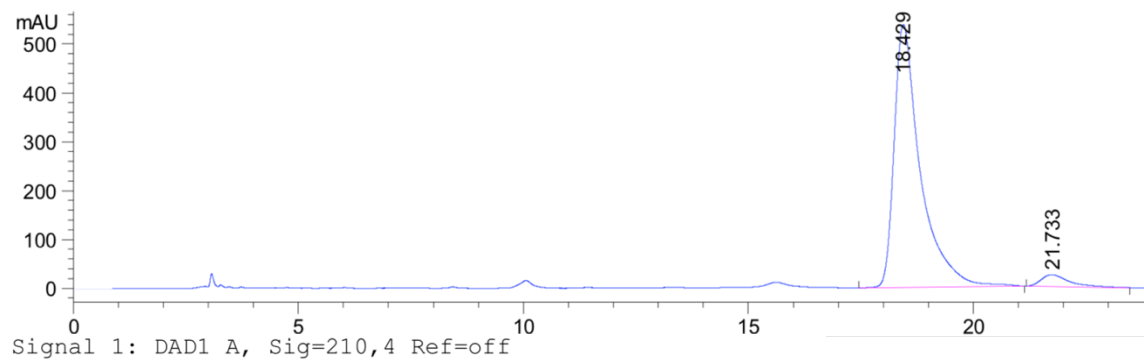
(±)-2-(1,3-dioxoisindolin-2-yl)-N-(1-phenylbut-3-en-2-yl)acetamide



Peak #	RetTime [min]	Type	Width [min]	Area [mAU*s]	Height [mAU]	Area %
1	18.457	BV R	0.4429	4955.47949	135.42155	49.8705
2	21.655	BB	0.5359	4981.21240	109.15691	50.1295

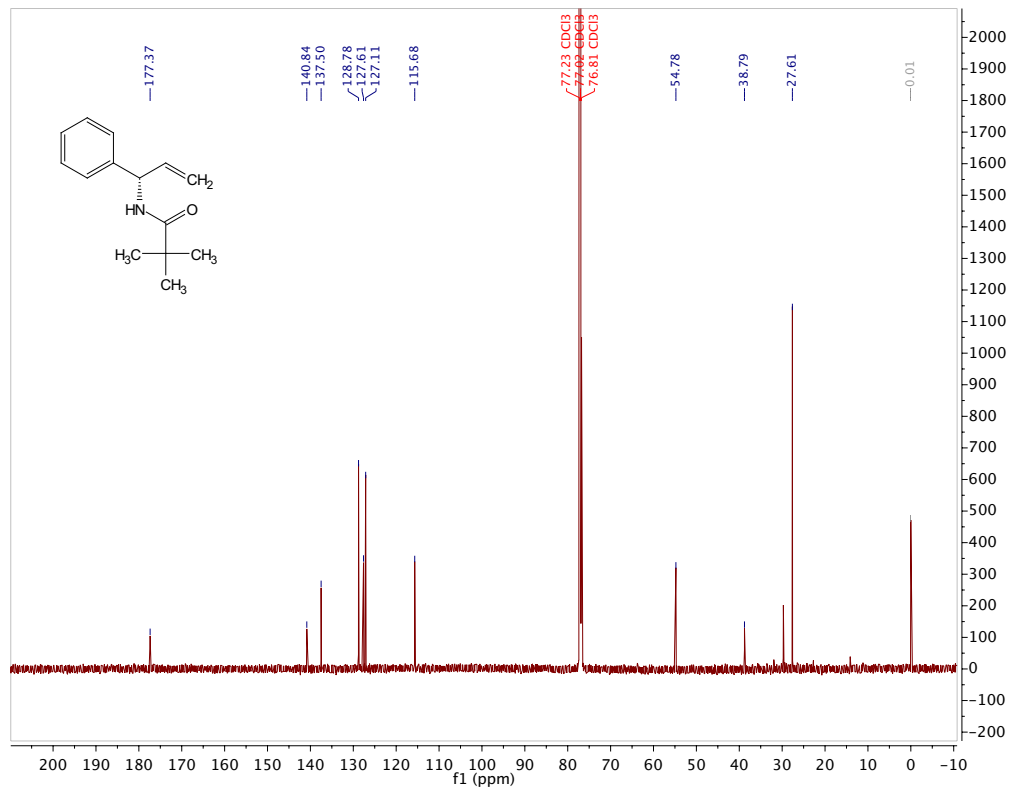
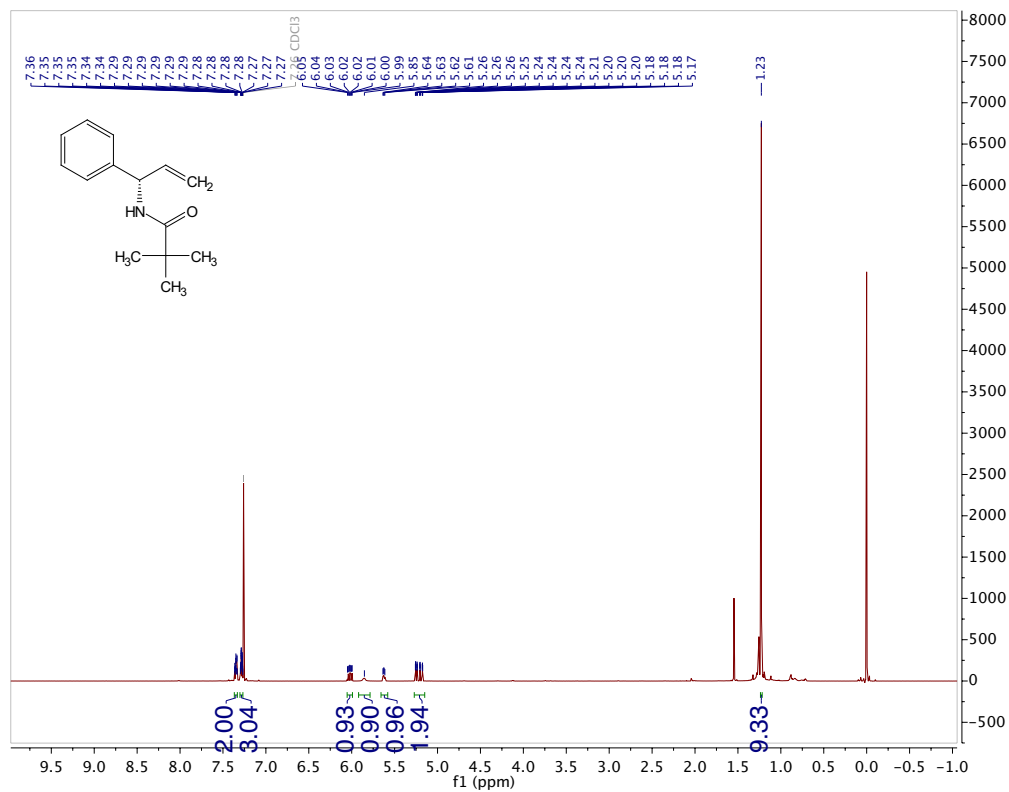
Totals : 9936.69189 244.57847

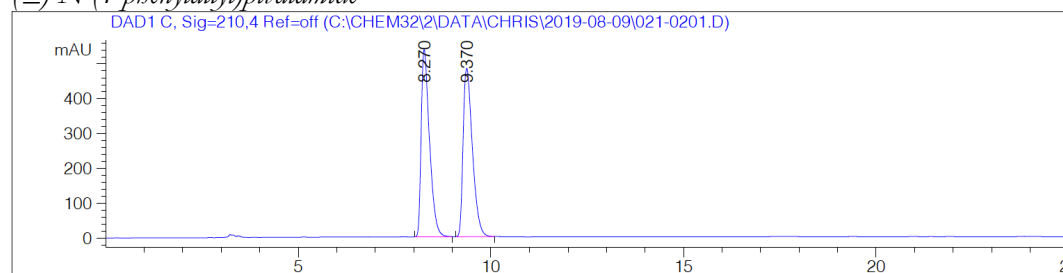
(R)-2-(1,3-dioxoisindolin-2-yl)-N-(1-phenylbut-3-en-2-yl)acetamide



Peak #	RetTime [min]	Type	Width [min]	Area [mAU*s]	Height [mAU]	Area %
1	18.429	BB	0.5074	2.18200e4	538.26617	95.4123
2	21.733	BV R	0.5099	1049.16833	24.14909	4.5877

Totals : 2.28691e4 562.41527

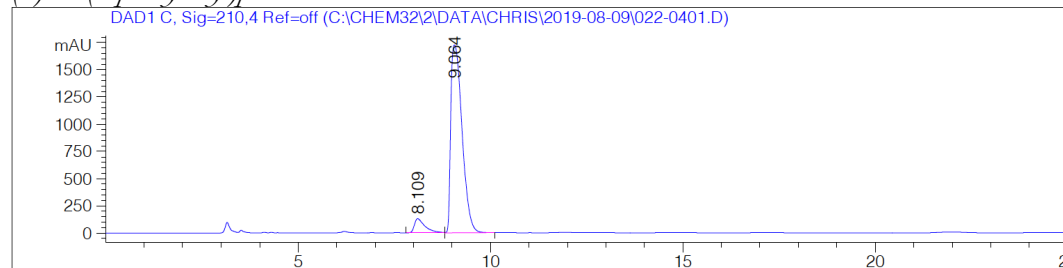
(S)-N-(1-phenylallyl)pivalamide

(±)-N-(1-phenylallyl)pivalamide

Signal 1: DAD1 C, Sig=210,4 Ref=off

Peak #	RetTime [min]	Type	Width [min]	Area [mAU*s]	Height [mAU]	Area %
1	8.270	BB	0.2251	7979.37158	537.64404	49.9904
2	9.370	BB	0.2526	7982.44971	483.54959	50.0096

Totals : 1.59618e4 1021.19363

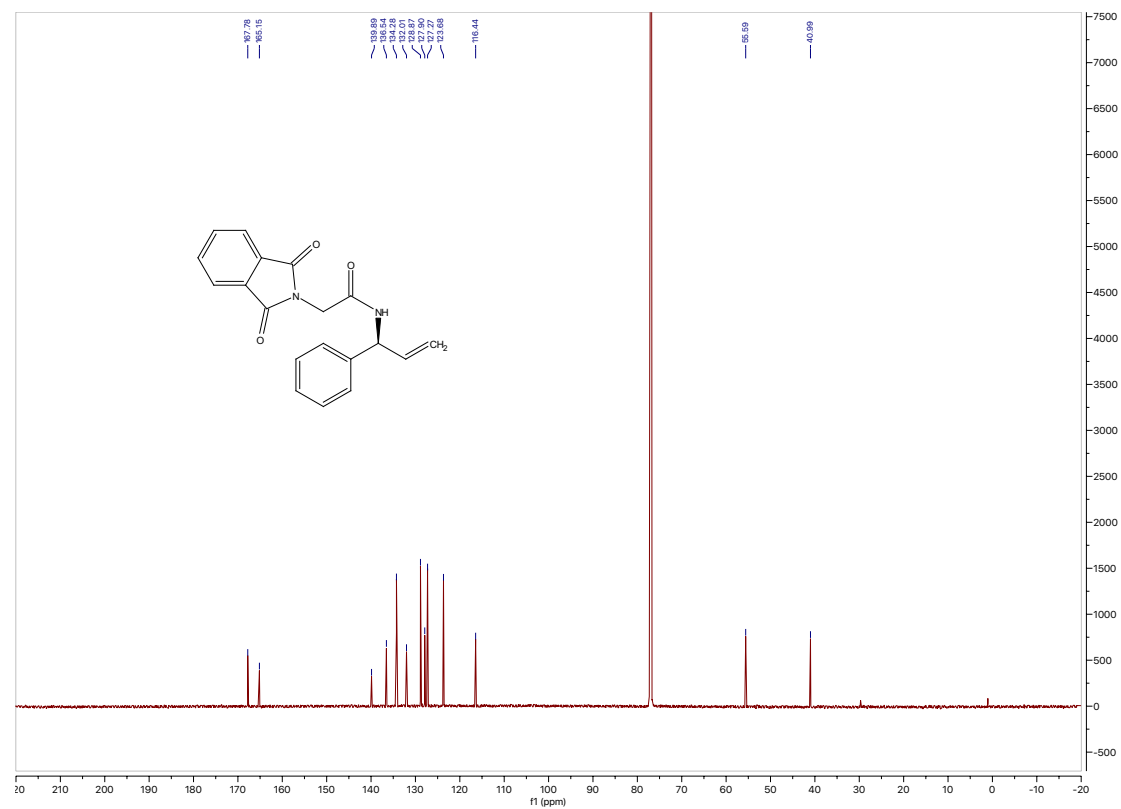
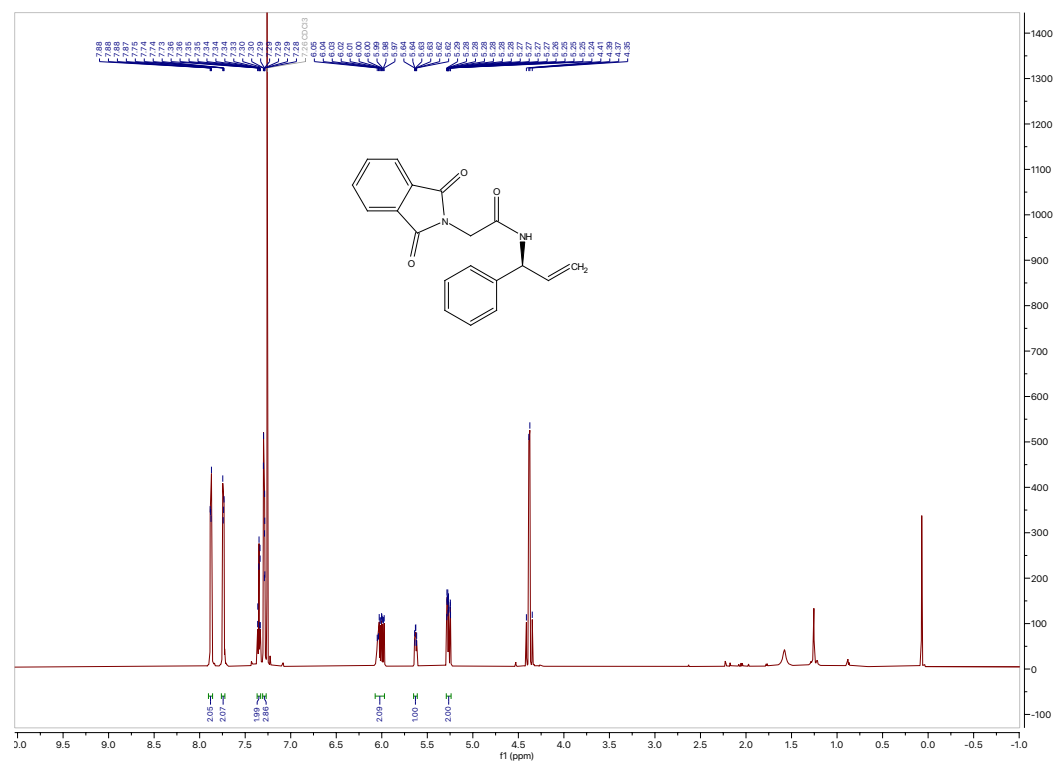
(S)-N-(1-phenylallyl)pivalamide

Signal 2: DAD1 C, Sig=210,4 Ref=off

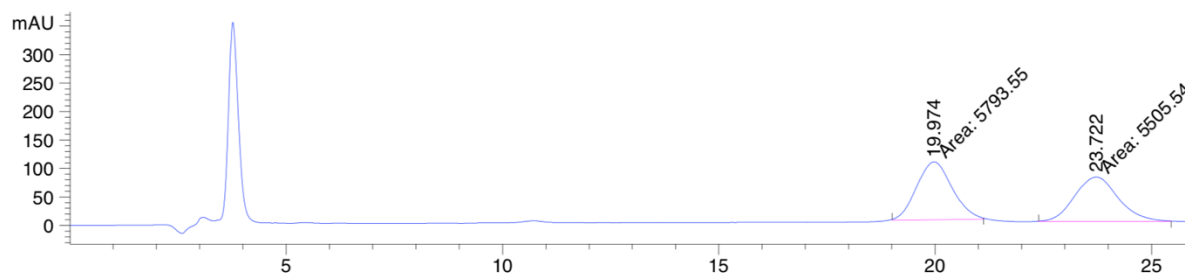
Peak #	RetTime [min]	Type	Width [min]	Area [mAU*s]	Height [mAU]	Area %
1	8.109	VV	0.2769	2515.46436	130.49010	6.6902
2	9.064	VB	0.3233	3.50839e4	1725.01147	93.3098

Totals : 3.75993e4 1855.50157

(S)-2-(1,3-dioxoisindolin-2-yl)-N-(1-phenylallyl)acetamide



(±)-2-(1,3-dioxoisindolin-2-yl)-N-(1-phenylallyl)acetamide

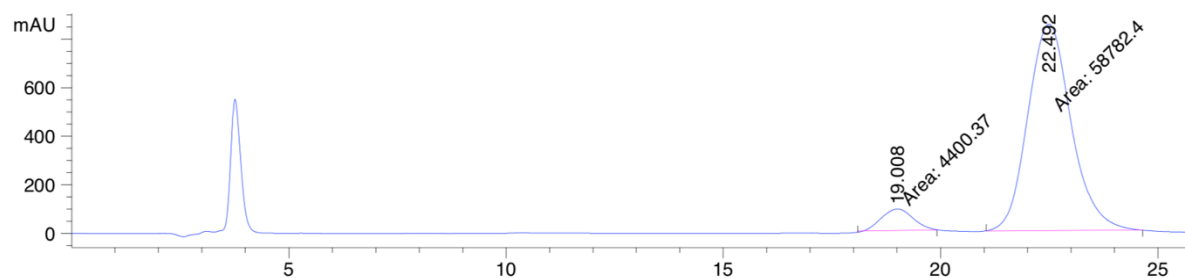


Signal 1: DAD1 C, Sig=210,4 Ref=off

Peak #	RetTime [min]	Type	Width [min]	Area [mAU*s]	Height [mAU]	Area %
1	19.974	MM	0.9513	5793.55469	101.50015	51.2745
2	23.722	MM	1.1756	5505.54199	78.05405	48.7255

Totals : 1.12991e4 179.55421

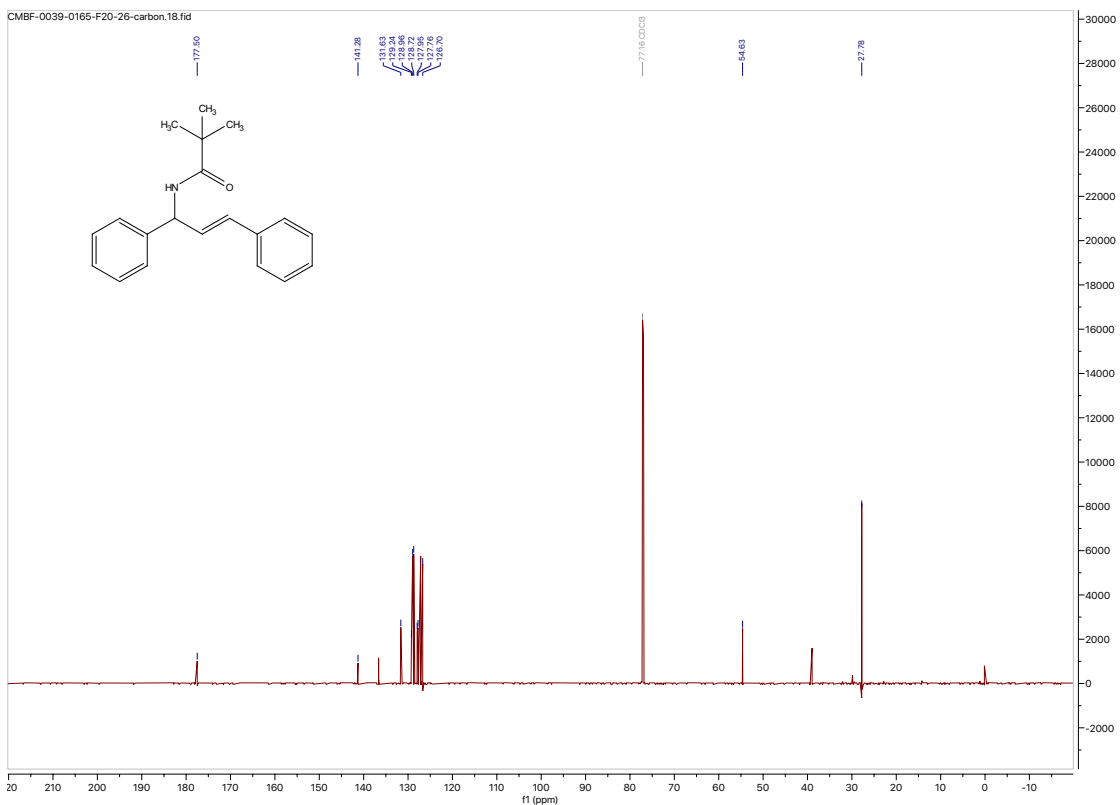
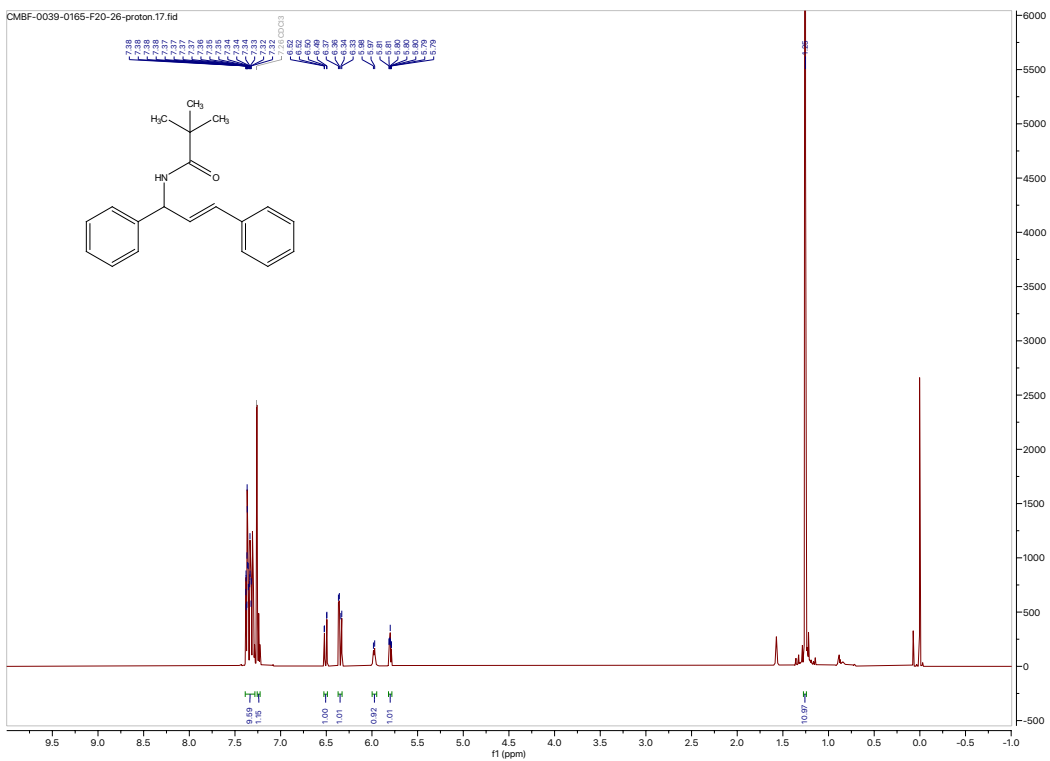
(S)-2-(1,3-dioxoisindolin-2-yl)-N-(1-phenylallyl)acetamide

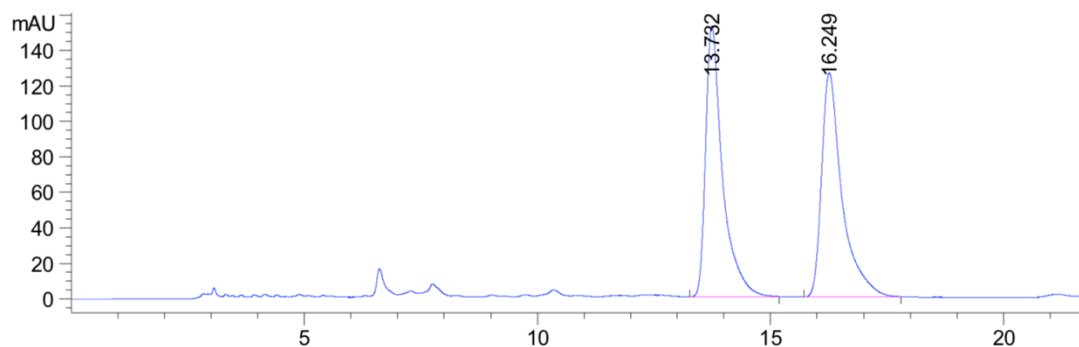


Signal 1: DAD1 C, Sig=210,4 Ref=off

Peak #	RetTime [min]	Type	Width [min]	Area [mAU*s]	Height [mAU]	Area %
1	19.008	MM	0.8312	4400.37354	88.22954	6.9645
2	22.492	MM	1.1531	5.87824e4	849.64386	93.0355

Totals : 6.31827e4 937.87340

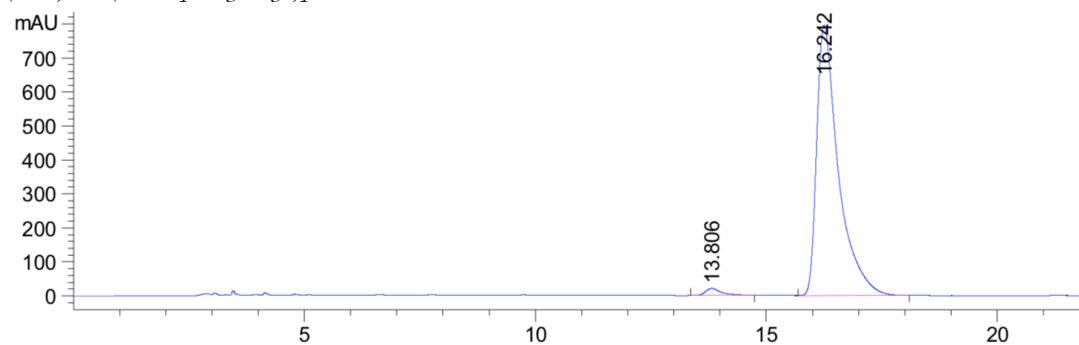
(S,E)-N-(1,3-diphenylallyl)pivalamide

(±)-(E)-N-(1,3-diphenylallyl)pivalamide

Signal 2: DAD1 B, Sig=230,4 Ref=off

Peak #	RetTime [min]	Type	Width [min]	Area [mAU*s]	Height [mAU]	Area %
1	13.732	BB	0.3546	3845.48267	152.53081	49.9790
2	16.249	BB	0.4231	3848.71924	126.26714	50.0210

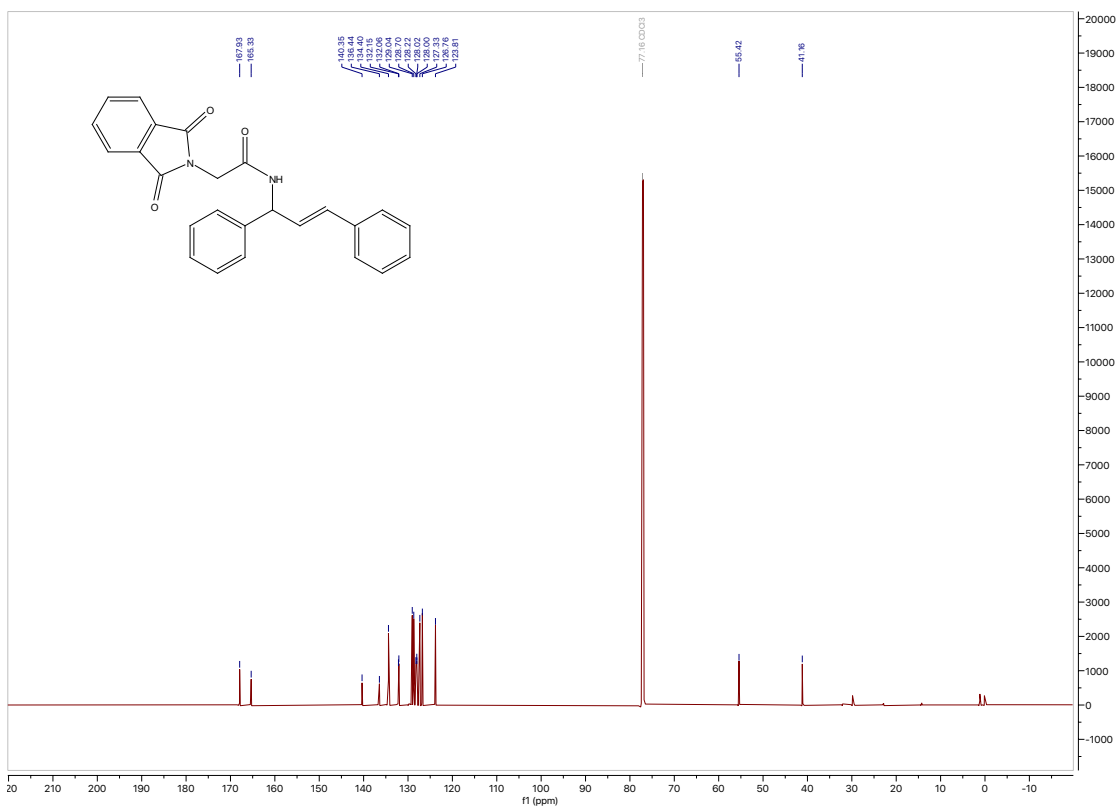
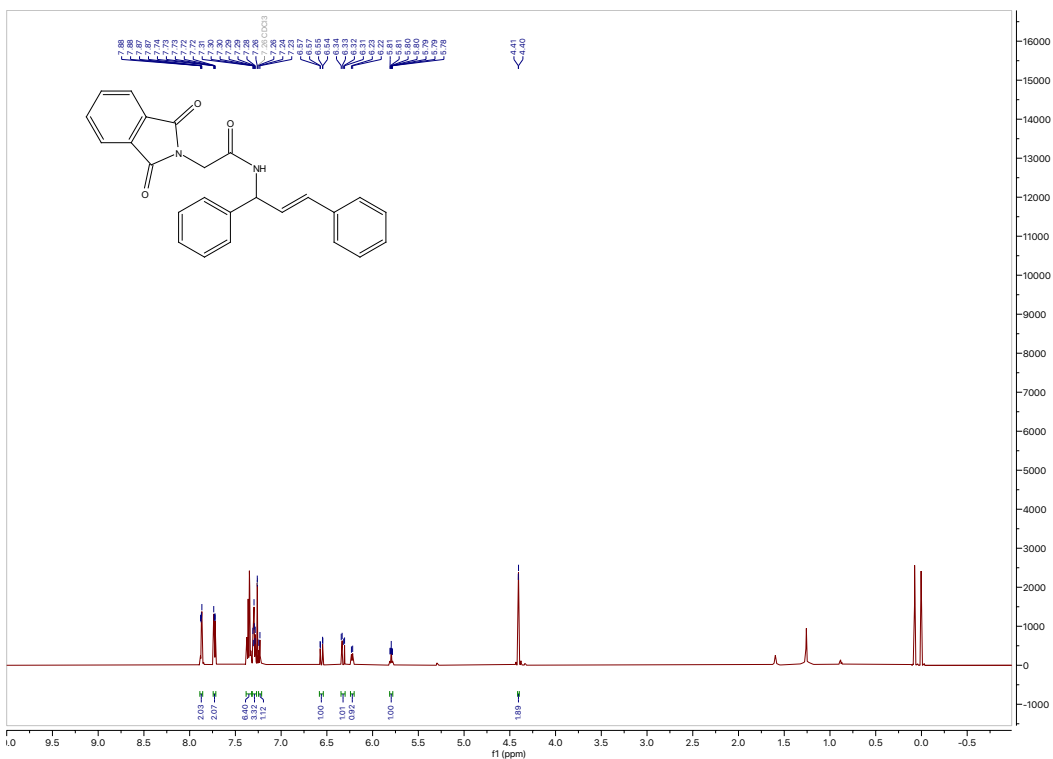
Totals : 7694.20190 278.79794

(S,E)-N-(1,3-diphenylallyl)pivalamide

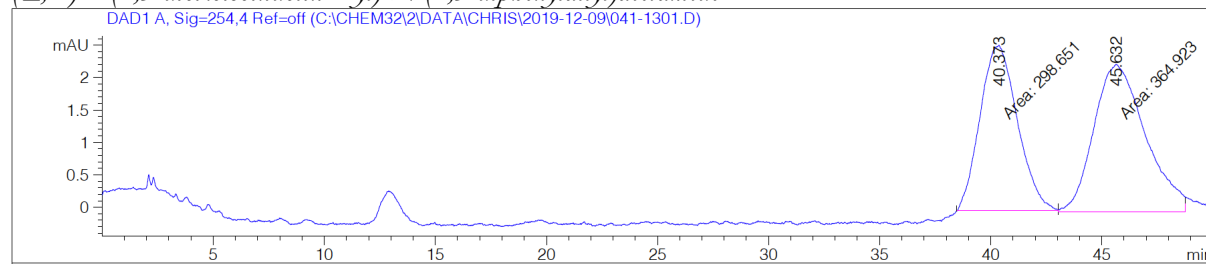
Signal 2: DAD1 B, Sig=230,4 Ref=off

Peak #	RetTime [min]	Type	Width [min]	Area [mAU*s]	Height [mAU]	Area %
1	13.806	BB	0.2922	508.97794	20.60517	1.9261
2	16.242	BB	0.4517	2.59169e4	795.23010	98.0739

Totals : 2.64258e4 815.83527

(S,E)-2-(1,3-dioxisoindolin-2-yl)-N-(1,3-diphenylallyl)acetamide

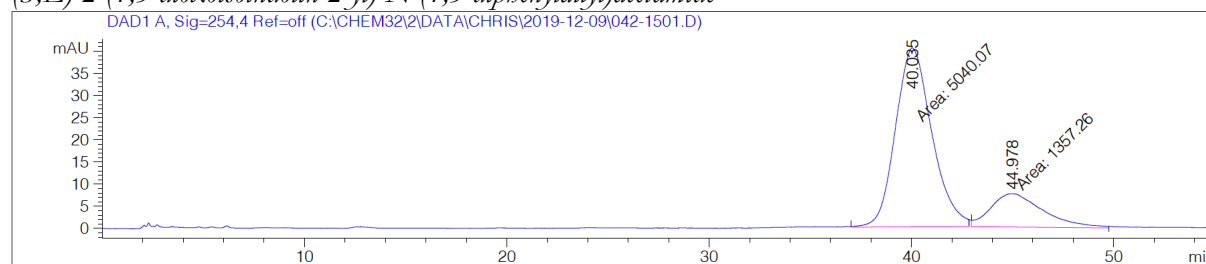
(±,E)-2-(1,3-dioxisoindolin-2-yl)-N-(1,3-diphenylallyl)acetamide



Peak #	RetTime [min]	Type	Width [min]	Area [mAU*s]	Height [mAU]	Area %
1	40.373	MM	1.9487	298.65140	2.55428	45.0065
2	45.632	MM	2.6789	364.92325	2.27036	54.9935

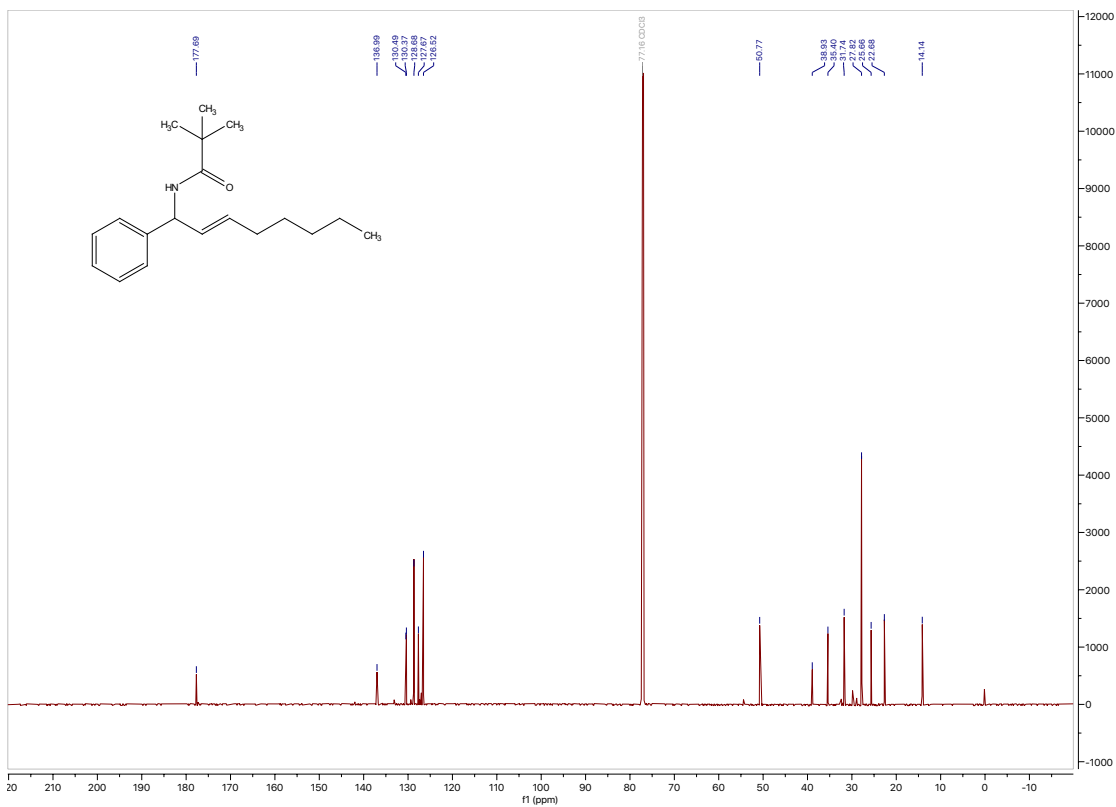
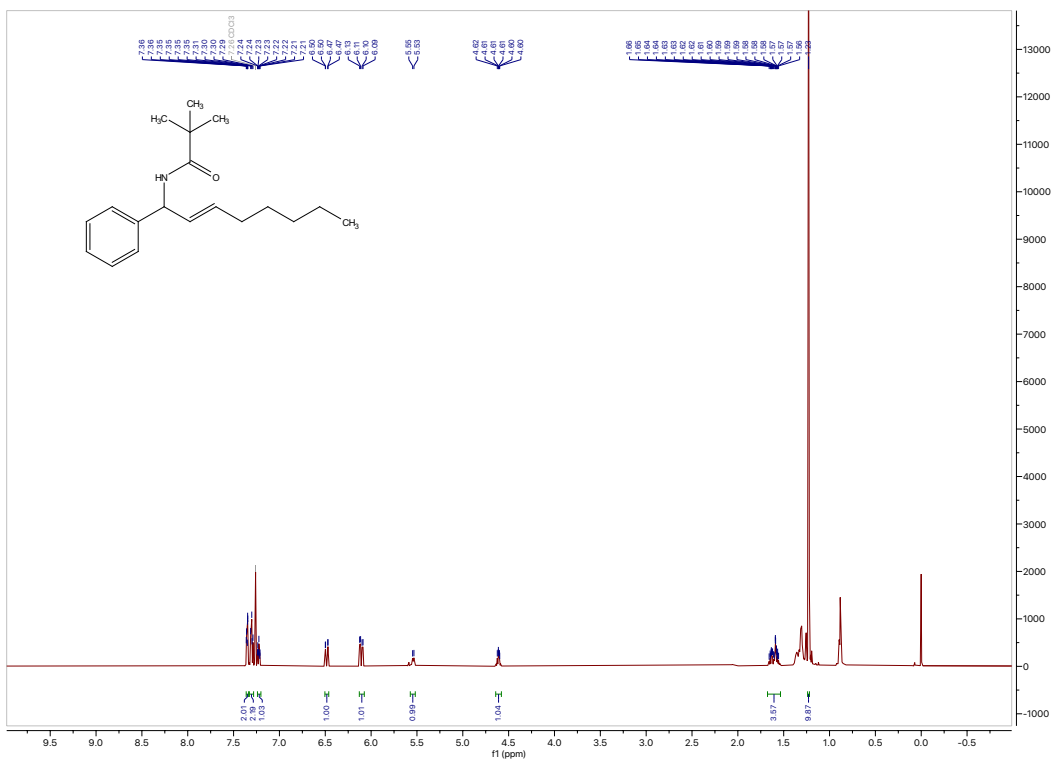
Totals : 663.57465 4.82464

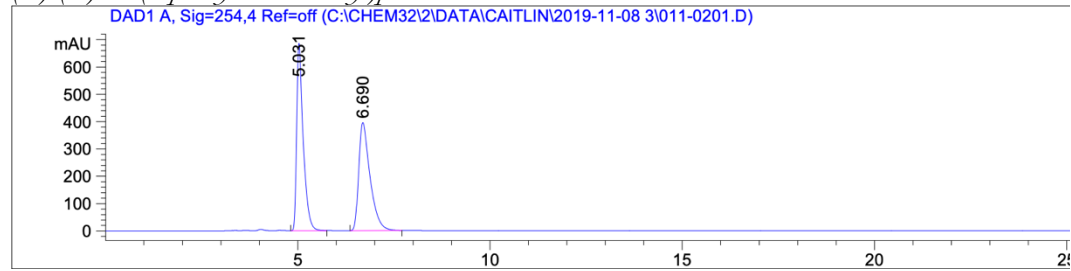
(S,E)-2-(1,3-dioxisoindolin-2-yl)-N-(1,3-diphenylallyl)acetamide



Peak #	RetTime [min]	Type	Width [min]	Area [mAU*s]	Height [mAU]	Area %
1	40.035	MM	2.0817	5040.07373	40.35269	78.7840
2	44.978	MM	3.0088	1357.25916	7.51837	21.2160

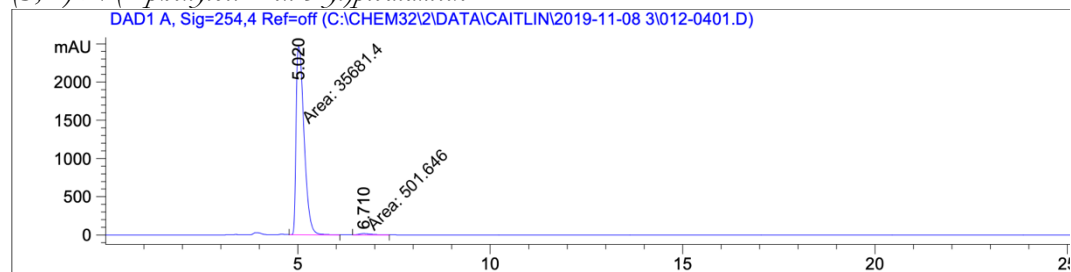
Totals : 6397.33289 47.87106

(S,E)-N-(1-phenyloct-1-en-3-yl)pivalamide

(±)-(E)-N-(1-phenyloct-1-en-3-yl)pivalamide

Peak #	RetTime [min]	Type	Width [min]	Area [mAU*s]	Height [mAU]	Area %
1	5.031	VB	0.1722	8128.28955	686.04407	50.1367
2	6.690	BB	0.3005	8083.97021	395.41028	49.8633

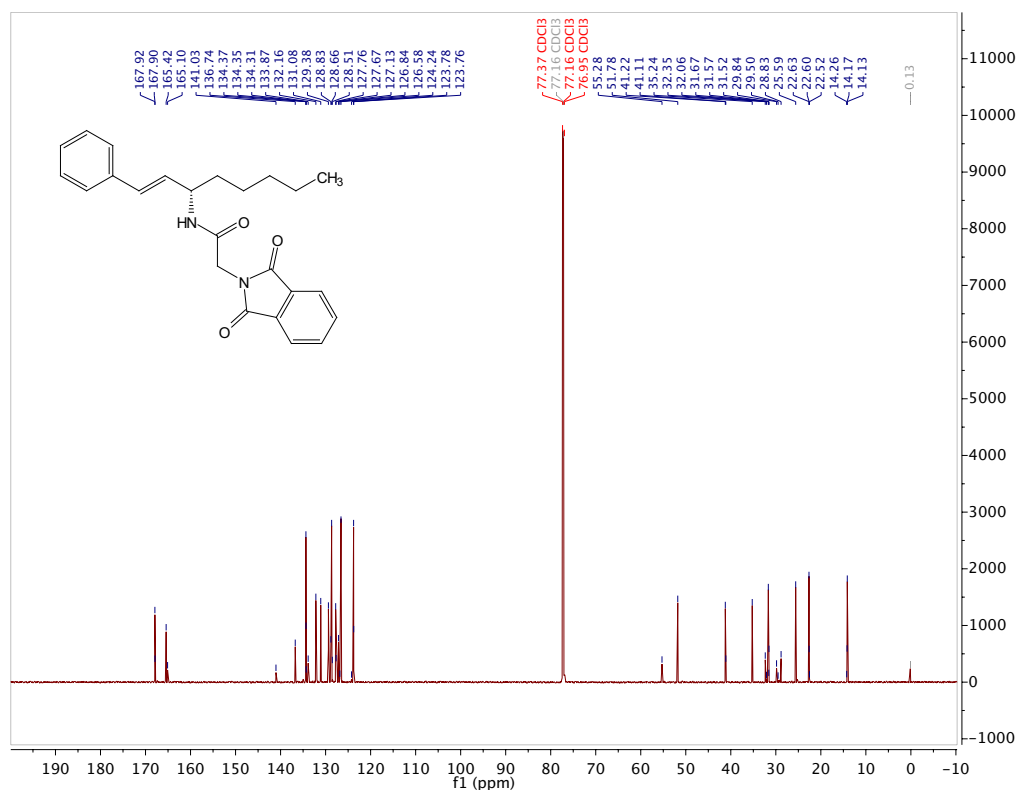
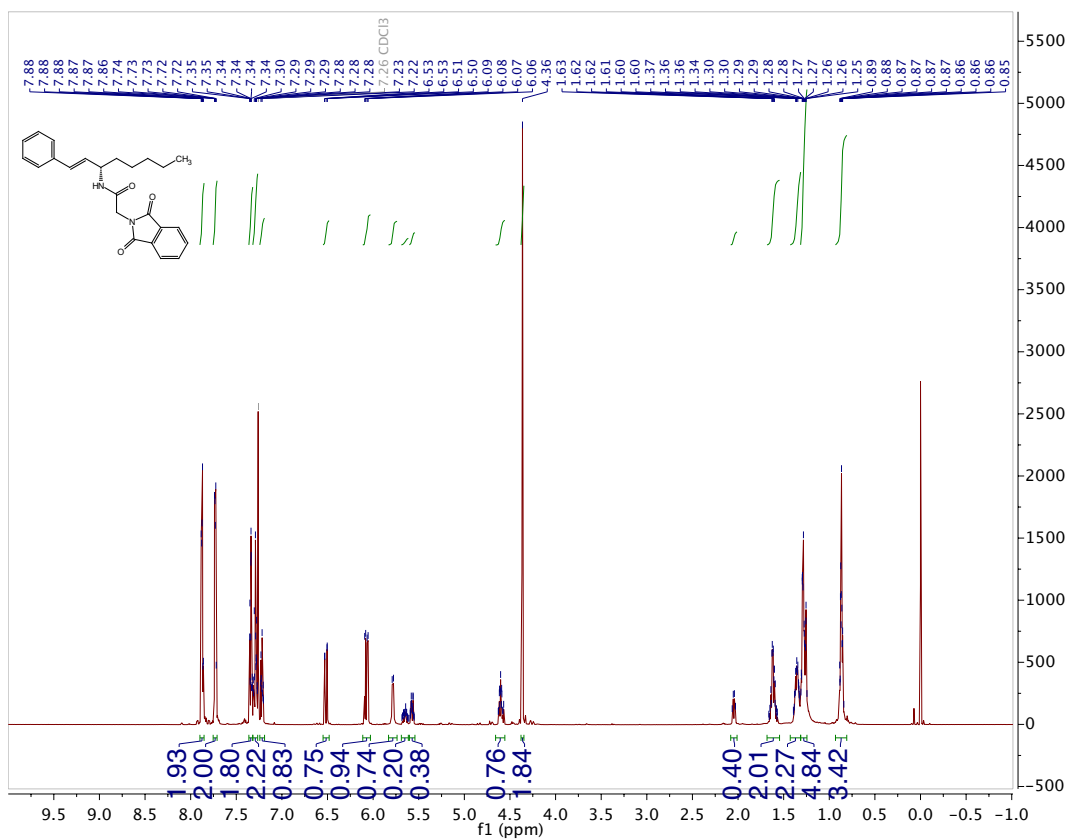
Totals : 1.62123e4 1081.45435

(S,E)-N-(1-phenyloct-1-en-3-yl)pivalamide

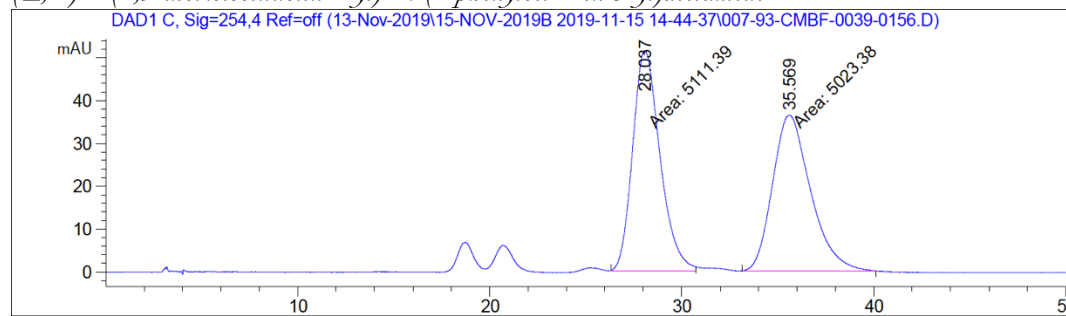
Peak #	RetTime [min]	Type	Width [min]	Area [mAU*s]	Height [mAU]	Area %
1	5.020	MM	0.2419	3.56814e4	2458.60937	98.6136
2	6.710	MM	0.4265	501.64560	19.60351	1.3864

Totals : 3.61831e4 2478.21289

(S,E)-2-(1,3-dioxoisindolin-2-yl)-N-(1-phenyloct-1-en-3-yl)acetamide



(±,E)-2-(1,3-dioxoisindolin-2-yl)-N-(1-phenyloct-1-en-3-yl)acetamide

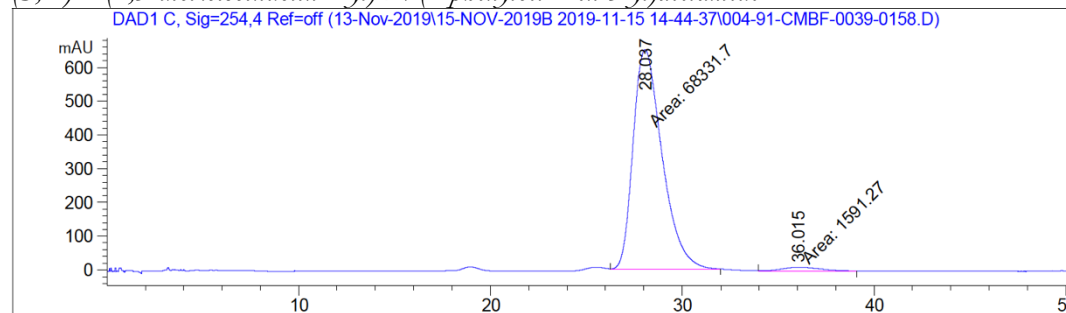


Signal 3: DAD1 C, Sig=254,4 Ref=off

Peak #	RetTime [min]	Type	Width [min]	Area [mAU*s]	Height [mAU]	Area %
1	28.037	MM	1.6556	5111.39160	51.45485	50.4342
2	35.569	MM	2.3009	5023.37891	36.38676	49.5658

Totals : 1.01348e4 87.84162

(S,E)-2-(1,3-dioxoisindolin-2-yl)-N-(1-phenyloct-1-en-3-yl)acetamide

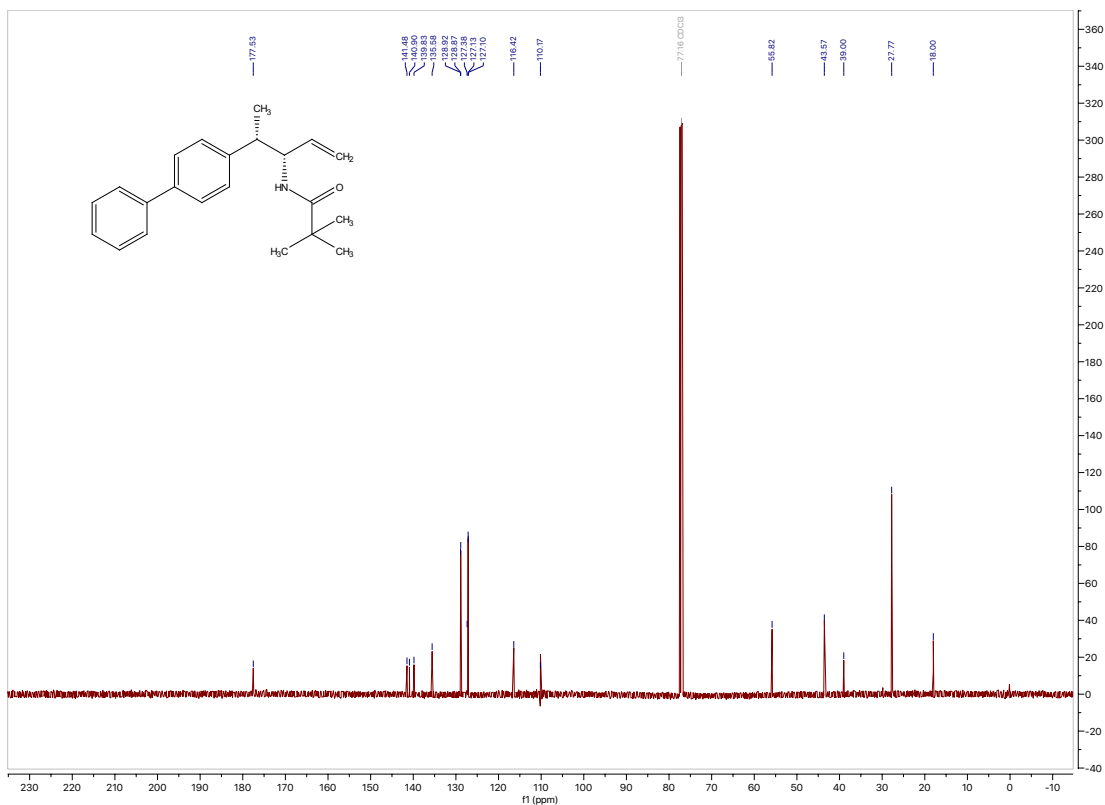
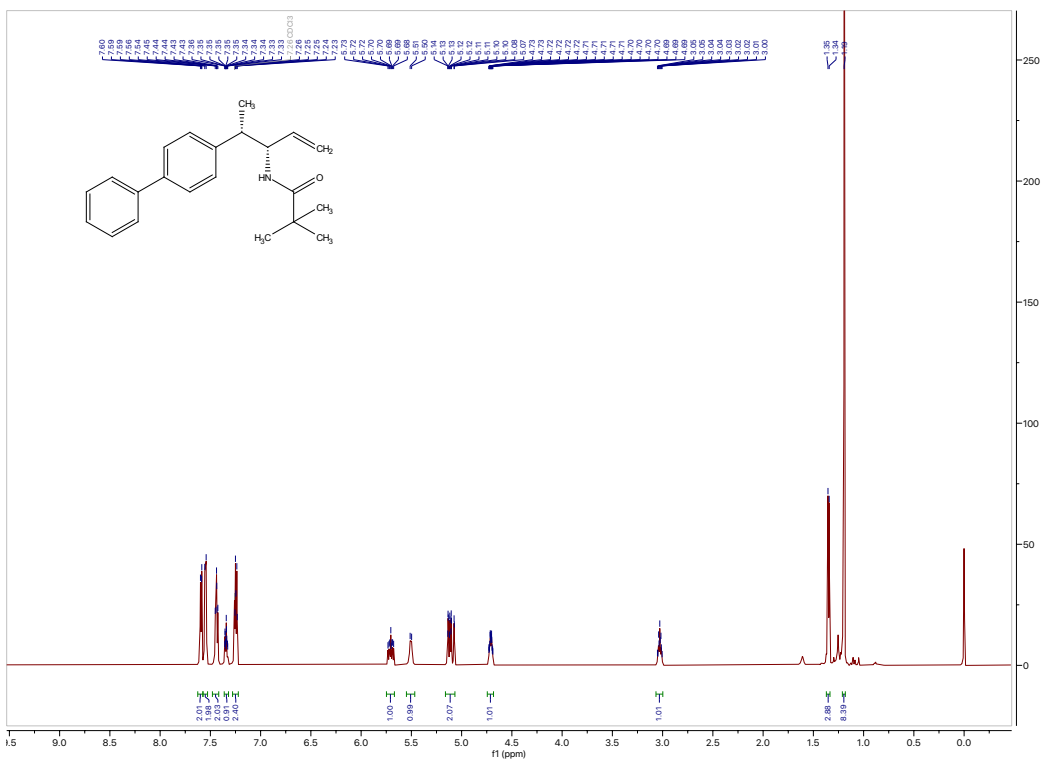


Signal 3: DAD1 C, Sig=254,4 Ref=off

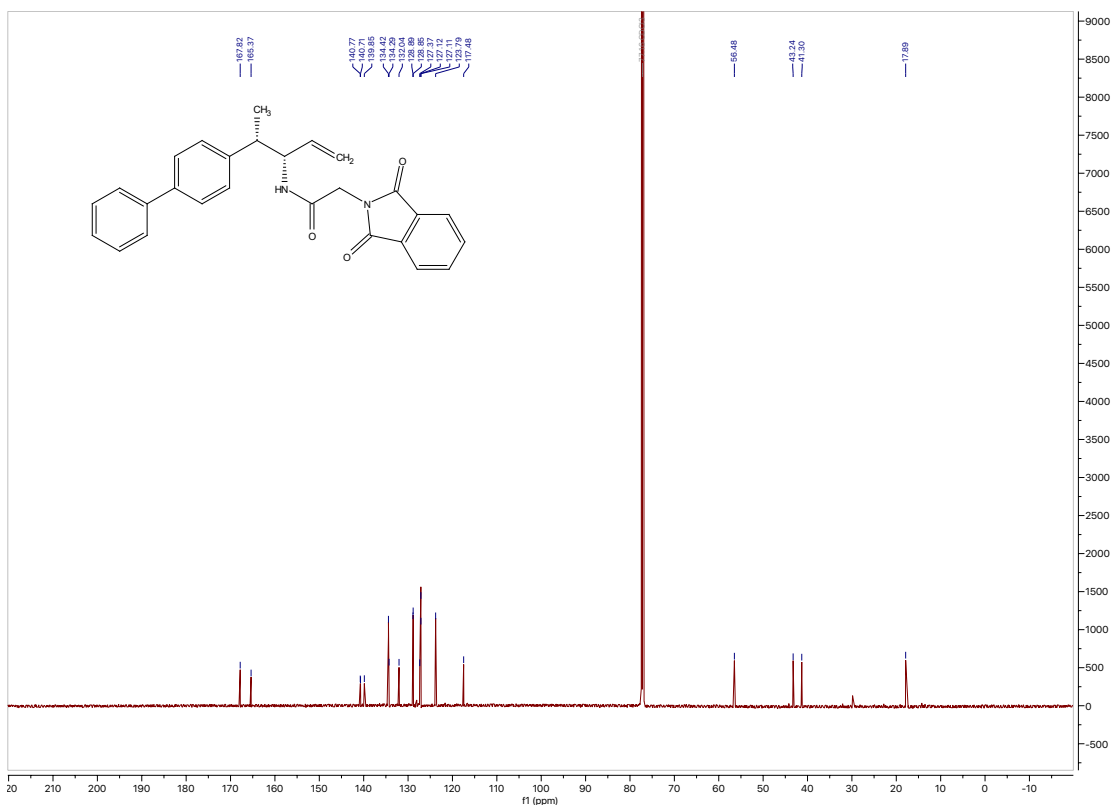
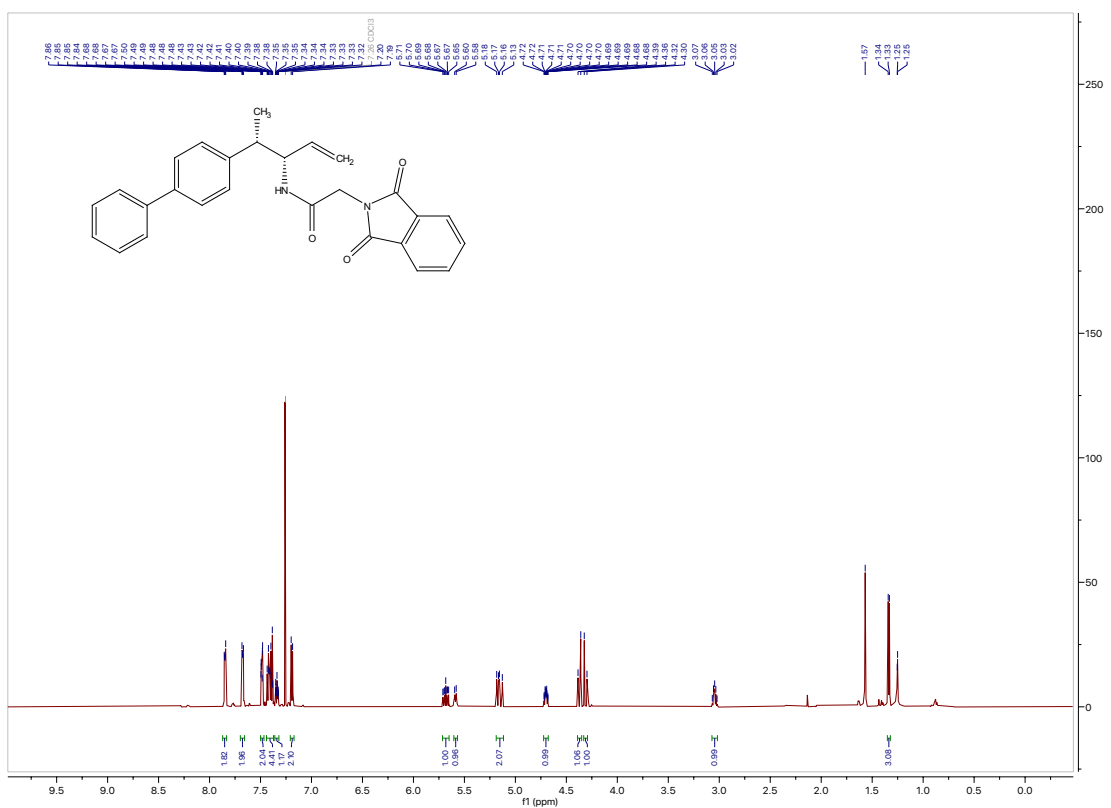
Peak #	RetTime [min]	Type	Width [min]	Area [mAU*s]	Height [mAU]	Area %
1	28.037	MM	1.7505	6.83317e4	650.59467	97.7242
2	36.015	MM	2.3517	1591.27356	11.27731	2.2758

Totals : 6.99230e4 661.87197

N-((3*S*,4*S*)-4-([1,1'-biphenyl]-4-yl)pent-1-en-3-yl)pivalamide



N-((3*S*,4*S*)-4-([1,1'-biphenyl]-4-yl)-2-(1,3-dioxisoindolin-2-yl)acetamide



3.10 References

- (1) Kazerouni, A. M.; Nelson, T. A. F.; Chen, S. W.; Sharp, K. R.; Blakey, S. B. Regioselective Cp*Ir(III)-Catalyzed Allylic C–H Sulfamidation of Allylbenzene Derivatives. *J. Org. Chem.* **2019**, *84*, 13179–13185.
- (2) Burman, J. S.; Harris, R. J.; B. Farr, C. M.; Bacsá, J.; Blakey, S. B. Rh(III) and Ir(III)Cp* Complexes Provide Complementary Regioselectivity Profiles in Intermolecular Allylic C–H Amidation Reactions. *ACS Catal.* **2019**, *9*, 5474–5479.
- (3) Lei, H.; Rovis, T. Ir-Catalyzed Intermolecular Branch-Selective Allylic C–H Amidation of Unactivated Terminal Olefins. *J. Am. Chem. Soc.* **2019**, *141*, 2268–2273.
- (4) Knecht, T.; Mondal, S.; Ye, J.-H.; Das, M.; Glorius, F. Intermolecular, Branch-Selective, and Redox-Neutral Cp*Ir^{III}-Catalyzed Allylic C–H Amidation. *Angew. Chemie Int. Ed.* **2019**, *58*, 7117–7121.
- (5) Ye, B.; Cramer, N. A Tunable Class of Chiral Cp Ligands for Enantioselective Rhodium(III)-Catalyzed C–H Allylations of Benzamides. *J. Am. Chem. Soc.* **2013**, *135*, 636–639.
- (6) Ye, B.; Cramer, N. Chiral Cyclopentadienyl Ligands as Stereocontrolling Element in Asymmetric C–H Functionalization. *Science*, **2012**, *338*, 504–506.
- (7) Ye, B.; Cramer, N. Chiral Cyclopentadienyls: Enabling Ligands for Asymmetric Rh(III)-Catalyzed C–H Functionalizations. *Acc. Chem. Res.* **2015**, *48*, 1308–1318.
- (8) Newton, C. G.; Kossler, D.; Cramer, N. Asymmetric Catalysis Powered by Chiral Cyclopentadienyl Ligands. *J. Am. Chem. Soc.* **2016**, *138*, 3935–3941.
- (9) Hyster, T. K.; Knörr, L.; Ward, T. R.; Rovis, T. Biotinylated Rh(III) Complexes in Engineered Streptavidin for Accelerated Asymmetric C–H Activation. *Science*, **2012**, *338*, 500–503.
- (10) Jia, Z.-J. J.; Merten, C.; Gontla, R.; Daniliuc, C. G.; Antonchick, A. P.; Waldmann, H. General Enantioselective C–H Activation with Efficiently Tunable Cyclopentadienyl Ligands. *Angew. Chem. Int. Ed.* **2017**, *56*, 2429–2434.
- (11) Trifonova, E. A.; Ankudinov, N. M.; Mikhaylov, A. A.; Chusov, D. A.; Nelyubina, Y. V.; Perekalin, D. S. A Planar-Chiral Rhodium(III) Catalyst with a Sterically Demanding Cyclopentadienyl Ligand and Its Application in the Enantioselective Synthesis of Dihydroisoquinolones. *Angew. Chem. Int. Ed.* **2018**, *57*, 7714–7718.
- (12) Baker, R. W. Asymmetric Induction via the Structural Indenyl Effect. *Organometallics* **2018**, *37*, 433–440.
- (13) Baker, R. W.; Turner, P.; Luck, I. J. Electronic Control of Metal-Centered Chirality in H5:KS-Indenyl-Sulfanyl and -Sulfinyl Rhodacycles of Phenylpyridine, *Organometallics*, **2015**, *34* (9), 1751–1758

- (15) Baker, R. W.; Radzey, H.; Lucas, N. T.; Turner, P. Stereospecific Syntheses and Structures of Planar Chiral Bidentate $\eta^5:\kappa^2$ -Indenyl-Sulfanyl and -Sulfinyl Complexes of Rhodium(III). *Organometallics* **2012**, *31*, 5622-5633.
- (16) Marder, T. B.; Calabrese, J. C.; Roe, D. C.; Tulip, T. H. The Slip-Fold Distortion of π -Bound Indenyl Ligands. Dynamic NMR and x-Ray Crystallographic Studies of (η^5 -Indenyl)RhL₂ Complexes. *Organometallics* **1987**, 2012–2014.
- (17) Hart-Davis, A. J.; Mawby, R. J. Reactions of π -Indenyl Complexes of Transition Metals. Part I. Kinetics and Mechanisms of Reactions of Tricarbonyl- π -Indenylmethylmolybdenum with Phosphorus(III) Ligands. *J. Chem. Soc. A* **1969**, 2403–2407.
- (18) Westcott, S. A.; Kakkar, A. K.; Stringer, G.; Taylor, N. J.; Marder, T. B. Flexible Coordination of Indenyl Ligands in Sandwich Complexes of Transition Metals. Molecular Structures of $[(\eta^5\text{-C}_9\text{R}_7)_2\text{M}]$ (M = Fe, R = H, Me; M = Co, Ni, R = H): Direct Measurement of the Degree of Slip-Fold Distortion as a Function of d-Electron Count. *J. Organomet. Chem.* **1990**, *394*, 777–794.
- (19) Trost, B. M.; Ryan, M. C. Indenylmetal Catalysis in Organic Synthesis. *Angew. Chem. Int. Ed.* **2017**, *56*, 2862–2879.
- (20) Piou, T.; Romanov-Michailidis, F.; Romanov-Michailidis, M.; Jackson, K. E.; Semakul, N.; Taggart, T. D.; Newell, B. S.; Rithner, C. D.; Paton, R. S.; Rovis, T. Correlating Reactivity and Selectivity to Cyclopentadienyl Ligand Properties in Rh(III)-Catalyzed C–H Activation Reactions: An Experimental and Computational Study. *Journal of the American Chemical Society* **2017**, *139*, 1296-1310.

Experimental References

- (1) Yan, Z.; Chong S.; Lin, H.; Yang, Q.; Wang, X.; Zhang, W.; Zhang, X.; Zeng, Z.; Su X. Design, synthesis and biological evaluation of tetrazole-containing RXR α ligands as anticancer agents. *Eur. J. Med. Chem.* **2019**, *164*, 562-575.
- (2) Abe, I.; Nakao, Y.; Nakahara, T. *N*-Pivaloyl Methyl Esters as Novel Derivatives of Amino Acid Enantiomers for Chiral-Phase Capillary Gas Chromatography. *Chem. Lett.* **1997**, 629-630.
- (3) Burman, J. S.; Harris, R. J.; Farr, C. M. B.; Bacsa, J.; Blakey, S. B. Rh(III) and Ir(III)Cp* Complexes Provide Complementary Regioselectivity Profiles in Allylic C–H Amidation Reactions. *ACS Catal.* **2019**, *9*, 5474-5479.
- (4) Wang, Y.; Wang, J.; Li, G.-X.; He, G.; Chen, G. Halogen-Bond Promoted Photoactivation of Perfluoroalkyl Iodides: A Photochemical Protocol for Perfluoroalkylation Reactions. *Org. Lett.* **2017**, *19*, 1442-1445.
- (5) Brooks, J.; Xu, L.; Wiest, O.; Tan, D. S. Diastereoselective Synthesis of Highly Substituted Tetrahydrofurans by Pd-Catalyzed Tandem Oxidative Cyclization–Redox Relay Reactions Controlled by Intramolecular Hydrogen Bonding. *J. Org. Chem.* **2017**, *82*, 57-75.
- (6) Yuan, Q.; Yao, K.; Liu, D.; Zhang, W. Iridium-catalyzed allyl-allyl cross-coupling of allylic carbonates with (*E*)-1,3-diarylpropenes. *Chem. Commun.* **2015**, *51*, 11834-11836.

- (7) Wang, Y.- M.; Buchwald, S. L. Enantioselective CuH-Catalyzed Hydroallylation of Vinylarenes. *J. Am. Chem. Soc.* **2016**, *138*, 5024-5027.
- (8) Fall, Y.; Berthiol, F.; Doucet, H.; Santelli, M. Palladium-Tetraphosphine Catalysed Heck Reaction with Simple Alkenes: Influence of Reaction Conditions on the Migration of the Double Bond. *Synthesis* **2007**, *11*, 1683-1696.